University of Strathclyde,
Department of Electrical and Electronic Engineering

A long-Range Spectroscopic Methane Leak Sensor System Using a High Power Raman Amplifier

By David Mitchell

A thesis presented in fulfilment of the requirements for the degree of Doctor of Engineering

April 2010

Copyright Statement

Signed: *Date:*

Acknowledgments

Firstly, my thanks go to Walter, not least for his help in putting this thesis together and helping me to get my report writing skills to where they are today. This is more of an achievement than one might think unless one has been privy to some of my earlier reports. Aside from this, thanks for having the belief in my ability to pull through even when things may have appeared otherwise. More generally, I feel I have benefited from your supervision, being given an almost free hand to pursue topics of interest. My ideas were met with an ideal blend of enthusiasm and a healthy scepticism that drove me to make my work more rigorous. Finally, thanks for the exposure to international conferences and the good times we had at those. Your support in Prague made all the difference to my confidence.

I would also like to thank Kev, who had the misfortune of being assigned to helping me turn my high power amplified source into a complete sensor system. During this time, I feel we worked together tremendously well and developed and understanding and rapport that we otherwise might not have had. Working through stressful situations was made considerably easier with your good humour (and when your humour wasn't good, you usually vocalised whatever I was feeling more eloquently than I could in any case). This was of course backed up with a strong work ethic and an organised, no-nonsense, positive approach, which helped me develop and better organise my investigations. I believe these qualities were vital to the success of the project. Thanks for all the laughs and making the lab work seem easier.

Furthermore, I would like to extend my thanks also to everyone who helped out in the field trials and preliminary experiments; Ian with his ability to magically produce kit that fits with everything else and makes everything work and his stint at the field trials, which nearly landed him in hospital from exposure, Keith, Michael and James in particular for having the presence of mind to take photographs of the field trials. All of the above took time out of their work to embark on something much less pleasant! I would also like to acknowledge the support of Graham, for seeming to know where everything is and whether it is working, George for listening to my theory problems and providing help or appropriate reading. Thanks everyone in the group for their input, laughs and conversation, in particular Arup, who still won't share his wife's true curry recipe with me and Joao, who was always good fun. Thanks to Carole, Sadie and Rachel for your conversation and support.

Thanks also go to OptoSci, for being a part of an exciting project and choosing me to carry it out. In particular thanks to David Moodie as an industrial supervisor with a healthy scepticism and high standards that demand the best from people. Your practical approach and unerring intuition regarding electronic equipment was much appreciated. Thanks all for the Guinness times!

Last, but by no means least, I'd also like to extend thanks to Federica for helping keep me fed (though not nearly enough!) and clothed (far too much!) during my frantic writing up time and for putting up with me when I was feeling less than jovial.

Abstract

Wide area gas leak monitoring is a necessary but costly exercise in industrial areas where hazardous gases are stored, transported or released as by-products. The problem arises from having inspectors perform time-consuming patrols over long distances traversing potentially difficult terrain. One prominent example of this is the leak inspection of continental natural gas pipeline networks. In order to increase the speed and efficiency of these inspections, a long-range helicopter or vehicle mounted optical spectroscopic sensor system is proposed, where the spectroscopic probe signal is launched over the open test path and methane is detected by analysing the backscattered signal from the ground. Using high-quality, low-cost, optical communications sources and receivers, the near-IR spectroscopic sensor system can be built economically whilst high sensitivity is achieved, despite the relative weakness of near-IR compared to the fundamental far IR absorption lines, using the sensitive wavelength modulation spectroscopy (WMS) technique. The technique of stand-off methane measurements using the surface backscatter of a WMS signal from arbitrary terrain has been demonstrated effectively in previous work and commercialised at short range (~10m). The main difference between the 10m system and the proposed 100m system was the output signal power required to obtain the necessary received signal power at the detector for methane detection. Using a simple geometrical argument, a factor of 10 greater range results in the need for a factor of 100 increase in signal power to achieve the same received power level at the detector. With typically 10mW signal power used in the 10m systems, ~1W should be required for detection at 100m.

The strongest near-IR methane overtone lines are in the region of 1650nm at which tuneable diode laser sources are available with up to ~20mW maximum output power. The development of a high power 1650nm amplifier represents the main focus of the work, given that none are currently available. Combining a commercially available, high-power EDFA, with a gain band around 1530-1580nm, with a fibre Raman amplifier (FRA), which amplifies any signal using a pump of optimally ~13.2THz higher frequency than the signal (for germano-silicate fibres) via the stimulation of the inelastic Raman scattering, allows amplification at 1650nm using the output from an

EDFA. Given this, a 1650nm WMS signal from a diode laser can be used to seed the stimulated Raman scattering (SRS) of a 1540nm pump from a high power EDFA, resulting in a high power, amplified 1650nm WMS signal. Raman amplifiers are particularly attractive because of their excellent noise figure and simple construction, essentially requiring only a length of gain fibre and some means of (de)multiplexing the signal and a pump waves. With power levels of the order of W in both the pump and signal waves propagating within the fibre system, stimulated Brillouin scattering (SBS) represents the main obstacle to the realisation of the high power fibre amplifier system.

Several Raman amplifier designs were modelled and tested, using a range of fibre types and pumping configurations. Good accordance was achieved between the models and the experiments and 2.36W of high quality 1650nm signal power was produced in the counter-pumped DSF system from a 20mW DFB signal laser and a 5W Keopsys pump EDFA. SBS was suppressed in the system using the fact that the gain bandwidth of SBS is considerably narrower than that of SRS, allowing propagation of an SBS-free broad bandwidth pump without affecting Raman gain. In the case of the narrow bandwidth 1650nm WMS signal, SBS was suppressed by emulating bandwidth broadening through optimisation of the wavelength modulation parameters used primarily for WMS, resulting in the distribution of the wavelength modulation over the Brillouin gain length.

With a successful amplifier system developed, short range methane measurement experiments were conducted at 11m with methane integrated path concentration levels of 10000, 1000 and 100ppm.m using the minimum possible output signal power to achieve a 3:1 gas SNR. Having validated the geometrical argument for the intensity of backscatter as a function of range along with the signal power required for acceptable sensitivity in the 11m methane sensing measurements, the maximum range of the sensor system was calculated to be 260m. The system was taken to field trials at 105m using a make-shift transmit and receive system, which consisted of a collimator/expander and a 30cm Fresnel lens respectively. Background level methane was detected with a SNR in considerable excess of 3:1 using the backscattered WMS signal from wood, concrete and white laminate and 100ppm.m sensitivity was demonstrated.

Table of Contents

Chapter 1 Introduction and Background

1.1 Background and Justification

Methane is invisible, odourless and flammable gas and is the main constituent of natural gas. This makes it an important energy source and it is piped over long distances to be used and sold across continents. However, it is explosive at around 5-15% molar concentration in air [1.1] meaning that leak monitoring of storage areas as well as the gas pipeline infrastructure is required. This can present a major inconvenience to oil and gas companies, since the pipes can stretch for thousands of kilometres and also pass under inaccessible terrain, making these inspections very laborious and expensive with handheld detectors and impractical for a network of point sensors. In addition, storage areas can be large and gas clouds can migrate away from point sensors, which could allow a leak to go undetected. The result of these factors is essentially that environmental monitoring in the oil and gas industry is an unavoidable and costly exercise, while at the same time the methods of detection are fallible.

One method of overcoming the difficulty in inspecting large areas and also the constraints of point sensors, is to have a remote sensor system that could be attached

to a helicopter or suitable vehicle to allow greater speed and coverage in the case of gas pipelines or wide areas. The vehicle equipped with a remote sensor system becomes a mobile environmental monitoring tool, capable of rapid leak inspection over large areas, such as pipeline networks. Apart from the possibility of vehicle based detection, the long range sensor could be fixed on a platform to allow more thorough and flexible inspection of an area than an array of fixed point sensors. These configurations enable fast, flexible detection and should lead to a considerable increase in efficiency and reduction in the cost of environmental monitoring for large areas, while at the same time improving the chances of detecting a methane leak. Although some long range and vehicle mounted detectors have been produced as reviewed in this chapter, an ideal solution has not yet been realised in terms of cost, weight, size and performance.

The most practical way of constructing a long-range, remote hydrocarbon monitor is through the development of an open path optical sensor system. The obvious practical barrier to this, is that over long ranges, say a feasible helicopter altitude of >100m, the collection of the signal backscattered from the ground is inefficient and therefore a low noise signal detection scheme and a high launch power are required. Furthermore, it is necessary to be able to detect small increases of methane concentration against a background (~340ppm.m at 100m, assuming a round trip) [1.2]. Various technologies providing potential solutions to this problem are discussed in the following section.

1.2 Environmental Monitoring in Industry

Until the early 1990s, hydrocarbon detection was mainly conducted using pellistors as distributed point-sensors, or flame-ionisation detectors as portable, hand-held sensors. Pellistors operate by passing a current through a bare wire and, in the presence of a hydrocarbon, oxidation takes place at the surface of the wire, resulting in a resistance change and hence unbalancing a Wheatstone bridge. The voltage required to rebalance the bridge is used as a quantitative guide to the methane concentration present [1.3]. The flame ionisation detector is a portable device used

to investigate the presence of flammable species. It operates by ionising flammable species through flame ignition. The resulting ions are drawn to electrodes and produce a current. The current level represents the concentration of flammable gas or vapour [1.4]. Initially, spectroscopic detectors were conceived to replace widespread pellistor point sensors and hand held flame ionisation detectors (FID) as a result of a number of weaknesses associated with these detectors, which are outlined below [1.3].

Although pellsitors are a well established technology, highly sensitive and have a modest unit cost, they have the disadvantage of degradation over time, requiring regular recalibration and hence they have a high cost of ownership. Furthermore, there are several important failings regarding the pellsitor. Firstly, it can only detect the presence of a gas below the upper flammability concentration limit, which means that a sudden gas leak could lead to no reading from the pellistors. Secondly, they are inherently unsafe since they feed a relatively high current into the test area and deliberately cause oxidation of hydrocarbons around the detector. Finally, they are not gas specific and report the presence of many hydrocarbons with no indication of which [1.3].

In the case of the hand-held flame ionisation detector, they come with obvious safety implications. Carrying even a well-shielded flame, into an area that may contain explosive leaks is inadvisable in principle. In addition, it is not gas specific, only useful if the detector is located within the leak cloud and produces a warning for anything flammable in the air while destroying any species it finds [1.5]. It was the recognition of these failings in available monitoring systems that resulted in the development of commercial optical sensing systems as an alternative in an attempt to avoid some of these issues. Arising from the sphere of optical gas sensing, various point and hand-held sensors exploiting absorption spectroscopy were developed.

1.3 Optical Spectroscopy for Methane Sensing

1.3.1 Conception of Spectroscopic Methane Sensing

The concept of detecting methane using optical spectroscopy for industrial sensing was originally devised by C. Moore in 1964, [1.6] where methane was injected into the cavity of a He-Ne laser in order to suppress stimulation of its primary $3S_2$ to $3P_4$ transition, which is responsible for output at 3.3923μm. This wavelength, matches a strong methane absorption line, meaning that light at this wavelength experiences considerable attenuation though a methane sample. Given the presence of a large amount of methane in the laser cavity, the $3S_2$ to $3P_2$ dominates in its place, resulting in stimulation of the unabsorbed 3.3912μm emission. It was hypothesised that the sensitivity to the presence of methane in the cavity was very high and that the concentration of the methane could be determined by the relative strength of the two output wavelengths. Later, this coincidence was exploited in a methane sensor using one He-Ne laser on the methane absorption line and another whose output was unabsorbed by methane as a reference, and subsequently a system with a dual wavelength He-Ne (one on and the other off-line) to achieve the same effect [1.7,1.8].

1.3.2 Spectroscopic Sensing in Industry

Having identified optical spectroscopy as an exploitable tool for environmental monitoring, it was only after some time that it became fully feasible in a commercial sense. With the increasing interest in optics for telecommunications, solid state optical devices became much less expensive and therefore practical, low-cost, spectroscopic methane sensors could be designed by exploiting this component set. Optical sensors, both point and remote are generally superior, in terms of cost (particularly when considering the total cost of ownership), flexibility (integration with other systems such as control and optimisation), applications, (gas specific or several targets) and reliability while offering similar performance in terms of sensitivity and response time compared with flame ionisation detectors and pellistors [1.3]. Initially, it was convenient to use LEDs or even thermal sources as the means of producing radiation at wavelengths that would be absorbed by hydrocarbons, such

as methane, for use in spectroscopic sensing systems. In their simplest form, they may consist of a pair of filtered LEDs, or similar broad bandwidth source whose emission frequency band covers a strong absorption line of the target gas and a pair of optical detectors [1.3]. One of the LEDs will be incident on a detector through a gas cell that has access to the atmosphere around it and the other LED-detector pair is sealed from the surrounding environment. They report a detection on the reduction of received powers from one of the LEDs in relation to the other. Two LEDs are used in most cases to mitigate the risk of false alarms caused by fluctuations in current to the LED. Like pellistors and FIDs, these are often point sensors, but can be directed across a path. They require considerably less re-calibration than the pellistor, since carrying out their task does not degrade the components significantly and they do not require high currents or flames to carry out the detection, making them inherently safer.

Building further upon the concept of spectroscopic point sensors, there are still improvements to be discussed. Firstly, these detectors still feed electrical current to the inspection area, which can still give rise to the ignition of a methane leak. In addition, a separate LED and photoreceiver set are required for each sensor, and over a large area and this can become expensive. Lastly, the signals from the point sensors must be protected from electrical interference to maintain a reasonable sensitivity. To avoid these disadvantages, it would be convenient if light could be fed from a source through optical fibre to and from the inspection points [1.3]. This makes it possible that only one optical source is required for the wide area system, the inspection point could fit into small spaces, there would be no electrical current at the inspection sites and the network would be immune to electrical interference. However, the realisation of this requires some consideration. Firstly, practical propagation through standard optical fibres requires operation in the near-IR where the methane absorption is considerably weaker. Secondly, using one source to address many points demands a powerful source or a technique that can be used with low signal power.

1.4 Coherent Near-IR VS Incoherent Mid-IR Spectroscopic Signal Sources

The fundamental absorption lines in the mid-IR band are by far the most efficient in terms of absorption of photons by the methane, with the strongest of the fundamental at around 3.3μm being a factor of around 200 stronger than the strongest of the near-IR at around 1651nm [1.3]. This immediately favours building a system that operates in the mid-IR band, however the implications of building a complete mid-IR sensor system require consideration beyond this. Taking these into account, it can make detection using coherent near-IR sources far superior to a high quality mid-IR LED-based sensor initially in terms of sensitivity. One of these considerations is that the sensitivity of a spectroscopic sensor is heavily dependent on the spectral power density of the source and the inexpensive, off-the-shelf mid-IR sources available include LEDs and thermal sources, whose output bandwidth is far in excess of that of single-mode diode lasers available in the near-IR. The result is that, of the total output power of the broad bandwidth, mid-IR device, only the small proportion of its spectral power coinciding with methane absorption lines is absorbed. The fractional absorption of the source's output as it passes through a cloud is proportional to the ratio of the gas linewidth to the source. If the absorption line is broader than that of the source, the maximum fractional absorption is achievable. The relative (to when the laser and gas linewidths are approximately equal) reduction in fractional absorption with respect to spectral power density is illustrated in Figure 1.1.

Considering high quality, commercially available LED sources, their linewidth is such that they suffer a penalty of a factor of ~3000 in terms of fractional absorption compared to a narrow bandwidth, source (relative to the absorption line). In addition, diode laser sources can output 10-20 times more optical power than LED sources, meaning that the total absorption depth for a narrow-band, single-mode laser output, such as that from a DFB centred on an absorption line is at least 30000 times greater than that of a mid-IR source. The result of this simple spectral comparison is that, even when considering the relative near and mid-IR line strengths (factor of 1/200 to near IR absorption)[1.3] and the fact that an LED source may address up to

ten methane lines (factor of 10 improvement to mid-IR absorption) [1.3], a near-IR communications DFB laser output on a strong near-IR overtone line is absorbed at least 10 times as much as a thermal or LED source in the mid-IR. This figure is obtained taking the factor of 30000 improvement from increased fractional absorption and greater output power of the near IR compared to mid-IR sources and dividing it by the factors that favour mid IR, such as line strength and number of absorption lines addressed simultaneously.

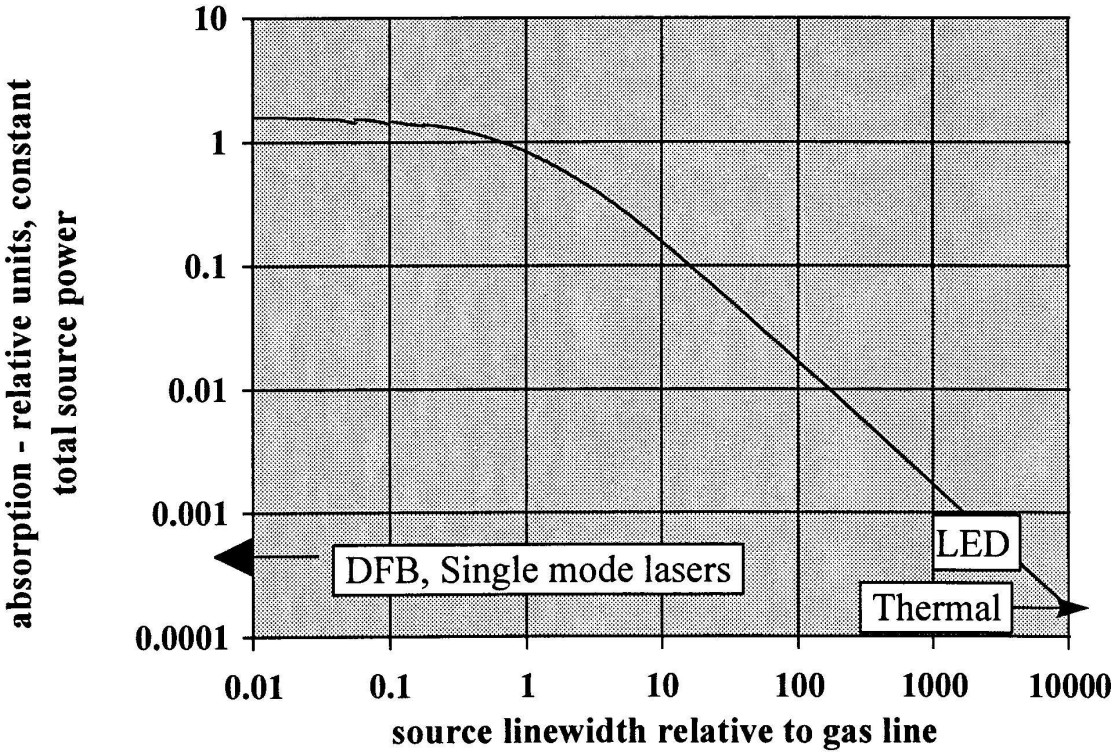

Figure 1.1 Relative absorption as a function of ratio of source to gas linewidths. Extracted [1.3]

In addition to the advantages of coherent near-IR sources over incoherent mid-IR sources with respect to the interaction with their apposite absorption lines, the detection configurations of the competing system types also bear interesting comparisons. When considering both the mid-IR and near-IR bands, it should be taken into account that at room temperature, the background thermal radiation is much stronger in the mid than near-IR and this reduces the ultimate sensitivity of any mid-IR system. Taking detector areas of the same area and band gaps of 750meV and 350meV for near and mid-IR detectors respectively, the fundamental dark current of the mid-IR detector is around three orders of magnitude greater than that

of the near IR detector. Hence, near-IR systems can be more suitable for the detection of methane from a small signal power in a complete, commercialised system than mid-IR, as doing so in the mid-IR band would require cooled IR detectors to eliminate the dark current for a useable sensitivity. At liquid nitrogen temperatures, the performance of a typical InAsSbP mid-IR detector becomes comparable to that of an InGaAs near-IR detector at room temperature [1.3].

With respect to coherent sources suitable for the spectroscopic detection of hydrocarbons in the near-IR, the advancement of techniques and systems was largely a result of the development of improved near-IR diode lasers in the mid 1990s for optical communication applications. One particularly useful laser, and most relevant to the project is the DFB (Distributed Feedback) laser. The DFB diode laser is suitable for spectroscopic gas sensing because it is readily modulated and wavelength tuneable over a few nm, stable, energy efficient, low noise and has narrow output bandwidth (typically between ~1-10MHz). These lasers can produce in the region of 1-20mW CW output power and maintain their strongly single-mode output as a result of their distributed grating structure of their active region, which forms a narrow bandwidth cavity. This means that the selected mode experiences very considerable gain compared with any others, resulting in strong suppression of sidebands [1.9].

Many gases that require monitoring in industry have absorption lines at near-IR wavelengths, meaning that these communications diode lasers can find applications in sensing. The original development of these lasers provided sources with wavelengths up to 1550nm. The result was that high quality, single-mode near-IR tuneable lasers were being produced in large quantities and hence at a low cost, which lead to greatly increased interest in tuneable diode laser spectroscopy (TDLS) as a means of gas sensing. Some further development was still required to reach the preferred 1651nm and 1665nm methane lines, but this was easily realised given the existing technology, with Shimose and Okamoto from the Anritsu Corporation developing a single-mode 1.66μm DFB diode laser. Having access to high quality,

cheap lasers that were easily modulated made trace gas sensing of hydrocarbons using a laser in an industrial context more readily realisable [1.10].

Given that a near-IR laser could be multiplexed in an optical fibre network addressing detection points around a site, it follows that communications fibre components could be employed both for their high quality in terms of performance and reliability and also in terms of their price. Mass production of the appropriate components for a sensor network leads to a significant cost reduction in the system build. In addition it allowed the use of near IR detectors, such as those made from InGaAs which do not require cooling, rather than the mid-IR detectors, such as InAsSbP and HgCdTe, which require cooling because of their small band gaps necessary for the detection of low energy photons.

1.6 TDLS with WMS

Having established that the use of a near IR DFB provides an improvement in terms of fractional absorption and overall sensitivity, we now examine a practical application enabled by the use of the DFB, namely that of wide area monitoring via a network of fibre fed cells. Although this is an application quite different from remote sensing, the techniques and advantages they provide are instructive.

It should be recalled that a DFB laser is considerably more expensive than LEDs and therefore, more must be done to allow extensive multiplexing. This is exacerbated by the fact that, although a 1651nm DFB laser can be made using the same materials and production techniques as a C-band 1550nm DFB, it is a wavelength not used in communications, thus keeping the cost higher than that of a standard communications laser. In order to offset the cost of using a laser diode as the optical signal source, at least 100 inspection points must be addressed [1.3]. Having employed a low noise communications source and photoreceiver, it then falls to the detection technique to maximise SNR from the low power resulting in maximised multiplexing.

In applying a detection technique to sense small increases in methane level, the following factors should be considered. Firstly, there is still the need for self-referencing, analogous to the second LED on a mid-IR point sensor. Using the DFB, this is achieved in the technique. By sweeping the laser's output wavelength across the absorption line, a differential absorption is found in the presence of methane (off-line and on-line), and not for a reduction in received power arising by other means. This can be achieved using one tuneable source rather than using two non-tuneable sources for normalisation of optical power at the receiver. Using a tuneable laser to carry out the spectroscopic sensing as described, is known as Tuneable Diode Laser Spectroscopy (TDLS).

It is through the use of a narrow bandwidth, tuneable diode laser that the application of techniques associated with a high SNR become possible. For this purpose, the well established Wavelength Modulation Spectroscopy (WMS) technique is employed. The concept is that by applying a wavelength dither to the narrow bandwidth (compared to the gas absorption linewidth) probe signal as it is swept across the gas line, the received power is, in the presence of methane, an amplitude modulated AC signal. This occurs as the sinusoidal wavelength modulation interacts with the absorption line profile. Firstly, detecting in AC allows the reduction of 1/f noise by setting the dither and hence detection frequency to the region of at least 10^4Hz [1.11,1.12] and secondly, it allows the use of phase-sensitive detection using a lock-in amplifier (LIA). The LIA acts as an electrical band pass filter, which can be centred on the detection frequency, thus excluding noise at frequencies outside of its bandwidth. It then amplifies the filtered signal, producing a DC level that is proportional to the depth of the AC amplitude modulation.

Given the ability to select the pass frequency of the AC signal, it is possible to select a harmonic of the gas signal. 1f detection, i.e. that at the frequency of the wavelength dither is often used, or alternatively detection can be carried out at a higher harmonic, often 2f. This involves detection at twice the wavelength dither frequency, and this is sometimes chosen to enable more effective isolation of signal

amplitude modulation arising from differential gas absorption from amplitude modulation as a result of current modulation on the laser used to induce the wavelength modulation [1.10]. Using phase sensitive detection and optical power in the region of tens of micro-Watts, the sensitivity can extend to a methane level of around 2.5ppm.m [1.3]. The unit ppm.m is used to measure 'integrated path length concentration,' or 'average concentration path-length product', which takes both the concentration of the gas cloud and path length of the light through the gas into account. The total absorption by the methane molecules depends upon the total number of molecules a beam of light encounters. This in turn depends upon the concentration of the molecules with respect to volume, and the path length of the cloud through which the beam travels. Hence 3ppm.m represents light passing through a 1m cloud of a concentration of three methane molecules per every million, or a cloud of one part-per-million concentration and path of 3m.

A sensor network system using TDLS with WMS as described above represents the state of art in current optical point sensor networks. However, if the discussion returns to the case of leak inspection of pan-continental natural gas pipelines, such a network of point sensors is still not a feasible solution in terms of cost because of the implied size of the sensor network.

1.7 Remote TDLS with WMS Signal from a DFB Laser

1.7.1 Principle of remote Gas Sensing Using a Backscattered WMS Signal from Arbitrary Surfaces

It was the lack of flexibility with regard to where leak detection could be carried out using point sensors (i.e. they are only likely to be deployed where there is a high, foreseeable risk of a leak) that initially led to interest in the development of stand-off hand-held spectroscopic sensors. These sensor systems would be a direct replacement for the hand-held FIDs, except that they would carry a significantly smaller risk of igniting any flammable species in the air on a large scale, would be gas specific and could be used over some distance, meaning that the operator need

not necessarily stand in the gas cloud to detect the leak. It is here that the advances in networked point sensors can be applied to remote sensors. Given a methane detection technique for trace methane detection from low powers, it follows that hand-held, remote detection systems could be produced using the same principle, as they operate under similar received power conditions to achieve a similar sensitivity.

The proposed system in the work detailed within this thesis is an open path optical sensor, where the absorption of radiation by the target gas is detected by measuring the backscattered signal from the ground around the inspection area, analogous to previous work [1.12] but at longer range. A TDLS-WMS signal, which is tuned to the wavelength of a methane absorption line is directed from the helicopter, or suitable vehicle, through the test path and is backscattered from the ground around the gas pipe back to a detector system on the helicopter. A schematic showing the concept of the open path spectroscopic sensor system is shown in Figure 1.2.

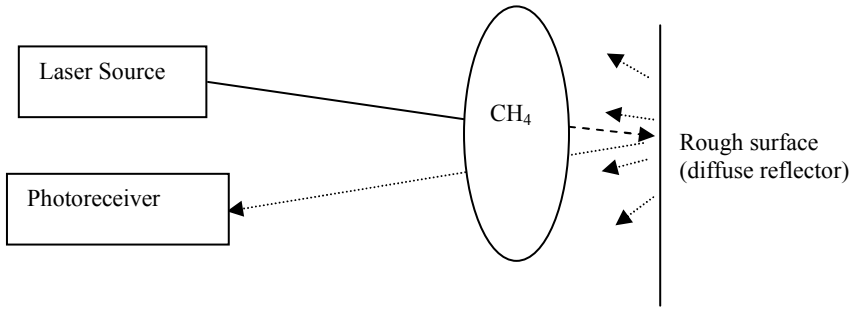

Figure 1.2. Schematic of Open Path Methane Detector Principle of Operation

In Figure 1.2, light is transmitted through the methane cloud and scattered from the ground at the back of the test path. The received power is then measured using a photoreceiver via a collection lens.

1.7.2 Realisation of a Practical Stand-Off Spectroscopic Sensor Based upon review of Commercialised Systems

Although the proposed long-range remote sensor addresses a new function, and a near-IR methane detector with a range of more than 100m is, to the best of our knowledge, not commercially available, some short-range variants are. These can be

discussed to provide proof of principle for the long-range sensor. Making use of the advances in DFB lasers and spectroscopic techniques mentioned in the previous section, a group published papers pertaining to a remote WMS-TDLS based methane sensor in 1992, which used the 1.66μm DFB laser locked to the centre of a methane absorption line using a gas cell and feedback mechanism based on maximising the 2f signal by adjusting the laser temperature [1.10]. They had two different modes of detection, the simplest of which was to launch the signal beam along a test path and directly into a receiver, as in the configuration typical of the early LED spectroscopic sensors. Alternatively, the signal could be directed at some surface at the end of the test path and the backscattered signal was collected and processed.

Clearly the backscatter method put considerable limitations on range and sensitivity, as well as changing the set-up required. As a result of the smaller collected signal in the backscatter mode, a pre-amp stage was required to amplify the signal from the photoreceiver before feeding to the lock-in amplifier. The output wavelength was dithered about the centre of the methane line at high frequency (5.35MHz) and the 2f signal was obtained. 2f was preferred because the 1f signal has a significant DC offset as a result of the residual amplitude modulation (RAM) arising from the current induced amplitude modulation, although 1f detection was also investigated [1.10]. This DC bias is greatly reduced in the case of 2f detection and arises here to a much lesser extent because of the non-linearity of the laser's output power as a function of input current and the gas absorption of the RAM. Using the 2f signal therefore allows greater signal amplification by the LIA before saturation is reached. The small DC offset was removed from the 2f signal by adding a correction function to the current modulation through which the frequency modulation was applied [1.10].

One problem with any backscatter system is that the magnitude of the gas signal, whether f or 2f, depends not only upon the amount of methane present, but is also directly proportional to the received power at the detector. In the case of a moving remote backscatter system, both the reflectivity of the backscatter surface and the range at which the backscatter takes place can be variable. In order to counter this, a

reference is required and in this case the ratio between the f and 2f gas signal is taken to remove this return power dependence [1.10].

Using the direct configuration, they detected 50ppm.m methane in air, with a SNR of 150 using a 1.3s averaging time. They extrapolate this to 0.3ppm.m sensitivity assuming a SNR of 1 is acceptable, however it is common for a SNR of 3:1 to be used and hence 0.9ppm.m should be noted for comparison. These values are comparable with the mid-IR He-Ne detectors, but require no cooling of the detector or source [1.10]. When operating in backscatter mode, experiments were carried out at 5m, into a 5000ppm.m sample using a wooden board and a concrete block as targets. In the case of the wooden board, the sensitivity was extrapolated to 50ppm.m, and in the case of concrete, which was found to be 40% less reflective than the wooden board, which will presumably have lowered the sensitivity by a corresponding proportion but a value was not published.

Concentrating on similar work conducted later by some of the same personnel as the previous system, Iseki et al continued to realise a commercial system [1.12] based on the 1992 lab demonstrator shown previously in Figure 1.3.

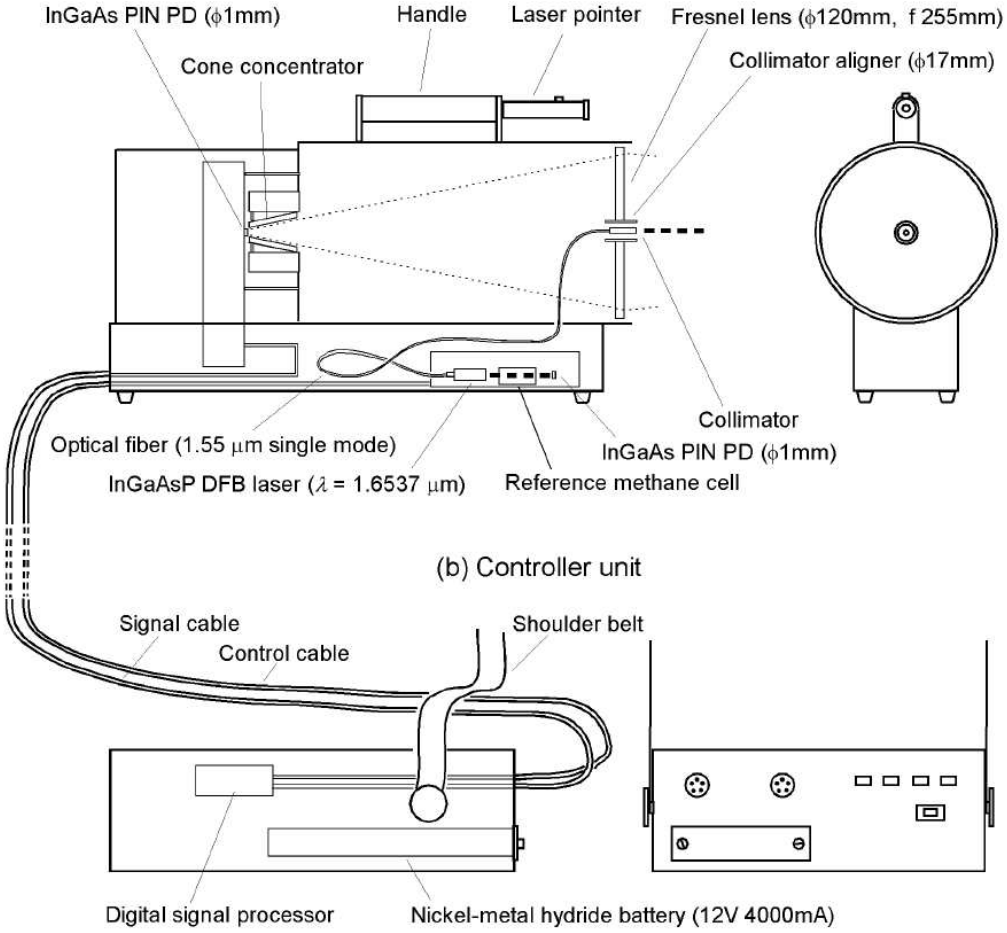

Figure 1.3 Iseki et al Commercial portable sensor system. Extracted [1.12]

The principle was the same as before, with the laser illuminating a surface at the other end of a test path, and the backscatter power being collected by a 120mm Fresnel lens onto a 1mm PIN photodiode with low noise pre-amp. In addition to the Fresnel lens, they also installed a cone concentrator to further increase the collection efficiency as shown in Figure 1.3. The cone concentrator concept is useful in non-imaging roles such as this and literature can readily be found on the concept [1.13]. This is one of the modifications to the lab demonstrator to construct a hand portable detector. The 10kHz laser modulation and reference signal were fed from a control unit, which also housed a lock-in amplifier of time constant 100ms. The relationship between LIA settings and detection rate and bandwidth are discussed in Section 2.2.2. The 2f signal was used and quantitative methane measurements could be made of the path integrated concentration via a PC with the appropriate software. Given that access to a PC may not be possible, the unit could be used as a sniffer,

wherein an alarm would sound if the signal became strong enough (they quote the example of a signal that would indicate 100ppm.m)[1.12].

In terms of performance, it was claimed that it could detect a 450ppb.m gas leak at 6m, again assuming SNR of 1 and using an MgO target. MgO is a highly reflective and almost perfectly Lambertian target material, making it an excellent control material, but not a realistic everyday surface. That is to say, it reflects almost around 99% (at 1550nm) of light falling on it, and distributes the reflected light almost evenly in a hemisphere. A perfectly Lambertian reflector has yet to be realised and so MgO is the nearest approximation available. In order to qualify their results, they carried out an extensive analysis of backscatter from common everyday materials referenced to MgO, which was very useful as a literature comparison in this work. From this backscatter study they deduced that their sensor should be able to detect a small leak of $10cm^3$/min at a range of 3m [1.12]. The main difference between the concept system and Iseki's commercial system being the inclusion of a reference gas cell for maintaining the laser locked to the methane absorption line. The system was successfully tested in outdoor conditions [1.12].

Given the proof of concept of remote spectroscopic detection using WMS, it follows that the main difference between carrying out detection at 5-10m and 100m is the relative backscattered signal intensity. Therefore, should enough signal output power be available, similar performance in terms of sensitivity should be possible at longer ranges. The main obstacle however, is that there are currently no suitable high power near-IR (1650nm) sources or amplifiers available. The same can also be said for high power, tuneable narrow-bandwidth mid-IR sources that could be used for WMS. A rule of thumb for remote systems is that to match the backscattered signal power for sensing at 10m, a factor of 100 more output power is required at 100m[1.14]

1.8 Selection of the Laser Source

1.8.1 Mid-IR Sources: State of Art and Design Implications

The rationale in the design with respect to optical source is discussed in this section. Given that no suitable, high power source is commercially available in the near or mid-IR for methane sensing, the implications of designing a high power source for each band is discussed. Firstly, the mid-IR is considered as an obvious starting point because of its stronger fundamental absorption lines compared with those of the near-IR. To compete with or exceed a near-IR WMS sensing system in terms of detection sensitivity from small signals, a system operating in the mid-IR would need to be based around a narrow bandwidth source capable of the same WMS technique discussed in previous sections. Methods of producing this narrow bandwidth mid-IR output include difference frequency generation (DFG) and optical parametric oscillation (OPO).

In the case of an OPO system, a pump oscillates within a cavity through a nonlinear material, such as a periodically poled lithium-niobate (PPLN) non-linear crystal. Two waves are produced from the pump, whose sum frequency is equal to that of the input pump. Historically these waves are known as the signal and idler waves. The proportion of the frequencies of the idler and signal waves, and hence the obtained wavelength can be determined by angular phase matching through adjusting the polarisation state of the input pump relative to the axis of the crystal[1.15]

DFG is similar to OPO, except that the signal wave is input along with the pump to achieve the desired difference frequency in the idler. In doing so, the threshold power for the effect is lowered. There is extensive literature on their operation, but brief descriptions of their operating principle can also be found [1.16]. The relative power of the signal and idler waves are determined by the angular phase matching in DFG systems.

DFG and OPO systems are not widely used for several reasons. Firstly, their phase matching and hence their output power or wavelength respectively is strongly

dependent upon temperature and the relative positions of all the components, meaning that they must be very carefully controlled in an oven. Secondly, they are complex in themselves and will often require an amplifier system to pump them, making them even more complex. Finally, given their alignment sensitivity, they are delicate and may not fare well in real, operational conditions. These factors result in OPOs and DFGs being expensive and often bulky, in terms of both the device itself and in terms of managing their operating conditions. In both cases, relatively narrow bandwidth, tuneable emission is achievable [1.15].

Despite the disadvantages associated with DFGs and OPOs, some reasonably successful systems have been constructed, as will be discussed in the review section on remote imaging systems. However, considering the temperature and vibration controls such a system would need to maintain crystal alignment as well as the cost of PPLN crystals (variable (2009), but in the region of £10000), a system using this approach would still be relatively bulky, expensive and more prone to failure than a near-IR communications based source. From a practical point of view, producing a high quality near-IR signal is simpler than one in the mid-IR, even though it has been demonstrated that high quality mid-IR can be produced.

Some advancements in the development of laser sources could lead to major improvements in producing convenient, high quality, narrow bandwidth, low cost, mid-IR output, in particular the quantum cascade laser. These operate in the mid-IR band, lasing via multiple intra-band transitions, and as such their emission wavelength is determined by the construction of the diode lattice rather than the materials used and their associated band structure. Their operating wavelengths are generally too long to be used around 3.3μm for methane, but this could be achieved conveniently and economically in the future with improved production techniques or strain compensation, although the latter may result in reduced reliability [1.17]. Their CW power is in the mW range at room temperature and they are capable of producing pulses with a peak power in the order of Watts. They are often constructed in a DFB configuration and hence produce single-mode, narrow bandwidth signals. Not currently mass produced for either the sensing or

communications industries, these QC lasers remain relatively expensive compared to C and L band DFB lasers.

1.8.2 Near-IR Sources: Design Implications

The alternative to mid-IR detection is to build a system in the near-IR, targeting the relatively weak methane overtone lines, the strongest of which are in and around 1651nm and 1665nm. This allows the construction of a fibre-optic system using communications amplifiers, components and near-IR communications detectors, thus mitigating many reliability, cost and alignment issues associated with bulk optical systems. The main challenge with this configuration is the generation of high power at 1651nm to achieve the required range for the system. As mentioned, there are currently no amplifiers commercially available at 1651nm and the development of this is the main piece of work detailed within this thesis. Despite the relative difficulty of detecting methane using the weak near-IR previously outlined, a fibre amplifier or laser system would have significant advantages over a bulk optical mid-IR system. Firstly, the implementation of a fibre amplifier or laser results in a very robust system without the requirement for precise alignment, whereas bulk optical systems are extremely sensitive to alignment. Fibre amplifiers, in particular, are insensitive to vibration and temperature effects. This is particularly important in the case of a sensor system that is required to be fixed to vehicles, as vibration and temperature fluctuations are to be expected and as such, might cause instability in the fibre laser.

Secondly, a fibre system is expected to be lighter and more compact than a bulk mid-IR system. In the case of a mid-IR system like those outlined in the previous section, it is probable that vibration resistant optical stages would have to be employed to accommodate the bulk optics reliably, and these normally have considerable mass. The mid-IR system would also require cooling and temperature control, and in addition to these factors, many batteries may be required to give the system a long operational lifetime because of their optical inefficiency compared with fibre amplifiers. With all of these factors taken together, it is probable that such a mid-IR system could weigh hundreds of kilograms, which presents a problem in the role of a

helicopter mounted sensor system, whereas a system in which all components are fibre coupled may only weigh around 10kg, including the optical sources.

Thirdly, a fibre system build can be carried out using standard communication fibre components, which because of their mass production, are considerably cheaper than relatively small volume mid-IR bulk optical materials. As a requirement of communications components, they tend to be very reliable compared to corresponding mid-IR components and it would therefore be expected that such a system would be less likely to develop a fault through normal operation. In general, fibre laser and amplifier systems can achieve higher efficiencies because of the additional beam confinement and the possibility of convenient, long interaction lengths.

1.9 Exploitation of Stimulated Raman Scattering as a Vehicle to a High Power 1651nm Signal

1.9.1 Background to Raman Amplifiers

Based upon the discussion thus far, it was decided that using a near-IR detection system would help realise the most effective, reliable system. This section concentrates on the exploitation of communications amplifiers in order to design a suitable high power 1651nm spectroscopic source. The techniques and components are introduced as is the rationale for their incorporation.

There are two main communications fibre amplifiers that can be considered for the task of amplifying 1651nm in the communication set. They are, the Erbium Doped Fibre Amplifier (EDFA), which is a well established communications amplifier typically used to amplify signals between 1530nm and 1570nm and secondly, the Raman amplifier, which is becoming more popular in communications with the increased availability of high power diode lasers [1.18]. The EDFA is not of immediate use, but the Raman amplifier can be, since it operates by the stimulated

inelastic scattering of its pump, thus amplifying a signal at a longer wavelength than its pump. The significance of this is that the main parameter governing the gain of the Raman amplifier is the frequency difference between the pump and signal waves, rather than an absolute wavelength, meaning that its application is not restricted to the most popular communications wavelengths [1.18]. The frequency shift resulting from the inelastic scattering is around 13.2THz in standard optical fibre, or around 110nm at 1550nm, meaning that if high power is obtainable at around 1540-1550nm, then high power stimulated scattering is available at around 1650nm using a Raman amplifier. As mentioned, high power standard communications amplifiers (EDFAs) are available in the C-band, and so high optical power at around 1550nm is readily generated; hence a Raman laser or amplifier system is a practical solution to obtaining a high power 1651nm output.

Raman amplifiers are becoming increasingly popular in communications with the increase in power available from diode lasers. This is because a signal can be amplified in a standard communications link without inserting repeaters, or EDFAs in-line, nor amplifying the signal to a high power to begin with. Hence an existing link can be upgraded with minimal disruption. In Raman amplification, a pump wave of one Stokes shift shorter wavelength than the signal requiring amplifying can be inserted into the fibre together with a signal [1.19]. Using this technique the system can have a net gain of 1, cancelling fibre losses. In this way, the noise is minimised because of the long interaction length and low peak power and gain.

In terms of producing high power at 1651nm from a pump at ~1550nm, either an external oscillator - fibre Raman amplifier, or a fibre Raman laser needs to be designed. The former implies that, as in the short-range hand-held sensor systems, the optical signal source can be a tuneable communications DFB laser and the high power is provided via an amplifier system. DFB butterfly packages are very stable and rugged when properly controlled, and this would, in conjunction with a fibre Raman amplifier, make a very stable source that is highly resistant to external effects. In the fibre Raman laser, the Raman scattering stimulates through the build-up of spontaneously Raman scattered photons in a fibre cavity and hence the DFB is

not required. The TDLS and WMS modulation would be applied directly though the laser cavity, most likely provided by a pair of Bragg gratings, or a Bragg grating and a cleaved end [1.20].

Fibre lasers can be problematic in that they suffer from vibration and temperature sensitivity in terms of output stability. The master oscillator fibre amplifier (MOFA), where a laser is used to provide the seed for the stimulation of Raman scattering, as opposed to a fibre laser system is a convenient method of maintaining stable, single-mode operation and smooth tuning whilst avoiding the disadvantages of mechanically modulating and thermally controlling a Fibre Bragg Grating (FBG) using an in-house built mount to produce the wavelength modulation and temperature control. In addition, when considering the company developing the sensor, it is worth taking into account the previous work and system configurations developed. A distributed methane sensing network was developed using optical fibre addressed gas cells, with a WMS gas sensing signal being produced by a DFB laser[1.3]. With the sensing elements already in place and the fabrication and assembly for this established, it was convenient to base the long-range, remote system on the foundations already laid. Furthermore, work is continuing on processing the resultant signals from this existing sensing scheme, obtaining better quality data, meaning that any further development could be applied to any new system based upon the same scheme [1.21,1.22].

1.9.2 Realisation of a High Power 1651nm Signal from an All-Fibre Amplifier System

As mentioned, the high power 1541nm pump can be supplied by existing communications EDFAs. This helps the system to meet the design requirements, in that a lightweight, energy efficient, reliable and low cost optical power source may be produced from all fibre components. The EDFA is a well established and reliable technology, which was conceived at Southampton University as an efficient single-pass, low noise amplifier for communications in 1987 [1.23]. The principle of an EDFA is that an optical fibre is doped with erbium, a rare earth, to act as the radiative atom. The optical fibre acts to confine the pump wave, usually at 980nm,

to maximise excitation of the erbium, while also confining a seeding signal in the same narrow cross section, leading to a configuration conducive to maximising amplification efficiency. The 980nm radiation excites erbium ions from the ground state $^4I_{15/2}$ to $^4I_{11/2}$ where non-radiative relaxation occurs to the metastable $^4I_{13/2}$. From this long-lived state, amplification can take place when radiative relaxation is stimulated in the presence of a seed wave of the appropriate photon energy. This stimulated transition results in emission such that most EDFAs amplify in the C-band and have a peak gain between 1530nm and 1560nm, depending on their construction. Different lengths, pumping wavelengths and pumping schemes can be used to maximise gain at a given wavelength or produce greater overall gain depending upon the application [1.24]. They provide a very high efficiency because of their beam confinement within the fibre that is unsurpassed in any other type of amplifier [1.25]. EDFAs are also available in the longer wavelengths of the communications wavelengths (L-band), to around 1620nm (Keopsys), although such a unit is currently (as of December 2009) very expensive when compared to C-band variants. Extensive literature is readily available on this well established technology [1.25].

It was decided that a discrete Raman amplifier, together with the existing DFB signal source and a high power, 1540nm pump EDFA was the best combination to produce a high power, low noise methane sensing signal with minimum further development and maximum integration with existing products. The principle is that the EDFA output is scattered in a fibre gain medium by a Stokes shift at around 110nm and the 1651nm DFB output can seed the scattering from 1540nm, resulting in an amplified version of the WMS signal. Typically, Raman amplifiers and EDFAs are in direct competition for the same signal boosting role in communications [1.18], however when used together they enable parametric amplification across much of the optical fibre transmission window.

A Fibre Raman Amplifier (FRA) system can be constructed from standard communications fibre and fibre components, which is commensurate with the overall strategy in development of using off-the-shelf products where possible. A schematic of the proposed system is shown in Figure 1.4. Essentially, a Fibre Raman Amplifier

(FRA) can consist of WDMs for multiplexing and demultiplexing the pump and signal, and a reel of optical fibre as a gain medium along with a signal source and appropriate pump. The simplicity of this is significant, in that the cost of the Raman amplifier system is little more than the cost of the signal laser and the high power EDFA, meaning that a custom 1650nm amplifier can be constructed for approximately the same price as a high power 1550nm EDFA. The amplified output is directed from the transmit telescope to a target surface, from which it is backscattered. The backscatter is focussed onto the photodetector via receive optics and processed by the LIA and oscilloscope.

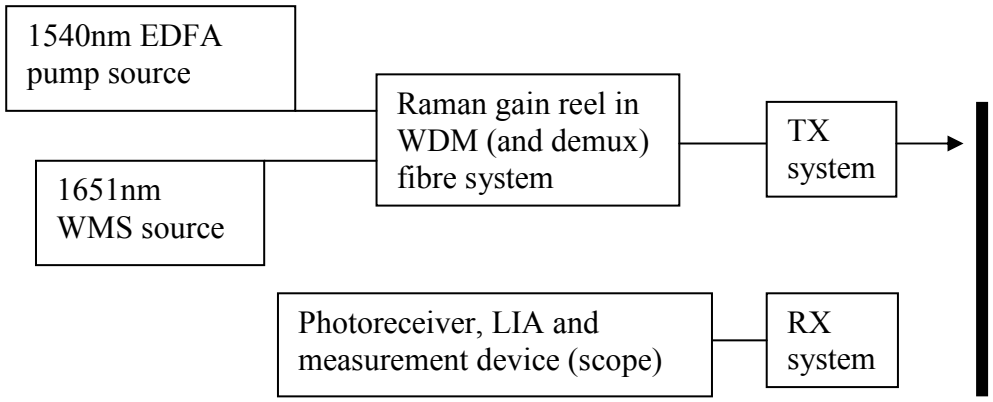

Figure 1.4 Proposed system sensor system schematic using Raman amplified source directed over open path to scenery surface

With regard to the efficiency of the Raman amplifier, there will be some power lost in the Raman amplification stage, mostly as a result of unscattered or 'residual pump', however even given this, a Raman amplifier system pumped by an EDFA should still be very efficient compared with other amplifier types.

While designing a high power fibre system, it is expected that certain obstacles will present themselves, for example Stimulated Brillouin Scattering (SBS) and multipath interference (MPI). SBS, like Stimulated Raman Scattering (SRS) is an inelastic scattering effect, which creates a backward travelling Stokes wave that experiences a very high Brillouin gain after threshold is reached. The Stokes shift is much smaller in SBS than SRS, as the scattering is with low frequency acoustic phonons rather than the high frequency optical phonons associated with SRS. If care is not taken,

increasing the power in the fibre system can result in scattering an increasingly large proportion of input power back out of the fibre, particularly when noting that the gain of Brillouin scattering is much stronger in standard fibre than that of Raman scattering. This is a difficulty associated with optical fibre systems in general, particularly those that require narrow bandwidths or high power. In the case of the required optical source, both of these conditions are present.

Multipath interference occurs when the signal takes more than one path to the detector, thus resulting in beating. This can arise from double-Rayleigh scattering (DRS), but can also result from pairs of reflection sites in the gain fibre, at splices and connectors for example [1.18]. DRS arises from the Rayleigh scattering that occurs in all fibres. At high optical powers, even fibre lengths of <10km can produce significant Rayleigh backscatter powers (~mW). It should be noted that both SBS and DRS backscatter will experience Raman amplification and the effect can become strong very easily after scattering becomes significant. If the amplified Rayleigh backscatter becomes strong enough, it too can produce a significant, secondary Raman-amplified Rayleigh-scattered wave now in the direction of the signal (hence the name DRS). This wave matches the signal frequency and causes beat noise in the signal [1.14]. Despite these obstacles, it is apparent from the review process that a near-IR DFB-fibre Raman amplifier system is the most commercially viable solution to remote sensing at >100m in an airborne sensing system in terms of cost, weight, size, reliability and stability with sensitivity comparable to that of a point sensor network.

Despite having chosen the system to be designed based on the discussion so far, it is instructive to consider other remote sensing systems already on the market for comparison with the proposed system and to consider features they offer that might be applicable in its design.

1.10 Review: Remote Methane Sensors

1.10.1 Review: Imaging Methane Detectors

There have been numerous methane sensors that have attempted to go further than integrated path methane detection (and quantification) and have extended to imaging, adding the benefit of being able to 'see' the leak and hence be more able to identify its source. In their simplest form, some imagers are essentially IR cameras, and operate on the assumption that leaked gas is at a different temperature to the atmosphere, at least until it has been leaked for some time. This device is clearly only of any value when investigating a site where it is known that there is a leak, as a tool to help find its source. It is quite clear that despite its simplicity, low cost and, assuming it 'sees' the leak, its advantage of leak visualisation compared to 'sniffing' (generates an alert on detection of the gas in the detection path) for a leak over a narrow path, it is completely unreliable as an actual leak detector, and not at all quantitative. Although not immediately relevant to the review, this method has perhaps inspired further development in remote spectroscopic methane sensors. Several systems are outlined in this section, some using the near-IR technology as discussed and others preferring instead to operate in the mid-IR at the fundamental absorption line. The improvements in methane sensing, in terms of cost, sensitivity and techniques as discussed previously have been exploited in the creation of these imaging systems. As with remote sensors, both near and mid-IR systems have been developed.

1.10.2 Vehicle Mounted Near-IR Methane Imager by SRI

A system is under development at SRI (December 2009), where they have proposed using a Raman amplified near-IR DFB source, in a similar approach to the one under consideration in this thesis. However their target range is in the region of 30m with a 100mW signal from their Raman source as opposed to in excess of 1W [1.26]. Given this, their Raman amplifier is of a very different configuration and is presumably limited by SBS. They, like the other hand-held devices began with an unamplified DFB transmitting 5mW and achieved a 15m range, where 18ppm.m above background methane was detected, which is similar to the performance of the

systems cited previously. The main purpose of their sensor was to be mounted on a van in order to detect and deduce the source of methane leaks via imaging.

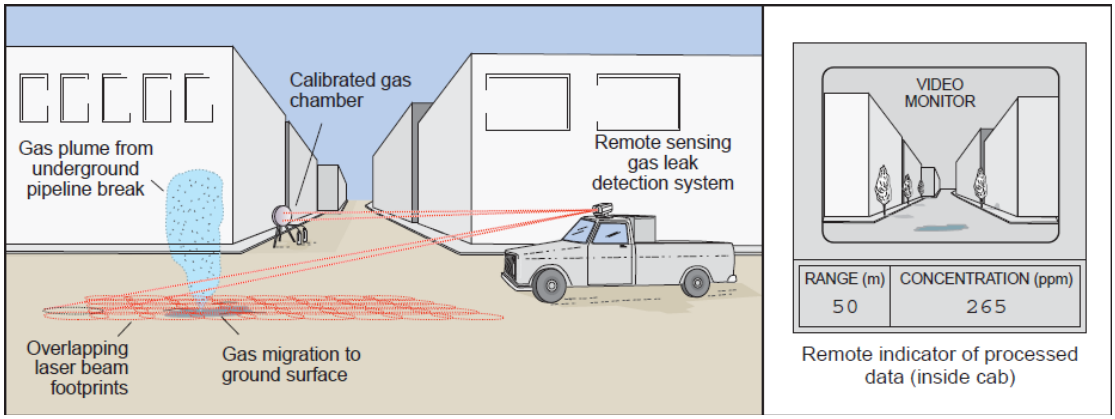

Figure 1.5 Schematic of SRI methane sensor. Extracted [1.26]

Figure 1.5 shows the vehicle conducting a patrol using the sensor system. The turret mounted source can be directed anywhere in its field of view and performs a raster scan pattern. Building up a profile of absorption, along with images from the camera and range data from a laser rangefinder, the operator receives data as shown on the RHS of the diagram. This is an interesting system with respect to the work in this thesis but as yet their Raman amplifier and resulting performance data are not yet in place and no attempt appears to have been made at producing high power or suppressing SBS. The imaging technique used in their system could be applied to the system in this work if required.

1.10.3 Mid-IR (DFG) Portable Methane Imager

A commercially available mid-IR imaging system that produces its mid-IR signal through DFG is described and a schematic of their system is shown below in Figure 1.6. The 1064nm source is a diode pumped Yb-doped fibre amplifier seeded by a small Nd:YAG laser, which improved the compactness of the system considerably compared with the cooled high power Nd:YAG laser used in a van mounted system [1.6]. Alternate pulses of on and off-line are transmitted so that the background is taken with each measurement. The 30GHz tuning is conducted by tuning the DFB. They have attempted to optimise the ratio between background IR radiation and backscattered signal by physically scanning the direction of their signal using a raster

scanner across the backscatter target. They have designed their imaging system such that each scan reading illuminates one single pixel at a time on a 256 element linear array, as viewed by their collection optics.

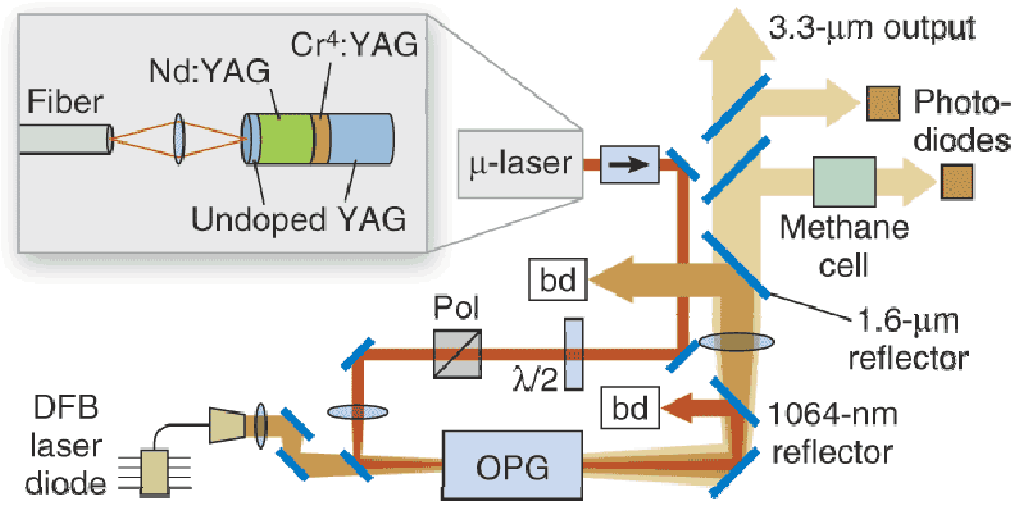

Figure 1.6 DFG system for 3.3μm sensing signal. Extracted [1.27]

The sweep scan of the CCD array is conducted synchronously with the illumination sweep and hence the only current from the array arising from background is coming from one element of the array, upon which all of the collected backscatter is also incident and only during the short pulse gate. The detector was able to detect leaks of a rate 2-40g/hr depending upon the wind speed. The image of a methane cloud is shown in Figure 1.7. On the left-hand image the return power was shown as a function of spatial co-ordinates (displayed as low return power/high absorption - white), which allowed an absorption-space image to be formed. The one on the RHS is a normalisation of the first using an off-line, unabsorbed signal for the absorbed signal to be subtracted from. This leaves an image which only contains gas absorption information as a function of spatial co-ordinates.

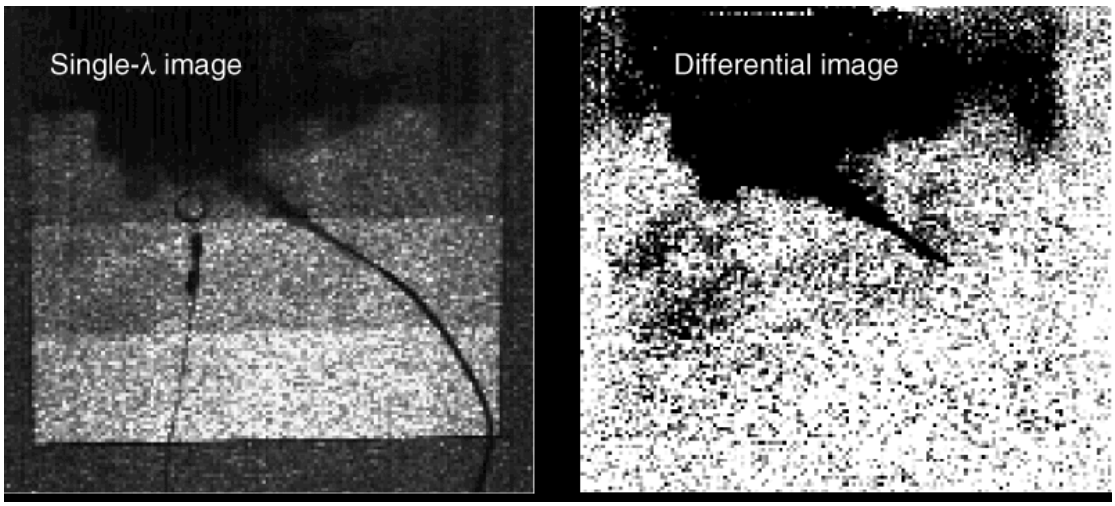

Figure 1.7 Output images from Sandia Methane imager showing a methane cloud. Extracted [1.27]

The unit has been packaged in a man portable casing and consumes 150W electrical power in total with an output mid-IR idler of 400mW (7μJ pulses of the order of ns) thus can be powered using a portable battery, albeit with a relatively short operation time. They have not quoted a range for their system, but judging by the quality of the images and the resolution required to 'see' a gas leak, together with photographs of the system in operation, it appears that the system is designed for use over around 10-20m.

1.10.4 Hand-Held Near-IR Imaging System

Using a similar system to that of Iseki's point sensor, Miles Padgett et al produced another commercial system and performed end-user trials [1.28]. This was another near-IR TDLS system. It was found from these trials that the performance of the optical methane sensor was similar to that of an FID at a range of around 5m, achieving 10ppm.m as a point sensor. Several demonstrator units were distributed to end-users. A schematic of their system is shown below in Figure 1.8. However, the main and eventual goal of the unit by Miles Padgett was to produce an imager, recognising the need to help inspectors actually locate leaks, which can be difficult with a single beam pointer. A scanner is installed into the head, which then makes a scanning grid and produces a 2-D transect of the methane cloud, as shown in Figure 1.9, similar to the concept in the SRI system

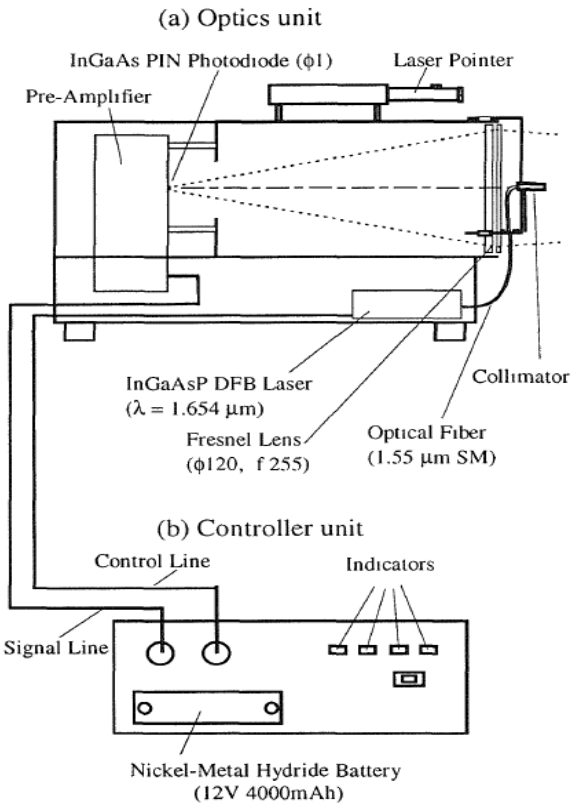

Figure 1.8 Schematic of Miles Padgett et al system. Extracted[1.29]

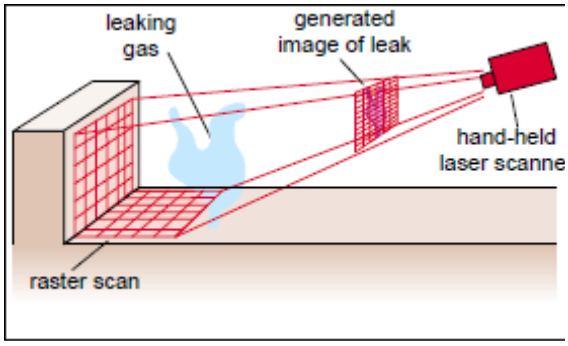

Figure 1.9 Schematic of proposed raster scan pattern for improved cloud imaging by Miles Padgett et al. Extracted [1.29]

This concludes the discussion of methane leak imagers, and the review turns once more to a remote laser pointer style design.

1.10.5 Long Range Near-IR Methane Sensor

A high altitude methane leak sensor has been designed by Physical Science Inc [1.30], wherein a system was made that could operate in two modes, one for 100m and another for high altitude around 1000m. It centred around one transceiver unit, which comprised a Galilean telescope as the send optics and 25cm (effective diameter) parabolic mirror and a standard 1.5mm^2 InGaAs detector upon which the light is concentrated using a lens. When detecting in the 100m regime, they used a standard 20mW 1651nm DFB as their source and in the high altitude regime they chose a specialist L-band EDFA amplified 1618nm source.

The reasons for choosing the 1618nm absorption line of methane were two-fold. Firstly, the much lower line strength of the 1618nm (~1% line strength of 1651nm) line allowed methane sensing over 1km without saturating the sensor with background. In addition to this, it allowed the use of an L-band EDFA developed by Keopsys. Given the wavelength of the power EDFA, this would be a very costly device. At high altitude, the sensor was able to detect 5000ppm.m leaks, making a single scan per second. With more relevance to the >100m system described within this thesis, the DFB, along with the same transceiver was able to detect 10ppm.m traces of methane at 30m. It is not known what their target backscatter surface is, but considering the results achieved by other remote sensors cited here, it is likely that it may be somewhat optimal. So far as the literature search concluded however, there were no journal publications pertaining to these achieved ranges, though being a commercial system developed by a company that would be expected to protect its IP, a full disclosure of results may not be available, but an internal paper was found. [1.30]. The results were taken with stationary scenery, and it is expected that the performance will fall with speed.

1.10.6 Other Uses of Remote TDLS and Summary

The potential for use of remote TDLS systems are too numerous to include an exhaustive list, but it is not a difficult exercise to envisage or find several high profile examples of uses aside from detection of hydrocarbons and other species for industrial environmental monitoring. Other examples include the measurements of

concentrations of greenhouse and pollutant gases, as environmental issues become increasingly significant. Generally measurements are made at high altitude from an aircraft, but rather than backscatter from the surface, a high power source, which is usually pulsed, is launched through the air and the Raman or Rayleigh backscatter from the gas is measured (depending upon the technique used to identify the species.) Raman backscatter can be used to identify gases from their Raman spectra, or the Rayleigh backscatter can be processed using absorption spectroscopy techniques. This type of system is known as a LIDAR (Light detection and ranging.) Other applications of long-range near-IR sensing target gases include CO_2 sensing as a means of finding evidence of respiration to assist in directing rescue efforts in a variety of circumstances or security purposes.

With the large number of potential applications for near-IR TDLS, it is desirable to design a system that is as flexible as possible. The amplifier systems described in this thesis is well placed in this respect, with a broad gain band. With respect to gain bands signals in the range 1610-1700nm can potentially be amplified to around 1.5-2W using the Raman amplifier. Signals in the range of 1530-1570nm can be amplified to around 8W using a C-band power EDFA without the Raman amplifier stage. It is conceivable that with appropriate switching, a user may be able to change the output of the power amplifier to a broad range of wavelengths, producing a multi-Watt WMS source to target one of many, or even several in a cycle, absorption lines of interest. The only additional hardware required to achieve this are different spectroscopic sources (DFB or VCSELs at the apposite wavelength.) If a broadly tuneable WMS signal source could be added to the system, it would make the source alone a valuable spectroscopic tool.

1.11 Aims and Objectives

1.11.1 Overall Aims

The overall aim of the project was to design a long-range (>100m), open path, single ended methane leak sensor system with a 100ppm.m sensitivity (above background).

The detection would take place by the collection of the WMS signal backscattered from arbitrary scenery. Sufficient backscattered signal power for the required methane sensitivity would be provided by the design and inclusion of a high power (>1W) 1651nm CW fibre Raman amplifier system for the amplification of the WMS signal.

1.11.2 Statement of Objectives

Having identified the need for a feasible long-range, low cost, light-weight, energy efficient open path optical sensor for efficient large area monitoring and the techniques and hardware to be used, it remains to break the task of its design and construction down into its constituents. A reasonable programme would entail the following

1) Consideration of backscattered power. In order to make an informed construction of a long-range sensor, a study of backscatter from common surfaces should be made. This should enable an estimate for the required output power of the amplifier system to be developed, since the sensitivity of WMS techniques based on the power at the receiver is well characterised. In order to do this, there are two preliminary stages
    a. The formulation of a theoretical diffuse backscatter model, assuming a collimated beam at the output and a hemispherical beam radiating from a diffuse reflector. This model can extrapolate long range performance given data from short range methane detector systems. From literature a typical ratio of collected backscattered signal compared to the output was quoted in a long-range helicopter-borne spectroscopic sensor review paper as 10^{-6} for a 25cm diameter collector at a typical helicopter altitude of around 150m [1.14]. Also, reflectivities of common surfaces can be sourced in a review.
    b. Measurements of backscattered power from a range of common surfaces using sensor send/receive optics to compare with the model to test the overall system performance in the context of systems already developed in terms of anticipated sensitivity as a function of range and output power.

2) Design, testing and optimisation of a high power 1650nm WMS source, using an amplified DFB. The amplification is carried out by the EDFA-pumped Raman amplifier. Within this objective, there are numerous major sub-objectives.
    a. Formulation of theoretical amplifier models for various gain fibres to guide the design and construction of Raman amplifiers
    b. Construction and characterisation of prototype Raman amplifiers using different gain media.
    c. Stimulated Brillouin Scattering is expected to produce strong back reflections if not properly addressed. It must be suppressed in the pump wave and the signal before full-power tests can be carried out. SBS suppression techniques should be reviewed, modelled and tested as appropriate.
    d. Minimising cost of unit. Wherever possible, the system should be made with cost in mind at all stages
3) Integration of the amplified source into a remote sensor system, with appropriate receiver
4) Testing in lab and in field at concentration levels from background to achieve 100ppm.m sensitivity at 1-200m range, to match the sensitivity of point sensors.

1.12 References

[1.1] Akifumi Takahashi, Youkichi Urano, Kazuaki Tokuhashi, "The global distribution of methane in the troposphere," Journal of Loss Prevention in the Process Industries, Volume 11, Issue 5, pgs 353-360, (1998)

[1.2] L.P Steele, P.J. Fraser, R.A. Rasumussen, "The global distribution of Methane in the Troposhere" Vol 5 Issue 2, p125-171, (1987)

[1.3] B. Culshaw a, G. Stewart a, F. Dong a, C. Tandy b, D. Moodie, "Fibre optic techniques for remote spectroscopic methane detection from concept to system realization" Sensors and Actuators B 51 (1998) 25–37

[1.4] D.J Morgan, "Construction and Operation of a Simple Flame ionisation Detector for gas Chromatography," Journal of Scientific Instruments, Vol 38, No 12, pg 501, (1961)

[1.5] Ben van Well, Stuart Murray, Jane Hodgkinson, Russ Pride, Rainer Strzoda, Graham Gibson and Miles Padgett "An open-path, hand-held laser system for the detection of methane gas" J. Opt. A: Pure Appl. Opt. **7** (2005) S420–S424

[1.6] C. Moore, "Gas-laser frequency selection by molecular absorption," Appl. Opt. 4, 252-253 (1965)

[1.7] W. B. Grant, "He-Ne and CW CO2 laser long-path systems for gas detection," Appl. Opt. 25, 709-719 (1986)

[1.8] K. Uehara, "Alternate intensity modulation of a dualwavelength He-Ne laser for differential absorption measurements" Appl. Phys. B 38, 37-40 (1985)

[1.9] Rudiger Paschotta, "Encycolpedia of Laser Physics and Technology," pg 128, Vol 1, Published by Wiley and Sons in October 2008 ISBN10 3527408282, also available free online http://www.rp-photonics.com/distributed_feedback_lasers.html

[1.10] Kiyoji Uehara and Hideo Tai, "Remote detection of methane with a 1.66-μm diode laser," Appl. Opt. 31, 809-814 (1992)

[1.11] R. S. Eng, A. W. Mantz, and T. R. Todd, "Improved sensitivity of tunable-diode-laser open-path trace gas monitoring systems "Appl. Opt. 18, 3438(1979).

[1.12] Takaya Iseki, Hideo Tai and Kiyoshi Kimura "A portable remote methane sensor using a tunable diode laser" Meas. Sci. Technol. 11 594–602 (2000)

[1.13] Roland Winston, Juan C. Miñano, W. T. Welford, "Non-Imaging Optics" Elsevier Academic Press (2005)

[1.14] A.G. Berezin , S.V. Malyugin, A.I. Nadezhdinskii, D.Yu. Namestnikov, Ya.Ya. Ponurovskii, S.G. Rudov, D.B. Stavrovskii, Yu.P. Shapovalov, I.E. Vyazov, V.Ya. Zaslavskii "Remote helicopter-borne detector for searching of methane leaks" (Review) Spectrochimica Acta Part A 66 803–806 (2007)

[1.15] Rudiger Paschotta, "Encycolpedia of Laser Physics and Technology," pg 478-483, vol 1 Published by Wiley and Sons in October 2008 ISBN10 3527408282, also available free online www.rp-photonics.com/optical_parametric_oscillators.html

[1.16] Rudiger Paschotta, "Encycolpedia of Laser Physics and Technology," pg 722 Published by Wiley and Sons in October 2008 ISBN10 3527408282, also available free online www.rp-photonics.com/sum_and_difference_frequency_generation.html

[1.17] Je´rome Faist, Federico Capasso, Deborah L. Sivco, Albert L. Hutchinson, Sung-Nee, G. Chu, and Alfred Y. Cho. "Short wavelength 3.4 μm. quantum cascade laser based on strained compensated InGaAs/AlInAs" Applied Physics Letters Vol. 72, Number 6 pg 680-682. (Feb 1998)

[1.18] Jake Bromage, "Raman Amplification for Fiber Communications Systems" Journal of Lightwave Technology Vol. 22, NO. 1, pgs 79-93 (January 2004)

[1.19] Mohammed N Islam, Chapter 1, vol 1, "Raman amplifiers for Telecoms" Springer, (2004)

[1.20] Govind P. Agrawal Chapter 8, "Non-linear Fibre Optics" Academic Press, Harcourt, Brace Jovanovich, Publishers (1989)

[1.21] A. L. Chakraborty, K. Ruxton, W. Johnstone, M. Lengden and K. Duffin, ″Elimination of residual amplitude modulation in tunable diode laser wavelength modulation spectroscopy using an optical fiber delay line″, Optics Express, Vol. 17, No. 12, pp9602-9607, (June 2009)

[1.22] J.R.P. Bain, G. Stewart, K. Duffin, M. Lengden, K. Ruxton and W. Johnstone, "Recovery of absolute gas absorption lineshapes using TDLS at arbitrary modulation indices", International Conference on Field Laser Applications in Industry and Research, Grainau, Germany, (6-11 September 2009)

[1.23] R.J. Mears, L. Reekie, I.M. Jauncey and D. N. Payne: "Low-noise Erbium-doped fibre amplifier at 1.54pm", Electron. Lett., 23, pp.1026-1028, (1987)

[1.24] http://www.rp-photonics.com/erbium_doped_fiber_amplifiers.html

[1.25] P. C. Becker, N. A. Olsson, Jay R. Simpson "Erbium-doped fiber amplifiers: fundamentals and technology" Academic Press (1999)

[1.26] internal report obtained from http://www.sri.com/rd/Remote_Gas_Leak_Sensor.pdf in June 2008.

[1.27] Article from laser Focus World, March 2004 Issue. (Livermore, CA) Obtained from link:

www.laserfocusworld.com/display_article/201624/12/none/none/Feat/Portable-laser-based-imager-offers-efficient-hydrocarbon-detection in June 2009, System designed by Sandia National Laboratories

[1.28] Ben van Well, StuartMurray, Jane Hodgkinson, Russ Pride, Rainer Strzoda, GrahamGibson and Miles Padgett, "An open-path, hand-held laser system for the detection of methane gas" J. Opt. A: Pure Appl. Opt. 7, S420 S424 (2005) doi:10.1088/1464-4258/7/6/025

[1.29] Russ Pride, Miles Padgett, Rainer Strzoda, Stuart Murray, Sven-Ake "Implementation of Optical Technologies for Portable Gas Leak Detection" internal project report. (2004)

[1.30] Richard T. Wainner, Mickey B. Frish, B. David Green, Matthew C. Laderer, Mark G. Allen, and Joseph R. Morency "High Altitude Aerial Natural Gas Leak Detection System, Program Final Report"
Covering the Period October 2004 through December 2006. Printed April 2007

Chapter 2 Theory

2.1 Introduction

Having set the objectives in Chapter 1, a more in-depth treatment of the underlying principles and techniques employed to design the system is presented. This chapter gives an introduction to the relevant description of TDLS using WMS. The models of the amplifier system, pertaining both to the behaviour of SBS and SRS and their parameters are discussed, and these models will then be validated in the experimental investigations, which can be found in Chapter 4.

In order to establish the output power requirements of the Raman amplifier, it is necessary to consider diffuse backscatter of light from common, rough surfaces that might be found in industrial areas. This should allow a connection between output signal power and the detection limits at a given range to be made, based upon the expected received backscatter power. This backscatter intensity model was constructed in Excel, enabling the user to adjust parameters and predict the performance of the system, or to establish the design requirements to achieve a given performance. Data from similar experiments are cited to support the theory and to validate extrapolations made for modelling the performance ceiling of the system.

The main focus of the this chapter is concerned with Raman scattering as applied to the design of a practical, low cost, reliable, high-power Raman amplifier. Several practical

considerations in Raman amplifier design, particularly with respect to the selection of the optimal gain medium, only become significant in the specific case of high-power, high-gain, narrow signal bandwidth, continuous wave (CW) systems. These considerations are described from the point of view of designing a practical, commercial Raman amplifier system. Having discussed Raman gain media, a description of the computer modelling used to guide the building of the Raman amplifier is included. With the theory and practical considerations laid out for the construction of an optimised Raman amplifier, the theory governing SBS is then introduced quantifying the effect that can ruin the performance of the system. Methods of mitigating its effects are described.

2.2 Spectroscopic Gas Sensing

2.2.1 Background of Near-IR Optical Spectroscopy

The system is a remote methane sensor system, using Tuneable Diode Laser Spectroscopy (TDLS) to detect traces of methane close to the ground, or some surface. The system needs to have a high sensitivity to serve as an effective tool for environmental monitoring, as background methane and 100ppm.m increments thereupon should be detectable. This has led to the selection of TDLS with WMS as the detection technique and the principles behind these and an explanation of how they are used to fill this role are included.

The principle of spectroscopic sensing is that a given molecule has a unique set of quantized rotational and vibrational energy states, and if a photon with energy matching a transition between two compatible states is incident on the molecule it may be absorbed, using the photon energy to excite the molecule to a higher energy state. These quantized transitions give rise to a set of distinct absorption lines (or absorption spectrum), each with an associated absorption cross-section. A laser beam, whose frequency matches one of these absorption lines, will experience absorption upon transmission through a gas cloud, proportional to the number of molecules the beam has

come into contact with and the absorption cross section of the gas line. Hence the transmitted intensity can be related to the incident intensity through the Lambert-Beer law $I = I_0 e^{-\alpha N l}$. I is the transmitted radiation intensity exiting a gas cloud, I_0 is the intensity incident on the gas cloud, l is the length of the absorption path, N is the molar concentration of the gas and α is the absorption coefficient, which is a parameter attributed to a given gas cloud representing the amount of radiation absorbed per metre through it and is governed by the wavelength dependent absorption cross-section of the molecules in the gas.

Using the relationships above and the knowledge of absorption peaks arising from the energy transitions, α can be plotted as a function of wavelength. Plots for various gases can be recovered from a number of databases. A near-IR sample of transmission data is taken from a database showing the transmission of radiation through a 1m gas cloud with a 22 degree Celsius ambient temperature with a 1% molar concentration in air (10000ppm.m), as shown in Figure 2.1-2.3, starting with the standard C-band EDFA window in Figure 2.1.

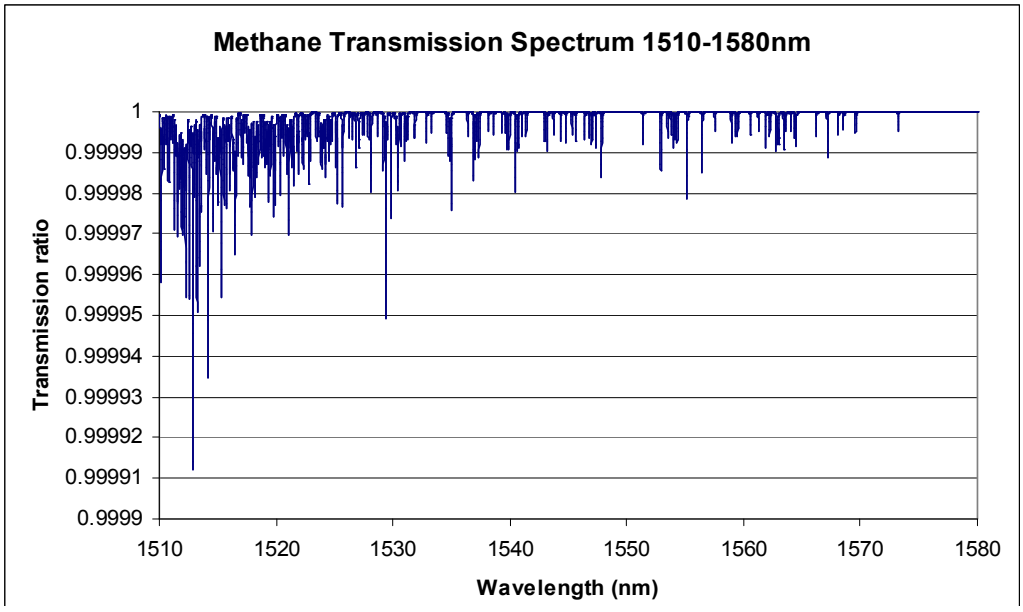

Figure 2.1 Methane transmission spectrum in the standard EDFA amplification window. Resolution 0.00875nm (70nm over 8000 points)

As can be deduced from the methane absorption spectrum in the EDFA amplification band, there are no strong absorption lines within this window. This helps vindicate the choice to design a new amplifier suited to a more effective absorption wavelength rather than exploiting present amplifier technology.

Figure 2.2 shows the methane transmission spectrum in the L-band and beyond. It is here that the first of the strong methane near-IR overtone lines are found. The position of the first few lines shown in Figure 2.2 are at the very fringe of the L-band communications amplifier component set. As discussed in Chapter 1, acquiring an amplifier in this band is very expensive.

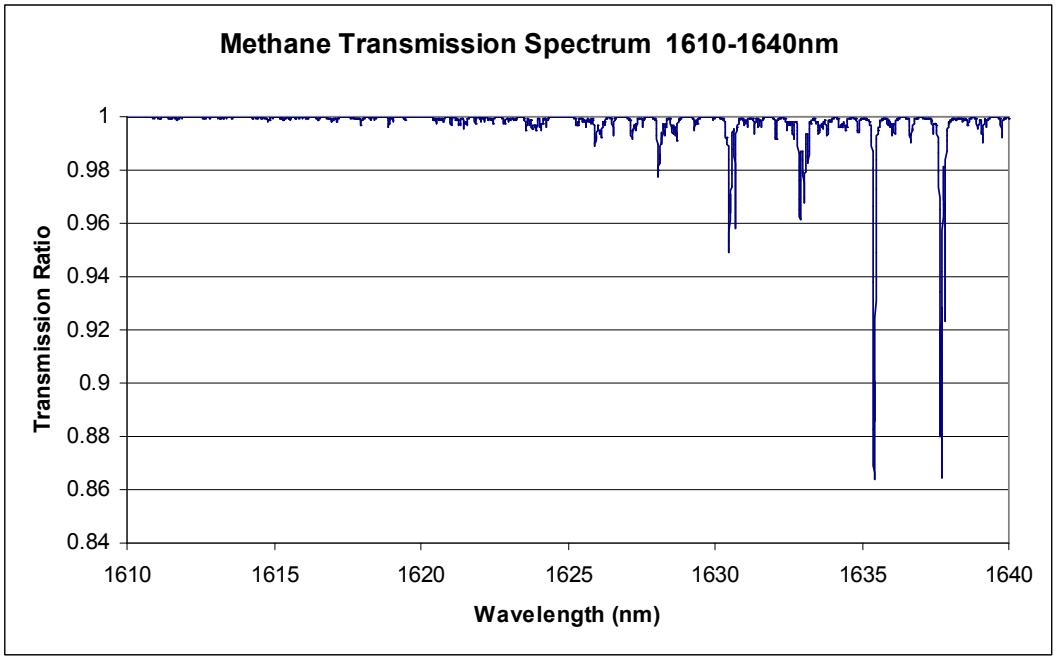

Figure 2.2 1% Methane transmission spectrum in 1610-1640nm. Resolution 0.00375nm (30nm/8000 points)

Figure 2.3 shows the methane transmission spectrum to include the strong near-IR overtone absorption lines of interest. It can be seen that the strongest of these is found at 1650.95nm, but there are other lines that would suffice. Current L-band

communications amplifiers do not address this band, hence to make use of these absorption lines, a new amplifier is required.

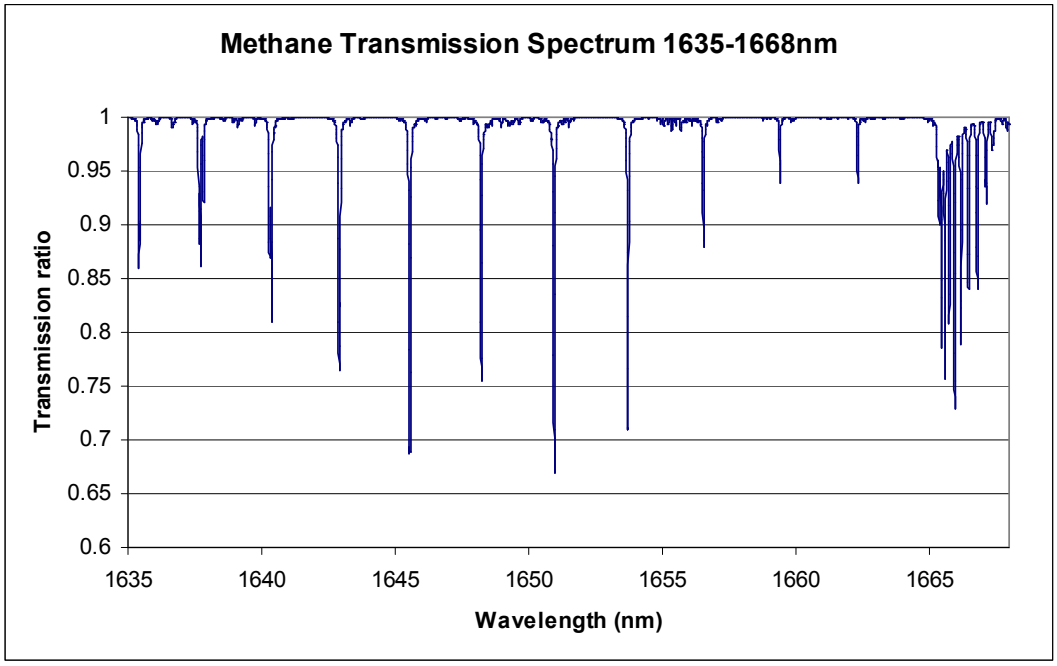

Figure 2.3. 1% Methane transmission spectrum between 1635-1668nm. Resolution 0.004125 (33nm/8000 points)

Given that methane is clearly identifiable by an absorption spectrum, together with knowledge of the location of strong absorption lines, it follows that its presence can be detected by the same principle. In the case of a spectroscopic detector, the transmission of light tuned to an absorption line of the target gas is monitored after traversing an inspection path. A decrease in received optical power at a detector can be used to indicate the presence of the gas.

2.2.2 Tuneable Diode Laser Spectroscopy

In the following section, TDLS with WMS is described as a technique both to ensure that methane is responsible for the optical power decrease and also to achieve high sensitivity measurements is discussed. For simplicity, TDLS is initially described in the context of a point sensor system. In TDLS, the laser's output is wavelength scanned

across an absorption line at low repetition frequency (typically 5Hz) to obtain the gas lineshape, which provides data on the pressure since higher pressure induces further collisional broadening to the gas line, changing its absorption profile. The technique of sweeping the probe laser over the absorption line provides self-referencing, since the wavelength transit over the absorption line provides a zero-reference (while the sweep is off-line) that should allow distinction between gas absorption and any other cause of transmission decrease. This is because gas absorption is wavelength dependent, and the presence of the target gas would cause a change in received power over the scan, whereas other artefacts in the path of the beam do not. The differential absorption over the scan is typically measured using a communications style InGaAs photoreceiver.

Sweeping the laser output wavelength also makes it simpler to find the gas line and its peak absorption, negating the need for very accurate temperature tuning. Figure 2.4 illustrates the first (wavelength scan) stage in the TDLS detection technique. In fact, this is technically all that is required to detect the presence of a particular gas. This slow wavelength scan leads to an advantage that the system has over simple, non-tuneable optical sensors. A gas sensor system without any wavelength scan or modulation would be unreliable as a decrease in received optical power could be caused by source degradation (i.e. diminishing output power), debris or insects entering the test path, as well as absorption by the target gas [2.1].

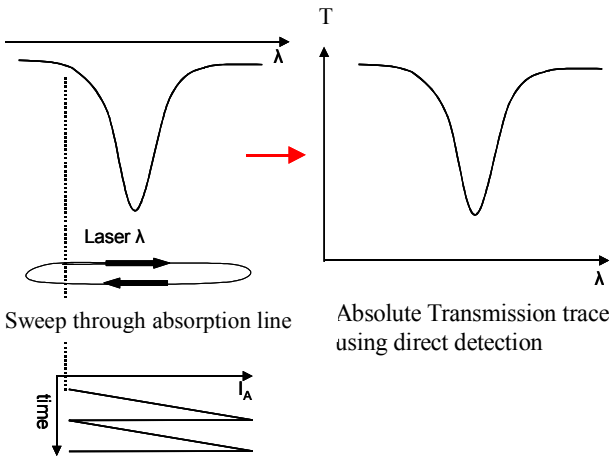

Figure 2.4. Direct Detection TDLS technique with 5Hz gas line scan

As can be seen in the schematic of the direct scan and signal recovery technique, shown in Figure 2.4, the wavelength is ramped slowly over the gas line tracing out its shape before returning quickly to the start of the cycle once more. This direct method of detection with its intrinsic self-referencing and supplementary data collection such as pressure and gas concentration make sensor systems using this type of TDLS highly reliable, low maintenance and yet simple, which when used in a network of sensors is easily integrated with environmental control systems [2.1].

Direct TDLS has the advantage over other TDLS techniques of being relatively simple to implement and requiring little signal processing or equipment for gas detection. However the direct method is not practical in all situations because of the relative insensitivity of making DC measurements. Now considering the case of remote, trace, spectroscopic methane detection, SNR is an important issue, since it is expected that signals backscattered to the sensor from an arbitrary granular surface are small (~200 nW) because of the distances involved (>100m) and the potentially poor reflectors and directionality of the beam (typically ~20% total reflected power backscattered in all directions - refer to section 2.2). It is anticipated that background power incident on the detector could easily exceed this, particularly in real, outdoor conditions. In addition it is required that the sensor system is capable of detecting small traces of methane (340ppm.m based upon background 1.7ppm methane over a round trip path length of 200m), which would result in a relatively insignificant proportion of the carrier power actually contributing to the gas signal (refer to Figure 2.3), assuming the relatively strong 1650.95nm overtone absorption line is used. Hence, using the direct method as described before would involve detecting a small change in a small signal, which would involve the use of specialised sources, detectors and controllers [2.2].

To enhance the SNR of the sensor system and hence the sensitivity of standard equipment to that required in the case of remote trace methane detection, WMS is applied, as introduced in Chapter 1. The starting point is the same with a 5Hz scan

across the absorption line, but a higher frequency sinusoidal wavelength modulation is superimposed upon it as shown in Figure 2.5 a) and b).

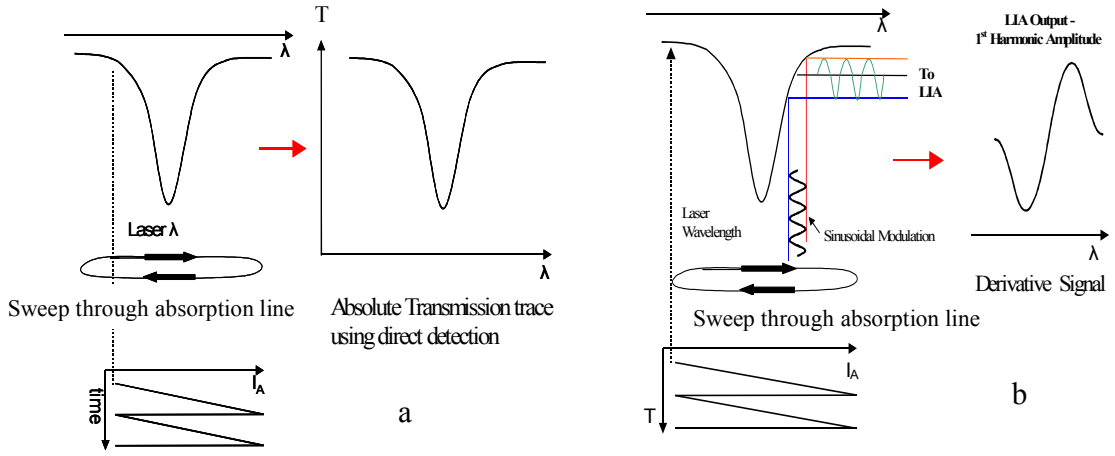

Figure 2.5. Modulation schemes and resultant signals for a) direct and b) WMS TDLS techniques

The techniques of (a) direct and (b) wavelength modulated TDLS are illustrated in Figure 2.5 for comparison, where transmission and lock-in amplifier (LIA) signals are plotted as a function of wavelength in a) and b) respectively. TDLS using the WMS technique retains the slow sweep as in a) to capture shape of the gas line but also has a smaller sinusoidal dither applied to it at a higher frequency as can be seen in b). If the target gas is present, the sinusoidal wavelength dither of the incident signal interacts with the gas absorption line, resulting in a corresponding amplitude-modulated gas signal, the magnitude of which is proportional to the gradient of the gas absorption line at the part being scanned by the probe signal, as shown in Figure 2.5b. The frequency of the amplitude modulated signal matches the dither frequency [2.1].

The reason for applying the wavelength dither is that it allows AC detection to be carried out using a lock-in amplifier (LIA) to rectify the signal. The benefits of conducting AC detection as opposed to DC are two-fold. Firstly, if the system's noise spectrum is taken

into consideration, detection can be carried out at a frequency point on the noise spectrum where noise is low. 1/f noise, a quantum electro-dynamical phenomenon arising from the laser source, is a strong source of noise at low frequencies, but falls off sharply with increasing frequency. The second benefit is that the LIA acts as an electrical band-pass filter, removing noise outside of its pass band from the signal before the amplification stage.

In order to minimise 1/f noise, the detection (and hence dither) frequency is typically set somewhere in excess of 10^4Hz. A LIA locks to an AC signal of given frequency and phase determined by a reference signal, which is fed into the LIA. An appropriate phase shift can be applied to the input reference signal to obtain the appropriate detection phase by the user, so that a gas signal from the photoreceiver and the phase shifted reference can be synchronised, allowing the signal to be passed and amplified by the LIA. Having removed much of the noise spectrum, the LIA amplifies the electrical AC signal and rectifies it as a DC signal. The DC signal is proportional to the size of the amplitude modulation arising from gas absorption, whose maximum (over a ramp sweep) depends upon the integrated path concentration (this is the integral of the gas cloud concentration with respect to path length) and signal power falling on the receiver.

In the case of first harmonic detection, the frequency selected is that of the wavelength dither frequency, (NB the dither frequency is the modulation rate, not to be confused with the dither depth) or in the case of second harmonic detection, double the wavelength dither frequency [2.1]. Considering how the factors mentioned could affect the design of the remote sensor system, the LIA detection bandwidth is an important parameter. Naturally it is desirable to have a narrow LIA bandwidth as this will exclude more noise, effectively forming a narrower bandwidth band-pass filter, however this requires a longer time constant, which in turn reduces the number of data points that can be taken per unit time. This data rate limitation consequently imposes a trade-off between the detection speed of the sensor system and the sensitivity, which is particularly important in the case of the sensor system being mounted on a fast moving

vehicle, such as a helicopter, since it demands a compromise between airspeed and density of inspection measurements for a required sensitivity. As an illustrative example, a helicopter may be flying at around $50ms^{-1}$ to carry out a pipeline inspection. In order that a reasonable inspection density is taken, say at 1m intervals, the absolute minimum ramp sweep frequency is 50Hz. Within this ramp, ideally there should be a large number of data points, but taking a minimum reasonable number of 10 points per ramp, we then require a time constant between measurements of 2ms. Using the relationship relating detection bandwidth to time constant $BW = 1/4\tau$, where τ is the time constant and BW is bandwidth; this restricts the sensor system's band pass to a minimum of 125Hz. This example assumes that there is no averaging of the signal from the LIA. Although this is a considerable improvement over the case of no filtering, it still represents a two order of magnitude increase in white noise pass compared with detector systems using the same technique, but unbound by the detection speed requirement [2.2]. A basic, but instructive LIA tutorial can be found on the Bentham website [2.3].

As mentioned in Chapter 1, the current dither used to apply the wavelength modulation also causes amplitude modulation in the output of the signal laser at the same frequency. On initial consideration, this may seem to be an inconvenience, since it is an amplitude modulation of the same frequency that the sensor system relies upon for the detection of methane and in many ways it can be. However, this AC signal can be used to normalise the gas signal's dependence upon received power out of the relationship. This is possible because, as mentioned the LIA is phase sensitive and the FM and AM effects on the laser from the current dither are phase separated. Hence, it follows that the amplitude modulation arising from the interaction of an absorption line and the frequency dither, and the amplitude modulation resulting purely from the current dither are separable when using phase-sensitive detection. The gas absorption signal magnitude can be normalised to the magnitude of the RAM, so that the gas signal level is dependent only upon the integrated path concentration of the gas and not the received power. This is necessary because the backscattered power is variable in the case of a

moving, remote sensor system because of the changing backscatter level from different surfaces. In the general case however, the FM and AM components are not in quadrature, which means that the net, maximised AM resulting from FM-methane line interaction will contain some component of the RAM. In addition, the RAM will change slightly over the wavelength sweep with the presence of methane along the inspection path since the beam is partly absorbed. The current-induced AM component encroaching onto the 1f gas signal results in a raised, non-zero baseline, which restricts the maximum gain that can be applied by the LIA to the gas signal before saturation and hence this places a limit on sensitivity. A method for reducing this to increase system detection sensitivity will be outlined in Chapter 6.

2.2.3 Theoretical Treatment of Individual Components of WMS Signal and their Origin

Given that the absorption of a gas line is dependent upon the wavelength of the probe beam (i.e. the position on the absorption line being probed), and that the amplitude of the probe signal is dependent upon the laser diode current, which is varied to change the wavelength, a mathematical description is formed to express the relationship between the intensity modulations resulting from the gas line and from the laser. This can be found in previous work [2.4]. The equation linking the incident intensity of a laser upon a gas cloud and the emergent laser power is the Lambert Beer law once again. This can be simplified in the relevant case of small absorptions as shown in Eqn 2.1

$$I = I_0(1 - \alpha_{(\upsilon)} N.l)\,. \qquad \textbf{Eqn 2.1}$$

where I is the laser intensity after transit through a gas cloud of length l, concentration N and the frequency (υ) dependent absorption per unit length per unit concentration is α. It should be recalled that the emergent intensity modulation on the laser, after transit through the gas cloud will be a function arising broadly from two actions. The first is the amplitude modulations arising from the current ramp and dither. Given the

properties of non-ideal lasers, the intensity of the laser output will change appreciably over the wavelength ramp, as will the depth of the amplitude dither. With wavelength being a function of diode current, it is reasonable to say that, if the laser parameters are kept constant, the laser output intensity as well as the dither amplitude modulations are functions of output wavelength, albeit indirectly. The second arises from gas absorption, which is directly wavelength dependent. This also requires individual treatment because $\alpha(\upsilon)$ is a function of wavelength. Starting with the current induced amplitude modulation, an argument describing the instantaneous intensity of the amplitude ramped and modulated signal is formulated.

$$I_0 = I(\upsilon) + \Delta I(\upsilon)\cos(\omega t) \qquad \textbf{Eqn 2.2}$$

where ω is the modulation frequency and t is the time for which the modulation has been applied. Together they have the significance of representing the phase angle of the dither. Hence, substituting Eqn 2.2 for the incident laser intensity I_0 in Eqn 2.1, we obtain Eqn 2.3

$$I(\upsilon,\alpha) = \left(I(\upsilon_c) + \Delta I(\upsilon_c)\cos(\omega t)\right)\left(1 - \alpha(\upsilon)Nl\right) \qquad \textbf{Eqn 2.3}$$

where υ_c is the laser output centre wavelength, $\Delta I(\upsilon_c)$ is the wavelength dependent intensity modulation amplitude. This expression now takes account of the wavelength dependent (via current tuning of the laser) output intensity, and intensity modulation depth from the dither, as well as the wavelength dependant gas absorption.

Since the narrow bandwidth output of the laser is scanning and dithering on a gas line, α is a function of frequency through the frequency dependence of effective absorption cross section. Assuming a small dither frequency deviation ($\delta\upsilon$) about the laser's output centre frequency υ_c, the absorption as a function of wavelength with respect to the gas (Voigt) lineshape can be approximated using a Taylor series expansion to the second order with reasonable accuracy [2.1,2.4] as shown in Eqn 2.4

$$\alpha(\upsilon) \approx \alpha(\upsilon_c) + \frac{d\alpha(\upsilon_c)}{d\upsilon}.(\upsilon - \upsilon_c) + \frac{1}{2}.\frac{d^2\alpha(\upsilon_c)}{d\upsilon^2}.(\upsilon - \upsilon_c)^2 \qquad \textbf{Eqn 2.4}$$

This expression for the absorption profile about υ_c is also substituted into Eqn 2.1. The resultant expansion of terms can be found in the referenced work, but the main result of this analysis was that the individual harmonic components of the gas signal can be resolved as terms of the expansion. The first harmonic component as received by a LIA in the 1f detection mode, which is of most significance to this work, is as follows in Eqn 2.5 as an example of a harmonic component of the gas signal. The expansion of the second harmonic can be found in the referenced work [2.4]

$$I_\omega = \Delta I(\upsilon_c).\left(1 - \alpha(\upsilon_c)N.l\right)\cos(\omega t) - I(\upsilon_c).\frac{d\alpha(\upsilon_c)}{d\upsilon}N.l.\delta\upsilon.\cos(\omega t - \psi) \qquad \textbf{Eqn 2.5}$$

The first term of Eqn 2.5 is the RAM from the current dither, taking into account its absorption in the presence of methane. The second term is the intensity modulation resulting from the frequency dither-absorption line interaction; (note the phase shift term). It should be noted that any harmonic component of the gas signal can be selected in theory, however typically either the first is used because it has the largest magnitude and is relatively convenient to recover data from, or the second so that RAM can be largely excluded from the gas signal, allowing higher gas signal amplification by the LIA without saturation when compared to 1f. 2f detection often results in improved sensitivity but to the detriment of recoverable information.

From this analysis, it can be seen that the first harmonic gas signal is proportional to the gradient of the gas absorption line over which the dither takes place as well as the integrated path length absorption. Additionally, there is a component dependent upon the RAM, whose magnitude depends upon the construction of the laser via its current tuning characteristic at the modulation frequency. A high frequency-tuning rate with

respect to current leads to a smaller RAM component for the same wavelength dither and therefore allows the gain of the LIA to be set higher because only the gas signal is being amplified. A relatively low current tuning characteristic (i.e. more current dither is required to attain the requisite wavelength dither) is useful if a RAM reading is required, as the required current modulation to provide the frequency dither is relatively high, which leads to a strong laser output intensity modulation.

For simplicity, the Voigt distribution of the gas line and its derivative have not been included in this treatment, but this does not affect the relevant conclusions that can be made based upon the description above. It can be seen that the gas signal, or a given absorption line, is directly proportional to the integrated path gas concentration and the signal power and this is true of all harmonics. This supports the assertions that

1) Normalisation of received power is required with respect to the backscattered power from the target surface. If the target surface changes, then so too will the amplitude of the gas signal for the same gas cloud as a result of more power falling on the receiver.
2) It is acceptable to use either the RAM or another signal harmonic as a reference, since each harmonic of detection is directly proportional to the signal power, and is proportional to the integrated path concentration because the $I(\upsilon_c)$ term appears across all harmonic components. This means that the ratio between e.g. the first and second harmonics could be used to determine the integrated path concentration (the ratio is only dependent upon gas parameters). The advantage of using RAM for normalisation is that it is the most accurate way to normalise backscatter power out of the signal, while the advantage of using a higher harmonic as a reference is that it still allows removal of RAM from the output signal at its source, while providing acceptable referencing.
3) The system would benefit from equipping with an imaging scheme such as those discussed in Chapter 1, since the integrated path concentration holds no information regarding the proportion of path length and concentration through

the gas cloud i.e. a long cloud of low concentration is indistinguishable from a small cloud of high concentration.

Having considered the key parameters affecting a WMS-based sensing system, the discussion can proceed to the implications of using arbitrary scenery from which to backscatter the signal.

2.3 Backscatter Photometry

2.3.1 Characterisation of Diffuse Backscatter Surfaces

Since the long-range system operates on the basis of capturing a backscattered signal from arbitrary terrain, some consideration of the reflectivity of common surfaces and the nature of the backscattered light is necessary to determine the total power back at the detector, given a fixed launch power. This is important in the modelling of the sensitivity of the system and in determining the power requirements of the Raman amplifier. Most surfaces are diffuse reflectors as a result of their granular surface texture, where the term diffuse describes a surface upon which an incident beam of radiation would have its power scattered over a hemisphere radiating outward from the point of incidence (excluding that which is absorbed at the surface). This is not to be confused with a perfectly Lambertian surface, which scatters all of the power *evenly* over the hemisphere. Indeed such a surface has yet to be realised, and so the term 'Lambertian' refers to an ideal diffuse surface. Some materials are close to ideal, the closest of which is Magnesium Oxide, which can be used as a black or white reference target for comparing the backscatter behaviour of other diffuse surfaces. Some diffuse targets actually scatter incident optical power more obliquely than a Lambertian surface would. It is therefore important to examine the backscattered light over a range of angles so that problem surfaces can be identified as well as gaining an approximation of the level of backscattered power expected [2.5]. It is expected that most surfaces have some specular component of backscatter and therefore detection will be carried out

approximately normal to the target surface, both in terms of the incident signal and the receiver. Some work has previously been carried out on the reflectivity of arbitrary surfaces over a range of incidence angles by other groups for a similar purpose and the method of obtaining these characterisations is outlined and their results presented [2.5]. Using their reflectivity results, calculations can be made linking received signal power and output carrier power from the Raman amplifier source.

The results from their investigation were as follows in Figure 2.6. A laser beam is split equally between a reference detector and incidence upon the face of each of the test targets. The test targets were mounted upon a rotating plinth, through which the effective incident angle and detection angle could be varied (the signal output and the detector were fixed normal to the face of the target along the same optical axis and the target was rotated.) The differential absorption, referred to in Figure 2.6 is used to remove any effect variable laser output power might have on the results. The laser output was split with half of the power directed onto a detector connected to a LIA and the other half being reflected onto the target surface via a small mirror. The differential absorption is the ratio of the backscattered power to the reference power. The reflectance unit per solid angle takes the collector size and range into account to assist with extrapolation to longer range (i.e. a collector of the same size subtends a smaller solid angle from the backscatter surface, hence less backscattered power is received at longer ranges).

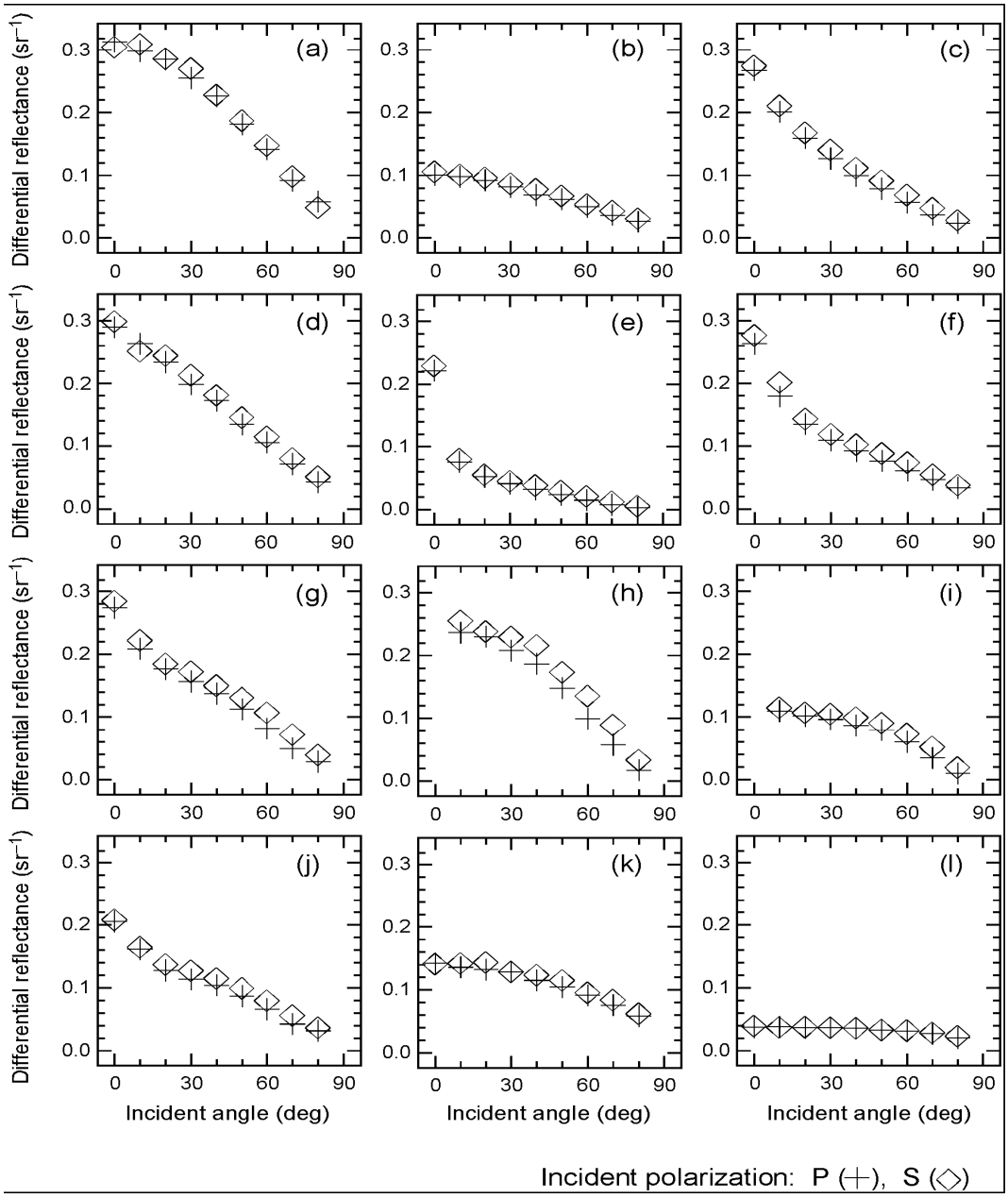

Figure 2.6. Iseki's backscatter results. Differential Reflectance of a range of common materials as a function of angle of incidence Targets key with reference to Figure 2.6: (a) magnesium oxide, (b) sand paper (number 400), (c) cardboard, (d) white wallpaper, (e) black wallpaper, (f) wooden board (Japanese cedar), (g) a frosted white tile, (h) a polished white tile, (i) imitation marble, (j) mortar, (k) concrete and (l) asphalt. Owing to specular reflection, the apparent differential reflectances at normal incidence are too large to be shown in (h) and (i). Extracted [2.5]

Another study was made at the University of Glasgow by Miles Padgett et al [2.6] in which a portable diode-array spectrometer was used to measure the reflection properties of wet and damp soil and tarmac. The measured backscattered proportions are shown in Table 2.1

Material	Angle to normal (θ)		
	15°	45°	75°
Spectralon reference	100 % (by definition)		
Soil (clay type)	36.9 %	50.0 %	131.9 %
Damp soil	*16.4 %*	*18.6 %*	*56.4 %*
New tarmac (3 months old)	6.5 %	6.9 %	18.1 %
Wet new tarmac	*3.4 %*	*2.6 %*	*3.3 %*

Table 2.1. Reflectivity of common surfaces as measured by Miles Padgett. Extracted [2.6].

In addition snow backscatters around 60% of incident light, and would make a very good surface around which to attempt long range gas sensing. Most surfaces tested backscatter between 10-30% of incident light compared to the Spectralon (MgO) control for between 0-30 degrees incidence angle, but potential 'problem surfaces' include concrete, tarmac, particularly when wet and imitation marble. Although it is extremely unlikely that (imitation) marble will be a real target surface, it is instructive when considered along with the wet tarmac result, as it suggests that poor backscatter will be collected from materials with a dark colour and perhaps a glossy surface [2.6]. The poor backscatter performance of tarmac could be because of its light absorbing nature associated with its dark colour. The difference between new and mature tarmac could be either the wet tarmac scatters light with a relatively large reflective component compared to the diffuse part (thus perhaps missing the detector), or that new tarmac is darker and more absorbing than mature tarmac, which may have a layer of lighter coloured dust on top. The fact that wet tarmac performs increasingly poorly compared to three-month-old tarmac with increasing angle tends to indicate that the issue is that wet tarmac is more specular, which could be an issue when using the sensor system in

real outdoor conditions (e.g. wet). It should be noted that the measured reflectivity of clay soil above 100% suggests that it scatters radiation more obliquely than the 99% Lambertian MgO surface, most likely a result of its extremely granular surface.

2.3.2 Modelling of Backscattered Power with Range

For the purposes of calculating the required launch power to carry out TDLS, the common 10-30% reflectance from an average surface is taken (let us say 20%) and ~150nW is required at the detector to match the sensitivity of the hand held system over 100m, the required launch power can be calculated from an approximation based upon the radar equation, with the exception that the outgoing radiation front is small compared to the size of the target (i.e. the case of a collimated beam incident on the ground/the target surface is greater than the spot from the signal laser and that the entire collection optic is illuminated by backscatter).

$$P = \frac{P_0 R d^2}{4L^2} Sin\theta \qquad \textbf{Eqn 2.6}$$

These parameters are arranged on Figure 2.7 for clarity.

Referring to Eqn 2.6 and Figure 2.7, P is the backscattered signal power at the detector, P_0 is the power incident on the backscatter surface. R is the surface reflectivity at the backscatter target surface, d is the aperture width of the receiver, or any collector used to collect the backscatter, L is the range between the target surface and the receiver, and θ is the angle between the normal from the receiver to the target surface, to take into account that if the target surface and detector are not parallel, the detector aperture appears to be smaller to incoming light.

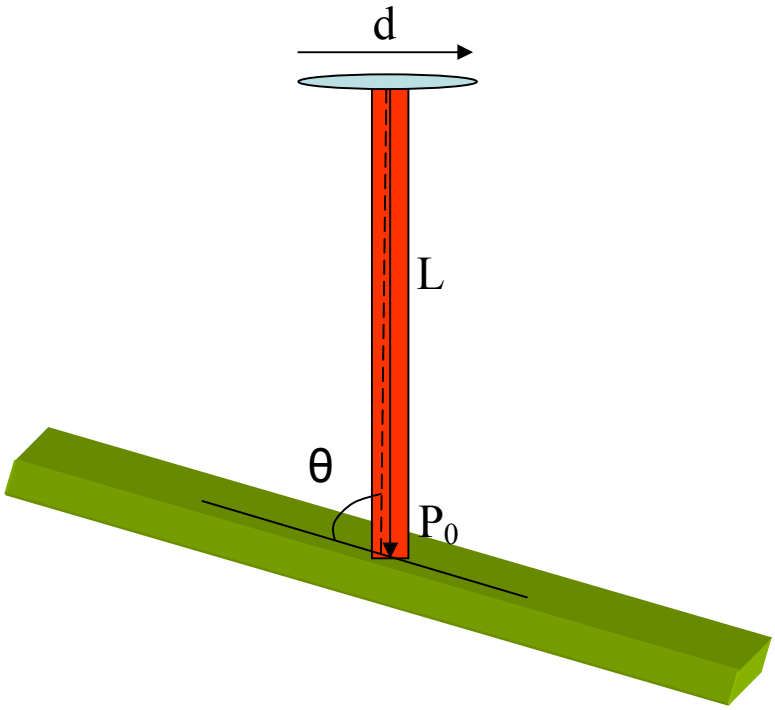

Figure 2.7 Schematic of backscatter model parameters

With reference to Figure 2.6 and using some typical data in Eqn 2.6 an expected output power requirement can be determined. Setting required received power to be around 150nW on the detector and distance from the ground to the receiver L = 100 m, receiver aperture diameter D = 0.30m and the backscatter ratio R = 15% at normal incidence (i.e θ, the angle of the surface to the incident radiation = 90 degrees) it is expected that around 1W output power would be required to match these parameters. This will be verified in Chapter 5 by detecting methane samples while using the minimum possible launch power. These results will be used to extrapolate a required signal power for matching performance at 100m using an inverse square relationship between range and required launch power to maintain a given received backscatter power at the receiver.

In further support of the 1W power requirement, recall that the Miles Padgett system achieved a 10m range using around 10mW of optical launch power [2.6]. Hence, if Eqn 2.6 holds up to 100m, this suggests that a 1W signal would be required to scale the range

of the 10m system up to 100m with the same methane sensitivity. A simple Excel model was constructed, which allows launch power, reflectivity, receiver aperture, target attitude relative to the line of sight of the receiver (θ in Figure 2.7) and attenuation (including that from the collection lens) to be input and the range to be varied with a slider. The model returns received power as a function of all of these parameters. Alternatively "goal seek" (a feature on MS Excel) can be used to fix a required receive power while varying one another parameter. For example maximum range could be found given a fixed output power, or so could a required output power given a fixed range.

2.4 Optical Fibre

2.4.1 Background, Basic Theory and Parameters

Optical fibres are central to the project and progress in fibre amplifiers has provided the means of building the remote sensor system. Some treatment of the theory of optical fibres is included in this section to form a foundation for the study of optical fibres as Raman gain media. Many of the parameters referred to in terms of the SRS theory are introduced here. Optical fibres are constructed from glass and guide light through the principle of total internal reflection as the method of confinement. Fibre optics became a field of study in the 1950's, but manufacturing techniques producing fibres with characteristics recognisable in terms of those made today began in 1970, with fibre losses of 20dB/km available (c.f. 1000dB/km from early fibres) and by the late 1980s, 0.2dB/km was achieved, where losses are dominated by the fundamental Rayleigh scattering[2.7]. There are specialised glasses available that exhibit a lower Rayleigh scattering level at 0.05dB/km, but the figure of 0.2dB/km is typical of standard communications fibres manufactured today [2.7]. With the rapid improvement of optical fibres together with the progress in laser technology, optical fibres became important in the study of Non-Linear Optics, since optical fibre is a convenient way to

confine an electromagnetic wave within a small cross section, allowing high intensities as well as allowing relative ease of mixing waves over long interaction lengths. Some of the basic principles of fibre optics will be addressed in this section, followed by a treatment of the origins of non-linear effects in optical fibres before discussing stimulated Raman and Brillouin scattering as relevant to the project.

Figure 2.8 shows the index profile of a simple step-index fibre. The higher core index causes light to be totally internally reflected at the interface and hence propagate along the fibre. Indeed there are various profile structures available depending on the application, some following the principle of an abrupt step in the index and some with a gradual transition of refractive index, or graded-index fibres and within these main groups there are a range of variations.

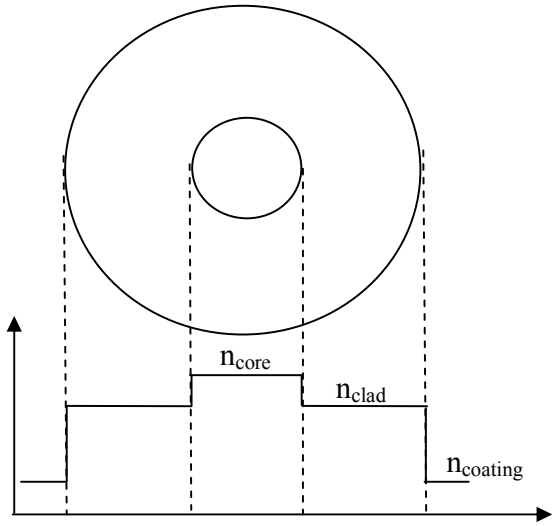

Figure 2.8 Schematic of step-index fibre refractive index profile.

Two important parameters in a fibre's construction are the refractive index difference between core and cladding as well as the core diameter. The refractive index parameters can be put in a more useable form as refractive index contrast as shown in Eqn 2.7

$$\Delta = \frac{n_1 - n_2}{n_1} \qquad \textbf{Eqn 2.7}$$

Where in Eqn 2.7 n_1 and n_2 are the refractive indices of the core and cladding respectively. Eqn 2.7 represents the core-cladding index difference. The refractive index difference is achieved with different dopant levels and types in the cladding and core, although the bulk material is silica glass in both cases. GeO_2 is commonly used in the core to increase the refractive index, although P_2O_5 is also used. Boron and fluorine can be used to lower the refractive index of silica glass and are hence suitable as cladding dopants [2.7]. Another important parameter to describe a fibre is the V number. This is mainly used to determine the mode behaviour of light inside the fibre.

$$V = ka\sqrt{(n_1^2 - n_2^2)} \qquad \textbf{Eqn 2.8}$$

Eqn 2.8 relates the V number to the fibre and wave parameters, where k is the wavenumber, or $\frac{2\pi}{\lambda}$; a is the core radius and square root term is the numerical aperture (NA). The numerical aperture is also defined as the sine of the maximum angle relative to the fibre axis that allows a ray to be guided within the core. The significance of the V number is that its value indicates how many modes the fibre will allow to propagate in the core. If the value is less than 2.405, the fibre supports one single mode and hence setting V equal to 2.405 designates λ as λ_{cutoff}, which represents the wavelength that must be exceeded to maintain single-mode operation in the fibre. This is the standard for communications cabling since it is necessary for the data to follow only one path length, as multiple modes would scramble the arrival of bits at a receiver over a long distance. This criterion is usually achieved by adjusting a, the core radius. In the case of building a Raman amplifier it is important to minimise the mode-field diameter to maximise light intensity, upon which non-linear effects such as inelastic scattering are dependent. Mainly for this reason, only single-mode fibres are used throughout the project [2.7].

2.4.2 Interaction of Light with Optical Fibre Lattice

As an electromagnetic wave, light propagating along a fibre is governed by Maxwell's equations Eqns 2.9-2.12, as is the dielectric medium through which it travels.

$$\nabla \times E = -\frac{\partial B}{\partial t} \qquad \textbf{Eqn 2.9}$$

$$\nabla \times H = J + \frac{\partial D}{\partial t} \qquad \textbf{Eqn 2.10}$$

$$\nabla . D = \rho_f \qquad \textbf{Eqn 2.11}$$

$$\nabla . B = 0 \qquad \textbf{Eqn 2.12}$$

In the particular case of a dielectric medium, such as optical fibre, there are some terms that become zero, in particular Eqn 2.10 no longer requires the **J** term, which represents current density, of which there is none and Eqn 2.11 equates to zero since the free charge density ρ_f is 0. Defining the remaining terms of the Eqns 2.9-2.12, **E** and **H** are the electric and magnetic field vectors, **D** and **B** are the electric and magnetic flux densities respectively, all in SI units. E and H fields are the cause of **D** and **B** flux and hence they are related

$$D = \varepsilon_0 E + P \qquad \textbf{Eqn 2.13}$$

$$B = \mu_0 H + M \qquad \textbf{Eqn 2.14}$$

Where ε_0 and μ_0 are the permittivity and permeability of free space respectively, and **P** and **M** are the induced polarizations arising from the electric and magnetic fields respectively. **M** is zero in non-magnetic materials, such as in the relevant case of an optical fibre. Using the above relations, the wave equation for the propagation of an

electromagnetic wave in a medium can be obtained. Taking the curl of Eqn 2.8 and using Eqns 2.14, 2.9 and 2.13 to replace **B** and **D** with **E** and **P**, the wave equation is obtained as shown in Eqn 2.15. Using $\mu_0\varepsilon_0 = 1/c^2$

$$\nabla^2 \times E = -\frac{1}{c^2}.\frac{\partial^2 E}{\partial t^2} - \mu_0 \frac{\partial^2 P}{dt^2} \qquad \textbf{Eqn 2.15}$$

The response of dielectrics to light is non-linear to intense electric fields, meaning that the propagation medium does not oscillate identically to the driving electromagnetic wave. In effect the polarisation of the charges in the medium cannot match the strong driving field oscillations, which in turn gives rise to some anharmonic motion of the electrons. In terms of Maxwell's equations, the **P** term must represent the sum of linear and non-linear polarisation components, which is significant only in the presence of an intense field. The non-linear components normally observed are of second and third order. Second order non-linearity gives rise to effects such as sum frequency and second harmonic generation arises from asymmetry in the molecules of the medium, and hence this effect is very small in silica fibre, whose molecules are symmetrical. The lowest order non-linearity that silica fibre exhibits significantly are of the third order, which are responsible for four wave mixing and difference frequency generation [2.8].

$$P = \varepsilon_0 \left(\chi^{(1)} E + \chi^{(2)} EE + \chi^{(3)} EEE... \right) \qquad \textbf{Eqn 2.16}$$

In Eqn 2.16, **P** represents the charge polarisation, and $\chi^{(j)}$ the j^{th} order susceptibility. The third order susceptibility is also responsible for inelastic scattering, which is a separate category of phenomena, and is directly related to the Raman gain coefficient. The third order susceptibility results from a combination of electronic and nuclear contributions. A detailed explanation of the underlying principles of SRS in terms of the

non-linear polarisation vector in the dielectric can be found for further reading on a more fundamental level [2.9].

The results of significance from this are that isotropic glass fibres are suitable for inelastic scattering as they exhibit third order non-linearity even though they do not exhibit those of the second, and that fibres with a higher third order susceptibility are more conducive to Raman Scattering. The further reading reference [2.9] also proceeds to analyse the Raman gain coefficient of Germanium and Flourine doped fibres starting from fundamental principles.

2.5 Principle of Raman Scattering

Spontaneous Raman Scattering was named after its discoverer, C.V. Raman [2.10]. The investigations that led to its discovery were inspired by the discovery of the Compton effect through which, X-Ray radiation was emitted as 'Bremsstrahlung' or 'braking radiation' from high energy electrons losing energy through collisions. It was hypothesised that any electromagnetic wave should follow a similar behaviour, losing energy to molecules in its propagation medium while giving rise to a lower energy, scattered photon. Its relatively late discovery and even later exploitation can be explained by the fact that it was difficult to induce and observe the effect without doing so purposefully, since it is a weak phenomenon and thus difficult to instigate without strong, coherent sources [2.11].

Inelastic scattering forms a separate category of third order non-linear effects, which includes Raman and Brillouin Scattering, wherein some of the scattered photon energy is transferred to the propagation medium. The classical wave model is considered qualitatively, as a full mathematical description is quite laborious. When electromagnetic radiation interacts with a molecule within a dielectric, the bound

electrons oscillate with the frequency of the radiation. This dipole oscillation results in re-radiation of the wave at the same frequency, but with a phase shift, whose angle is dependent on the molecule, giving rise to the concept of refractive index in the medium. However, the lattice molecules oscillate at a range of frequencies at room temperature and are capable of a range of stable oscillations, hence the re-radiated light from the dipoles contains the sum or difference terms between the incoming wave and a lattice vibration frequency, giving rise to a frequency-shifted wave. This frequency-shifted wave, arising from inelastic scattering, is known as the Stokes Wave. With respect to Raman scattering, this difference frequency corresponds to the excitation energy of a metastable high (optical) frequency lattice vibration, or optical phonon. In pure silica, this results from the bending of the Si-O-Si bond, whereas in optical fibre it is a combination of the bending motions of Silicon, Germanium and Silicon-Germanium molecules [2.12].

The Raman scattering process can also be considered in terms of Solid State Quantum Mechanics. The pump photon (from the beam being scattered) can excite a short-lived virtual phonon, which decays to a more stable optical phonon energy level, re-radiating most of the energy as a Stokes photon. Phonons are quantized lattice vibrations that can transfer energy to or from the lattice via interaction with photons. The photons involved in the interaction are annihilated and effectively replaced by lower frequency Stokes photons, which in effect results in a separate, frequency shifted beam in the scattering medium. Without stimulation, this occurs approximately 1 in every 10 million scattering events in bulk silica [2.12]. The lattice is heated or cooled when a phonon is created or annihilated respectively through the inelastic photon scattering. The latter case, giving rise to an anti-Stokes wave of a Stokes shift higher frequency than its pump, is orders of magnitude less probable than the converse case of the wave losing energy to the lattice, since the upper phonon energy state is considerably less occupied at room temperature than the lower and will not be considered further [2.12]. Given the weakness of even the relevant Raman Stokes wave generation, the effect must be stimulated to be of practical use.

2.6 Stimulated Raman Scattering and the Raman Amplifier

2.6.1 Principle of Stimulated Raman Scattering in a Raman Amplifier

The principle of Raman amplification is based upon the stimulation of Raman scattering wherein, given enough pump power, the Raman scattered photons stimulate further scattering when they reach a threshold density and the Stokes wave experiences gain. Raman lasers produce SRS in this way; building up enough spontaneously scattered photons from a strong pump, usually in a highly non-linear fibre, so that the stimulation threshold is exceeded. A resonant cavity would be used to maximise the photon density within desired gain band, reflecting the Stokes signal to reduce the lasing threshold, and a pump reflector would be used to increase efficiency, lowering the input pump power required. This is the main difference between a Raman laser and a Raman amplifier. A Raman amplifier does not use a cavity to build up stimulated scattering, but the scattering is instead stimulated by injecting a seed wave into the gain medium, which is the signal to be amplified at the desired Raman Stokes wavelength together with the pump. The seed signal lowers the SRS threshold considerably, since the build-up of spontaneous Raman scattering is not required to initiate the process. Raman scattering stimulated from spontaneously Raman scattered photons is an unwanted effect in the Raman amplifier and constitutes ASE, which depletes the pump and can cause beat noise with the signal as well as broadening of the output signal bandwidth.

The quantum model of Stimulated Raman Scattering is illustrated in Figure 2.9, which demonstrates the propagation of the pump and signal in the fibre, the molecular vibrations giving rise to phonons and the resulting energy transitions.

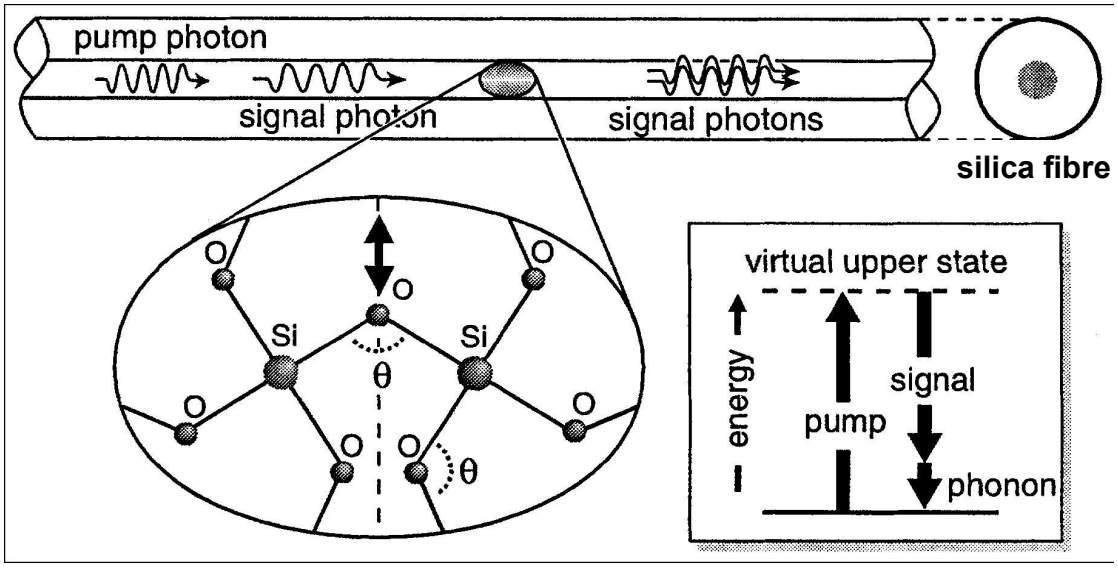

Figure 2.9. Raman Interaction and Energy Level Diagrams. Extracted from source [2.12].

The pump is chosen to be of a single Stokes shift higher frequency than the required signal frequency and a signal beam of sufficient intensity to stimulate the scattering at the peak Raman Stokes shift is launched into the same fibre. The Raman scattered pump photons are then duplicates of the Raman seed signal and in this way the signal is amplified. For standard single-mode communications fibre, the peak Stokes shift is approximately 13.2THz, which is around 110nm when obtaining a ~1650nm signal. A Raman amplifier's gain spectrum depends mainly on the *frequency difference* between pump and signal and not strongly on the absolute wavelength. This is because, as can be seen in Figure 2.9, the pump excites the molecule to a virtual state, which removes the specific transition energy requirement (meaning this can occur for a wide range of wavelengths), and the phonon is excited during the relaxation from this virtual state. The remaining energy not exciting the phonon continues to propagate as a Stokes photon, which is a duplicate of the signal, a Stokes shift lower frequency than the original pump photon.

Stimulated Raman scattering (SRS) and therefore Raman amplifiers are polarisation sensitive, as a Raman scattering event resulting in a polarisation change is considerably

less probable than one that duplicates polarisation. The effective gain coefficient is approximately an order of magnitude lower for orthogonal waves as co-polarised [2.12]. The gain coefficient, as will be discussed later in this chapter, is a fibre parameter that determines the strength of the interaction between pump and Stokes signal in producing SRS. However, the gain coefficient is not dependent upon relative direction between signal and pump waves, since at a given optical phonon frequency there is a large and even spread of k-vectors, meaning that momentum can be conserved regardless of direction. The dispersion relation would allow SRS completely irrespective of direction, but confinement in an optical fibre limits SRS to co or counter-propagation with respect to pump [2.12].

2.6.2 Stimulated Raman Scattering Rate Equations

Having discussed SRS, it is required that some consideration of its quantification takes place. The evolution of the pump and signal waves along the fibre can be described by two coupled differential equations respectively, Eqns 2.17 and 2.18.

$$\frac{dP_S}{dz} = \frac{kg_R}{A_{eff}} P_P P_S - \alpha_S P_S \qquad \textbf{Eqn 2.17}$$

$$\frac{dP_P}{dz} = -\frac{\omega_P}{\omega_S}\frac{kg_R}{A_{eff}} P_P P_S - \alpha_P P_P \qquad \textbf{Eqn 2.18}$$

Eqn 2.17 represents the change in signal power per unit length, where the first term on the RHS represents Raman gain in the z length interval and the second term on the RHS signal attenuation. Eqn 2.18 represents the change in pump power per unit length, where the first term on the RHS represents pump depletion due to SRS and the second term fibre attenuation. Defining the terms of the equations, k represents a factor determined by the polarisation mode overlap of the pump and signal over the length interval z. It is a constant whose value lies between around 0.1-1, depending upon the relative pump and signal states of polarisation [2.9, 2.11, 2.12]. The value of k is

approximately 0.55 when using an unpolarised pump, by taking an average of the orthogonal and parallel interaction strengths. This issue will be discussed in more detail later in Section 2.7.4. P_S and P_P are the signal and pump powers (S and P subscripts denote signal and pump parameters respectively throughout, unless otherwise stated), z the length of the gain medium interval, α is the fibre attenuation per unit length, and g_R is the Raman gain coefficient, which when divided by the effective area becomes the more commonly used parameter 'Raman gain efficiency' with units $(W.km)^{-1}$ and ω is the frequency of the wave (S or P). A_{eff} is the effective mode field of the pump and signal, which may not be the same in general. To take account of this, the mode field overlap integral is used to calculate overlap efficiency, η, whose inverse can be factored directly with area, to form the effective area (A_{eff}) for the pump and signal wave together, as shown in Eqn 2.19. This simply takes account of the fact that the pump and signal only interact in the region in which they overlap. Hence, if ψ is a function representing the radial field distribution (cylindrical symmetry) of the mode and the subscripts have their usual meaning, Eqn 2.19 applies [2.9].

$$A_{eff} = 2\pi \frac{\int \psi_S^2 r dr . \int \psi_P^2 r dr}{\int \psi_S^2 \psi_P^2 r dr} \qquad \textbf{Eqn 2.19}$$

The effect of this is small in the cases relevant to this work, and in a simple model this term could be simplified to being the mode field area of either the pump or the signal, which are similar, being separated by around 13.2THz. This approximation assumes that both the pump and signal waves satisfy the single-mode propagation condition in the fibre. The parameters affecting Raman gain per unit length have been introduced, and Raman threshold is introduced at this point to provide a fuller background to the theory of SRS before the discussion moves to practical aspects of amplifier design.

The SRS threshold is not of great importance to an amplifier system that is being seeded because, as discussed, threshold is considerably reduced while injecting a seed into the

gain fibre. Clearly, the seed used to stimulate the SRS is the WMS signal that requires amplifying. The seeding becomes highly efficient at high powers, where the interaction strength between the pump and signal is strong (see Eqns 2.17 and 2.18). It is predicted that with a pump of several Watts, much of the energy can be scattered from the pump into the 1651nm carrier beam [2.11, 2.13]. It is worth considering the relationship between the parameters governing SRS threshold as well as making a note of the threshold to avoid ASE. The threshold for the stimulation of Raman scattering from build up of spontaneous Raman scattering has the following relationship with the fibre parameters as shown in Eqn 2.20[2.11]

$$P^{th} \approx \frac{16 \times A_{eff}}{k.g_R L_{eff}} \qquad \textbf{Eqn 2.20}$$

Eqn 2.20 shows the relationship between the threshold pump power P^{th} in Watts and the fibre parameters, where g_R and $L_{eff,}$ are Raman gain coefficient and effective gain length respectively.

2.7 Considerations in Raman Amplifier Design

2.7.1 Outline of Considerations

Having introduced Raman scattering and the Raman rate equations, some of the considerations involved in producing a Raman amplifier system using commercial optical fibres are discussed:

1. **The suitability of various Raman gain fibre media.** One of the key parameters determining suitability of a fibre for Raman amplification is the Raman gain efficiency (g_R/A_{eff}). In order to enable consideration of common communications fibres as potential gain media, a method for determining the Raman gain efficiency from standard parameters is included. See Section 2.7.2.

This is necessary because standard communications fibre datasheets often contain no information on Raman gain efficiency or non-linear coefficient. Despite this, standard communications fibres comprise an important part of the sourcing process because in addition to Raman gain efficiency, media must be considered in terms of overall merit. This takes additional factors into account, such as attenuation (dB/km), insertion loss (splice losses etc dB), Rayleigh (dB/km) and splice backscatter (the latter is difficult to quantify, qualitatively this will be higher given a greater difference between core composition of gain fibre and standard fibre in components) and cost. Many non-linear fibres, despite often having high Raman gain efficiencies stated in their datasheets, may have similar or inferior overall merit to standard fibres in terms of the application under consideration.

2. **Co-Pumping VS Counter-Pumping Scheme**: These carry different benefits and characteristics, between which the optimum must be decided. See Section 2.7.3
3. **Polarisation Effects:** Raman gain is strongly polarisation dependent, denoted by the k value in the Raman gain rate equations. This can have up to a 10dB influence on the effective Raman gain coefficient and the output power is exponentially dependent upon this. The effect that this is likely to have on the system is calculated, and it needs to be determined whether polarisation dependence can be used to maximise gain, or whether it needs to be mitigated where possible. See Section 2.7.4
4. **Modelling the Amplifier:** A suitable model is chosen to build a theoretical picture of various Raman amplifier designs to assist with an optimal build. See Section 2.8

2.7.2 Approximation of Raman Gain Efficiency for Selection of Raman Gain Media

The rate equations of the Raman amplifier have been introduced and these are central to developing a Raman amplifier, however the origin of the gain coefficient should be

considered in order that appropriate fibre gain media can be selected. Eqn 2.21 is the relationship between parameters governing the Raman gain coefficient [2.14].

$$g_R(\nu) = \frac{\sigma_0(\nu)\lambda_P^3}{c^2 h n^2(\nu)} \qquad \textbf{Eqn 2.21}$$

Where $\sigma_0(\nu)$ is the 0˚K (extrapolated) Raman cross-section, λ_P is the Pump wavelength and h, n and c have their usual meanings. It should be noted that for pump waves of wavelength 1300-1550nm, the dependence of Raman gain upon absolute pump wavelength is very weak in comparison to wavelength difference between pump and signal as a result of negligible electronic resistance in this wavelength region [2.15]. The absolute wavelength dependence is hence largely ignored in applications around these wavelengths, and shall be in the case of this work henceforth. In addition, most data used to characterise the gain media is at 1550nm, giving approximately the correct result in the case of the project without absolute wavelength scaling in any case. The main variable of interest to determine Raman gain is the net Raman scattering cross-section of the fibre core material. This is dependent upon the Raman scattering cross-sections σ of the glass itself as well as the cross-sections and concentration of dopants found therein.

The 0˚K Raman cross-section, can be calculated from using the measurable Raman cross-section of the glass at temperature T. the Raman cross-section varies with temperature as shown in Eqn 2.22 [2.14].

$$\sigma_T(\nu) = \frac{\sigma_0(\nu)}{N(\Delta\nu, T) + 1} \qquad \textbf{Eqn 2.22}$$

where the population factor N is deduced using Eqn 2.22.

$$N(\Delta\nu, T) = \frac{1}{e^{\left(\frac{h\Delta\nu}{kT} - 1\right)}} \qquad \textbf{Eqn 2.23}$$

Esentially Eqn 2.22 and Eqn 2.23 convey that the Raman cross-section (for Stokes emission) decreases with temperature, as the population of upper phonon states begins to populate. As the Undoped bulk silica is inefficient at Raman scattering, as it has a low Raman cross-section. However, as introduced in the section on optical fibres (Section 2.4), the core of a fibre is doped in order to induce the requisite refractive index change between core and cladding, primarily for controlling beam confinement. This is helpful with respect to Raman amplifier construction since Germanium GeO_2, which is commonly used to raise the index of the core of many communications fibres, has a Raman scattering cross-section that is approximately an order of magnitude higher than that of silica [2.6]. Additionally, increased germanium doping tends to favour narrower beam confinement, which in turn gives rise to higher intensities and thus efficiency for non-linear effects such as Raman scattering. A diagram of the Raman spectra of high purity bulk samples of the glass formers in optical fibres is shown Figure 2.10 as part of a study to determine optimal fibre formulation for gain media for Raman lasers. It shows the strength of Stokes waves for a series of glass formers as a function of wavenumber given a constant pump power at 19436cm^{-1}.

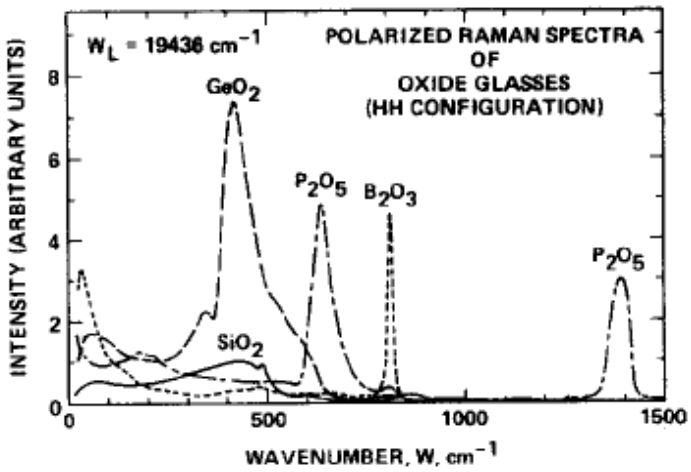

Figure 2.10 Raman Scattering Spectra for glass forming substances and dopants. Extracted [2.16]

Given knowledge of relative Raman cross-sections of common dopants and glasses, it is possible to model the expected Raman gain of Germanium doped fibres. Most companies providing optical fibre will be able to provide data on Raman gain coefficients and profiles for their products, so an exhaustive study of Raman gain with respect to dopant concentration was not carried out. However, a relationship between peak Raman gain coefficient and Germanium doping is cited from other work, which included a study of modelling Raman gain from fibre parameters, which can be utilised in providing a preliminary model of how a particular fibre should perform. This, together with consideration of the other parameters in the rate equation, Eqn 2.17, can be used to gain some intuition regarding which types of fibres could be used as Raman amplification media. Eqn 2.24 has shown reasonable agreement with experimental investigation[2.14]

$$g_{Rpeak} = \frac{n_2^2}{2n_1^2\lambda_{SPeak}}\left[1.046 + 0.0833 \times x_{GeO_2}\right] \times 10^{-13} \qquad \textbf{Eqn 2.24}$$

Where g_{Rpeak} is the peak Raman gain of the fibre, n_1 and n_2 are the core and cladding refractive indices respectively, λ_{Speak} is the wavelength of the Stokes wave at the Raman peak in microns and x_{GeO2} is the % molar Germanium concentration. It may be even more difficult to obtain the actual germanium concentration of the optical fibre without having to make a special request once more for detailed information. The Sellmeir equation relates the refractive index step of a fibre to the germanium concentration in the core and wavelength and Sellmeir equation coefficients are available in several catalogues for various optical glasses with given germanium dopings. From this, data can be obtained linking refractive index step to germanium doping concentration. A sample of this data had been collected previously from one such source for this purpose [2.14] and this data has been used to plot an approximation of the dependence of refractive index on Germanium doping. This should make it easier to perform a review of possible fibres, since the core refractive index should be available on data sheets of standard fibres not originally intended as gain media. Five data points were plotted

using the Sellmeir equation for silica with a range of germanium concentrations, and a function generated from a line fit on MS Excel as shown in Figure 2.11.

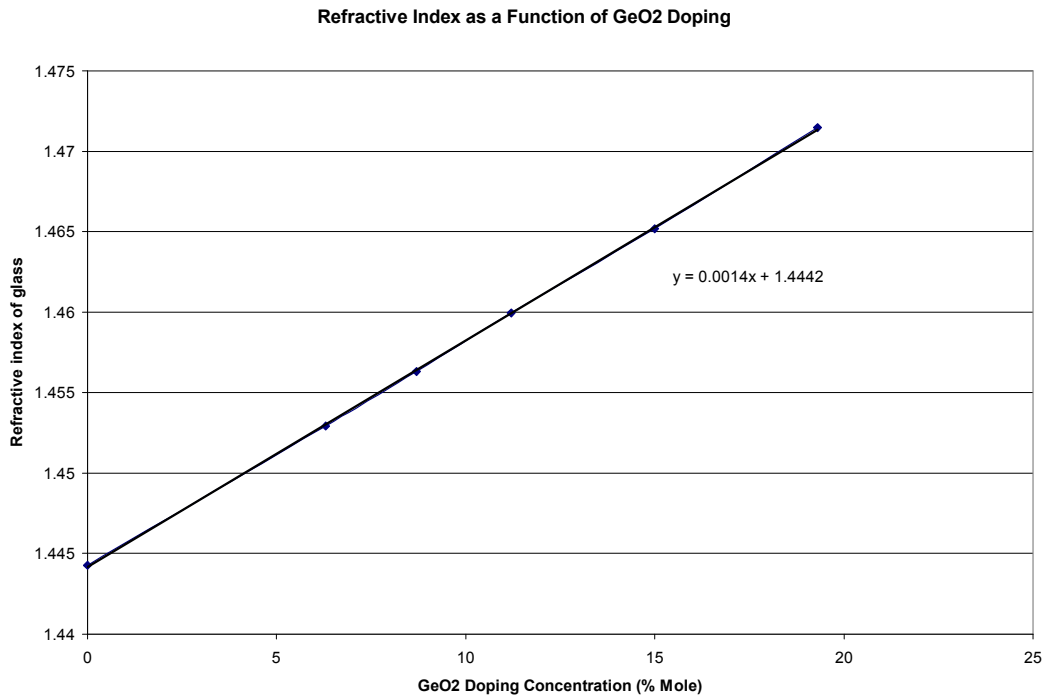

Figure 2.11 Refractive index of silica fibre as a function of Germanium concentration.

Figure 2.11 shows the linear dependence of the refractive index of silica glass upon germanium doping concentration, yielding the Eqn 2.25

$$x_{GeO_2} \approx \frac{n_1 - 1.4442}{0.0014} \qquad \textbf{Eqn 2.25}$$

Together with Eqn 2.25, Eqn 2.24 should allow an approximation of the peak Raman gain of standard step index fibres such as DSF, DCF and standard SMF-28 style fibres. Given those relationships it becomes a matter of substitution to extend this approximation to numerical aperture, or the commonly provided cut-off wavelength, as provided in the Section 2.4. Once the refractive index step is known in a step-index

germano-silicate fibre, whether through knowledge of the cut-off wavelength or NA, the germanium concentration can be approximated and the approximate Raman gain found. Other work of interest found a relationship between the Raman gain and the chromatic dispersion, however in this case, the usefulness is limited as the non-linear coefficient is also required to obtain an absolute value, and this is not necessarily easier to obtain than the Raman gain coefficient [2.17]. A third investigation explored the same problem for step index fibres, using refractive index difference Δ as the input parameter [2.18]. They found a relationship, again through empirical means as follows

For GeO_2 doped core fibres Eqn 2.26 applies

$$g_R(\times 10^{-14} m/W) = 2.75 + 2.16|\Delta| \qquad \textbf{Eqn 2.26}$$

And also for fibres with a Fluorine doped cladding Eqn 2.26 is used

$$g_R(\times 10^{-14} m/W) = 2.75 - 0.32|\Delta| \qquad \textbf{Eqn 2.27}$$

2.7.3 Pumping Configurations in Raman Amplifiers

Raman amplifiers can have several pumping configurations that affect the gain dynamics, as well as signal quality and overall achievable output power. These configurations are co-pumping and counter-pumping corresponding to the relative direction of propagation of pump and signal through the gain medium. It is also possible to employ a combination of the two and each configuration has their relative strengths, although bi-directional pumping was not investigated because of the increased complexity of additional high power isolation, and hence system insertion loss required in implementing it safely. Co-pumping is the most intuitive design and produces the greatest gain over a short total gain medium length. A short length is desirable as this minimises backscatter and cost. The shorter required length results from the fact that the gain is proportional to the product of the pump and signal power, so when the signal is small, there is a large pump available to provide some gain. The greatest gain is found

in the mid section of the gain fibre, where the signal is significant but the pump has not been strongly depleted. However, there are disadvantages to co-pumping, the most notable of which is the high pump to signal noise transfer due to the fast nature of the SRS process. In addition, the profile of the signal power evolution with respect to displacement along the fibre means that the signal power is large over a significant proportion of the fibre by experiencing strong gain in the early to mid stages of the fibre. Although this scheme may allow the use of a shorter fibre, it may make some unwanted non-linear effects, such as SBS more difficult to suppress.

Counter-pumping is a commonly used scheme in communications because of the low pump to signal noise transfer. The noise transfer is reduced since the pump fluctuations are averaged over the length of the fibre. This can be easily understood if the signal is considered to be propagating in the presence of a pump that experiences a sudden change in amplitude. In the case of co-pumping, one part of signal (co-propagating with the fluctuation) experiences a different pump power over most of the gain length and will hence experience a different overall gain and a different output power. In the context of many fluctuations, this results in an amplitude varying/noisy signal given a noisy pump. In the case of a counter-pumped amplifier, any signal will experience gain from the entire pump beam launched during the signal's transit time through the fibre and will, in effect experience an averaged pump amplitude. In co-pumped amplifiers, this averaging can be partly achieved by chromatic dispersion in longer fibres, but this is more relevant to the case of distributed amplifiers in communications networks [2.11]. In addition, the counter-pumped signal is much less likely to suffer from ASE, as the factor of 16 in Eqn 2.20 for co-pumped SRS threshold is replaced by a factor of 21 in the case of counter-pumped SRS, and is usually not observed. ASE should be avoided if possible, but should it be initiated it is likely that its onset in the forward direction (relative to the pump) will make it less likely to initiate in the backward direction because of the added pump depletion and hence ASE should not generally propagate with the signal in a counter-pumped system [2.11]

Counter-pumped Raman amplifier systems, despite generally needing a longer overall length of gain fibre, tend to produce a very high proportion of their gain towards the end of the fibre (with respect to the signal) compared with co-pumped systems. This is because the relatively small inserted signal, at the signal injection/residual pump exit side of the fibre, interacts with the depleted pump and hence the pump-signal power product and consequently the gain is small (see eqn 2.17). Towards the end of the fibre, where the pump is launched, the signal will have become significant because of the long path over which it has been experiencing small, incremental gain, where it then interacts with a strong, undepleted pump. Therefore in a relatively short section of fibre, a strong pump interacts with a strong signal and produces high gain. This is very useful in helping to suppress Stimulated Brillouin Scattering (SBS) in particular, by potentially producing a large signal over a short section of gain fibre. Like SRS, SBS threshold is inversely proportional to length as will be discussed in Section 2.9. Using counter-pumping to shorten the length over which the signal is large has been demonstrated as the sole method of suppressing SBS in a high power Raman amplifier, where a CW, counter-pumped system was employed with a very small seed signal (<1mW) in the presence of a very strong pump (~40W) [2.19]. This is not practical in the case of the system here, since a much higher efficiency is required (c.f referenced work efficiency of <10%) and 40W is more difficult to obtain at 1540nm than 1120nm. In addition, because of the high gain, the referenced system would be very sensitive to any back-reflection from splices and hence the care, techniques and equipment used in the assembly of this amplifier would be critical.

2.7.4 Polarisation Effects in a Raman Amplifier

As outlined, the SRS interaction between orthogonal pump and signal waves in a Raman amplifier is approximately an order of magnitude weaker than co-polarised waves. Consequently, some consideration needs to be made regarding the various methods that could be employed to address this. In the case of two co-propagating linearly polarised waves of different frequency, their relative state of polarisation (SOP) is not maintained.

Given that the optical fibre is wound onto a spool, causing birefringence, and that fibres investigated are not polarisation maintaining (PM), it can be expected that a wave will not maintain its original SOP. Also, two waves separated by 100nm will not maintain their relative SOP for more than a few metres (depending upon the fibre). It can therefore be concluded that the factor k in the gain equation cannot simply be determined by launching a co-polarised pump and signal to achieve k = 1, nor will orthogonally polarised waves perform as poorly as though k=0.1. In both cases, and all intermediate relative launch polarisations, k is a value somewhere between the two extreme cases for all but very short or PM fibres. Studies on the issue have been undertaken [2.20].in order to quantify how sensitive a FRA is to polarisation effects, given polarisation mode dispersion (PMD) parameter of the gain fibre, and good results have been achieved. If two linearly polarised waves, a pump and signal of frequency ω, co-propagate, the polarisation coherence length l_c is given by Eqn 2.28[2.20]

$$l_c = \frac{4}{(\omega_P - \omega_S)^2 D_P^2} \qquad \textbf{Eqn 2.28}$$

D_P is the PMD of the gain fibre, which is often available from fibre datasheets, but is also found from $D_P = \sqrt{\langle \Delta\tau^2 \rangle / L}$ where $\langle \Delta\tau^2 \rangle$ is the differential group delay, which can be measured and L is the length if the fibre. Assuming the length of the Raman gain fibre to be long with respect to the coherence length, they found Eqn 2.29 holds for a co-pumped Raman amplifier system[2.20]

$$\frac{\Delta g}{g} = \sqrt{l_c / l} \qquad \textbf{Eqn 2.29}$$

Where Δg is the difference in Raman gain efficiency between the optimal and worst case polarisation matching and g is the Raman gain efficiency of the fibre. As an example, considering an SMF-28 style fibre with PMD of 0.05 and assuming pump and signal

waves are separated by a peak Raman Stokes shift of 13.2THz, the coherence length is approximately 9.2m, which in a 2km fibre results in a 7% range of effective Raman gain coefficient values available from the full range of relative pump and signal SOP. Given that the overall Raman gain is an exponential function dependent upon the Raman gain coefficient, a 7% reduction in g_R could make a significant difference in signal power. In the counter-pumped configuration, the polarisation dependent gain is found to be negligible for fibres with a PMD greater than 0.001ps.km$^{-1/2}$, which is a very low value for standard fibres and so polarisation is effectively removed from the design while counter-pumping is employed. A full vector treatment of polarisation dependent gain (PDG) in a Raman amplifier was published and can be read for a more in-depth analysis on this subject [2.21].

The two main results of this vector analysis were the elimination of PDG by choosing counter-pumped systems, while using a fibre with PMD >0.001ps.km$^{1/2}$ and also that the effect of PDG, should it arise, is linearly proportional to the degree of polarisation DOP of the Raman pump, assuming a linearly polarised signal, which is a point for consideration for pump design in a co-pumped amplifier.

With regard to building a Raman amplifier system, it must therefore be considered whether PDG will have any significant effect on the system and whether to utilise PDG to maximise the signal gain, or to use an unpolarised pump to eliminate any PDG in the system. Eliminating the PDG implies that polarisation control becomes unnecessary, which simplifies the system and reduces insertion losses and the need for system re-optimisation over time. In addition, it is likely that vibrations and shifts in temperature would give rise to shifts in the relative SOP between pump and signal, leading ultimately to signal power fluctuations and hence noise [2.12]. This might necessitate real time monitoring and polarisation optimisation or alternatively environmental control and special packaging of the fibre system, leading to increased complexity and reduced reliability. Finally, given that polarisation dependent gain is a factor of fifty less significant in counter-pumping systems, attempting to maximise Raman gain efficiency

through polarisation control means either, using a polarisation maintaining (PM) fibre, which is expensive, difficult to splice and of similar gain coefficient to SMF-28 (effectively double because of improved k), in a counter-pumped configuration; or necessarily using a co-pumped configuration. Given these factors, neutralising PDG as much as possible (i.e. unpolarised pump and counter-pumped configuration) should lead to the most robust system and avoid many operational problems. The result of this, however is that Raman gain efficiency is sacrificed, and that any effective Raman gain coefficient of fibres used will be around 55% of that achievable (taking the average of orthogonal and parallel k polarisation factors.)

2.8 Modelling of Optical Fibres as Raman Gain Media

2.8.1 Raman Amplifier Modelling by Iteration of the Raman Rate Equations

Given that the Raman gain coefficient can be obtained, the next stage of the theoretical development is to model the performance of the Raman amplifier. Firstly, a consideration of the type of model is required. The Raman system is high power and high gain, hence any model attempting to predict its performance must include a pump depletion term, unlike many communications model where the signal always remains small compared with the pump. This demands an iterative method of approximating the coupled differential rate equations. Using a simple iterative method to calculate the Stokes and pump power in small intervals (where the gain and pump depletion over the interval is small) provides acceptable accuracy, considering that there would be more significant uncertainty in actual power levels entering the gain medium in a real test system (and indeed exiting the gain medium to get to a detector). Matlab was used to calculate the Raman gain in one metre intervals over which the signal gain could be considered to be small increments and pump depletion was neglected until the following interval as shown in Eqns 2.30 and 2.31

$$P_{S(n+1)} = P_{S(n)} + k_{PS} g_R P_{P(n)} P_{S(n)} - \alpha_S P_{S(n)} \qquad \textbf{Eqn 2.30}$$

$$P_{P(n+1)} = P_{P(n)} - \frac{\omega_P}{\omega_S} k_{PS} g_R P_{P(n)} P_{S(n)} - \alpha_P P_{P(n)} \qquad \textbf{Eqn 2.31}$$

Where P_S and P_p are the pump and signal powers entering a length interval, k is the polarisation factor, which is a value less or equal to one depending on the degree of co-polarisation between pump and signal waves as discussed previously. In the case of designing the system, it was assumed that over the fibre lengths in use, and with no effort made to maintain polarisation, that this factor could be treated as 0.55, particularly since it seems desirable to use an unpolarised pump source. The gain coefficient and attenuation, as defined previously have length units of m rather than km, to match the 1m length intervals used in modelling.

2.8.2 Modelling Raman Signal Power as a Function of Interaction Length in OFS Raman Fibre

Using appropriate starting parameters, the evolution of the pump and signal power can be predicted as a function of displacement along the fibre. This can be used as a tool to find an optimal fibre length for the chosen fibre gain medium. If the fibre is too short, this will limit the output power available and the conversion efficiency, too long and it increases the effect of backscatter and undesirable non-linear effects as described in detail later in this chapter (Section 2.6). This implies that an informed compromise must be made. The modelling process was conducted initially for a specialist Raman fibre, supplied by OFS optics. The parameters, as provided by OFS are as follows in Table 2.2.

Parameter (Units)	**Parameter Value**
Effective Area @ 1550nm (μm)	18.7
Attenuation @1550nm (dB/km)	0.32
Raman Gain Coefficient $(W.km)^{-1}$	2.5
PMD $(ps/km^{-0.5})$	0.12

Table 2.2 Parameters for OFS Raman Fibre

A trace of the Raman gain coefficient was also included in the spec sheet for the fibre as shown in Figure 2.12. This is a useful resource for determining the usefulness of pump sources of known bandwidth, and although this spectrum is particular to OFS Raman fibre, the gain spectrum shape is indicative for most germano-silicate fibres, even though the peak Raman gain is unusually high.

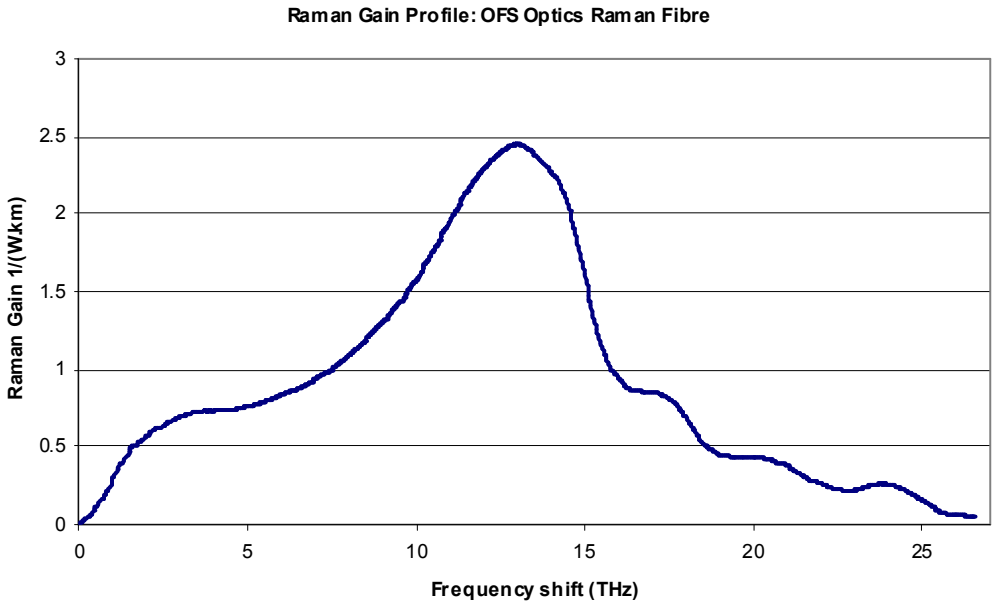

Figure 2.12 The actual Raman gain spectrum for the OFS Raman Fibre (Raman Gain as a function of Frequency Shift between pump and Stokes waves.)

The parameters used in the Matlab program for modelling OFS Raman fibre were as follows in Table 2.3. For the output power, the losses were considered to be around 1dB for both the pump and the signal. The expected, effective Raman gain for the system is 1.4

g_{eff} $(W.km)^{-1}$ Assuming k=0.55	1.4
Length of Fibre (km)	2.2
A15 & A16 Attenuation (@1550 and 1650nm in dB)	0.3, 0.33
Insertion loss (dB)	1
$Is_{(1)}$ Inserted Signal Power (mW)	4
$Ip_{(1)}$ Inserted Pump Power (W)	4

Table 2.3 Parameters used for modelling OFS Raman fibre

If the insertion losses are set to a feasible value such as 1dB on the input side (the system should be approximately symmetrical). The evolution of signal power is shown for illustration of the theoretical technique of finding an optimal length and for demonstration of how the gain behaves in a co-pumped Raman amplifier in Figure 2.13, which illustrates the point regarding signal evolution in a co-pumped amplifier, where most of the gain takes place in the mid-section of the fibre. There are low gain sections at the beginning where the signal is small and towards the end of the fibre where the pump is small through depletion. It is the distance at which the gain per unit length becomes small towards the end of the fibre that will be considered the optimal gain length. From Figure 2.13, this is in the region of 1.4km. It is also useful to look at the gain per unit length directly as shown in Figure 2.14.

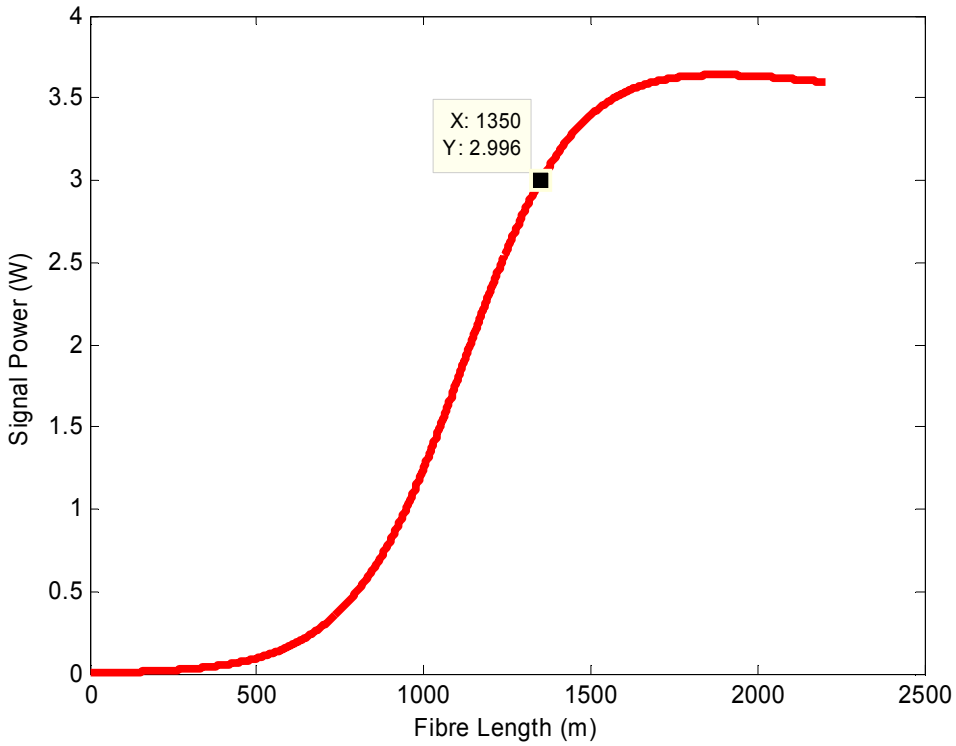

Figure 2.13 Raman Stokes Power (W) as a Function of gain length (m) assuming 0.5dB insertion loss and a maximum pump power pre-insertion of 5W

In the actual modelling process, a value should be chosen such as -3dB or -5dB of the maximum gain per unit length at which to end the gain fibre (as gain is falling off, or as shown on the RHS of Figure 2.14). This must be decided based upon maximising gain and minimising SBS and amplified backscatter. Considering Figure 2.13 in conjunction with Figure 2.14, it would seem more reasonable to use the -5dB gain/unit length (relative to the peak gain), since using -3dB results in a 700mW decrease of maximum overall gain. In addition, it would be useful to be able to see some Raman gain using lower pump powers for initial experiments. It should be noted that the gain per unit length, as well as the overall gain is smaller when using smaller pump powers, and hence a longer gain fibre is required for the same proportion of pump to signal transfer.

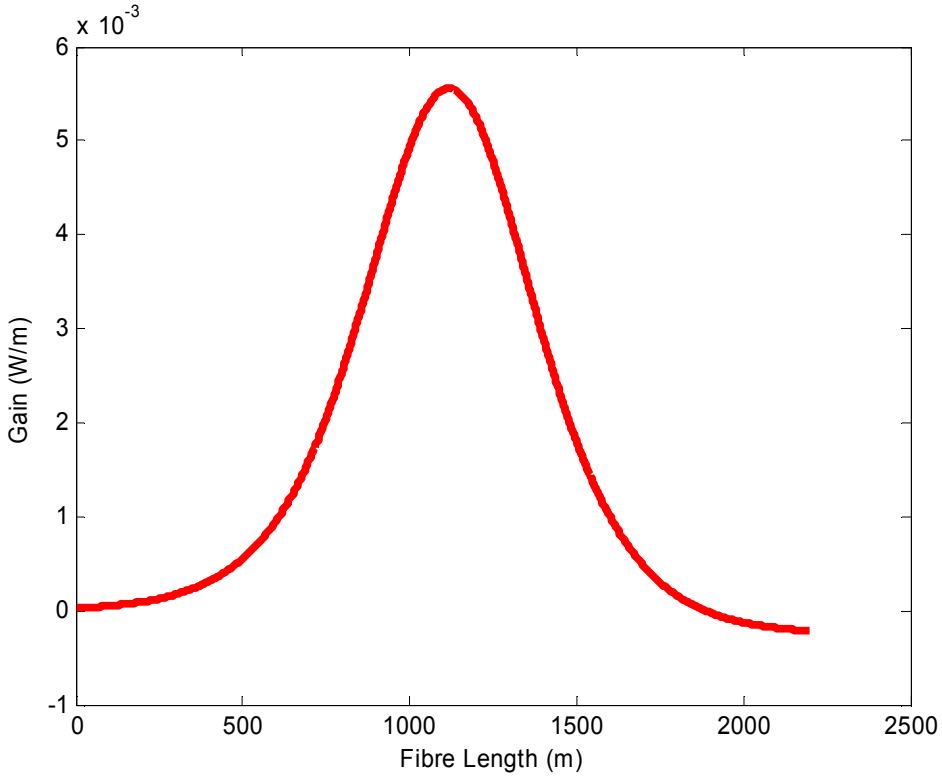

Figure 2.14 Power gain per unit length (W/m) as a function of distance along the fibre assuming a 0.5dB insertion loss for a 5W (4W) input pump and 5mW (4mW).

Further interpretation of Figure 2.13 and Figure 2.14 suggests that, should all unwanted non-linear effects be suppressed in an ideal amplifier system, there is still a length after which the Raman gain becomes less than the attenuation per unit length (where the gain per unit length is less than zero), and this sets an absolute ceiling for the length of gain medium regardless of SBS.

2.8.3 Modelling Standard Communication Fibre as a Raman Gain Medium and the Counter-Pumping Raman Gain Model

In the project brief it is stated that the system should be made from standard communications components; hence in order to reduce costs, other fibres that are commonly employed in the communications industry were investigated. SMF-28 style, single-mode communications fibre is the most common optical fibre in communications

networks and also the cheapest single-mode fibre. It also has the advantage of having the best splice compatibility with the communications fibre components, which also use this type of fibre. Like fibres are optimal for splicing to one another, because there is essentially no refractive index step or core mismatch at the splice, reducing losses and backscatter. Selecting a standard fibre not designed specifically for Raman applications also provides a good example of how the models linking fibre parameters can be used to determine the Raman gain efficiency.

From the values available from the fibre specifications, the most useful for estimating the Raman gain is the refractive index, which was provided in the form of numerical aperture. From various sources[2.11, 2.12].standard SMF has a Raman gain efficiency of around $0.5(W.m)^{-1}$, and hence this is a useful validation of the model.

Using Eqn 2.7 and the numerical aperture from the specification sheet to find n_1 to be 1.451, the Germanium concentration can be found from Eqn 2.25. This was calculated to be 4.86%, which in turn yields a peak effective Raman gain coefficient of $0.50(W.km)^{-1}$ using Eqn 2.24, which is consistent with the literature. Incidentally, the same calculation was conducted using the equation relating refractive index difference to Raman gain, Eqn 2.26, and this returned a Raman gain coefficient of $0.55(W.km)^{-1}$, which can be considered to be reasonable agreement. Given that the polarisation can be assumed to be scrambled over the gain length (recall that this is the counter-pumped case and the PMD is $>>0.001ps/km^{0.5}$) and k therefore takes the value 0.55, an effective gain efficiency of $0.28\ (W.km)^{-1}$ is obtained. The model parameters are included below in Table 2.4. The counter-pumping model is demonstrated using the standard single-mode fibre as a sample. From this, the differences in behaviour will be described between the co-pumped and counter-pumped models.

It is expected that given the longer length of fibre used in the case of a standard fibre as a gain medium, that it would be particularly advantageous to use a counter-pumped configuration to reduce the SBS gain length, as well as to improve the SNR. The

difference in the co and counter-pumped modelling is simply that the pump rate equation has its signs reversed, so that the change per unit length is the sum of the Raman depletion term and the attenuation term. This is because it is necessary to choose an end of the gain medium to designate as the start, but with the pump and signal counter-propagating, the launch side for one of the waves is the output side for the other.

Attenuation @1550nm, 1625nm (dB/km)	0.19-0.2 (use 0.2), 0.2-0.23(use 0.22)
Mode Field Diameter (μm) @1550nm	10.5 ± 0.8
NA	0.14
PMD ($ps/km^{0.5}$)	<0.2
Cut-off (nm)	<1260
g/A_{eff} as calculated $(W.km)^{-1}$	0.5
k	0.55
Insertion loss (Inserted Pump, signal)	0.5dB (4.5W, 4.5mW)

Table 2.4 Parameters collected from spec sheet and calculation to model Raman performance of standard single-mode communications fibre.

Using an iterative approach by taking sequential intervals to determine the parameters for the next interval rather than a fitting approach makes this necessarily so and conventionally, the signal direction is considered to be forward. Given this, an estimate of the residual pump power must be made instead of the actual input pump power, and this value can be perfected by adjusting the parameter until the input pump power is close to that desired. (i.e. the power that is likely to be inserted into gain medium from the pump launch side.)

The first model was constructed for the co-pumping of SMF, as obtaining a first approximation of the optimal length is more convenient from this configuration. Given the first approximation, further modelling is required, given that a longer length is required in the case of counter-pumping compared to co-pumping to achieve the same

gain. The evolution of the signal power in a 10km co-pumped SMF Raman amplifier is shown in Figure 2.15 for determining the length required in the following counter-propagating model.

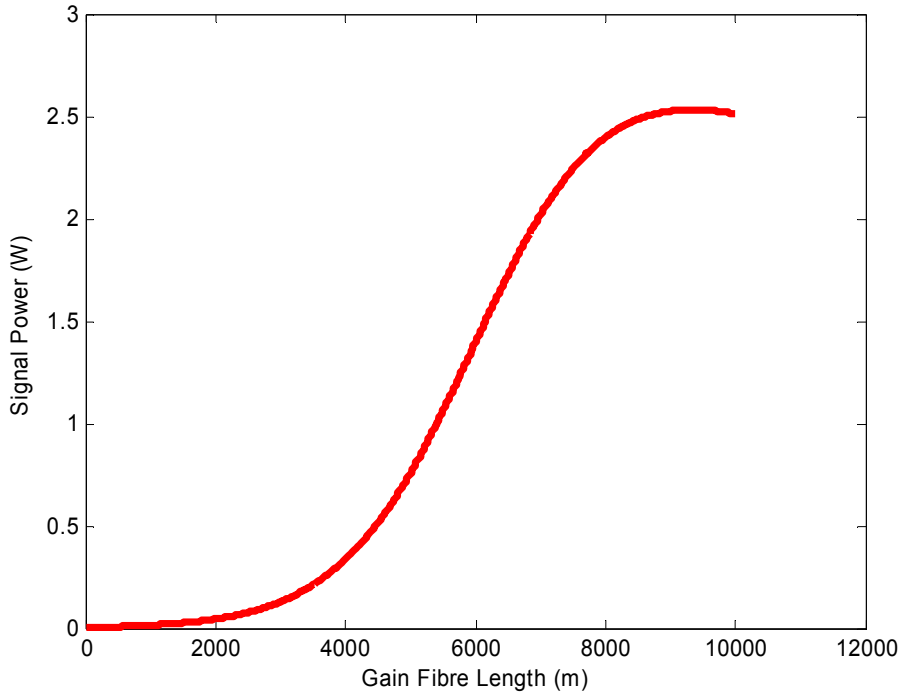

Figure 2.15 Signal Power as a Function of Fibre Length for standard single-mode fibre

The model of signal power as a function of distance along the gain fibre was run for the counter-propagating pump and signal using the same parameters and insertion losses as before (see Table 2.4), with the result shown in Figure 2.16

The counter-pumped model suggests that for a 10km fibre the output signal power is in excess of that calculated to be required for the application (~1W), as shown in Figure 2.16. One important note about the model is that, although the signal evolution is modelled here, it is not correct to assume that cutting the fibre back to 8km, for example, will result in the corresponding value for signal power at 8km in Figure 2.16. According

to the model result, this would reduce the output power to around 300mW. By simply taking the 8km point on Figure 2.16 and nominating this as the end of the fibre without re-running the model will result in taking account of pump depletion that would have occurred between 10-8km, but not the Raman gain over the same section. In order to calculate the actual power given a shorter length the model must be re-run with a new estimated residual pump as an initial parameter for the new fibre length. This process is more laborious than modelling co-pumping, and a model that would fit appropriate parameters would be more efficient for large data sets than the manual trial and improvement method employed for this model.

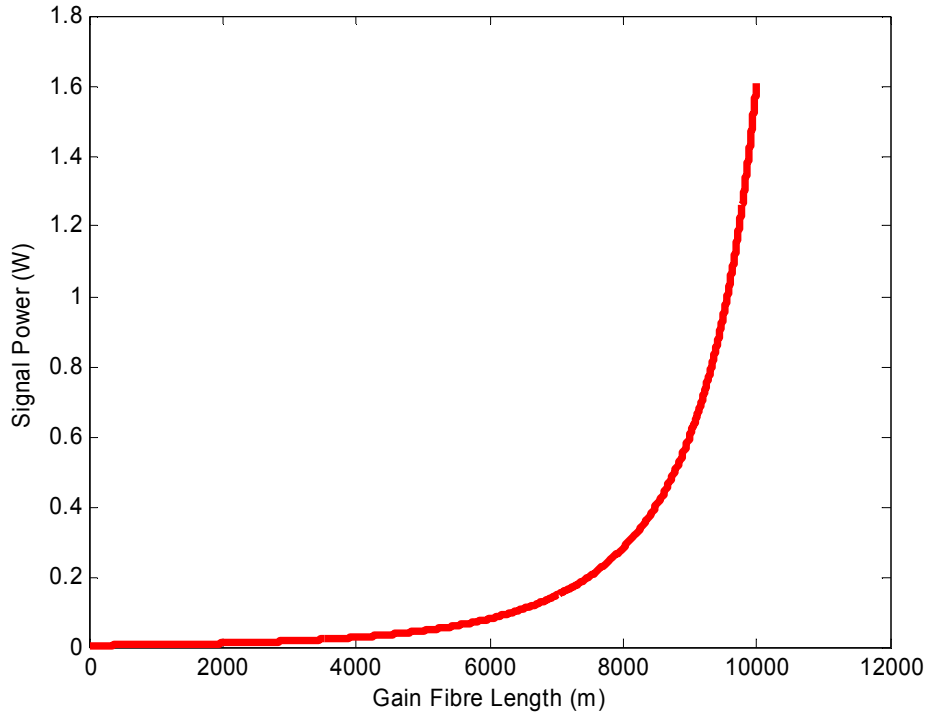

Figure 2.16 10km SMF-28 counter-pumped system output signal power as a function of gain fibre length.

As a demonstration for clarity, the fibre length is reduced to 8km and the model re-run with the same parameters as shown in Figure 2.17. Clearly, the result from re-running the model is very different from the case where the pump depletion in the unused length is included.

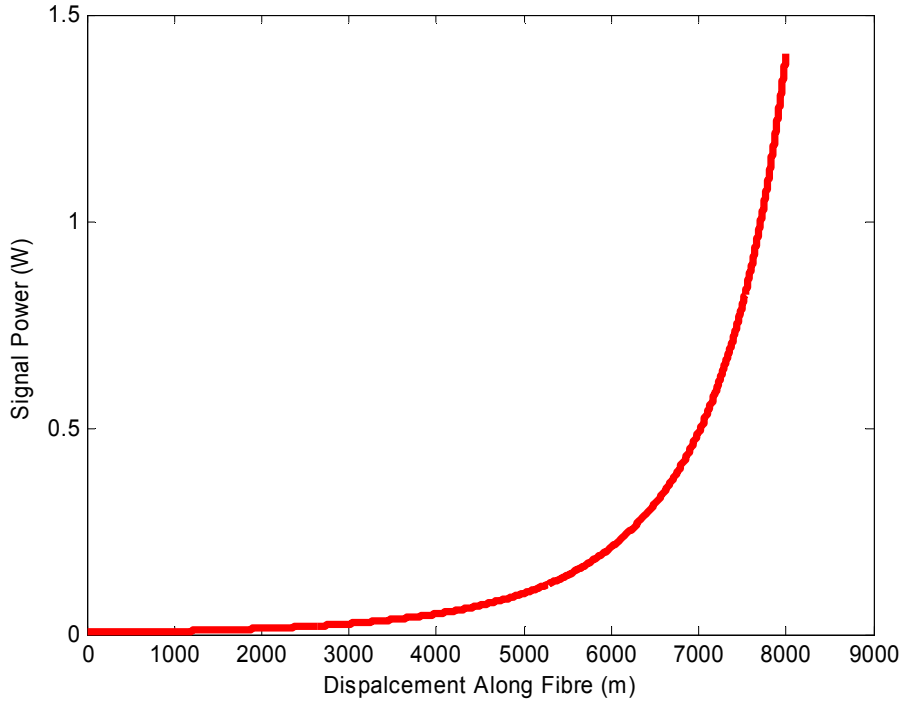

Figure 2.17 8km SMF-28 counter-pumped system output signal power as a function of gain fibre length.

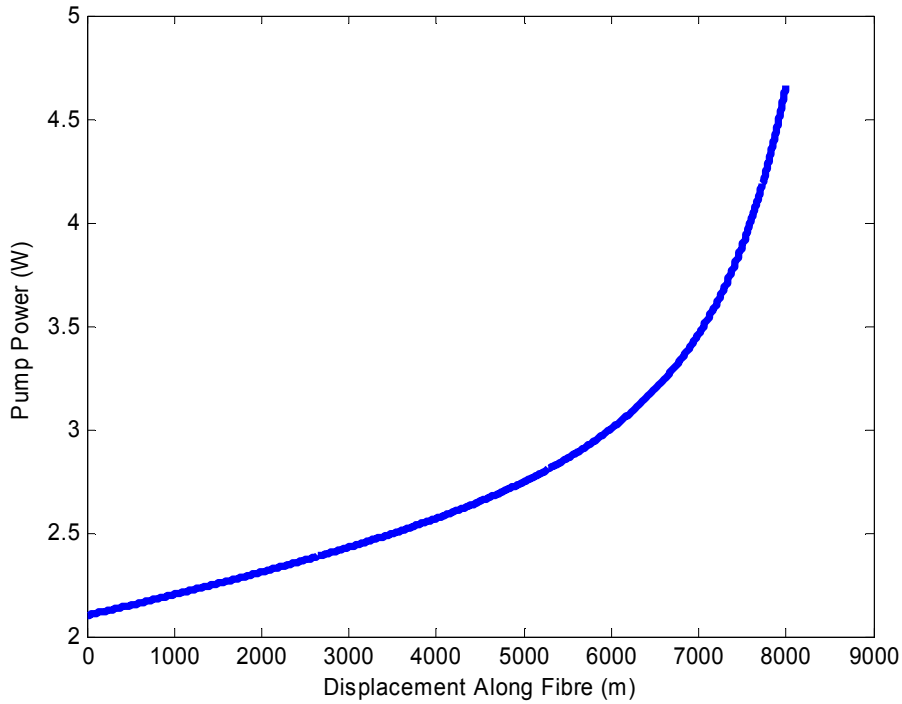

Figure 2.18 Pump Evolution in an 8km SMF-28 counter-pumped system.

This can be seen more clearly when considering the pump evolution model for an 8km fibre as shown in Figure 2.18.

Using Figure 2.18 as an example, firstly in general terms it can be seen that with respect to what the signal experiences, the pump is comparatively small at the signal input end, but maximum towards the end of the fibre (again with respect to the signal). It is hence clear why the model must be re-run in the case of changing the fibre length. Cutting the fibre from the new 8km length to 6km, for example would effectively change the input pump to around 3W instead of 4.5W.

2.8.4 Modelling Parameters of Dispersion Shifted Fibre as a Raman Gain Medium

With the process for counter-pumped modelling described, the parameters for modelling the DSF fibre are stated. This fibre will be modelled in both the co and counter-pumped configurations for comparison with the experimental results in Chapter 4. The parameters are listed in Table 2.5

Attenuation @1550nm(dB/km)	0.22
Mode Field Diameter(μm) @1550nm	8.1 ± 0.8
g/A_{eff} as provided$(W.km)^{-1}$	0.85
k	0.55
Insertion loss (Inserted Pump, signal)	1dB (4W maximum pump)

Table 2.5. DSF modelling parameters

Having discussed the issues regarding the design of a suitable Raman amplifier system, a more quantitative treatment of SBS is included so that it can be mitigated from the system

2.9 Stimulated Brillouin Scattering

2.9.1 Background of SBS in the Raman Amplifier

Propagating high powers (~W) in fibres present an additional set of challenges when compared to a fibre system operating at a few mW. Like SRS, SBS is another inelastic scattering process, but exciting lower energy acoustic rather than optical phonons as in the case of SRS. Consequently, the SBS excitation frequencies are lower and, as a result, the Stokes shift is smaller (~10GHz c.f. 13.2THz of SRS.) Other significant differences between SRS and SBS are the respective cross-sections in optical fibre. The cross-section of Brillouin scattering is approximately three orders of magnitude greater than that of SRS [2.22]. This means that the power threshold for SBS to begin to stimulate from spontaneous scattering and experience gain is three orders of magnitude lower than that of SRS, and is likely to occur in the system if care is not taken to prevent it. In addition, the gain bandwidth of SBS is much narrower than that of SRS (40MHz c.f. 7THz respectively)

In practical terms, the problem that SBS poses is that it depletes its pump; whether this is the Raman pump wave intended to pump the Raman Stokes wave, or the Raman Stokes wave (i.e. the amplified signal). This power is scattered backwards relative to its original direction of propagation, imposing a limit on the performance of the Raman amplifier through depletion and noise through amplitude oscillations in the signal. In addition, it can potentially cause damage to sources through potentially high backscattered powers, if the isolation is insufficient to deal with the backscattered power. Once SBS threshold has been reached, most additional (inserted pump or amplified signal) power is backscattered in the Brillouin Stokes wave [2.22]

The most intuitive way to qualitatively describe SBS is via wave theory, making the approximate assumption that the electric field distribution along the fibre is a sine wave at one given instant as shown in Figure 2.19.

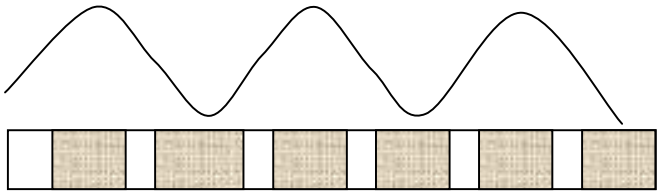

Figure 2.19. Illustration of E-field distribution in fibre giving rise to density/refractive index distribution by electrostriction

The wave gives rise to a periodic electric field distribution along the fibre, modulating the charge density periodically through a process known as electrostriction and hence the refractive index along the length of the fibre. This creates a temporary induced grating structure, which acts like a reflective Bragg grating reflector to the wave that induced it, since the periodicity of the refractive index steps will always match the maxima and minima of its pump wave with index steps at $\frac{\lambda}{2}$ intervals. Although the refractive index steps are small, they occur along the entire length of the fibre over which the power is high enough to stimulate the effect, meaning that the grating steps are very numerous, resulting in a high effective reflectivity. The density distribution as induced via the opto-electric effect is an acoustic wave, and hence it travels at the speed of sound in the fibre in the forward direction, causing a ~10 GHz Doppler shift in the backward travelling Stokes Wave, giving rise to the Stokes Shift.

As in the case of SRS, SBS can be described quantum mechanically, the process is the annihilation of a pump photon and the simultaneous creation of an acoustic phonon and a Stokes photon. In this interaction, momentum and energy must be conserved, and hence the following relation between the pump Stokes and phonon waves must be true. $\Omega_B = \omega_p - \omega_s$ and $k_A = k_p - k_s$ where subscripts p and s refer to pump and Stokes wave, and ω and k are frequency and wave vector respectively. Ω_B and k_A are the frequency and wave vector of the acoustic wave. In effect, this states that the energy and momentum of the acoustic phonon excited in the scattering equate to the difference

between the energy and momentum respectively of the respective (pump and Stokes) waves. Ω_B and k_A satisfy the standard dispersion relation as follows in Eqn 2.32 [2.22].

$$\Omega_B = v_A \mid k_A \mid \approx 2v_A \mid k_P \mid \sin\left(\vartheta/2\right) \qquad \textbf{Eqn 2.32}$$

Where v_A is the speed of sound in the medium and using the assumption that the Stokes and pump wave photons have approximately equal momenta so that $k_A = 2k_P$. It can be seen from Eqn 2.32 that the Brillouin Stokes shift is dependent upon scattering angle, unlike the zero dispersion Raman scattering. Since the consideration relates to an optical fibre, only the forward and backward directions (relative to the pump) are significant, furthermore it can be seen that in the case of the forward propagating Brillouin Stokes wave, where $\vartheta = 0$ there is no frequency shift and no phonon energy imparted. However the effect is maximised in the backward direction relative to the pump, direction where the scattering angle $\vartheta = \pi$. The result of this is that the Brillouin Stokes wave travels in the backwards direction relative to the pump, with the Stokes shift arising from the energy imparted to creating an acoustic phonon. When the threshold density of Brillouin scattered photons is reached they begin to stimulate more Brillouin scattering events of the same kind, causing the backscattered power to rise sharply with increased input power into the fibre [2.13].

2.9.2 Modelling SBS

SBS was modelled so that its occurrence could be predicted and minimized. The threshold equation for SBS is dependent upon the length and effective area of the fibre as well as the linewidth of the pump since the gain bandwidth of SBS is of the order 40 MHz (much narrower than that of SRS) and hence if a pump with a broader bandwidth than this is used, the threshold for SBS is raised considerably since a proportion of the pump power is falling outside of this bandwidth. This can be explained physically,

referring back to the explanation of SBS in Section 2.9.1, if it is considered that any other than a hypothetical, monochromatic source does not produce a sinusoidal electric field distribution, and therefore with a broader bandwidth source, the periodicity of the induced refractive index steps are less defined, reducing the reflectivity of the grating.

For the purposes of the SBS models, the SBS threshold is defined as the optical launch power at which the SBS backscatter level is measured to be 1% of that launched power. The same polarization factor k is applicable here as in the case for SRS. The 1% threshold power can be calculated using Eqn 2.33 [2.22].

$$\frac{k g_B P_0^{cr} L_{eff}}{A_{eff}} = 19 \qquad \textbf{Eqn 2.33}$$

Where P_0^{cr} is the threshold pump power required for 1% of the pump power to be backscattered in the fibre , L_{eff} and A_{eff} are the effective length and area of the fibre respectively, g_B is the peak Brillouin gain coefficient (at the frequency shift corresponding to the peak Stokes shift) given by Eqn 2.34 [2.22, 2.13].

$$g_B = \frac{2\pi n^7 p_{12}^2}{c\lambda_p^2 \rho_0 \nu_A \Delta\nu_B} \qquad \textbf{Eqn 2.34}$$

Where n is the refractive index of the fibre core, taken as 1.45, p_{12}, λ_p, ρ_0, ν_A and $\Delta\nu_B$ are the photoelastic coefficient in the direction of the pump, the Brillouin pump wavelength, the physical density of the fibre core, the acoustic velocity of the effective Bragg grating resulting from the pump's intensity distribution and the Brillouin linewidth respectively. For SMF-28 the Brillouin gain coefficient is 5×10^{-11} m.W^{-1} [2.14]. Taking the core area to be ~50μm^2, the Brillouin gain efficiency is 1000(W.km)$^{-1}$, which matches the condition that Brillouin scattering should be

approximately three orders of magnitude greater than that of Raman gain coefficient. Since the linewidth of the pump wave will be designed to be broader than the Brillouin gain bandwidth, the peak gain coefficient in Eqn 2.33 is replaced with that in Eqn 2.35 to take account of the optical power falling outside of the Brillouin gain bandwidth, assuming a Lorentzian wavelength distribution

$$\tilde{g}_B(\nu_B) = \frac{\Delta\nu_B}{\Delta\nu_B + \Delta\nu_P} \times g_B(\nu_B) \qquad \textbf{Eqn 2.35}$$

Where $\Delta\nu_B$ is the Brillouin gain bandwidth, which is nominally 40 MHz, $\Delta\nu_P$ is the linewidth of the wave that pumps the Brillouin Stokes Wave and the ~ symbol denotes the Brillouin gain that takes account of relative Brillouin gain and pump linewidths [2.13, 2.22]. In effect, the Brillouin gain is restricted to the convolution of the Brillouin gain and pump spectra. The SBS threshold can be modelled using the Eqns 2.33-2.35 in terms of bandwidth for a known fibre. Models were constructed in Matlab and Excel and they are compared with measurements in Chapter 4.

Parameters from a model in literature [2.22] were inserted into the model outlined in this work to test its validity. A 1 km system was modelled using a laser of bandwidth 100 kHz and scrambled polarisation, Brillouin gain bandwidth was taken to be 40 MHz and the effective area of the fibre was 50μm^2. The Brillouin threshold was 47.9mW in literature but that used for the purposes of modelling in this thesis returned the value 45.8mW for the same parameters. The difference between the models could be that standard fibre attenuation has been dismissed as insignificant in depleting the Brillouin pump in our model but nevertheless, the model is in good agreement with literature.

While considering what length to make the fibre gain medium, SBS is now a quantifiable consideration as well as Raman gain in terms of this, and hence most of the tools required to make an informed plan for a Raman amplifier of given performance

have been obtained. However given the relative cross-sections of SBS and SRS, attempting to build a system under the current conditions is excessively restrictive. Hence, well informed plans for Raman amplifier designs can only be made after the effect of any techniques to mitigate SBS have been taken into account in the modelling.

2.10 Suppression of SBS

2.10.1 Overview of SBS Suppression Strategies

It is clear that SBS is a factor limiting the performance of the system; therefore a theoretical study was performed with respect to its suppression. Given the optical power in the fibre system, Brillouin scattering will reach stimulation threshold in the 1540nm pump Raman pump wave and also the amplified gas sensing signal. In general, the method used to suppress SBS in a system is to use some method of pump broadening, where in this case 'pump' refers to any wave that experiences sufficient Brillouin scattering so as to stimulate the effect, whether the Raman 1540nm pump or the gas sensing signal [2.22].

Given that the FWHM of SRS and SBS gain peaks are around 7THz and 40MHz respectively, it should be reasonable to use a Raman pump source with a bandwidth in excess of hundreds of GHz without a significant penalty to Raman gain. The same, however is not true of the Raman amplified methane sensing signal. The linewidth of the gas probe signal must be considerably smaller than the gas linewidth to maintain detection sensitivity, as discussed in Chapter 1. Given this, other methods of suppressing the stimulation of Brillouin scattering were investigated, however they all exploit the fact that the SBS gain bandwidth is relatively small compared to that of SRS. The difference in some of the alternative methods is that some of these techniques are applied to the fibre itself rather than the Raman signal.

The principle by which SBS can be suppressed through the fibre is as follows. If it were possible to change the Brillouin Stokes frequency shift in part of the fibre relative to the rest by more than a Brillouin gain bandwidth, it would mean that this region of fibre would not contribute significantly to the SBS gain in the other part of the fibre system. If the SBS threshold condition were reached in both the part of fibre with the intrinsic Brillouin Stokes shift and the somehow modified section, a second, independent, frequency-shifted Brillouin Stokes wave would be generated. Taking this argument further, if half of the total length of fibre gave rise to one Brillouin Stokes shift and the other half, a different Brillouin Stokes shift, at least an SBS gain bandwidth frequency seperation from the first, the SBS threshold is increased by a factor of around two, since the gain length for each non-interacting Brillouin Stokes wave is halved. This can be extended by further factors given more equal segments of different Stokes shifts. The Stokes shift differences can be induced in a single, standard fibre in two ways; by applying either a temperature or strain distribution along the fibre. The other option, not using a single fibre is to splice a number of different fibres with different Brillouin Stokes shifts (resulting from different dopant levels and core sizes, together to achieve the same effect.) However, This can lead to increased insertion loss, system fragility and back-reflection.

2.10.2 SBS suppression By Applying a Strain Distribution along the Gain Fibre

One method of altering the SBS Stokes shift in a single fibre is to alter the tension applied to the fibre itself. Incidentally, this technique is becoming popular as a distributed OTDR strain sensing technique and associated literature can be found [2.23].

Recalling that SBS is an acoustic phonon interaction, this process can be considered to be analogous to tightening a guitar string to change the acoustic properties of the material. There has been some work regarding this type of suppression, and up to 8dB threshold increase has been achieved [2.24].In this work, they applied two different types of strain distribution; one a periodic, dual-state/rectangular distribution, thus

creating two strain states in the fibre, i.e. intrinsic and applied. In the second case they applied a stair ramp distribution of forty steps of steadily increasing strain. As expected they found that the rectangular repeated strain distribution led to a maximum threshold increase of 3dB (50%), given that there were at best two unrelated Brillouin Stokes waves with a half-fibre gain length regardless of additional strain/ Stokes shift difference. In the case of the stair ramp, they increased the linear, tensile strain in equal steps and achieved a 7.3dB increase in SBS threshold power. A representation of the strain distributions investigated is shown in Figure 2.20

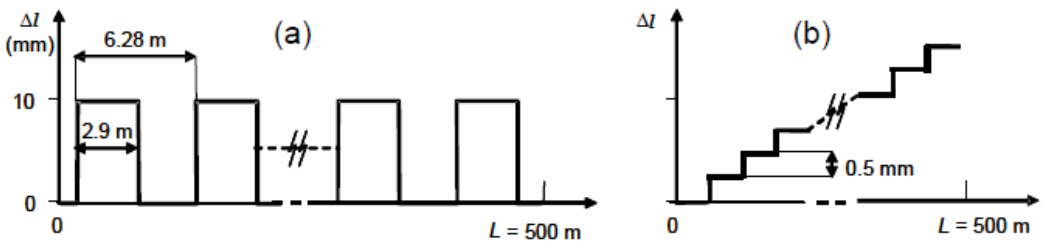

Figure 2.20 Strain Distributions for SBS suppression a) rectangular intervals, b) stair ramp. Extracted [2.24]

According to literature a strain of 4.5×10^{-3} produces a ~2% shift in the peak Brillouin Stokes shift [2.24]. This is demonstrated in their observation of the travel of the secondary SBS Stokes peak as a function of applied strain, where the strain distribution applied was that of a) Figure 2.20.

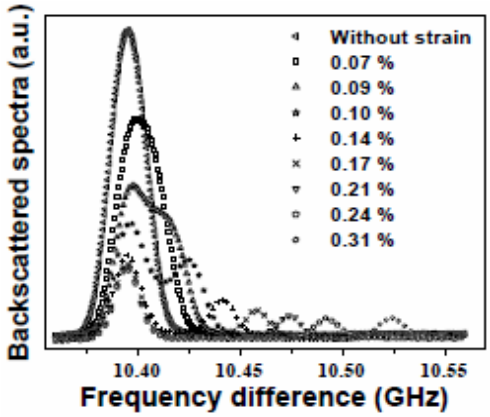

Figure 2.21 Backscatter Spectrum in configuration a) strained fibre for a range of strains. Extracted[2.24]

As can be seen from Figure 2.21, the secondary Brillouin Stokes wave generated in the strained regions becomes further separated in frequency from the intrinsic Brillouin Stokes shift with additional straining. Ideally, if a step configuration is to be used, and only a limited number of steps are practical, each step should move the Stokes shift a gain bandwidth away from the previous strain region to maximise suppression. These cited results demonstrate that, if required, such a technique could be effectively included in the system.

The method outlined constitutes a technique by which a fibre gain medium could have an increased SBS threshold in a standard type fibre, with no detriment to SRS and no alteration of the signal is required, so long as sufficient strain can be applied. From a practical point of view however, there are some difficulties. Firstly, the fibre will be wound onto a spool and it may be difficult to apply and maintain the correct tension. Furthermore, to induce an e.g. 10dB threshold increase in SBS threshold, which is reasonable for the signal power evolution in the system, at least ten different strain regions are required towards the end of the fibre, where the signal power is high. This would represent a considerable, practical challenge on a single spool, and in fact might require that the fibre is wound onto up to ten different spools. This subsequently makes the device bulkier than the original design for a single spool. Additionally changes in temperature would affect the tensions on the spools and might even cause a breakage, unless specialist spools that match the thermal expansion of the fibre are used. Finally, and very significantly, straining an optical fibre by the level required to achieve a considerable change in Brillouin Stokes shift results in a considerable reduction in lifetime and increase in fragility [2.25].This could compromise some of the system's key benefits, since it is required that it has a low cost of ownership and high reliability. Ultimately, this suppression method is instructive and could be used, should SBS not be suppressed by other means, but does come at the cost of complexity.

2.10.3 Temperature Distribution as a Method of SBS Suppression

The Brillouin Stokes shift of a fibre is also dependent upon fibre temperature, (irrespective of strain) and this can be exploited to suppress SBS in a similar way to strain. A group investigated this relationship experimentally and various temperature distributions were tested for their effectiveness in raising SBS threshold. The principle was found to be the same as for strain, in that changing the Brillouin shift by more than a Brillouin gain bandwidth from region to region provides an extra factor of threshold increase. As in the case of the dual-step strain distribution, a distribution consisting of two separate temperature regions provided a maximum of 3dB threshold improvement. Additionally, from their results the most successful temperature distribution, given the same overall temperature difference, was the one with the greatest number of temperature intervals, tending to a continuum. In those investigations, it was found that the Brillouin Stokes shift changed by 1.2MHz/°C and the SBS threshold was increased by a factor of just over three using a ramp temperature gradient with a total temperature difference of 140°C. This matches expectations, since they measured their Brillouin gain bandwidth to be 43MHz, meaning that four Brillouin gain bandwidths fit within the temperature distribution. The gain bandwidth refers to the -3dB (half-maximum) bandwidth, and hence there is some interaction between the Brillouin Stokes waves [2.26, 2.27].

Once again there are practical issues involved with this type of suppression. As in the case of the application of strain, separate reels are required. Secondly, to achieve a high SBS suppression a temperature difference of 400-500°C might be required. This has implications for fibre lifetime, in particular any polymer coating on the fibre, specialised fibre reels and also power consumption, bulkiness of ovens/heaters and safety associated with high temperatures.

2.10.4 Wavelength Dither as a method of SBS Suppression

Although bandwidth broadening of the gas sensing signal is not an acceptable solution, it is possible to emulate the effects of broadening with regard to SBS suppression whilst

keeping the instantaneous bandwidth of the signal small through the use of frequency modulation. As discussed in the TDLS theory, a frequency modulation is applied for the purpose of phase sensitive, AC gas detection. There is considerable flexibility in the modulation parameters chosen for the gas sensing, so long as the bandwidth of the photoreceiver and detection equipment is well in excess of the dither frequency. Hence, with carefully chosen frequency modulation parameters for the gas sensing and SBS suppression, both aims can be achieved with no additional equipment.

This technique was originally considered for SBS suppression in high capacity optical communication networks, where the optical power can be significant over long distances. In these cases, the bit sequence can be chosen to maximise effective signal bandwidth, or a separate wavelength dither can be applied that carries no information [2.28, 2.29]. The principle is that the effective bandwidth of the narrow bandwidth frequency dithered signal can be broad with respect to the Brillouin gain while considering the entire Brillouin gain length of fibre, since a range of frequencies are present along it at any given time. For this to be true, there is the condition that the frequency modulation is fast enough that at least the full peak-to-peak extent of the sinusoidal frequency modulation is swept through a whole number of times between the start and finish of the Brillouin gain region of the fibre, while the light travels through the fibre. That is to say, if the extreme spectral outputs λ^+ and λ^- of the sinusoidally dithered DFB's output are considered, the condition that the entire wavelength range should propagate within the Brillouin gain length at the same time (so that if at one end the wavelength is λ^+ it will be λ^- at the other) is required to maximise the effective bandwidth with a given modulation index. This gives rise to a simple mathematical condition linking the length of the fibre L, the speed of light c, the refractive index of the fibre's core n and the optimal dither frequency f [2.28]. The frequency should be, or be a harmonic of $f = \frac{c}{2nL_{gain}}$, where c is the speed of light, n is the refractive index of the fibre core at the signal wavelength and L_{gain} is the Brillouin gain length, which is the

length over which the signal is of sufficient power to bring the onset of SBS. For added clarity, the parameters are illustrated in Figure 2.22

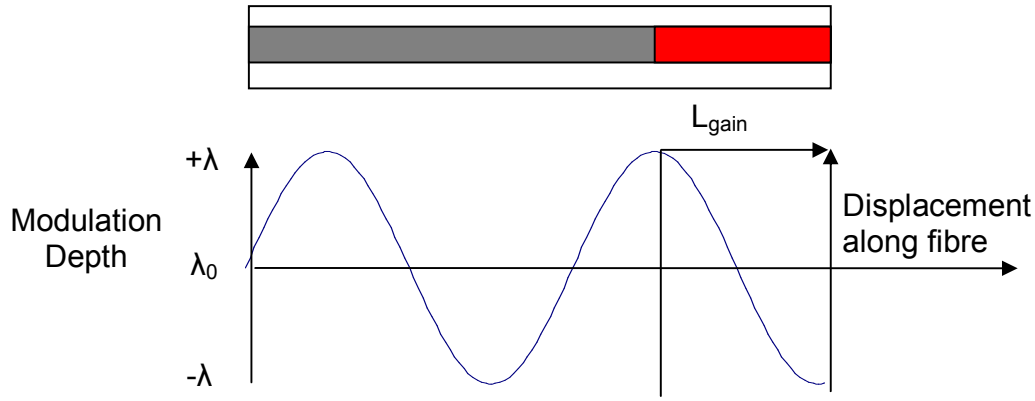

Figure 2.22 Schematic of SBS suppression using sinusoidal wavelength dither

With sufficient modulation index, it is expected that SBS and other undesirable effects such as interference from Rayleigh scattering should be efficiently suppressed. Fulfilling this condition, and given a modulation depth of, ideally several GHz the SBS threshold can be increased by a factor of around 100, recalling Eqn 2.35.

2.11 Summary

In summary, the theory discussed in chapter 2 has provided the basis for an informed design of a fibre Raman amplifier, taking all considerations for Raman amplifier design into account (including polarisation, fibre type and its bearing on gain, SBS occurrence and suppression) and treating these in the best way for the project requirements (low cost, high power, narrow signal bandwidth, low noise, robust, efficient). The reader should be in a position to predict the necessary amplifier output power required for a given design range and sensitivity, from TDLS and Backscatter sections 2.2-2.3. They should then be able to source an appropriate fibre, based on the considerations laid out, selecting an appropriate length and pumping configuration and implement necessary

SBS suppression techniques and parameters accordingly. Given these tools, the following chapter details the experimental technique involved in the development and characterisation of the amplifier system and characterisation of its performance as a methane sensor system.

2.12 References

[2.1] Peter Werle "A review of recent advances in semiconductor laser based gas monitors" Spectrochimica Acta Part A, 54, 197–236 (1998)

[2.2] B. Culshaw, G. Stewart, F. Dong, C. Tandy, D. Moodie. "Fibre optic techniques for remote spectroscopic methane detection - from concept to system realisation" Sensors and Actuators B 51 25–37(1998)

[2.3] 225 Lock-in Amplifier by the Bentham corportation. Obtained from http://www.bentham.co.uk/pdf/F225.pdf in February 2010

[2.4] Kevin Duffin "Wavelength Modulation Spectroscopy with Tuneable Diode Lasers: a Calibration-Free Approach to the Recovery of Absolute Gas Absorption Line-Shapes" Chapter 4, PhD thesis submitted to EEE University of Strathclyde, (2007)

[2.5] Takaya Iseki, Hideo Tai and Kiyoshi Kimura. "A portable remote methane sensor using a tunable diode laser" Meas. Sci. Technol. 11 594–602, (2000)

[2.6] Russ Pride, Miles Padgett, Rainer Strzoda, Stuart Murray, Sven-Ake "Implementation of Optical Technologies for Portable Gas Leak Detection" internal project report obtained through private communication in April 2007

[2.7] G.P Agrawal Chapter 1 "Non-Linear Fibre Optics," Academic Press, Harcourt, Brace Jovanovich Publishers 1989

[2.8] G.P Agrawal Chapter 2 "Non-Linear Fibre Optics" Academic Press, Harcourt, Brace Jovanovich Publishers 1989

[2.9] Karsten Rottwitt and Jørn H. Povlsen "Analyzing the Fundamental Properties of Raman Amplification in Optical Fibers" Journal of Lightwave Technology, Vol. 23, NO. 11, 3597, (November 2005)

[2.10] C. V. Raman and K. S. Krishnan, "A new type of secondary radiation," Nature, vol. 121, p. 501, 1928.

[2.11] Govind P. Agrawal "Non-linear Fibre Optics" Chapter 8, Academic Press, Harcourt, Brace Jovanovich Publishers, 1989

[2.12] Jake Bromage, "Raman Amplification for Fiber Communications Systems" Journal of Lightwave Technology Vol. 22, NO. 1, pgs 79-93 January 2004

[2.13] Billington, R, NPL internal report, "Measurement methods for stimulated Raman and Brillouin scattering in optical fibres" 1999 Freely available at web address (in April 2007) http://publications.npl.co.uk/dbtw-wpd/exec/dbtwpub.dll?&QB0=AND&QF0=ID&QI0=001741&TN=NPLPUBS&RF=Full+Record&DL=0&RL=0&NP=4&AC=QBE_QUERY

[2.14] Yuhong Kang "Calculations and Measurements of Raman Gain Coefficients of Different Fiber Types" Thesis submitted to The Faculty of the Virginia Polytechnic Institute and State University. Roger H. Stolen-Chair, Ira Jacobs, Ahmad Safaai-Jazi December 9, 2002 Blacksburg, Virginia

[2.15] N. R. Newbury, "Raman gain: pump-wavelength dependence in single-mode fiber" Optics Letters, Vol. 27, No. 14, July 15, 2002

[2.16] F.L Galeener, J. C. Mikkelsen, R.H Geils and W.J Mosby. "The relative Raman cross-section of vitreous SiO_2, GeO_2, B_2O_3, P_2O_5" App. Phys. Lett. 32(1) (Jan 1978)

[2.17] Frédérique Vanholsbeeck, Philippe Emplit, and Stéphane Coen "Complete experimental characterization of the influence of parametric four-wave mixing on stimulated Raman gain" 1960 OPTICS LETTERS / Vol. 28, No. 20 / October 15, 2003 Service d'Optique et Acoustique, Université Libre de Bruxelles.

[2.18] Chisato Fukai, Kazuhide Nakajima, Jian Zhou, Katsusuke Tajima, Kenji Kurokawa, and Izumi Sankawa "Effective Raman gain characteristics in germanium- and fluorine-doped optical fibers" / Vol. 29, No. 6 / Optics Letters 545 March 15, (2004)

[2.19] Yan Feng, Luke Taylor, and Domenico Bonaccini Calia "Multiwatts narrow linewidth fiber Raman amplifiers" Vol. 16, No. 15, Optics Express 1092921 (July 2008)

[2.20] E. Golovchenko, A. N. Phlipetskii, C. R. Menyuk, and L. Joneckis, ''Effect of randomly varying birefringence on the Raman gain in optical fibers,'' in *Conference on*

Lasers and Electro-Optics, Vol. 11 of 1997 OSA Technical Digest Series p.447 Optical Society of America, Washington, D.C., (1997).

[2.21] Q. Lin and G. Agrawal "Vector theory of stimulated Raman scattering and its application to fiber-based Raman amplifiers" 1616 J. Opt. Soc. Am. B/Vol. 20, No. 8/August 2003

[2.22] Agrawal Chapter 9 "Non-Linear Fibre Optics" Academic Press, University of New York, Academic Press, Harcourt, Brace Jovanovich Publishers 1989

[2.23] Hiroshi Naruse, Mitsuhiro Tateda, Hiroshige Ohno, and Akiyoshi Shimada "Dependence of the Brillouin gain spectrum on linear strain distribution for optical time-domain reflectometer-type strain sensors" Applied Optics Vol. 41, No. 34 (December 2002)

[2.24] J. M. Chavez Boggio, J. D. Marconi, and H. L. Fragnito "Experimental and Numerical Investigation of the SBS-Threshold Increase in an Optical Fiber by Applying Strain Distributions" Journal of Lightwave Technology, Vol. 23, Issue 11, pp. 3808, (November 2005)

[2.25] Kenneth D Fitchew "Technology Requirements for Optical Fiber Submarine Systems" IEEE Journal on Selected Areas in Communications Vol. SAC-1, NO. 3,

[2.26] J. Hansryd, F. Dross, M. Westlund, P. A. Andrekson, and S. N. Knudsen "Increase of the SBS Threshold in a Short Highly Nonlinear Fiber by Applying a Temperature Distribution" Journal of Lightwave Technology, Vol. 19, No. 11, 1691, (November 2001)

[2.27] Anping Liu "Suppressing stimulated Brillouin scattering in fiber amplifiers using nonuniform fiber and temperature gradient" Optics Express, Vol. 15, Issue 3, 977-984, (2007)

[2.28] Fishman, Daniel A.; Nagel, Jonathan A.; Park, Yong-Kwan "Reduction of stimulated brillouin scattering in a fiber optic transmission system" United States Patent: 5329396. Publication date 12/07/1994. (Access via "Patentsonline.com" in (April 2007)

[2.29] Adams, Laura Ellen; Bethea, Clyde George; Eskildsen, Lars Erik; Nykolak, Gerald, Rossevelt; Tanbun-Ek, Tawee "Optical system for reduced SBS" US patent number: 6331908. Published 18/12/2001

Chapter 3 Experimental Methods

3.1 Raman Amplifier Test Beds

3.1.1 Establishment of Measurement Parameters

This chapter details the experimental configuration employed in the initial practical build and characterisation of the 1651nm Raman amplifier and how the optimised amplifier system integrates as part of the remote methane sensing system. The first stage of the process was a consideration of which amplification and system degradation parameters would need to be measured and how the required measurements could be realised through the construction of an optical fibre test bed.

In the most basic terms, for Raman amplification to take place, pump and signal seed power, separated by the Raman Stokes frequency shift for silica need to be combined within the fibre gain medium. For the purposes of the investigations, it was required that they were combined in the gain medium while co and counter-propagating in separate configurations. The testing and characterisation of a Raman amplifier system requires the separate measurement of output signal and residual pump powers as a function of input pump and signal seed power. In addition to these basic requirements, the development of a low noise, high power amplifier system requires that backscatter, and in particular SBS power must be measured so that it can be characterised and suppressed. A number of individual configurations of the test beds were used for the characterisation of SBS in the different fibres and these will be

described separately. In addition to average measurements of output and backscattered power, time resolved power measurements were required. Also, for some purposes, knowledge of the wavelength spectra was required.

In addition to measuring each of the Raman amplifier parameters as stated, the use of an EDFA as a pump source for the Raman amplifier requires that its spectrum be controlled appropriately. The EDFA spectrum is controlled via a seed source and selection of this is an important part of the successful development of the amplifier system. In order to carry out development of the seed system, the monitoring of the spectra of the seed outputs and the resulting input pump to the Raman system is required, together with system characteristics and signal modulation parameters.

3.1.2 The Co-Pumping Test Bed

Given that the test bed would have to handle high optical powers and enable their measurement, this had to be given consideration, both in respect of safety and also with regard to making all of the required measurements. There are several possibilities to measure the high power outputs of the Raman system, but broadly they consist of either measuring the high power outputs using a thermal power meter at each output, or by splitting the power and measuring using InGaAs photoreceivers and power meters. The latter is clearly preferable, since with thermal power meters, only the power level is available, whereas photoreceivers can be used to observe a signal in the time domain. In order to measure the output power in this way, the power would have to be split in a readily characterised and repeatable way to deliver a useable power level to power meters. In addition to the practical measurement concerns, the safest way of handling high power is to keep all of the power in fibre, split a small, eye-safe proportion of the power to be measured and for the rest to be fibre fed to a beam dump, separating the user from the high power output. The most convenient way of splitting the power is with fibre taps couplers (of a high ratio.)

Figure 3.1 shows a schematic of the test bed for the initial, co-pumped Raman, SBS and seed investigations. Beginning from the LHS of the schematic, the 1651nm signal DFB laser is controlled via the temperature, current and modulation

controllers and injects the WMS signal into the Raman gain medium via a WDM and monitor tap. An isolator (60dB at 1650nm) is positioned between the DFB laser and the fibre system to prevent destabilisation of the DFB by backscatter from the amplified signal. The pump power from the EDFA is fed through the 1550nm arm of the WDM and follows the same route through the 20dB tap coupler into the gain medium. 1% of the total input optical power passes through the monitor tap and the remaining 99% into the gain fibre. This tap was placed before the input of the gain medium, so that pump and signal being launched into the gain fibre could be characterised in terms of power level and wavelength spectrum by interrogating the forward facing 1% tap arm. Any backscattered light from the gain fibre propagating towards the optical sources could be measured by interrogating the backward facing 1% arm (with respect to the pump) of the same coupler.

Having been confined within a single fibre and passed through a monitoring tap, the pump and signal waves co-propagate through the fibre gain medium. The amplified signal and residual pump waves output from the gain medium are demultiplexed via a second 1550/1650nm WDM, with a 20dB tap coupler on each of the output arms. This allows most (~99%) of the output power from both the signal and pump to be disposed of safely into fibre coupled beam dumps, allowing safe measurement of a small portion of the residual pump and signal via appropriate attenuation when necessary.

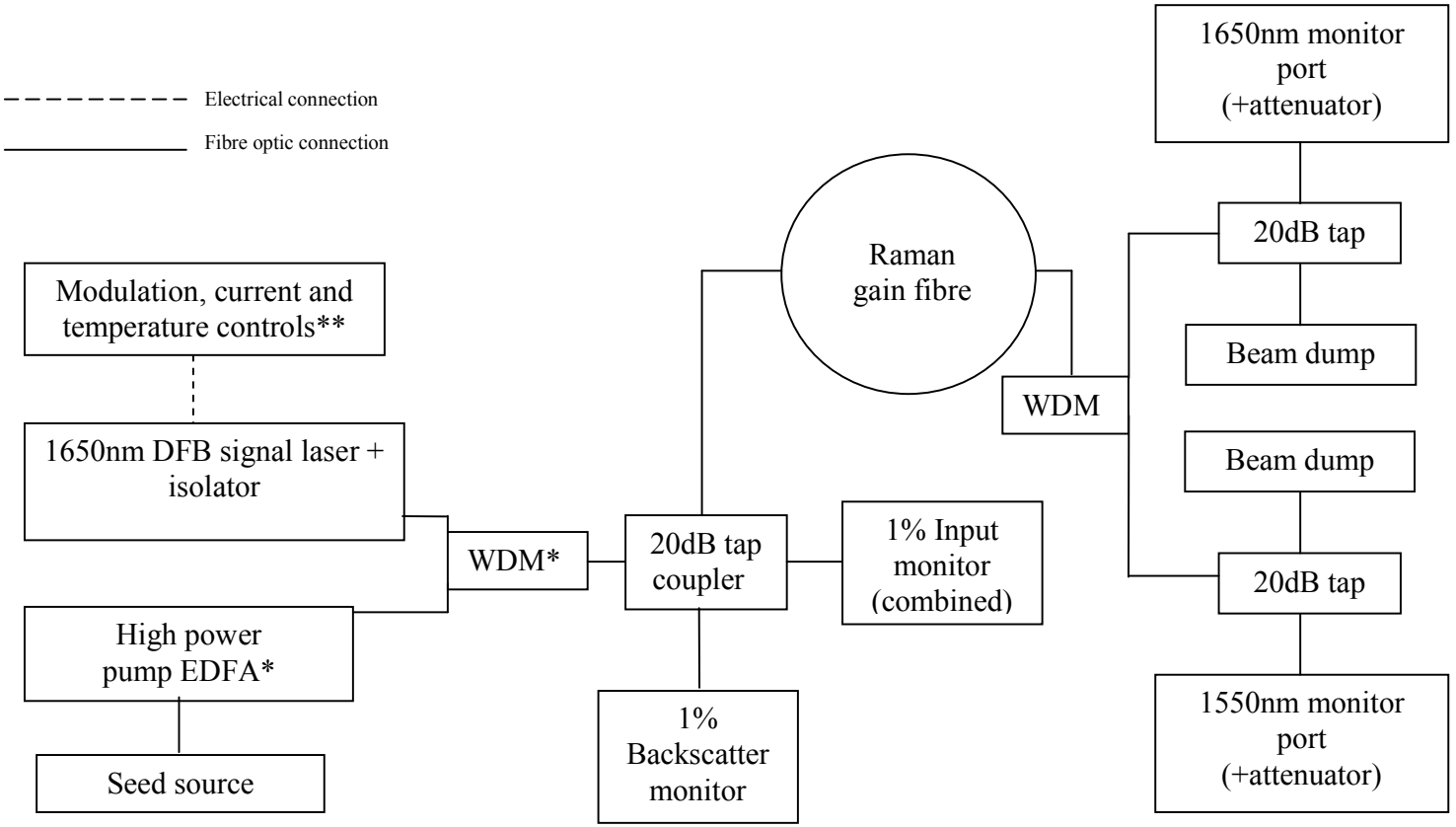

Figure 3.1 Raman test bed for the co-pumped configuration

The level of attenuation applied to the 20dB (1%) measurement arm of the tap depends upon the power being used in the experiment. Typically the in-line attenuators are chosen to maintain an output power in the range of -30 to 0dBm (1μW-1mW) to maximise sensitivity but avoid saturation effects in the Optosci InGaAs rack mounted power meters, LNP-2 photoreceivers. The in-line attenuators available were rated at 3, 5, 10, 15 and 20dB (50%-1% transmission) at 1550nm. Wavelength spectra measurements could be made at any port using the Optical Spectrum Analyser (OSA) as required.

The test bed configuration can be used for other measurements and characterisations, and the details of how this configuration is used are described in more detail along with the results of the investigations in chapters 4 and 5. In particular, with SBS gain being strongly dependent upon the optical bandwidth of the propagating light within the fibre, various pump seeds were designed to control the pump spectrum to obtain the required characteristics and their output spectra and those of the resulting pump outputs required measuring. Additionally, a separate configuration that includes a fibre resonator is required to measure the effective bandwidth of the wavelength dither of the signal used both for SBS suppression and WMS detection, whose spectrum is too narrow for the OSA to resolve.

In summary, the fibre test bed system enables various, individual measurements to be taken of signal, input and residual pump and backscatter power (averaged and time resolved) as well as their wavelength spectra via taps that ensure that the high power is separated from the experimentalist and equipment that would be prone to damage from it during Raman amplification investigations.

3.1.2 The Counter-pumped Test Bed

A similar test bed was required for Raman amplification experiments conducted in the counter-pumped configuration. Some improvements were made to the original co-pumped test bed design and details of the changes are discussed in Section 3.7.2 but are indicated by using dotted lines on the components that have been placed differently in the schematic of the counter-pumped test bed configuration, Figure 3.2.

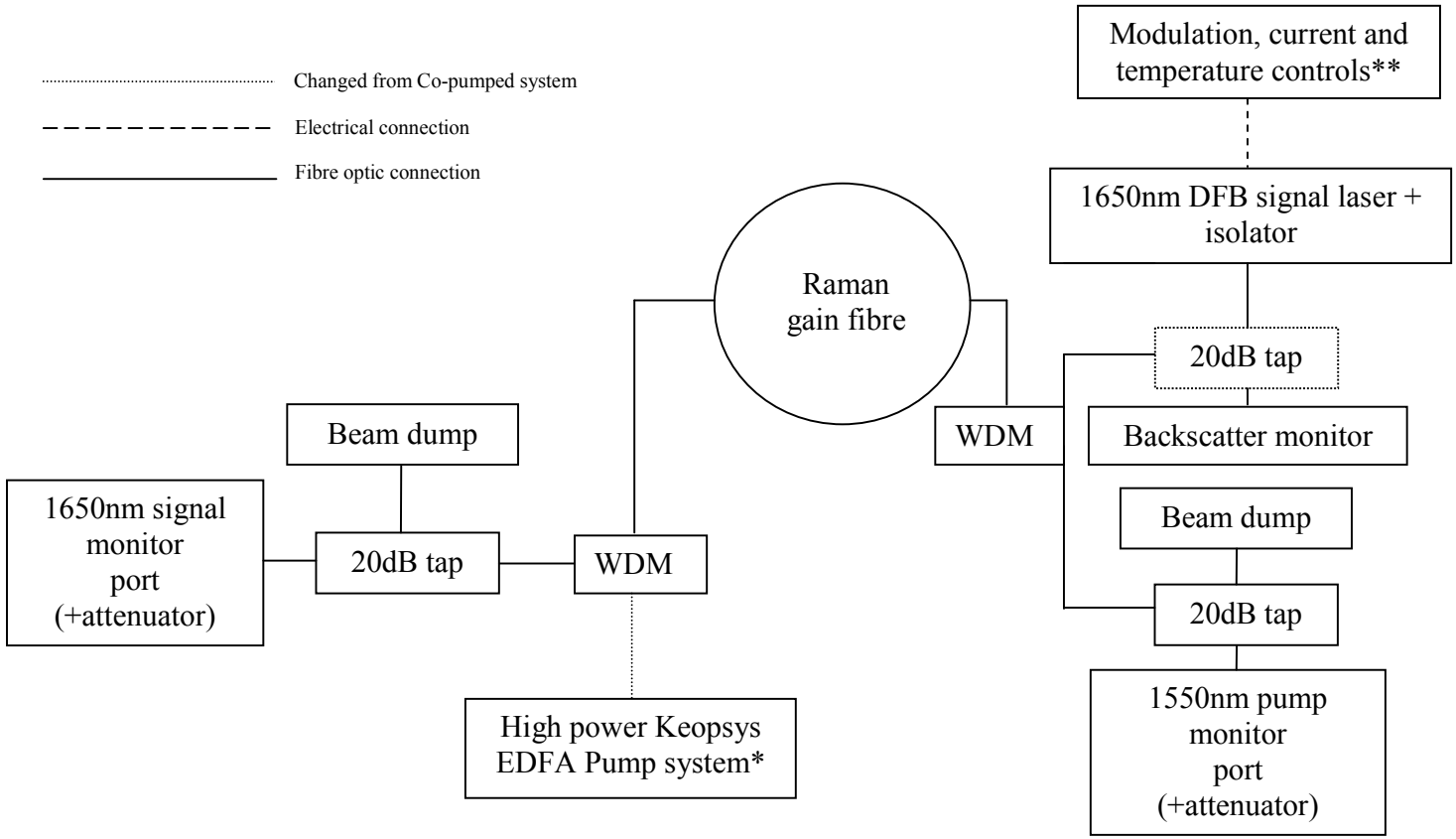

Figure 3.2 Schematic of counter-pumped Raman amplifier test bed (for SMF-28 and DSF)

The most obvious difference between the co and counter-pumped Raman systems lies in the fact that the main pump EDFA and the 1550nm beam dump have been swapped around so that the pump and signal can counter-propagate within the gain fibre. Additionally, the backscatter monitor tap was removed from the path of the pump in an attempt to reduce insertion loss and backscatter centres. This was made possible because SBS was fully suppressed in the pump during the initial experiments, which were carried out using the co-pumped configuration. However, monitoring of the backscatter arising from the narrow bandwidth signal was still required.

3.1.3 Additional Considerations for the Investigation of the Raman Amplifier

The test beds were used over the duration of the project for several different investigations and within these amplifier systems, there are a range of variations. Firstly, the EDFA pump can be either a 30dBm (1W) or 37dBm (5W) Keopsys benchtop EDFA, the 1651nm Raman seed can be generated by either a 5 or 20mW DFB and the Raman gain fibres used in investigations were OFS specialist Raman fibre, standard single-mode fibre and Sumielectric DSF (dispersion shifted fibre) as defined in Chapter 2.

At each of the monitor ports (signal, residual pump, backscatter and input monitor) it is possible to measure power level (averaged using an OptoSci power meter, or time resolved using a Thorlabs photoreceiver connected to an oscilloscope) or wavelength spectrum using an Agilent 86140B optical spectrum analyser (OSA). High power signal levels were at times monitored at high power from the 99% tap port and this was conducted using a pyrometer (thermal power meter). The exact combination of these options is stated for each of the individual investigations.

The three different fibres were tested as Raman gain media in co and counter-propagating configurations, including a specialist Raman fibre designed and marketed specifically as a medium for parametric Raman amplification, meaning a high Raman gain coefficient, relatively low attenuation and reasonable splicing

properties with standard fibre. This fibre is also the most expensive at around £1/m. In addition to this, systems were constructed of standard single-mode communications fibre and DSF, the former should make optimal splices with the test bed, but produces poor gain per unit length and the latter fibre provides a compromise between gain coefficient and splice compatibility with standard fibre and price when compared with the other two fibres. Given this range of gain fibre types, it was expected that an optimal amplifier type, in terms of overall merit, could be found or at least deduced for the application.

3.2 The Raman Signal Source and Drivers

3.2.1 DFB Signal Source

Throughout all of the Raman amplification experiments, a 1651nm DFB seed source is used as the source for the Raman signal seed. In some initial experiments, a 5mW laser was used and the rest was conducted using a 20mW variant. The selection will be stated in the case of each investigation. The current tuning rate of the 5mW laser was found to be 737MHz/mA in previous work [3.2].

The 20mW DFB laser was characterised in terms of current tuning by applying a 1V ramp @ 5Hz to the DFB while transmitting its output to a photoreceiver/oscilloscope via a fibre resonator (of FSR 0.4275GHz). This resulted in the observation of 78 interference fringes per ramp at the output of the interferometer, corresponding to a total frequency shift across the current ramp of 33.35GHz. The driving Thorlabs LDC 202B has a DC current tuning rate of 20mA/V and has a specified 3dB modulation cut-off at 3kHz, therefore the current ramp was ~20mA and the tuning rate deduced. The current tuning rate of the 20mW DFB laser was found to be 1.67GHz/mA. The output power of the 20mW DFB was measured using an optical power meter as a function of input current (as read from the LDC 202B current controller) and this characterisation is shown in Figure 3.3

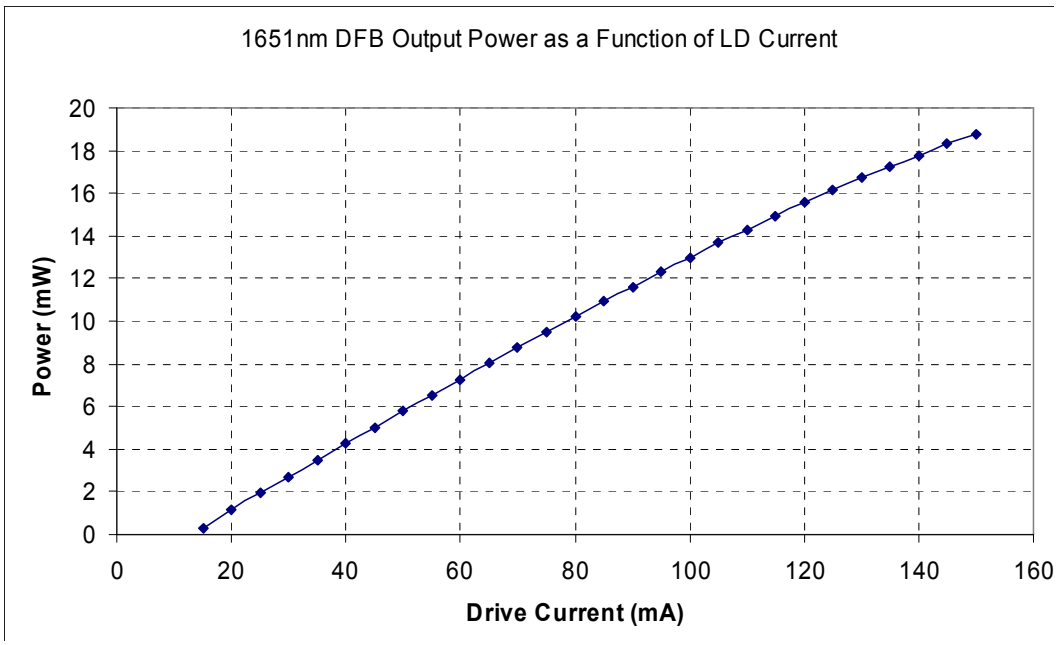

Figure 3.3 Output power as a function of drive current for the 20mW DFB signal laser.

3.2.2 Modulation Control

The DFB laser controls necessary for methane sensing and SBS suppression (as lumped in Figure 3.1** and Figure 3.2**, where the asterisks indicate their position within the configuration) are shown in Figure 3.4. The ramp was only applied during gas sensing experiments, whereas the dither was applied for all high power amplification experiments unless otherwise stated.

In order to produce a wavelength ramp and dither, a corresponding current ramp and dither was applied to the signal DFB laser. As can be seen in Figure 3.4, a bias T is used to mix the DC drive current and high frequency dither current before the swept and modulated current is fed to the DFB laser. This was necessary because the bandwidth of the laser drivers was restrictive in the dither frequencies that could be applied without approaching cut-off, where the driving modulation voltage provides decreased modulation at high frequencies (hundreds of kHz) when compared with that at low frequencies. A schematic of the bias T can is shown in Figure 3.5

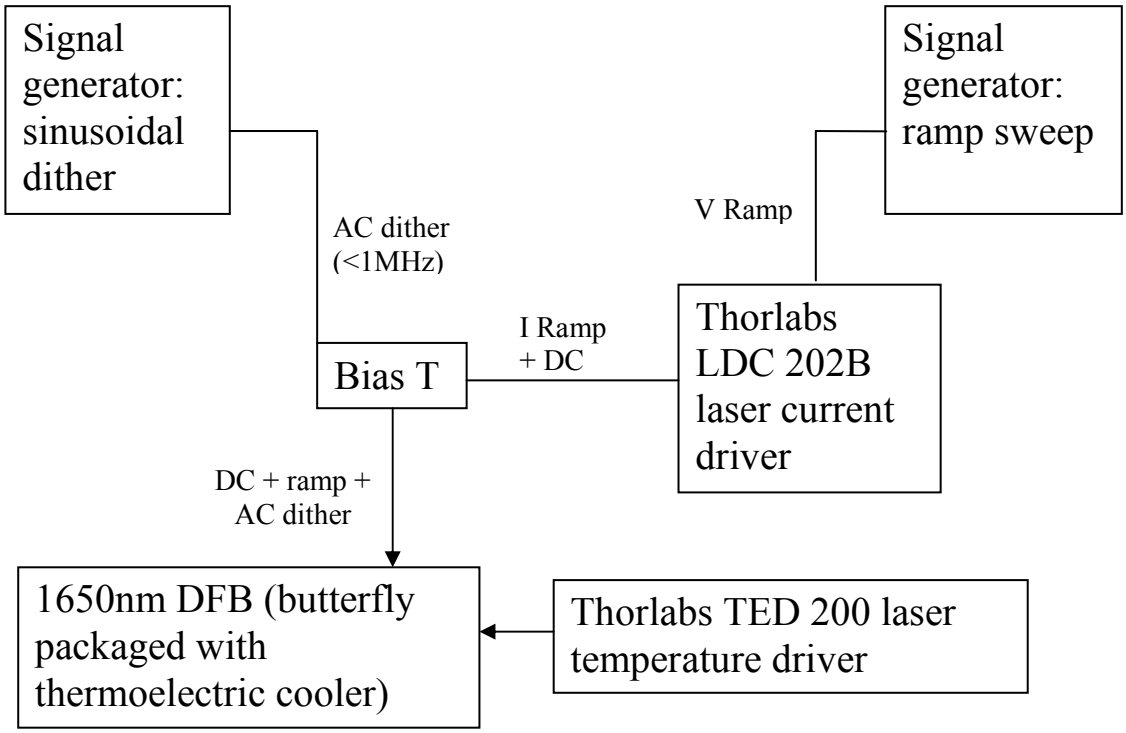

Figure 3.4 Laser control and modulation system

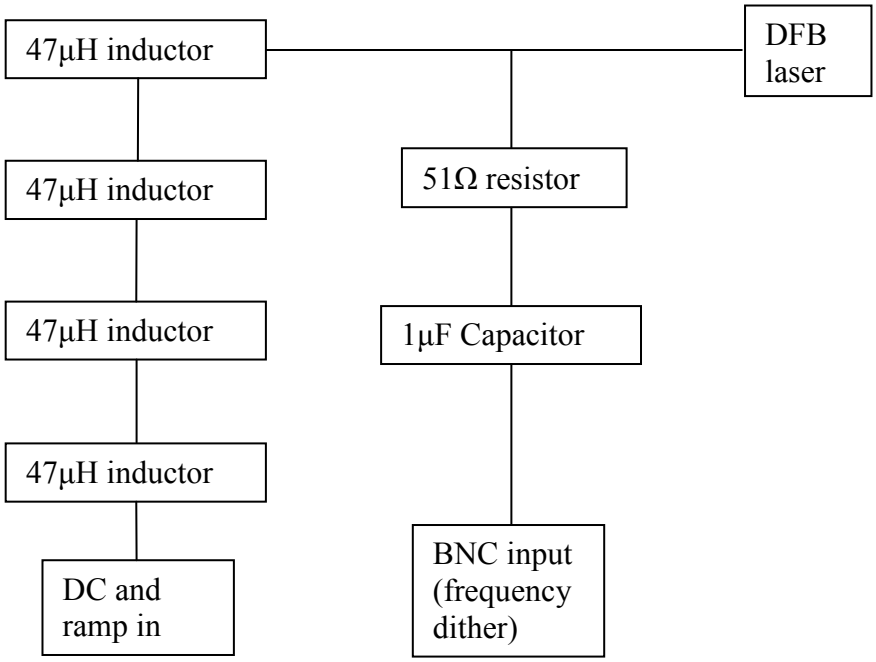

Figure 3.5 Schematic of Bias T for applying current modulation to DFB signal laser

The bias T passes only low frequency through the DC and ramp arm, where the cut-off is around 1kHz, on the other hand, any DC bias will encounter a very high resistance at the AC input via the capacitor with a low frequency cut-off of around 3kHz. This allows applied modulation and DC current to be fed directly to the laser diode unchanged, unlike the case where the modulation is applied via the current controller. It can be seen from the bias T schematic that there is no in-built protection against over-modulating the laser, as this was suspected of changing the modulation parameters applied. Therefore, care must be taken while setting the modulation parameters and it was practice that the modulation parameters were set and checked and the diode laser fed the appropriate bias before the AC modulation was connected to the function generator. This reduced the risk of applying a spurious modulation to the laser or a negative bias through the dither modulation while the DC bias was off. During gas measurements, the ramp was set at 1V pk-pk, resulting in a 20mA sweep, which in turn provided a frequency sweep of 33.35GHz. This could have been set higher if desired until the current would be reduced below lasing threshold from its 110mA DC setting (thus allowing around 165GHz sweep), but it was not necessary and further sweep depth would have had a strong effect on amplifier output power. When considering the dither depth available, it was recalled that the system is for methane sensing first, hence the modulation depth was limited to 3GHz, which corresponds to a modulation index of ~2 for the desired 1650.95nm line, which is optimal for methane sensitivity of the system. This was found to require 3.8V modulation via the bias T at the chosen dither frequency of 377kHz (chosen for optimal SBS suppression, as well as low multi-path interference (MPI) in Chapter 4 observed at the detector, see Section 4.10.3 for MPI). Given that the 3dB bandwidth of the photoreceivers used during gas sensing were around 1MHz, it was considered necessary to keep the modulation frequency under 500kHz to allow effective detection of the 2f signal without a significant response penalty.

3.3 Configurations for the Investigation of SBS of a Narrow Band Source

3.3.1 Configuration for the Observation of SBS of a Narrow Band Source

Having established the test bed configurations and the signal generation apparatus, it remained to carry out some preliminary investigations before Raman amplification could begin safely. Firstly, an experimental configuration is required to initiate and observe SBS in a narrow bandwidth signal. This validates the requirements that a broad bandwidth pump is to be used to pump the Raman amplifier and that the strategies considered in Chapter 2 for suppression of SBS of the signal are required to be put in place. A more detailed investigation into SBS backscatter of a narrow bandwidth source emission was undertaken in the OFS Raman and DSF fibre systems for comparison with theory in order to provide a more detailed insight into the effectiveness of wavelength dither as an SBS suppression technique for the amplified signal. This gives an insight as to whether SBS free, high power Raman amplification can take place with the proposed set of SBS suppression strategies before going ahead with the generation of high power signals. It was decided that, both the occurrence of SBS and its extent should be observed before work into its suppression and detailed modelling were carried out. The co-pumped OFS Raman fibre system was arranged with a power meter at the backscatter tap. The 1W Keopsys EDFA was seeded using a 'standard band' Santec tuneable laser set to 1550nm and its output launched into the Raman system via the pump input port. The backscattered power was measured as a function of input power for the 15MHz and 160MHz bandwidth modes of the tuneable laser. The 160MHz bandwidth emission is achieved via a fast phase modulation and the effective bandwidth was given in the product data sheet. The conditions are outlined once more along with the results in Chapter 4. This SBS observation arrangement is shown in Figure 3.6.

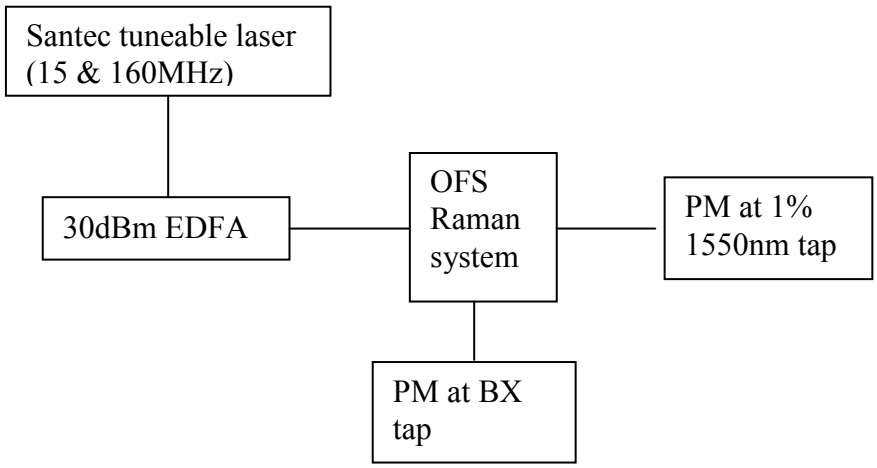

Figure 3.6 Configuration for observation of SBS of a narrow bandwidth signal

Comparing the signals at the 1550nm 1% tap (usually for residual pump on the co-pumped test bed) and the 1% backscatter taps, the proportion of backscattered power could be recorded as a function of input power for each of the bandwidth modes. The results are shown in Section 4.4

3.3.2 Configuration for the Investigation and Characterisation of SBS of a Wavelength Dithered Narrow Band Source

Further to this preliminary investigation, backscattered power was measured as a function of the frequency of the applied sinusoidal dither, which will be referred to as dither frequency, (for a constant input power and dither depth) and subsequently as a function of dither depth (i.e. the peak to peak frequency deviation of the laser) as at the optimal SBS suppressing dither frequency at constant input power.

SBS of the output of a narrow bandwidth source was deliberately instigated in the gain fibres, again in order to investigate the importance of dither frequency and dither depth parameters with respect to the suppression of SBS. For these investigations, a 1550nm DFB laser was used to seed the 30dBm (1W) Keopsys EDFA and backscattered power was measured as a function of dither frequency at a single dither depth in order to validate the relationship between optimal dither frequency for SBS suppression and fibre length by establishing optimal dither frequencies. The optimal dither frequency results for OFS fibre are shown in Section

4.4.2. In the second investigation, the DFB dither frequency was maintained at the experimentally determined optimum for SBS suppression and 1% backscatter powers (relative to the input power) were recorded for a range of dither depths for comparison with theory. This was conducted for OFS Raman fibre and DSF fibre amplifier systems. The configuration for the dither frequency and dither depth SBS suppression characterisations is shown in Figure 3.7.

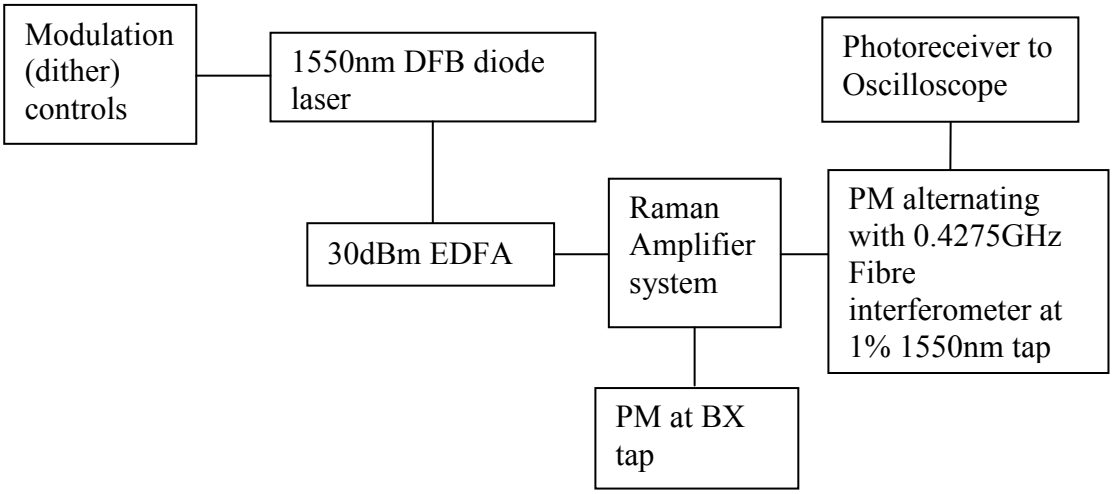

Figure 3.7 Configuration for the investigation of SBS backscattered power as a function of dither parameters

Given that the DFB laser's dither depth response to modulation is dependent upon the dither frequency, the dither depth was monitored using the 0.4275GHz FSR fibre resonator for each dither frequency setting. The modulation voltage was varied as necessary during the dither frequency investigation so that the same number of interference fringes were visible on the oscilloscope from the output of the resonator at each dither frequency, thus keeping the dither depth constant.

When measuring the 1% backscatter threshold as a function of dither depth, the dither depth had been found as a function of applied modulation voltage in a characterisation before the investigation. In order to do this, the dither frequency was set to the optimal SBS suppression frequency for the fibre being tested and the dither depth as a function of applied modulation voltage was determined using the 0.4275GHz fibre resonator. This was then used to characterise the dither depths used for SBS suppression at the required dither frequencies. Once more, this process was

repeated for each of the fibres tested because their optimal dither frequencies were different, potentially leading to a different response of the laser and drive electronics to dither voltage. The dither depths were measured to be 1.16GHz/V at 27.1kHz (for 4.5km DSF fibre) and 0.861GHz/V at 74kHz (for 1.4km OFS Raman fibre), which were found to be the optimal dither frequencies for suppressing SBS.

3.4 Development of Broad Bandwidth EDFA Seeds for Providing an SBS-Free Pump Source

In order to use an EDFA as a pump source for the Raman amplifier, its output spectrum must be controlled in order to supply photons that can be efficiently seeded to provide SRS at 1651nm in the Raman gain medium. The EDFA is an amplifier with a broad gain bandwidth and requires a seed, or signal in order to produce a useable, stable output spectrum. The seed source injects an appropriate band of photons to stimulate emission from the excited Erbium atoms in the main EDFA's gain fibre. In order to maximise the Raman amplification of a signal at ~1651nm, the seed spectrum must be optimised, and in order to achieve this several seed sources were designed and tested in terms of how their wavelength spectra affected the pump spectrum. These pump spectra could be compared with the calculated Raman gain efficiency of a 1651nm Stokes wave as a function of pump wavelength.

Given the characterisations of SBS arising from dithered narrow bandwidth sources (see Sections 4.3 and 4.4) together with the theoretical analysis of the required bandwidth to suppress SBS in the pump, it was clear that the bandwidth of the pump spectrum must be sufficiently broad to prevent the stimulation of Brillouin scattering of the pump power in the Raman gain medium. In addition, the output power and spectrum should be stable and it is required that the output is unpolarised to minimise noise in the output signal. The most convenient and economical way of producing a system that met the requirements was to employ a filtered ASE source. These sources were constructed using combinations of small benchtop EDFAs (OptoSci 10dBm Ed kit models) and a range of filters as well as a loop mirror to maximise the

ASE available for filtering. These filters included 1531nm and 1551nm CWDM filters, both with a ±7nm bandwidth, as well as a DWDM filter with 1538.87-1541.46nm pass band. Additionally a Dicon manually tuneable, band pass filter of bandwidth 0.2nm (at 1dB) and tuning range between 1529-1564nm was employed. The ASE source systems' output spectra were investigated with respect to changing the filter type and position within the optical system. The configurations of interest are described in more detail, along with their characterisations as discussed in Section 4.5.

3.5 Further Raman Amplification Investigations

Given a broad bandwidth pump and the appropriate SBS suppression techniques in the signal, Raman amplification could take place up to high power levels. Given this ability, polarisation dependent gain (PDG) was investigated for the broad bandwidth pump source using the co-pumped OFS Raman fibre system. In order to do this, the polarisation of the linearly polarised input signal was varied using a fibre polarisation controller, which was inserted into the system before the 1650nm input port. The signal power was maximised and minimised in turn with respect to input pump power at a number of different pump power levels to determine the extent of PDG, if any. The polarisation was altered by changing the position of the paddles on the polarisation controller. The main investigations involved the measurement of Raman signal and residual pump power while monitoring backscattered power as a function of input pump power, enabling validation of the Raman models as well as information on the maximum signal power available compared to the calculated requirement of 1W.

3.6 Construction of Raman Amplifier Systems and Special Fibre System Construction Techniques

3.6.1 Considerations in the Construction of Fibre Systems Using Specialist Fibres

During the construction of the Raman test beds, there were some considerations to make the system reliable and efficient. The two main considerations were that, in incorporating non-standard fibres into the system, the loss across splices can become significant and secondly, that standard FC-APC connectors are unsuitable for coupling power in the order of Watts.

With the test bed design established the fibre components were fused together into a complete system. This can be a complicated process when splicing different fibre types together and there is some discussion of the specialised techniques employed to do this while characterising the insertion losses of the system accurately. All of the splicing was carried out using a Sumitomo Electric Industries Type 35SE fusion splicer. These techniques include a method of monitoring the insertion loss of a splice while it is taking place and a technique for achieving improved splicing of unlike fibres in terms of minimising loss and backscatter.

3.6.2 Live Splice Monitoring

Building a high power fibre system with different fibres, both in terms of core size and composition, requires some techniques beyond those for normal splicing procedures. These techniques are used to monitor and minimise splice losses to allow the construction of an efficient and robust amplifier system. The required setup for live-monitored fusion splicing is detailed in this section, with a schematic of the required apparatus below in Figure 3.8, including details of the source receive module used to transmit a known power through a system and read the throughput in Figure 3.9. This process allows the measurement of individual splice losses while the splicing is taking place, rather than completing the entire system then measuring the total end-to-end loss. This allows more efficient location of a defective splice or connector and can be used as a tool to optimise a splice while it is taking place.

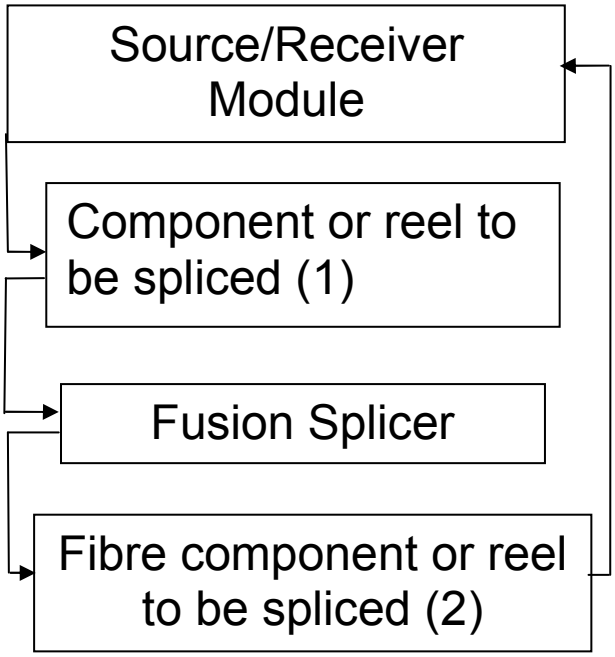

Figure 3.8 Schematic of live splice configuration

The signal is transmitted from the source receiver, through the system being spliced and the transmission is then read back at the photoreceiver.

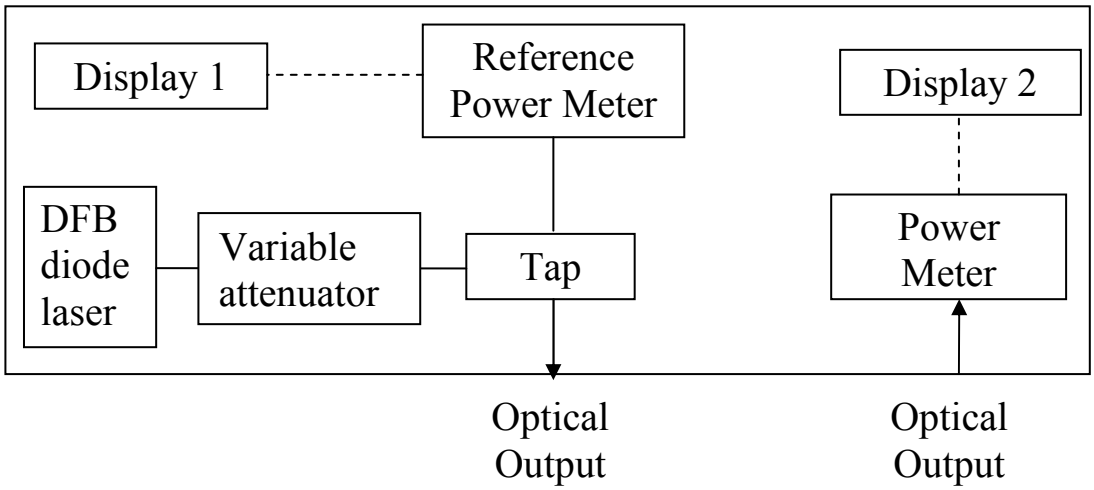

Figure 3.9 Schematic of source receiver unit.

In practice, the OFS Raman fibre reel was spliced to a standard communications fibre-optic component (tap or WDM), where one end of the fibre component was spliced with an FC-APC pigtail so that it can be connected to the output of the source receive unit, and the other was cleaned and cleaved. After cleaving, this free end of

the component is fitted with a bare fibre adaptor (BFA) so that it can fit directly into a power meter, or the receive port of the source receiver. This allows measurement of the insertion loss of the component and its connection to the source, so that this can be discounted against the loss across the whole system (component, fibre reel and the splice between them) to find the splice loss in isolation after the two items are spliced together. The aim of this is to acquire a more accurate value for the loss across the splice between the component and the specialist fibre, when only a value for total insertion loss will be available after splicing has taken place. The insertion loss of the fibre gain medium also needs to be taken into account for the same reason, but since in this example of splice monitoring the fibre is non-standard, it cannot be spliced to a pigtail for an accurate insertion loss measurement, since the loss in the splice to the pigtail could be significant and uncertain (the splice loss would almost certainly be more variable than the attenuation data from the manufacturer). Instead the loss should be taken from data supplied with the fibre module or reel.

After a note of the component insertion loss has been taken, the fibre end fitted with a BFA should then have the BFA removed, be cleaned and re-cleaved and placed in the fusion splicer along with the prepared end of the Raman gain fibre. The output end of the Raman fibre is cleaved and fitted with the BFA and plugged into the receiver part of the send receive unit so that the transmitted optical power through the joint can be measured and compared with the launch power. The overall system loss, minus the component loss and the loss over the fibre reel is the loss across the splice after it has taken place. In splicing two fibre components or reels together, the splice loss can be monitored live during the splice. This is of particular use in iterative diffusion splicing techniques, typically used on unlike fibres whose union is not straightforward and does not lend itself readily to a prescribed splice recipe.

3.6.3 Diffusion Splicing

Using diffusion splicing, fibres are fusion spliced together using an arc of relatively short duration, which builds an excess of material around the splice. This can be called the tack splice since its prime purpose is to form a rudimentary tack between the fibres with the cores aligned. The splice can then be re-arced to obtain a gradual melding of the cores of the fibres, with the surface tension of the liquefied cores

pulling them together during the arc. This gradual diffusion of the cores into one another as opposed to an abrupt change helps to reduce splice loss and Fresnel reflection between fibres with different core sizes and compositions as the coupling of the mode fields is more efficient and the refractive index step smaller.

There are different methods of setting a fusion splicer to perform a diffusion splice; it is possible to set parameters to conduct this in one splice program, but in the construction of the experimental system detailed here, it was conducted using a standard single-mode splicing program with a short arc duration to perform the initial 'tack' where the fibres are first fused with a subsequent series of re-arcs to improve the splice. This process was developed in preliminary investigations using spare standard fibre and samples of the OFS Raman fibre. The number of times that a splice joint should be re-arced can be determined using the live splice technique, where light is passed from component 1 through the splice into a receiver at the output end of component/fibre 2 (see Figure 3.8),as described previously. With successive re-arcs, the transmission across the splice should improve, but with a diminishing benefit with every arc. The transmission improvement should be monitored until two successive re-arcs gain no significant improvement, as over-arcing can begin to increase loss, make the splice very weak, or destroy it altogether.

3.7 Details of Raman Amplifier Systems

3.7.1 OFS Raman Fibre System

The first fibre tested was a specialist Raman fibre from OFS Fittel, whose parameters are stated in Chapter 2. The system was built in the co-pumping configuration and construction began around the gain fibre using the live monitored diffusion splice technique described previously. Building in this order rather than from the input side first allowed more convenient direct monitoring of the splice quality between the gain fibre and its adjacent components. A number of splice recipes were investigated in order to obtain the optimum splice between the standard fibre and Raman fibre of considerably smaller core and higher germanium doping concentration, but it was

found that the optimal procedure was the standard splice program followed by numerous re-arcs, i.e, the diffusion splicing routine and live monitoring as described previously. Typically, the tack splice reduced the loss across the junction to less than 10dB, and around 8 re-arcs would then bring the loss to around 0.3dB. The insertion loss of the Raman system from the source to the fibre gain medium and also the end of the fibre gain medium to the power meter including splices, components and patch cords but excluding the fibre attenuation in the fibre gain medium was 1.0±0.2dB (each side of the gain medium) at both 1550nm and 1650nm, as measured using the source receive unit for the 1550nm path and a 1650nm DFB of known output to measure the insertion loss along the 1650nm path. This parameter is not vital for quantifying the high power available at the high power output port based upon the 1% signal tap output. Only the ratio of the tap outputs is required for this, but it is necessary to have data on insertion losses into and out of the gain fibre so that the Raman output power can be compared with the theoretical predictions, since the models predict power at the end of the gain fibre based on power at the beginning of the fibre. Input pump power was deduced using the power monitor on the Keopsys EDFA unit and taking account of insertion losses as measured during the system build. The tap ratios, inclusive of additional attenuation added to the low power side of the tap couplers were 30.5±0.2dB at 1650nm and 35.3±0.2dB at 1550nm.

A high power (100mW-5W) pump is inserted into the system from the EDFA and therefore the connection should be considered. In the case of the co-pumped system, the Raman pump is fed from the EDFA via a specialised E2000 connector (E2000PS) specifically designed to carry high power as shown in Figure 3.10. This is then fed into a patch cord with an E2000PS connection on one side and a standard FC-APC connector with metallised ferrule on the other, which could then be connected to the standard FC-APC pump input connection on the test bed. A schematic of the connection is shown below in Figure 3.10.

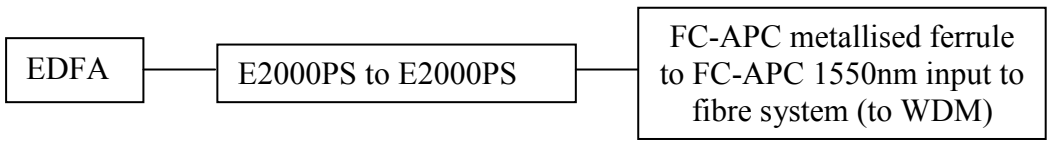

Figure 3.10 Schematic of connection between pump EDFA and pump input to the fibre system. Refer to * in **Figure 3.1**

The E2000 connector type clicks into its bulkhead, rather than manually aligning and screwing in like the FC-APC and this can reduce the chance of over-tightening connectors and makes the connection more consistent. It includes a spring-loaded dust-cover, which opens on connection into the bulkhead and otherwise remains closed to avoid contamination and scratching of the fibre end surface. The PS variant also has a tapered, expanded core at the termination to lower the intensity of the light and help reduce the chance of contamination or scratching of the fibre end-face. Scratching permanently increases loss and backscatter, in particular when the scratch is over the end of the fibre core. The loss is strongest when attempting to guide light from the damaged connector end into another connector rather than directly onto the photodiode of a power meter, and this point should be noted when attempting to locate a bad connection. Contamination from substances such as oil from the hands can lead to an increase in loss across the connection and furthermore can help trap highly absorbing contaminants on the surface, leading to a high loss. This can be rectified by cleaning with suitable solvent such as alcohol, but if the surface has become strongly absorbing while transmitting high power, oxidation may have taken place on the surface, which is essentially permanent.

In extreme cases, severe scratching or contamination can result in a fibre fuse in the case of connecting high optical intensities. Fibre fuse is where an absorbing artefact gives rise to a high build-up of heat, which cause the fibre to melt. This is most troublesome because the melting region of fibre travels backwards towards components since the molten glass becomes highly absorbing, converting most of the propagating laser power to heat. In the event of this, the procedure is to power down the high power source in the standard way as quickly as possible and cut away any burnt fibre and fibre components. A paper with good background information on the effects of end-surface contamination and fibre fuse can be found on the Furukawa website [3.1]

3.7.2 Standard Single-Mode and Dispersion Shifted Fibre Systems

The standard single-mode and DSF systems were of the same test bed configuration as shown in Figure 3.2 (although the DSF system was only tested in the counter-

pumped configuration), with the standard fibre gain reels (10km made from 4.5km and 5.5km reels spliced together) being replaced by the DSF reel in the same test bed. This became possible when it was clear that the standard single-mode system would be of no further use. Given experience with the OFS Raman fibre test bed, two alterations were made, which are marked with dotted lines in Figure 3.2. Firstly, it was found that the connection at the high power pump input port, as shown in Figure 3.10, was very prone to failure in terms of drastically increased insertion loss and burning, and on one occasion, resulted in a fibre fuse. The point in the connection at which problems occurred was at the connection at the FC-APC with metallised ferrule feeding into to an FC-APC connector with standard ferrule to connection as shown in Figure 3.10. These connectors simply screw in and out of a conjoining metal bulkhead, leaving variable insertion loss depending on the manually adjusted separation of the two connectors and the danger of damaging the end faces of the fibres by screwing them into contact with one another. There is also danger of contamination when the connector is exposed and scratching while fibres are being taken in and out of the bulkhead and it was factors such as those that were considered to be the main cause of frequent system failure. The 1650nm Raman seed signal is small and therefore a standard FC-APC (angle-faced to minimise Fresnel reflection at connector end-face to maximise stability) connection is used to insert the 1650nm beam from the DFB into the fibre system.

It was considered necessary to have the main EDFA connectorised, otherwise these costly units would be dedicated to only one test bed if spliced. In order to make this as reliable as possible, the input of the test bed was fitted with an E2000PS pigtail, which simplified the input and greatly reduced the frequency of system failures. It should be noted that a reliable, commercial unit should ideally have the EDFA spliced into the system and the connectors were only used for practical considerations not directly arising from the operation of a finalised system.

The insertion losses in the counter-pumped SMF-28 and DSF systems were 0.9±0.2dB insertion loss from the input to the fibre gain medium and 0.9±0.2dB between the gain medium and the power meter for 1550nm, and 1.1±0.2dB each side

at 1650nm, once more, all excluding the attenuation in the fibre reel. This has been omitted because the aim of taking the insertion losses either side of the gain fibre in the experimental investigation is so that the output powers can be compared with the theoretical values given by the Raman models, which calculate signal power and residual pump at the end of the gain fibre. The fibre attenuation is taken into account in these models, hence it does not need to be added as an adjustment to the experimental results. The relative transmission between high and low power taps was measured to be 31.7±0.2dB (~1200:1) at the 1650nm output and 39±0.2dB (~10000:1) at 1550nm. These effective tap ratios are inclusive of the addition of 10 and 20dB attenuators on the low power side of the tap to further increase the ratio. The same system was used for the DSF and the standard single-mode fibre, and the insertion losses and tap ratios remained unchanged when the gain fibre was replaced.

The second difference between the co and counter-pumping test beds was that, with SBS arising from the pump wave having been successfully suppressed in the OFS co-pumped system, the 20dB tap connected to the input side of the gain fibre thus constitutes a superfluous source of insertion loss in the path of the pump. The monitoring of backscatter arising from the signal was still relevant, however and so the tap was fitted at the 1650nm input. This allows backscattered signal power to be monitored without wasting tens of mW from the pump to insertion loss and the 1% tap arm as well as adding another pair of backscattering centres at the splices. If there were a large back-reflection of the pump wave, this could still be registered on the power meter since the WDM has a ratio of around 20dB, meaning that a readable amount of power would be seen on the occasion of a serious failure.

3.8 High Power Surface Backscatter and Initial Remote Methane Sensing Configuration

3.8.1 Extrapolation of Short Range Methane Sensing Performance to Long Range through Power Scaling

With the pump and signal effectively controlled and an optimised Raman amplifier having been constructed, it remained to build a transmit and receive system to direct the amplified 1651nm signal to a rough target surface, then collect backscatter from

the target. This allows the measurement of backscattered power from surfaces as a function of output power and range to validate models and extrapolations regarding sensitivity and range of methane sensing.

It should be recalled that the system is being designed as a long range (~100m) methane sensor that uses a backscattered WMS signal to inspect a chosen path for methane. It would be useful during the project to be able to test the sensor system in terms of methane sensing at short range in simulated lab environments, from which the performance of the system could be extrapolated as discussed in Chapter 2. Assuming that the only difference between methane sensing at short range and long range is the intensity of the backscattered light at the photodetector, it should be possible to calculate the required signal power as a function of range for a given methane sensing performance. In order to do this, two things required establishing; firstly the dependence of backscattered intensity on range from target to receiver, and also the signal power required to achieve a given performance at a given gas concentration at a given short range.

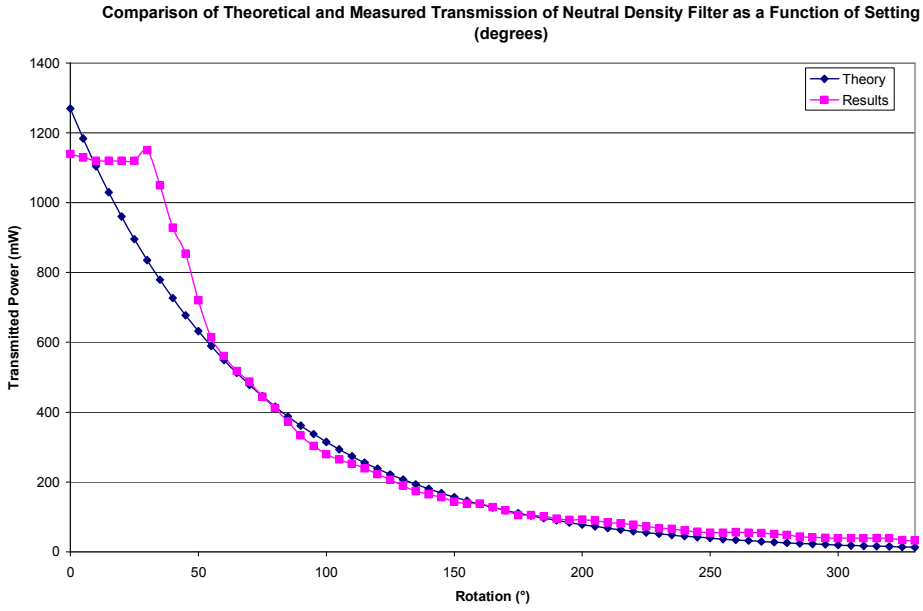

Figure 3.11 Characterisation of Neutral Density Filter. Refer to Figure 3.12***

The high power (99%) 1650nm output tap was fitted to a mounted collimator, which was directed towards a glass slide beam splitter to reduce the launched signal power

to the reflected power from the slide. The reflected power from the glass slide was then directed via a bulk optical variable attenuator. At either side of the glass slide and attenuator, the two lenses of a Kepler telescope beam expander were positioned as shown in Figure 3.12.

The bulk variable attenuator was essentially a neutral density film of graded optical density set in a disc, which could be rotated to set the attenuation. It could be adjusted to provide between 1% and 97.5% attenuation and was characterised by measuring the transmission of a 1.2W 1651nm signal from the Raman amplifier through the filter as a function of the position on the filter (degrees) using a pyrometer mounted on axis in the optical rail system. The characterisation of the filter and its comparison to theoretical (specified) values are shown in Figure 3.11. The specification states that the optical density of the filter varies with 2/330 per degree rotation. This characterisation was used to calculate the actual transmitted power given the power incident on the bulk attenuator.

The telescope system consisted of two biconvex BK7 lenses, the first of diameter 1.5mm and focal length 40mm, the second of diameter 4.5mm and focal length 120mm, expanding the beam by a factor of three.

The surface backscatter measurement configuration shown in Figure 3.12 was used both for quantifying backscattered power levels focused by the large (30cm diameter) Perspex Fresnel lens onto the Thorlabs photoreceiver unit as a function of distance from surface to receiver and for remote methane detection experiments. In the case of the backscattered power level investigations, the voltage levels output from the photoreceiver were read directly via an oscilloscope and had the background level subtracted from all of the results. This could then be back calculated to provide actual received powers to compare with theoretical backscattered power experiments. In order to convert the voltage level into an actual power, the expression $P_{\mu W} = 10^6 \times \left(\frac{V}{G\Re} \right)$ was used, where G is the transimpedence gain (set to 4.75exp(4)V/A) and $\Re$ is the responsively (0.9A/W at 1650nm).

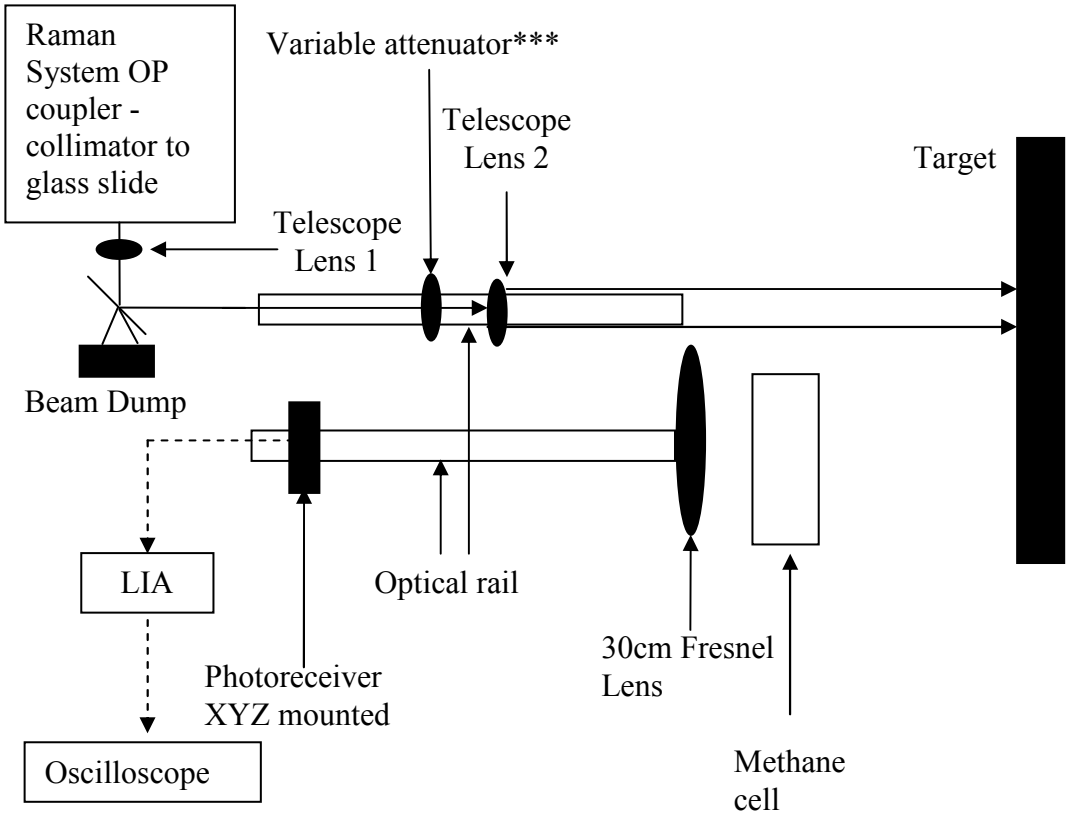

Figure 3.12 Schematic of Send/Receive optics

Stand-off methane sensing experiments were carried out using essentially the same apparatus as the backscatter investigation. The main differences were that the photoreceiver signal was sent to the LIA, whose output was then displayed by the oscilloscope, along with the requisite addition of a methane cell (box with transparent windows as will be described in Section 5.3.2) containing 0.1, 1 or 10% methane in a nitrogen-methane mixture placed in the path of the return beam. The gas cell was made up from two sides of clear Perspex and had an insertion loss of 1.8dB. The signal from the Thorlabs photoreceiver was preamplified at 40dB, before being fed to the Perkin Elmer Instruments 7280 DSP digital LIA. The LIA output was recorded onto a PC via Tektronix TDS3014 scope. Note that the 1% signal output tap was monitored during these experiments as well as using a pyrometer at the output beam as an additional method of monitoring the stability and magnitude of the output power.

In order to make optimised methane readings, the modulation index must be set to 2 for 1f and 2.2 for 2f detection. This means finding the optimal dither depth parameters on the laser, and so during initial gas measurements the gas signal, once obtained was maximised by changing the dither voltage. The optimal dither voltage at the chosen dither frequency and laser DC bias current level was taken to be the m = 2 and 2.2 for 1f and 2f detection respectively. This is an effective, if somewhat primitive way of optimising the WMS parameters, but the main point of interest here was only to optimise the gas signal strength, hence the treatment was considered to be appropriate.

3.9 Summary

The main outcomes of this chapter are that the test bed configurations for characterising the Raman amplifiers have been described along with the techniques used to construct them in addition to the types of measurements that they allow. The fibre system allows measurements to be made of input and output pump and signal, as well as backscattered waves. The measurements possible regarding these waves include spectral analysis, and (time resolved or averaged) power level. These can be conducted safely in fibre directly inserting connectors to the appropriate instruments. Additionally, the specific configurations for characterising SBS in the fibre systems have been described.

Given that the system would then be used in terms of methane sensing using signal backscatter at short range, the configuration for these stand-off gas sensing experiments has been described. This configuration allows measurable, adjustable, scaled down output signal powers while the amplifier was running at full power, to be launched in an expanded, collimated beam at a target surface. The surface backscatter was collected and the gas signal recovered in this configuration. In addition, the same configuration was used to validate the relationship between range and backscattered power to allow the scaled power gas measurements to be extrapolated to longer ranges.

3.10 References

[3.1] Koji Seo, Naoya Nishimura, Masato Shiino, Ren'ichi Yuguchi and Hirokazu Sasaki, Furukawa review "Evaluation of High-power Endurance in Optical Fiber Links" Freely available at web address. furukawa.co.jp/review/fr024/fr24_04.pdf

[3.2] Kevin Duffin "Wavelength Modulation Spectroscopy with Tuneable Diode Lasers: a Calibration-Free Approach to the Recovery of Absolute Gas Absorption Line-Shapes" Chapter 4, pg71 PhD thesis submitted to EEE University of Strathclyde, 2007

Chapter 4 Development of the Raman Amplifier System and Comparison with Theoretical Expectations

4.1 Aims of the Chapter

The aim of this chapter is to convey the results of the experimental investigations conducted to build and characterise the Raman amplifier systems against expectations resulting from the theoretical analysis of the systems. From these results, the mathematical models are validated, and a final high-power Raman amplified methane sensing signal source for inclusion into the remote methane sensor prototype system is developed and characterised.

Preliminary investigations using the OFS Raman fibre system are mostly concerned with confirming our understanding of the factors affecting Raman amplification and strategies to suppress SBS of the pump and signal. Given the results in the preliminary investigations of SBS, the requirement of a broad bandwidth pump source was established. Thus, the proposed broad bandwidth seed sources' spectra and those of the resultant pumps are shown and discussed. The initial investigations of SBS in narrow bandwidth sources also provided validation for the wavelength dither method of suppressing SBS. With SBS suppression in place in the pump and signal, Raman amplification experiments were carried out using the 1W and 5W EDFA units as the pump source.

Development of Raman amplifiers continued in order to achieve an optimal amplifier system and to provide a range of results using Raman gain media ranging from highly doped to standard fibre. From these results, the models could also be validated using experimental data from amplifiers made with fibres of low and high gain efficiencies over long and short gain lengths respectively in co and counter-propagating configurations, thus providing a full range of validation conditions.

Having established the preliminary results, the Raman amplification results are arranged in stages for each Raman amplifier system and this can be viewed collectively as the stages of a method of designing low noise, high power, efficient Raman amplifier systems using a combination of mathematical modelling and practical investigations.

The first stage of the method is concerned with the design of a Raman amplifier system, as directed by the model results in terms of power as a function of gain fibre length. This was generally chosen to provide adequate amplified signal power given the pump and signal source outputs available when the system was to be constructed. In the case of the OFS Raman system, this was chosen to maximise Raman scattering of the pump, whereas in the cases of standard SM fibre and DSF, there was consideration given to other factors that required using a shorter than optimal fibre to realise a useable amplifier.

The second step in the method is to characterise the system in terms of output signal and residual pump power as a function of input pump power while adjusting the SBS suppressing wavelength dither to optimise signal power before backscatter becomes a problem. This characterisation validates the Raman amplifier modelling, because the Raman models calculate output signal power and residual pump power given input pump and signal as well as fibre parameters as a function of distance along fibre. The calculated power levels from this model at the distance matching the length of gain fibre investigated in the practical experiments represent the predicted output parameters of the experimental configuration. Output pump and signal power

levels can be collated for the range of input pump powers available to produce output signal and pump power levels as a function of input pump power for a given signal power. In this way the output from the models and the experimental setup can be compared directly by measuring the output parameters as a function of the input pump power.

While increasing signal output via increased pump power in experiments, it is particularly important to monitor the signal quality for various problems that may occur. A discussion of the origin of these problems and how they can be identified and suppressed is included at the end of the chapter (Section 4.10). In the investigation of the OFS and DSF fibres, the SBS backscatter was characterised for validation of SBS suppression via wavelength dither and SBS models.

4.2 Calculation of Optimal Length of OFS Raman Gain Medium

The first stage in the construction of a Raman amplifier system, having already chosen the Raman gain medium around which it will be built, is to calculate an optimal gain fibre length using the amplifier model. This analytical method has been described in Chapter 2 and hence the results that determined the length of the OFS Raman fibre reel are shown directly. The theoretical signal evolution along the OFS Raman gain medium given 4W input pump and 4mW input signal at the start of the fibre in the co-pumped configuration is shown in Figure 4.1. Additionally, the gain per unit length is shown in Figure 4.2 using the same parameters.

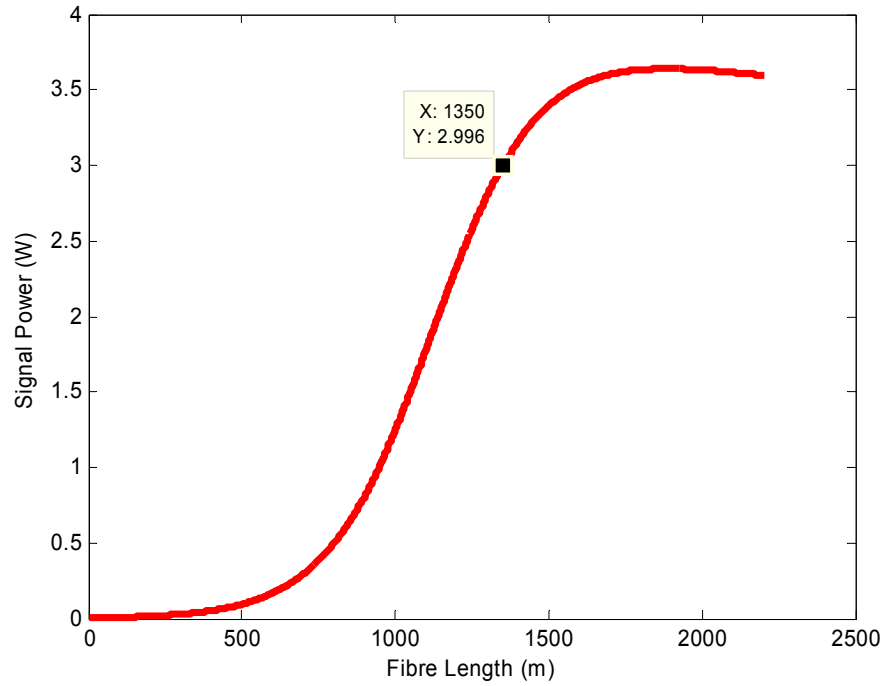

Figure 4.1 Signal evolution as a function of distance along fibre

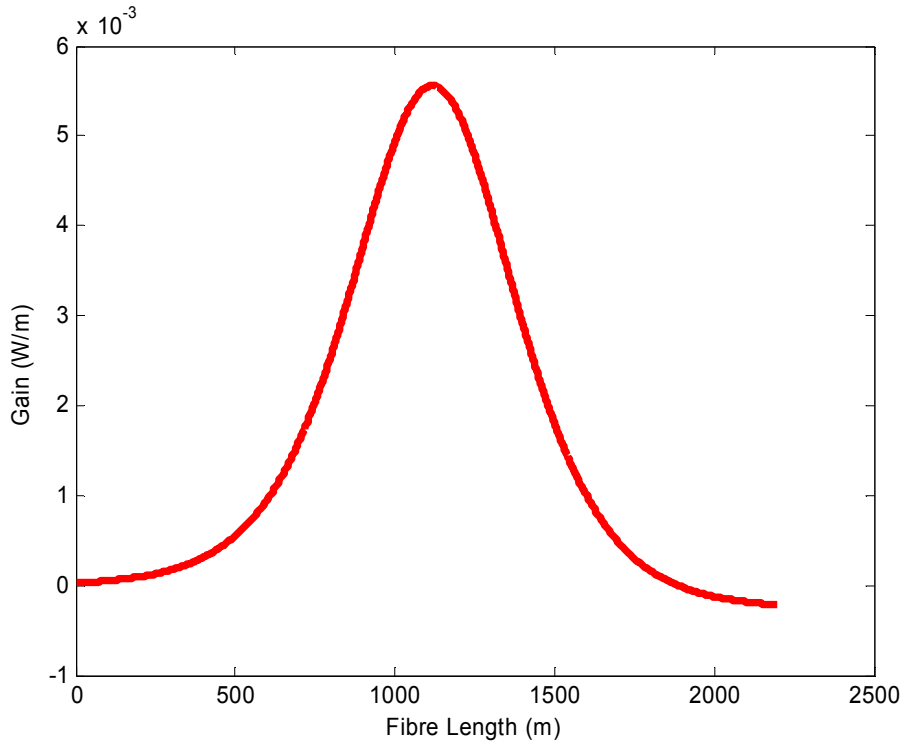

Figure 4.2 Power gain per unit length (W/m) as a function of distance along the fibre

From the results shown in Figure 4.1 and Figure 4.2, it was decided that a 1350m Raman fibre reel should be used for initial experiments, allowing a large proportion of the pump to be scattered into the Stokes wave. Using a relatively long fibre (with respect to the signal gain profile) also increased the probability of the occurrence of other non-linear effects that might require suppressing so that these can be identified and treated early in the design phase. In the first amplifier this was considered to be necessary in order to test potential SBS suppression strategies and identify any other effects that may be present in amplifier systems.

4.3 Preliminary Investigation of SBS Arising from a Narrow Bandwidth Source

From the theoretical analysis of the problem, it was apparent that SBS would impede the transmission of a high power 1540nm Raman pump through the Raman gain fibre, and any high power, narrow bandwidth 1650nm signal evolving within the medium. Given the considerable engineering resource potentially required to suppress SBS, the preliminary experiments were designed to test its actual extent in terms of transmitted power levels at which it appeared and backscattered power levels to be expected.

SBS of the output from a narrow bandwidth source in the Raman amplifier system was investigated, while at the same time, the effect of increasing the bandwidth of the same signal was observed. The aim of this was to observe the onset of SBS and to demonstrate the effect of signal bandwidth on SBS threshold. The OFS Raman amplifier system and test bed were arranged as shown in Figure 3.2 in Section 3.1.2, however, unlike the case of producing a Raman amplified signal, the 1W EDFA pump was seeded by the Santec ('standard band') tuneable laser of output bandwidth 15MHz at 1550nm, which is similar to that of a DFB diode laser. The laser was also equipped with a 'dither' function, which increased the bandwidth of the laser output to 160MHz according to the data sheet. The backscattered power level was

measured at the 1% backscatter tap as a function of insertion loss corrected input pump power. The results of this investigation are shown in Figure 4.3

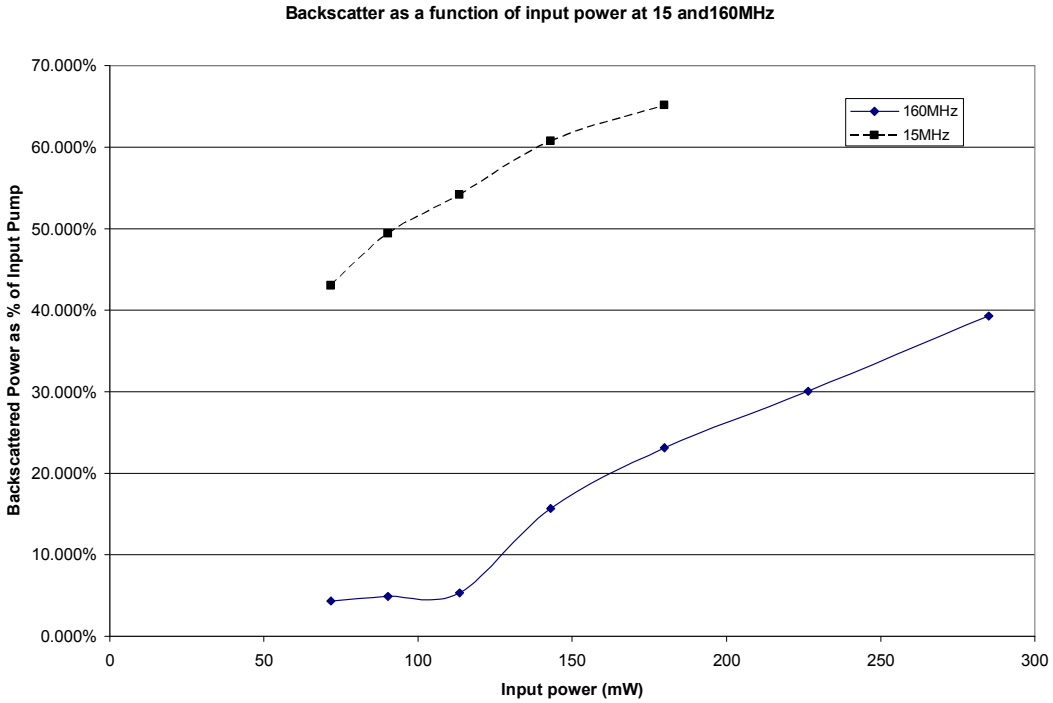

Figure 4.3 Proportion of backscattered power (%) as a function of input pump power (mW)

Figure 4.3 shows the proportion of the inserted power measured at the backscattered tap as a function of input power. The minimum input power shown in the figure was 72mW because this was the minimum launch power available from the pump EDFA while taking insertion loss into the fibre system into account. As SBS threshold is exceeded for any signal propagating within an optical fibre, the proportion of the propagating power scattered into the backward travelling Brillouin Stokes wave increases rapidly. The rapid increase in the proportion of the pump power being backscattered (not only the backscattered power level) distinguishes the SBS backscatter from Rayleigh and connector end backscatter as well as the backscatter level in cases where the SBS threshold is significantly exceeded. The SBS threshold can be defined in a variety of ways, one of which is, 'the inserted power at which backscattered power begins to increase rapidly' [4.1]. It should be noted that this definition is not that defined by Equation 2.31 in Chapter 2, but is useful in describing the results shown in Figure 4.3.

In the case of the 15MHz signal (top), this threshold appears to have been exceeded even at the lowest available input power level. Indeed the backscattered proportion of the signal is significant at over 40% and rising rapidly with input power. In the case of the 160MHz (bottom) series, it appears that an SBS threshold as described above is visible at around 115mW. Once this value is exceeded, most of the additional input power is backscattered out of the fibre. Comparing the two series, it can clearly be seen that the SBS threshold was increased in the case of the 160MHz series when compared to the 15MHz series, but after the SBS threshold was exceeded, it appeared that the proportion of backscatter would increase at a rate similar to that of the narrower bandwidth signal. The result of this indicates that SBS suppression by adjusting the bandwidth of the optical power in the fibre should be effective. However, it is also clear that the bandwidth required to propagate waves of the order of Watts in the fibre is considerably greater than those investigated using the tuneable laser. As a very rough calculation, assuming that the sharp increase in the proportion of backscattered power (115mW at 160MHz bandwidth) must be avoided in the 5W pump, we may scale the required bandwidth in the same way to say that 7GHz is the absolute minimum safe bandwidth for a 5W beam to be launched into this fibre system. That is not necessarily to say that any wave greater than 7GHz bandwidth is acceptable as a Raman pump, but it provides a threshold bandwidth under which there is a strong danger of damaging equipment, assuming that SBS threshold is proportional to pump bandwidth as obtained by combining Eqns 2.33 and 2.35.

4.4 Investigation of SBS of a Wavelength Dithered Narrow Bandwidth Signal in the OFS Raman Amplifier System

4.4.1 Principle of Suppressing SBS of a Narrow Bandwidth Signal Using Wavelength Dither

The principle underpinning the technique for suppressing SBS using a wavelength dither was described in Section 2.10.4. In summary, if a wavelength modulation is applied to a signal, the bandwidth, in terms of the stimulation of Brillouin scattering, is increased as the signal power is distributed over a broader spectrum as experienced by the whole fibre gain medium. This meant that the investigation of SBS of a wavelength dithered narrow bandwidth source was directly relevant to suppressing SBS in the Raman amplified signal.

4.4.2 Effect of Dither Frequency on the Efficiency of SBS Suppression using a Wavelength Dither

In order to provide optimised broadening, the dither frequency, i.e. the repetition rate of the dither modulation, needs to be chosen so that the full modulation bandwidth is present in the fibre all at once, i.e. the condition $f = \frac{c}{2nl}$ should be met (see discussion in Section 2.10.4), where f is the dither frequency, c is the speed of light in a vacuum, l is the Brillouin gain length and n is the refractive index of the medium. For the full 1350m length of the OFS Raman fibre, this required dither frequency is calculated to be 75.6kHz.

In order to verify the validity of the principle of using a dither to suppress SBS and also the dither frequency equation, SBS backscatter levels were investigated at a fixed dither depth over a range of dither frequencies. In this investigation, a 1550nm DFB laser was used to seed the 1W EDFA, the output of which was launched into the OFS Raman system and the backscatter measured. The output power of the EDFA was maintained at 20dBm (100mW), its lowest setting since it could be seen

from Figure 4.3 that it was easily possible to stimulate Brillouin scattering below this level and the backscattered power should be maintained at the lowest level practical for the safety of the equipment. The frequency of the wavelength dither was varied and the backscattered power monitored. Additionally, the dither was set at two different arbitrary depths (defined by the current dither depths as a % of the DC current level applied to the laser) in order to make a further qualitative observation of the effect of dither depth on SBS suppression, and upon optimal suppression frequency, if any. The results of this investigation for the OFS Raman fibre are shown in Figure 4.4.

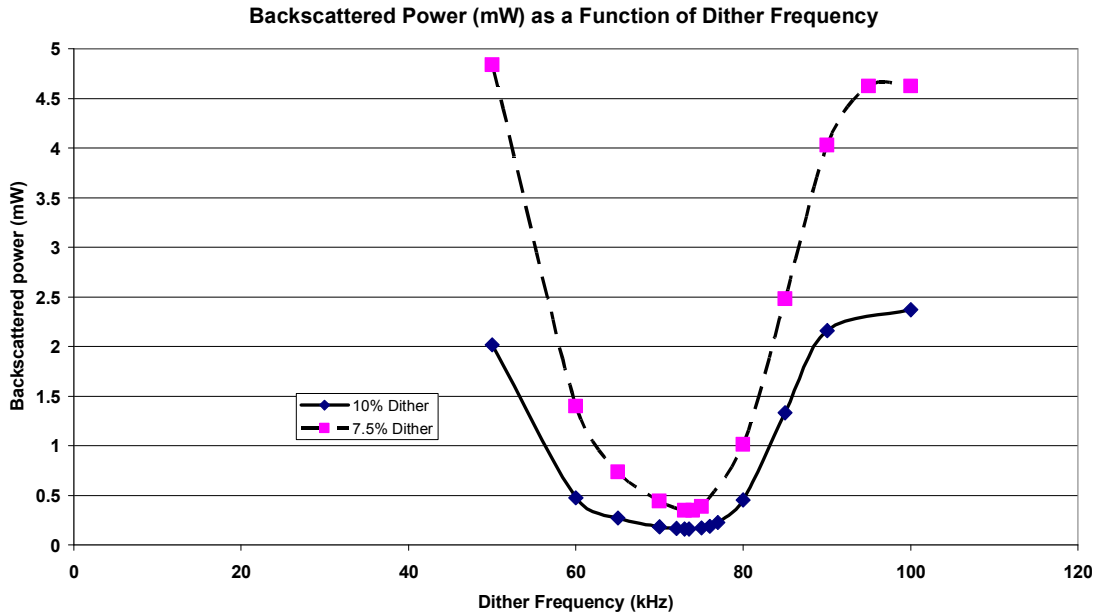

Figure 4.4 Backscattered Power as a function of dither frequency.

From Figure 4.4, it is clear that the effectiveness of frequency dither as an SBS suppression technique is strongly dependent upon the dither frequency. The optimal dither frequency was found to be 74.0±0.5kHz, which is in good accordance with the calculated value at 76kHz. In addition, increasing the dither bandwidth further increases the SBS suppression as expected and also increases the band of dither frequencies over which the SBS suppression could be considered to be effective. This is also intuitive, because the deeper modulation dissipates the spectral power over a boarder band, leading to an increase in SBS threshold for the signal and hence

a less pronounced dependence on optimising dither frequency at the same inserted power.

When applying the results of this investigation to the context of SBS suppression in the Raman amplified signal, it should be considered that this investigation was carried out using a pump wave whose power level did not change significantly during transit in the gain medium, except by the action of SBS. This is not so in the case of an amplified signal in the gain medium, where the input signal is small but increases potentially to Watts as it progresses through the gain fibre. This renders the equation for determining the optimal dither frequency ineffective for the application of selecting an optimal dither frequency for SBS suppression in the amplified signal, and the optimal dither frequency would be more readily determined empirically while Raman amplification is taking place, although the optimal dither frequency, if found empirically, could be used to gain a qualitative insight into the length over which the Raman signal becomes significant to support the models that calculate signal evolution along the fibres.

4.4.3 Effect of Modulation Depth on the Efficiency of SBS Suppression by Wavelength Dither in the OFS Raman Amplifier System

The positive result of the investigation of SBS suppression by wavelength dither invited further quantitative investigation of SBS suppression in the signal using wavelength dither, while underlining the potential importance of optimising the dither frequency to match the length of the fibre medium. SBS was investigated with regard to its response to effective bandwidth by varying the modulation depth of the 1550nm DFB, which was fed into the 1W EDFA. Using the same arrangement as before, the backscattered power was measured at the backscatter tap as a function of input power at a range of signal bandwidths. The results of this investigation are shown in Figure 4.5.

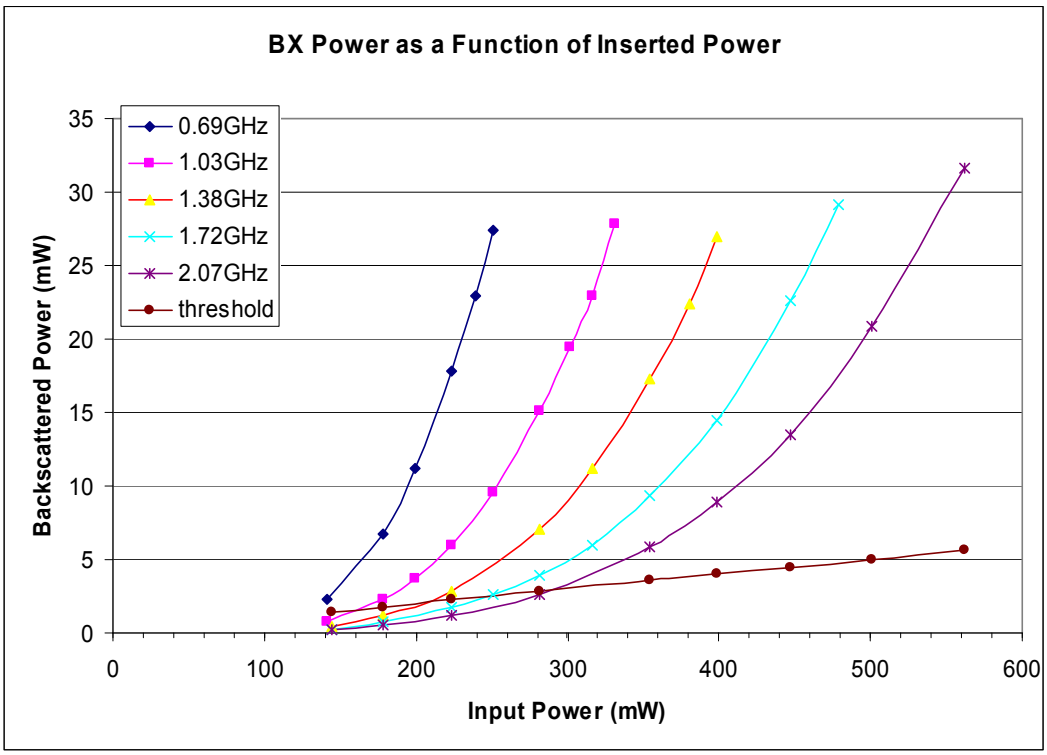

Figure 4.5 Backscattered power as a function of input power in the OFS Raman fibre system

In addition to the backscattered power as a function of input power in Figure 4.5, there is a plot of backscattered power equal to 1% of input power, and its intersections with the measured backscatter plots provide a 1% SBS threshold for each of the effective bandwidths launched, as defined using Equation 2.31 in Chapter 2. These threshold powers can be plotted as a function of bandwidth in order to form a relationship between SBS threshold and effective bandwidth and compare the experimental results with the calculated values.

Figure 4.6 shows the measured and calculated (from Equation 2.31) 1% SBS threshold power as a function of pump bandwidth for the 1350m OFS Raman fibre amplifier system. There is considerable discrepancy between the calculated threshold values and the experimental data, but this could be as a result of some approximations made in the SBS threshold calculations.

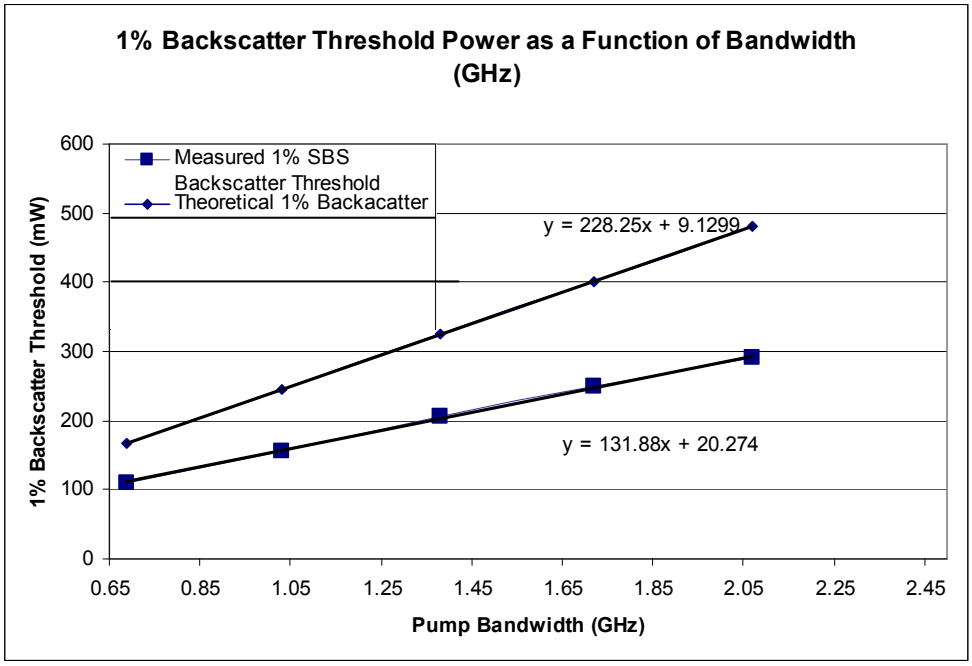

Figure 4.6 SBS threshold pump power as a Function of bandwidth for the OFS Raman fibre system.

Firstly, it was assumed that the sinusoidal wavelength dither depth was the effective pump bandwidth, given the optimised dither frequency, whereas this is not completely accurate. A sinusoidal modulation favours the frequency components at the extremities of the modulation (where the change in frequency is slow) in terms of the distribution of spectral power, which would allow some components of the pump frequency spectrum to exceed the SBS threshold before others. Additionally, it was assumed that all germanium doped silica fibres share a Brillouin gain coefficient, and the only fibre parameters varied between fibres modelled were effective area and length. This was considered to be acceptable because the variation in bulk photoacoustic properties of the germanium doped silica fibres should be small. The equation for a linear fit based upon the results is displayed on the plot and indicates that the SBS threshold power in mW for the OFS system is $P_{th} = 132 \times \upsilon_{pump} + 20$ where υ_{pump} is the frequency dither depth of the 1550nm DFB seeding the EDFA. This relationship should hold for signal bandwidths in excess of the 40MHz SBS gain bandwidth.

This, along with an optimal dither frequency for an amplified signal, should allow an approximate calculation of the 1% SBS threshold for any dither bandwidth. The dither frequency found to be optimal can be used as a tool to estimate the distance along the gain fibre at which Raman signal power becomes significant in terms of generating SBS, and the threshold as a function of bandwidth can be scaled with the effective Brillouin length. For the purposes of WMS targeting most of the near IR methane absorption lines, it is reasonable to have a dither depth of around 3GHz, [4.2] so calculations regarding suppression of SBS of the signal will be made using this as the effective bandwidth. Hence, using the OFS fibre as an example, the threshold over the entire fibre length for a 3GHz bandwidth signal should be around 400mW, but then given that the optimal SBS suppression frequency was around 200kHz (as will be seen in Section 4.6.1) rather than 74kHz, it could be argued that the SBS reaches threshold in the last ~1/3 of the fibre (since optimal dither frequency is inversely proportional to fibre length.) Given that the gain length is a factor of 3 less than that used to calculate the threshold if the entire fibre were involved in Brillouin Scattering, the SBS threshold increases by a factor of 3 to allow around 1.2W before SBS becomes significant (SBS threshold is inversely proportional to gain length, refer to Eqn 2.33). This was similar to what was observed, but the inaccuracy in finding the optimal dither frequency for a Raman amplified signal was considered to be too great to base a meaningful model upon this process. Hence it is not considered further.

4.5 Characterisation of Broad Bandwidth Seed Sources and the Resulting Pump Spectra

4.5.1 Configuration and Characterisation of Seed 1

With the need for a broad bandwidth pump source established, and investigations of the behaviour of narrow bandwidth sources within the gain medium, the

characterisation of the broad bandwidth seed sources and their resultant pump spectra using the two Keopsys units are discussed in this section.

This section gives an account of the configuration of the broad bandwidth source designated as Seed 1. A schematic of its configuration is shown below in Figure 4.7

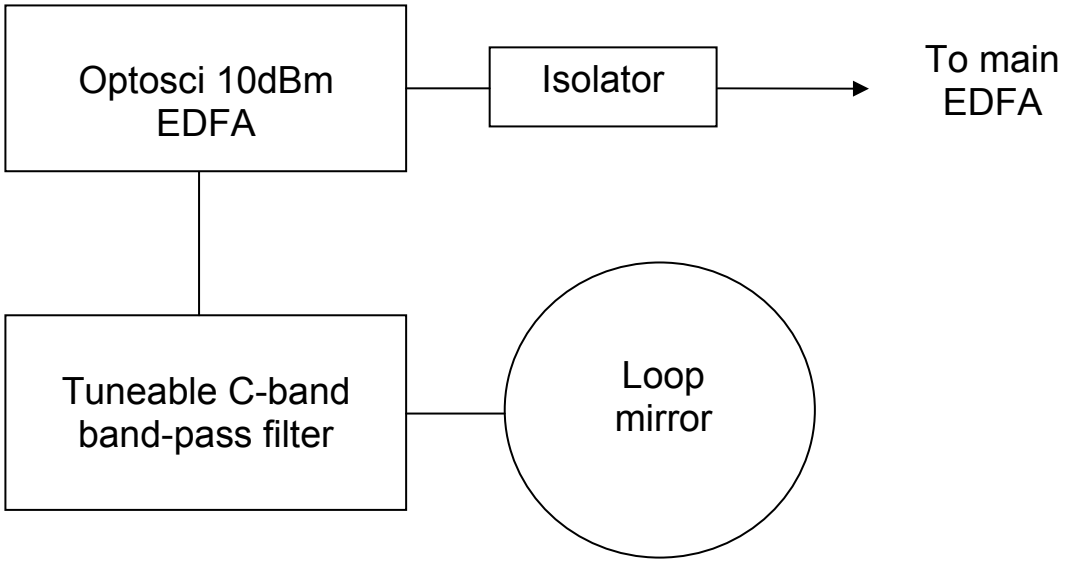

Figure 4.7 EDFA seed source system Seed 1

Seed 1, as defined in Chapter 3 was constructed to provide SBS-free pump power via the 30dBm EDFA for the OFS Raman fibre system. This seed was injected directly into the input port of the 1W pump EDFA, typically providing around 5-8dBm of broad bandwidth optical power centred on 1541nm, which was more than sufficient for its purpose. The output of the ASE source was inserted into an OSA, and the spectrum analysed. As can be deduced from Figure 4.8, the overall seed spectrum is a combination of the EDFA ASE spectrum and the amplification of the filtered ASE. The filter pass bandwidth is around 74GHz. Using this seed at this wavelength, the main 30dBm (1W) EDFA output had the form as shown in Figure 4.9. The monitor tap of the co-pumped Raman system was fitted with a 20dB attenuator and inserted into the OSA to bring the pump power well within safe limits for the equipment.

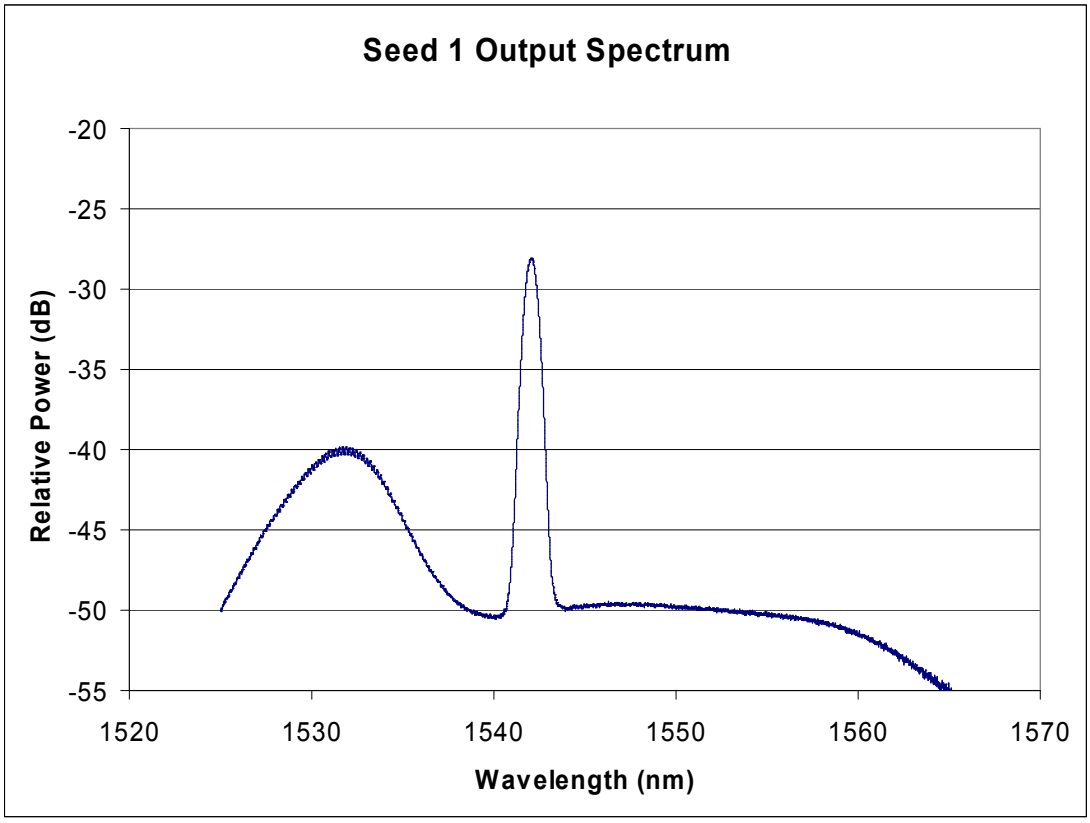

Figure 4.8 Optimised 1541nm seed output (Seed 1)

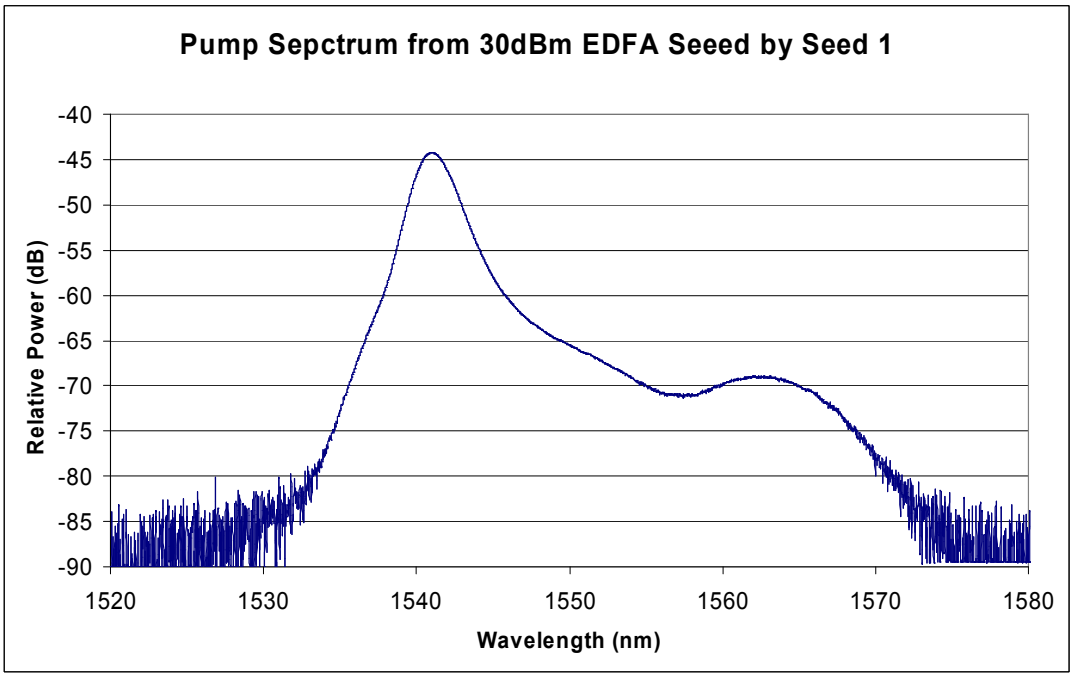

Figure 4.9 30dBm Keopsys EDFA output as seeded by Seed 1

From Figure 4.9, it can be seen that the majority of the power is distributed around the peak Raman pump wavelength of 1541nm for seeding stimulated scattering at 1651nm. The -3dB bandwidth of the main pump peak is 320±20GHz.

In order to confirm that the bandwidth of the pump source was sufficient to suppress SBS of the pump wave, the EDFA pump was launched into the OFS Fibre Raman system with no 1651nm Raman seeding signal and the backscatter power level was monitored. Using Equation 2.33 to substitute the Brillouin gain coefficient used in the threshold relationship, Equation 2.31, with an effective coefficient that takes account of source bandwidth, the effective pump bandwidth to suppress SBS of a pump in the 1350m OFS fibre is 17GHz and 85GHz for the 1W and 5W pumps respectively (taking the 1% backscatter of input pump threshold definition). The insertion loss corrected output power (not including attenuation in the gain medium of around 0.5dB over its length) was recorded as a function of insertion loss corrected input power and this is shown in Figure 4.10.

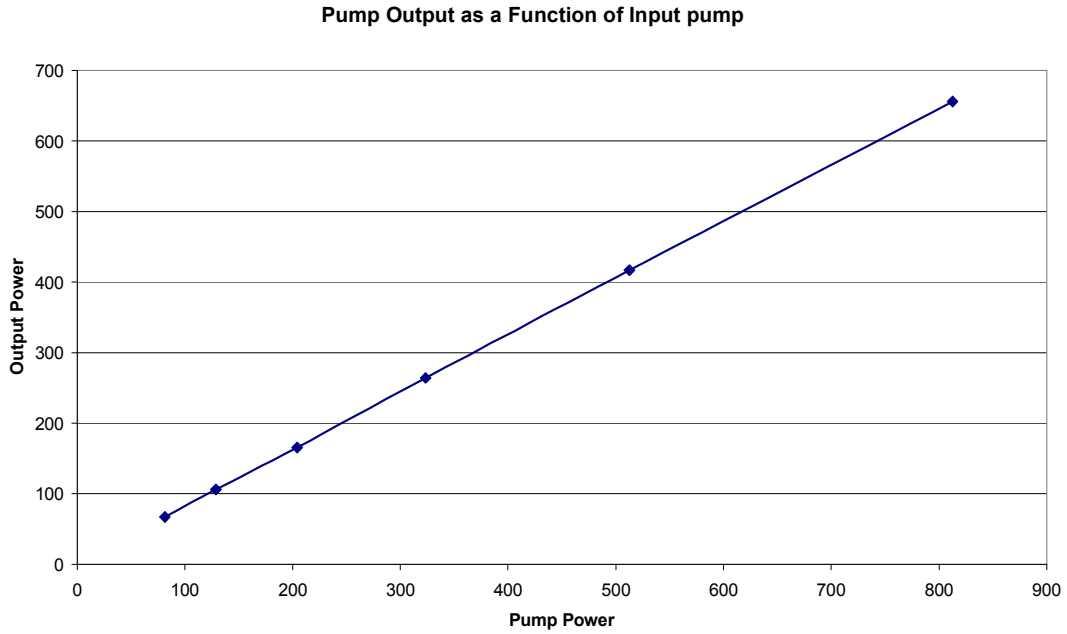

Figure 4.10 Output pump power as a function of input pump as seeded by Seed 1 with no Raman signal at 1651nm launched.

In contrast to the narrow bandwidth pump power transmitted through the Raman amplifier system, the pump as seeded by Seed 1 exhibits a linear relationship between input power and transmitted power. The implication of this is that no obvious SBS threshold power was reached for the full range of the 30dBm EDFA. This in turn suggests that Brillouin scattering of the pump is not being stimulated. In terms of building the high power Raman amplifier system, the significance of this is that the general concept and design of an unpolarised, SBS free, broad bandwidth source has been established.

With the insertion loss taken into account, there is some power discrepancy between input and output powers, most likely arising from uncertainty in loss measurements, spontaneous scattering, connector losses from the screw-in type connectors (which thus have a variable separation of end faces leading to variable insertion loss), and their degradation and also from variable bend loss depending upon how the fibres were arranged.

4.5.2 Discussion of the Need for a Replacement Seed for the 37dBm EDFA

It was found, however that this seed (Seed 1) was not as effective at seeding the 37dBm Keopsys EDFA in terms of producing an optimised pump spectrum when compared to the spectrum it produced with the 30dBm EDFA. There were two main issues discovered while using Seed 1 to seed the main EDFA. Firstly, the 37dBm EDFA has its gain peak at the longer wavelength end of the C-band, around 1560-1565nm, which is unsuitable for efficient Raman amplification of a 1651nm Stokes wave. This means that any seed that has some part of its output spectrum at around 1560nm is likely to seed a significant portion of the pump power to an unsuitable wavelength. Seed 1 allowed the pass of 1560-1565nm and hence caused this problem.

The second issue was that at high power, the pump's spectral profile, while being seeded by Seed 1, gave rise to strong Raman ASE at around 1650nm. This was because the spectral power density of the pump was sufficient to build up spontaneous Raman scattering within a relatively narrow band with respect to the

Raman gain bandwidth without the help of the 1651nm Raman seed signal from the DFB. This band of spontaneous Raman scattering then experienced considerable Raman gain. Aside from these operational issues, the tuneable filter was an expensive component, while non-tuneable communications filters could be employed at a much lower cost while increasing reliability and wavelength stability.

4.5.3 Demonstration of the Pump Spectrum Issues While Using Seed 1

The seeding of the 37dBm EDFA using Seed 1 with the tuneable filter set to 1542nm is shown for illustration of the problems caused. The seed with spectrum as shown in Figure 4.8 was injected into the 37dBm EDFA at 8dBm, which gave rise to a pump spectrum as shown in Figure 4.11.

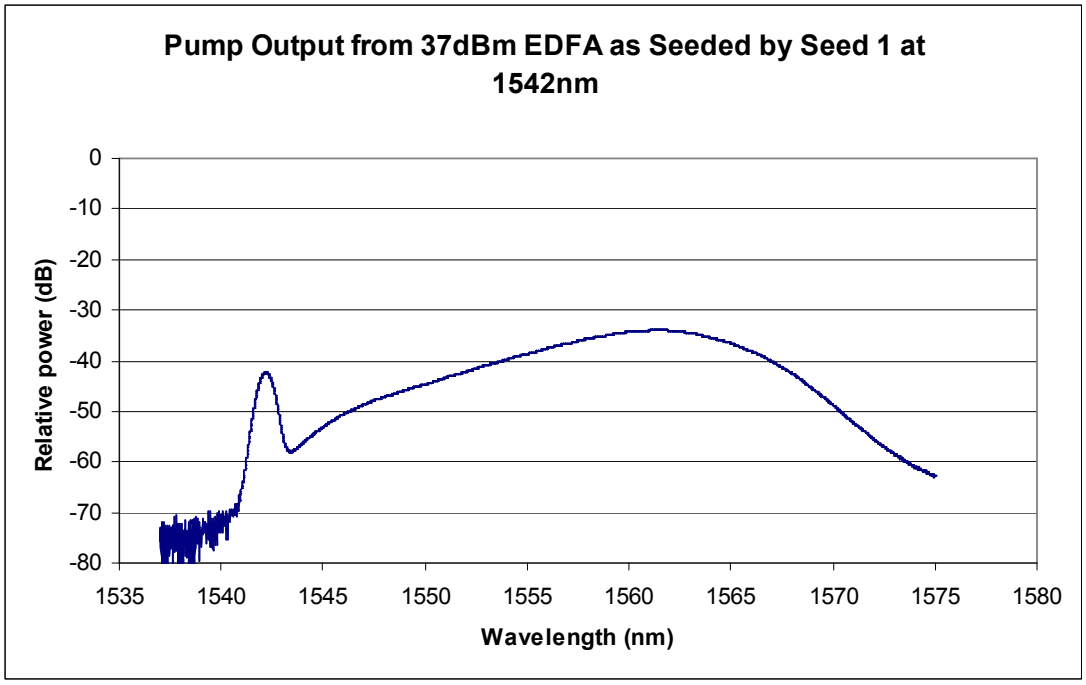

Figure 4.11 37dBm EDFA as seeded by Seed 1 at 1542nm

From Figure 4.11 it can be seen that, although a wavelength that is optimised for efficient Raman scattering to 1651nm has been selected via the tuneable filter, much of the power from the EDFA pump is ASE outside of the chosen, filtered ASE band. Furthermore, much of this ASE is at least 20nm away from the optimal ~1541nm peak, meaning that the effective Raman gain efficiency of the system is considerably reduced (recall the main Raman gain peak has a bandwidth of just under 10nm). It

should be noted that increasing the seed power to up to 8dBm had no noticeable effect on the proportions of power seeded into the desired region with respect to that lost to longer wavelength ASE at around 1560nm. The seed power from Seed 1 could not be increased further since it would cause the seed source to lase, which would have resulted in a strong, narrow bandwidth peak emissions from the EDFA and hence SBS backreflection in the Raman gain medium. In order to observe the suitability of Seed 1 for use with the 37dBm EDFA, the wavelength of the tuneable filter was increased within reasonable limits for pump seeding in an attempt to control more of the pump power, with the spectra shown in Figure 4.12 and Figure 4.13.

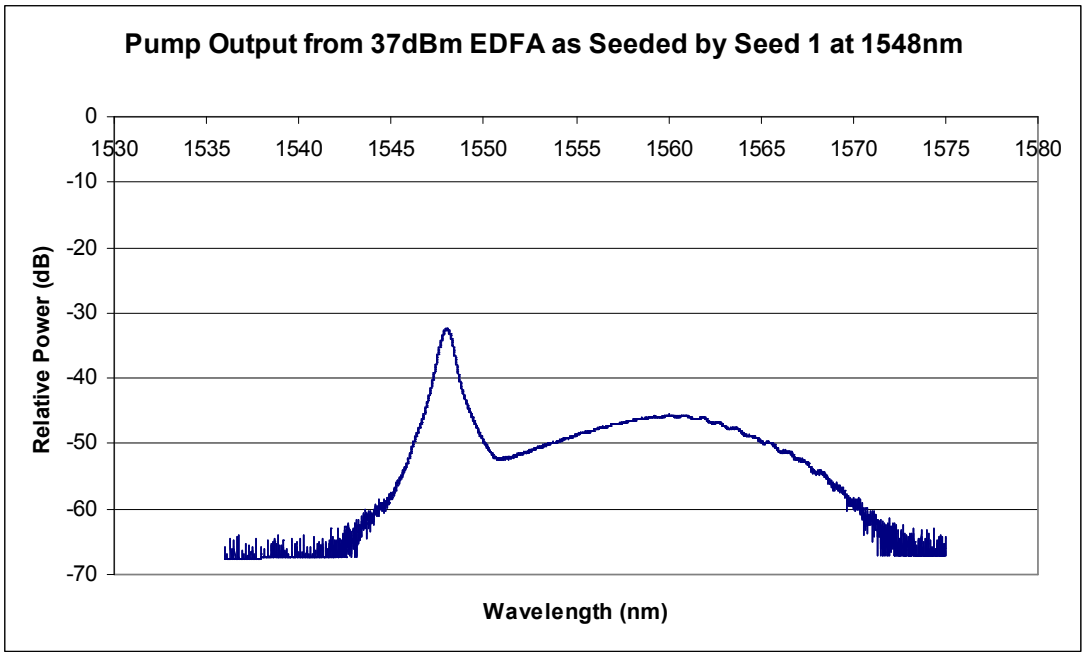

Figure 4.12. 37dBm EDFA Seeded by Seed 1 at 1548nm

From Figure 4.12 and Figure 4.13, it can be seen that the seeding becomes more efficient at controlling the EDFA output spectrum as the seeding wavelength approaches the 1560nm gain peak, therefore it can be inferred that Seed 1 would only provide effective pump control if it were to seed the main 37dBm EDFA at around 1560nm, otherwise much of the pump power is uncontrolled. This is impractical because pumping at 1560nm is likely to apply a significant penalty to the Raman

scattering efficiency of the system, outweighing any gains resulting from improved pump control.

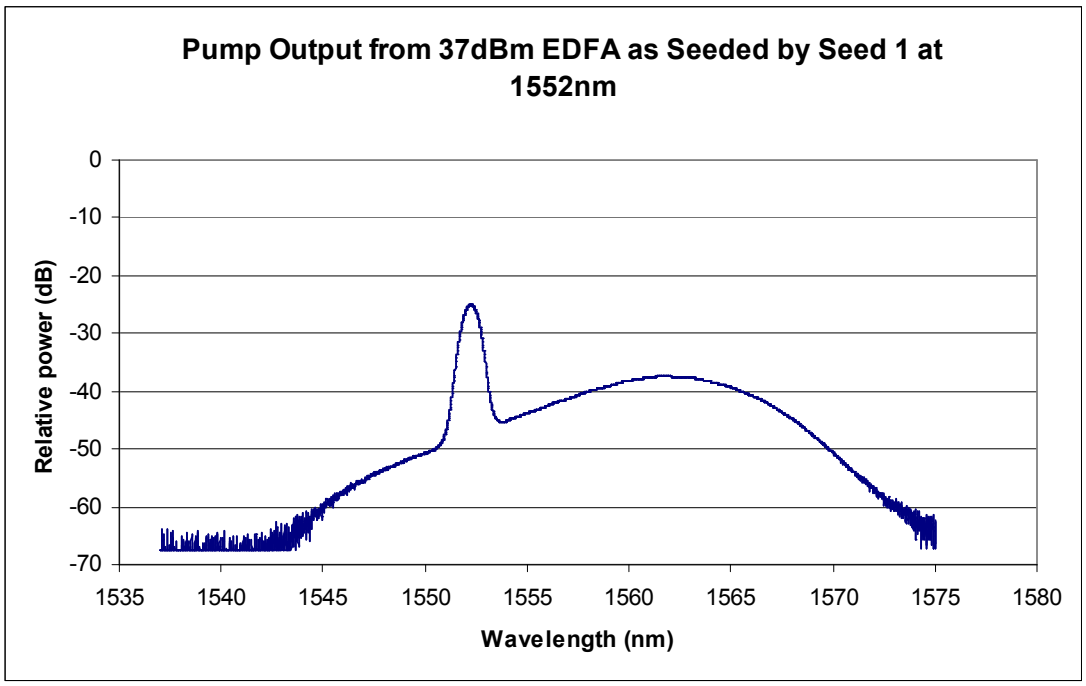

Figure 4.13 37dBm EDFA Seeded by Seed 1 at 1552nm

It was these results, along with the observation of Raman ASE while using Seed 1, which will be discussed separately, that led to the design and implementation of the broad bandwidth seed source defined as Seed 2, which is described in the following section. It should be noted that the tuneable filter was abandoned at this stage because its pass band was too narrow and allowed Raman scattering to stimulate from Raman ASE. Raman ASE is undesirable because it essentially depletes the pump through SRS without contributing to the WMS signal, thus wasting power and adding noise, particularly in the forward direction, where the ASE propagates with the signal, which can produce beat noise as well as random noise from spontaneous emission.

4.5.4 Configuration of Seed 2

The same principle of generating a broad bandwidth ASE signal from a small EDFA was used once more, but the filtering arrangement was changed to suppress more of

the 1550-1565nm seed output and different filters were used to produce a broader bandwidth ASE output. Light around 1560nm experienced optimised gain in the 37dBm EDFA unit, but is inefficient at Raman scattering to 1651nm in the Raman stage. This makes suppression of this wavelength important before the main amplifier stage if efficiency is to be maximised. A Schematic of Seed 2 is shown below in Figure 4.14.

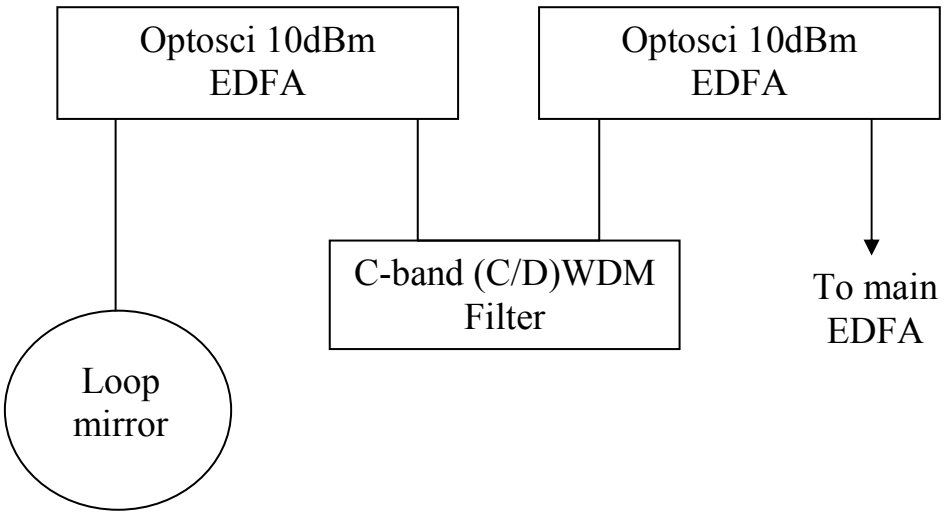

Figure 4.14 Schematic of Seed 2 configuration

Within this configuration, 1531nm and 1551nm CWDMs (with bandwidth ±7nm) and a DWDM (pass band 1538.87-1541.46nm) filter were inserted in turn for investigation and their apposite seed and pump spectra recorded. It was found that this was the optimal seed configuration type for control of the ASE output by the system while providing sufficient power to seed the main EDFA. Using two ASE producing EDFAs rather than one allowed improved filtration of ASE outside of the desired band compared to one ASE source with the filter in the path of the loop. This is because the filter could be placed at the output of an EDFA instead of in the loop. This configuration produced much more filtered ASE power than the case of placing the filter at the output of the seed system.

It was found that, in terms of maximising output power, placing the filter in the path of the loop mirror was most efficient, but this allowed the pass of the most unfiltered

ASE. Placing the filter at the output of the ASE source system allowed optimal control over the seed source's output spectrum; however this resulted in insufficient seeding of the small EDFA used to generate the ASE, resulting in a low output power. Having no seed led to the small EDFAs output power being spread over its entire gain band, which was then mostly filtered at the output. Hence the best compromise position was found to be between two EDFA sources as shown in Figure 4.14, so that a small, optimally filtered output was fed to the second EDFA, which would then boost the output power. This allowed more than 10dBm filtered ASE to be generated without the danger of lasing in the seed system.

4.5.5 Characterisation of Seed 2 Equipped with the 1551nm CWDM filter

Using the 1551nm (+/-7nm band) CWDM filter, the broad bandwidth seed output had a spectral power distribution as shown in Figure 4.15

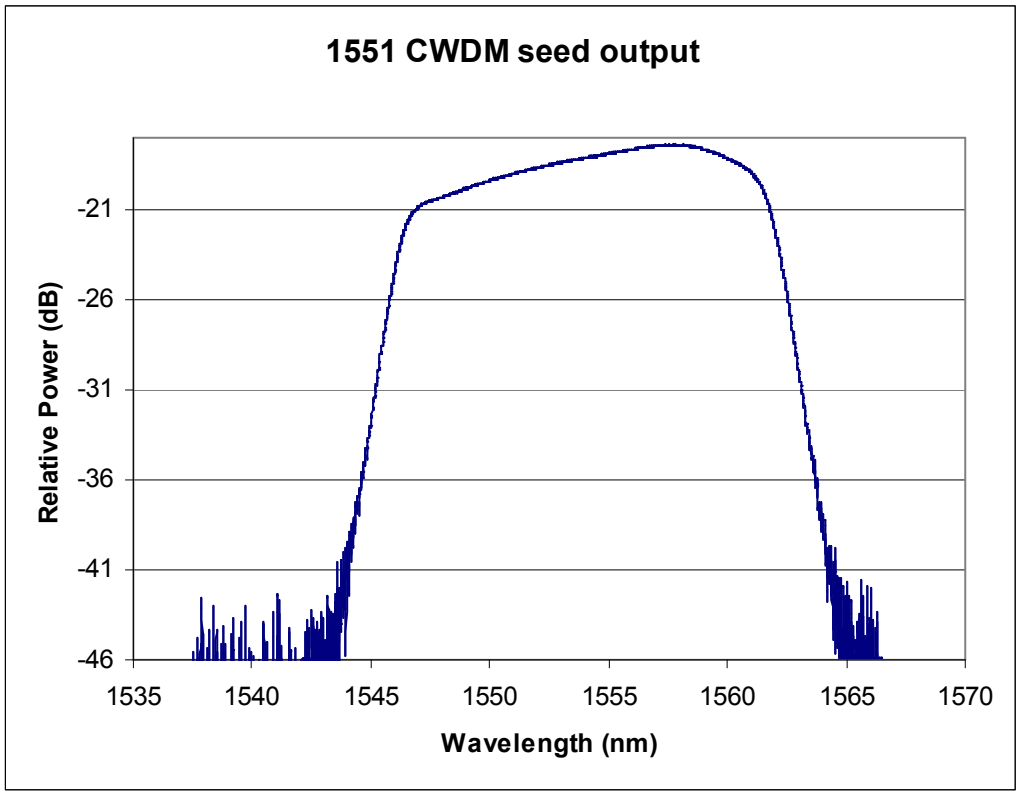

Figure 4.15 Output spectrum of Seed 2 with 1551nm CWDM filter

As can be seen from Figure 4.15, the spectrum of the seed output favours emission around 1560nm. This is likely to cause a large proportion of the main EDFA output to concentrate around this and lead to a lowered Raman scattering gain efficiency once again. Though one improvement is that, given the relative flatness of the seed output spectrum compared to the peak associated with the tuneable filter output, the EDFA pump output seeded by Seed 2 with the 1551nm CWDM is much less likely to experience Raman ASE in the Raman gain medium because of its reduced spectral power density. The efficiencies of the final Raman system pumped using the Seed 2 output with 1531nm CWDM and 1551nm CWDM in terms of Raman signal output power are compared at the end of the chapter (Section 4.11).

The pump as seeded using the 1551nm CWDM Seed 2 was fed to the 1550nm pump input port of the Raman amplifier test bed and the pump output spectrum was measured at the 1% monitor tap as shown in Figure 4.16. It can be seen that as expected, much of the pump power is seeded beyond 1560nm, from which Raman scattering to 1651nm is relatively inefficient. Being of considerably broader bandwidth than the pump spectrum seeded by Seed 1, it was expected that SBS should not be encountered using this pump spectrum.

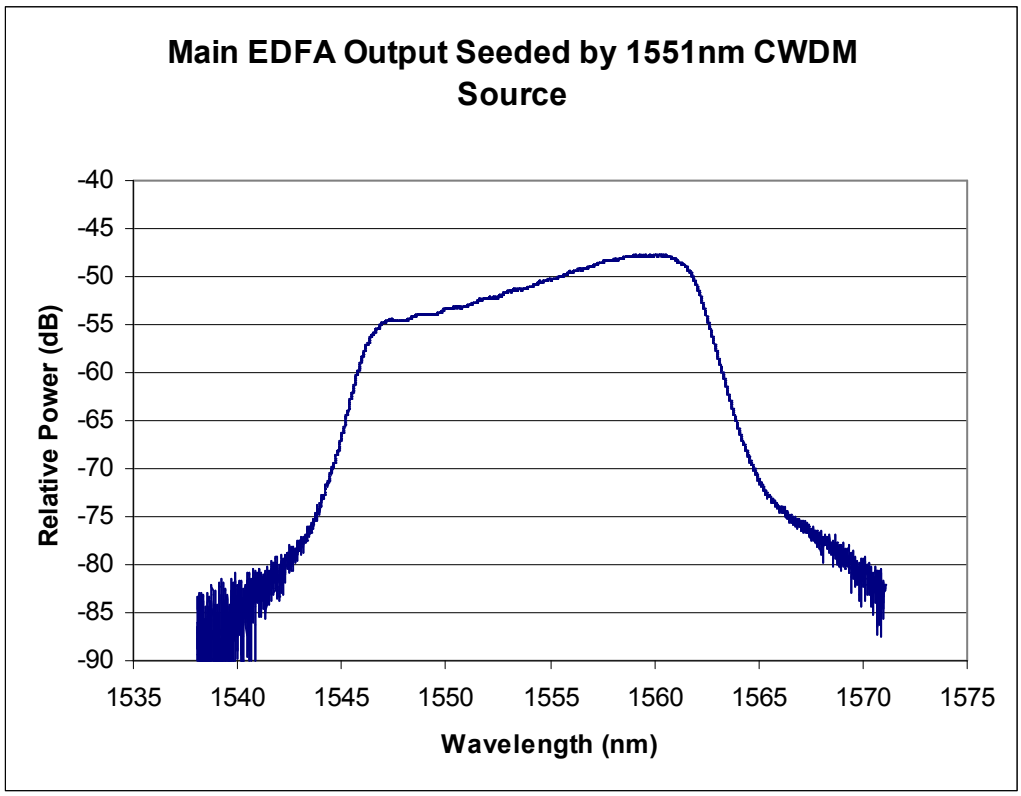

Figure 4.16 Output spectrum of main 37dBm EDFA as seeded by Seed 2 with 1551nm CWDM filter

4.5.6 Characterisation of Seed 2 Equipped with the 1531nm CWDM filter

As expected, the 1560nm biased seed has resulted in a pump spectrum whose peak is around 20nm longer in wavelength than the optimal pump wavelength at around 1540nm. It was therefore necessary to investigate the use of other communications filters. The 1531nm (+/-7nm) CWDM filter was considered to be more appropriate because it should not seed any of the EDFA's power to its strong peak 1555-1560nm band, but should peak close to 1540nm. Hence, the same seed configuration was used but a 1531nm CWDM filter replaced the 1551nm CWDM. The resultant output seed spectrum from Seed 2 is as shown in Figure 4.17. The seed spectrum suggests that there should be significant seeding of the main EDFA between 1535-1538nm, which is within the 3dB Raman gain band of 1541nm and there should be no significant seeding in the region of 1550-1560nm. Although not quite ideal, it should be a strong improvement over the 1551nm filter, which peaked most of the pump at

around 1555-1560nm, around 15-20nm away from the optimal 1541nm. The pump spectrum seeded by Seed 2 equipped with the 1531nm filter is shown in Figure 4.18.

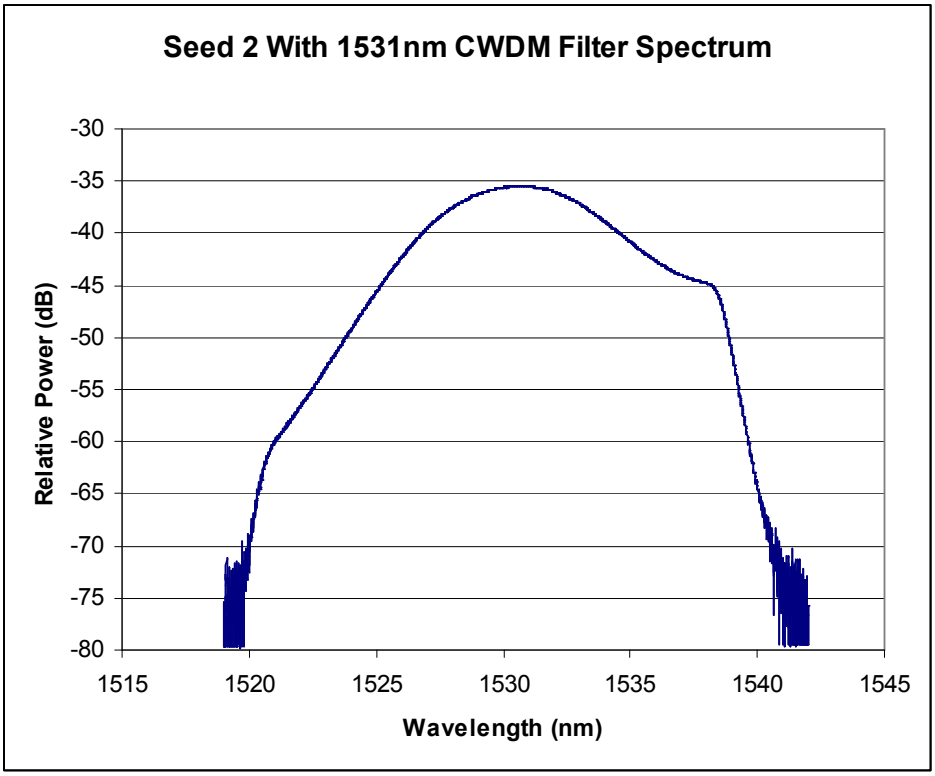

Figure 4.17 Output spectrum of Seed 2 with 1531nm CWDM filter in place

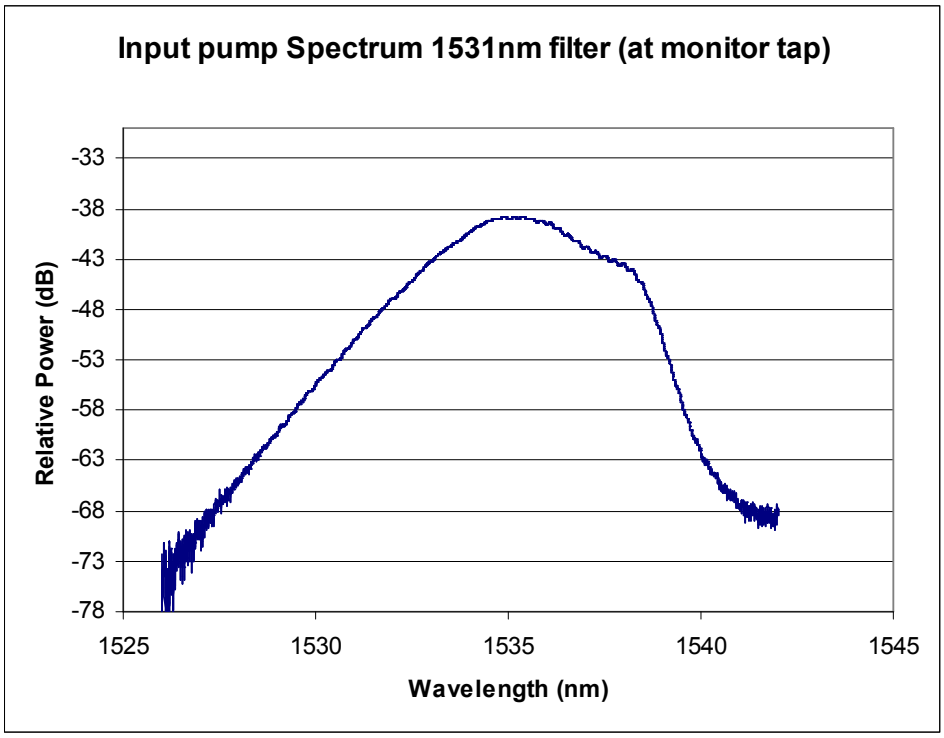

Figure 4.18 Output spectrum of main 37dBm EDFA as seeded by Seed 2 with 1531nm CWDM filter

Although the peak of the pump output is at around 1535nm using the 1531nm CWDM Seed 1, the power is still centred very close to the optimal pump wavelength compared to the other seed configurations investigated. Furthermore, the 1535nm peak is 30dB (facor of 1000) higher power than wavelengths longer than 1540nm c.f. 10-15dB in Seed 1, making the source less likely to seed the pump power at the longer wavelengths that see high gain in the 5W pump EDFA.

For an indicative analysis of how the pump spectrum should affect the effective Raman gain efficiency, the Raman gain spectrum of OFS Raman fibre was normalised and plotted as a function of wavelength from data supplied by OFS. The Raman gain spectrum for Raman scattering to 1651nm in OFS Raman fibre was compared with the normalised pump output spectrum (resulting from the seeding of the 37dBm EDFA by Seed 2 with the 1531nm CWDM filter) on a linear plot as shown in Figure 4.19

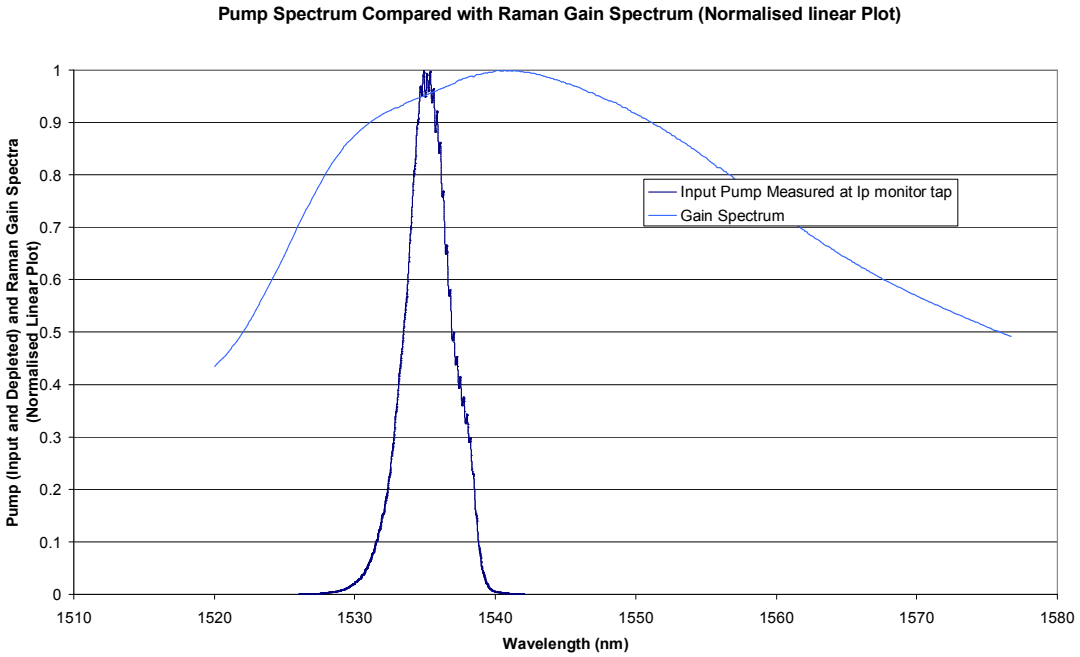

Figure 4.19 Comparison of Raman Pump spectrum as controlled by Seed 2 (1531nm CWDM) and the main peak of the Raman Gain Spectrum for OFS Raman Fibre for Raman scattering to 1651nm

Considering Figure 4.19 and the spectra of the other seeds, this source is close to optimal. It is very close to the peak Raman gain efficiency for pumping a 1651nm Stokes wave, and does not produce significant Raman ASE spectral density since it has a considerably broader bandwidth peak than Seed 1. A discussion of Raman ASE, together with an example of its occurrence at significant levels can be found in Section 4.10.2. For this reason, it can also be considered to be of sufficient bandwidth to avoid SBS in the fibre systems tested. Furthermore, the tuneable filter has been replaced by a relatively cheap telecommunications component, which does not require any tuning or maintenance to maintain the same pass band over time. Comparing this to Seed 2 equipped with a 1551nm filter, the effective Raman gain coefficient could be around 30% worse if the 1551nm CWDM were used since it centred on around 1557nm. This value was obtained by considering the Raman gain spectrum on Figure 4.19 and comparing it with the pump spectrum arising from the 1551nm Seed 2. Although the Raman gain spectrum shown in Figure 4.19 is for OFS Raman fibre, it is quite indicative for other Germanium doped fibre types, such as DSF and standard SMF. The doping concentration differences between the fibres only changes the peak Raman scattering frequency by at most a few nm, hence it is

valid to consider other pump spectra with respect to the normalised OFS fibre gain spectrum in Figure 4.19.

4.5.7 Characterisation of Seed 2 Equipped with the 1540nm DWDM filter

In an attempt to further optimise the wavelength of the pump output spectrum, a DWDM filter was used in place of the 1531nm CWDM with a pass band between 1538.87nm to 1541.46nm (at 1dB). This was expected to seed a higher proportion of the EDFA's power close to the optimal 1541nm pumping wavelength, while still maintaining a broad enough pass band to suppress Raman ASE and SBS. The seed output with the DWDM filter fitted was as shown in Figure 4.20

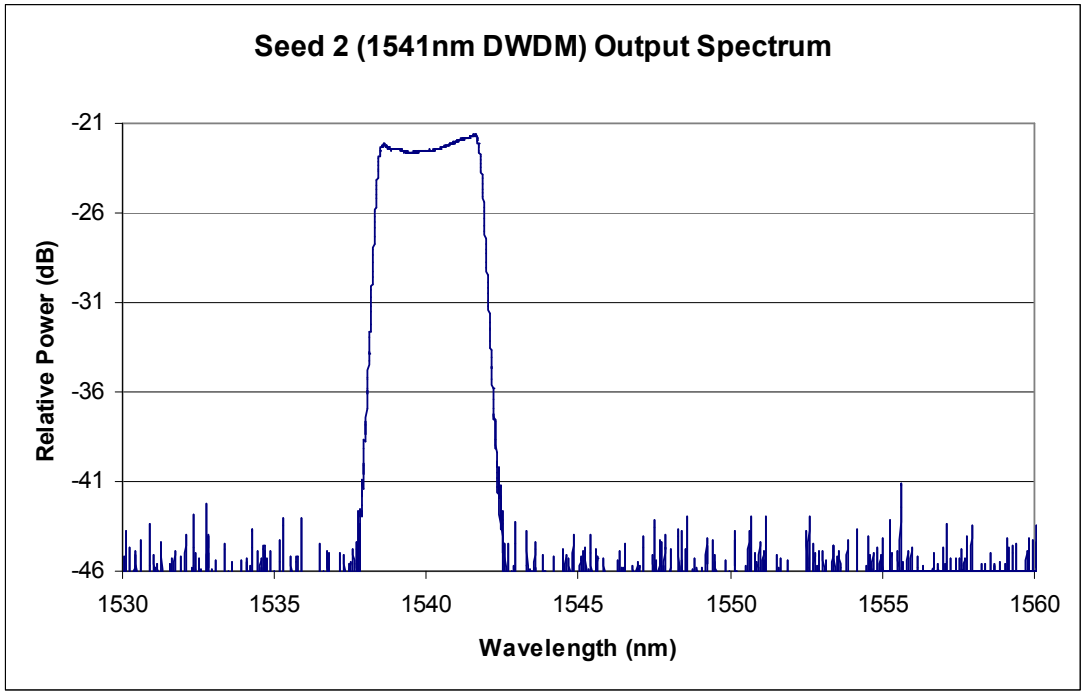

Figure 4.20 Output spectrum of Seed 2 with 1540nm DWDM filter

Using Seed 2 equipped with the DWDM filter to control the output of the 37dBm EDFA, the pump spectrum was as shown in Figure 4.21. As can be seen, the pump output band is well contained within what could be considered to be an ideal band around the optimal pumping wavelength. However, given the shape of the EDFA gain spectrum, this has created a sharp peak in the pump spectrum at around 1542nm, which could potentially give rise to Raman ASE (Section 4.10.2) or lasing

in the main EDFA (this was not observed in the main EDFA, but was a foreseeable risk), meaning that the 1531nm variant of Seed 2 was preferred. During testing, the DWDM variant of Seed 2 produced very similar results to the 1531nm CWDM in terms of Raman gain, and so with no measureable benefit to using the DWDM filter, but some risks and extra cost, it was abandoned as a broad seed filter. With an optimised seed created, this marked the end of the preliminary investigations.

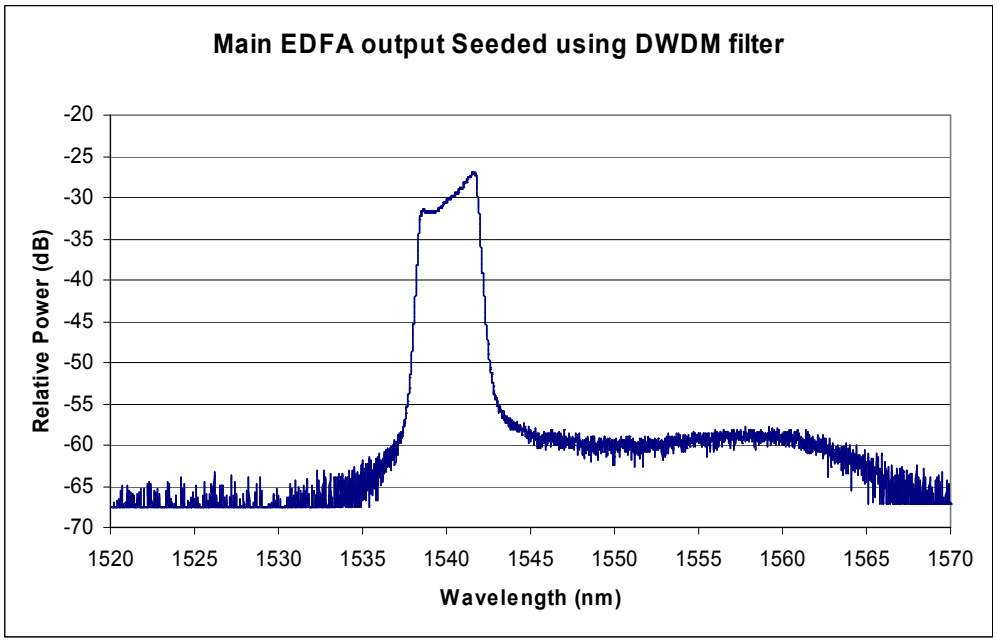

Figure 4.21 Output spectrum of main 37dBm EDFA as seeded by Seed 2 with 1540nm DWDM filter

During investigations using Seed 2 with any of the filters, there was no SBS backscatter observed. In particular, Seed 2 equipped with a CWDM filter produces a considerably broader bandwidth than Seed 1 with the tuneable filter, therefore the stimulation of Brillouin scattering would not be expected from Seed 2.

4.6 Characterisation of Initial Raman Amplifier System

4.6.1 Characterisation of Amplified Signal Power as a Function of Input Pump Power in the OFS Raman Fibre System

Having suppressed SBS of the pump wave through the development of an appropriate seed source and proven the principle of the chosen SBS suppression technique for the signal (i.e. wavelength dither), it remained to attempt Raman amplification of a 1650nm signal. The 1W EDFA pump seeded by Seed 1 was used as the pump for the amplification of the signal from the 5mW 1651nm in the OFS Raman fibre. Testing Raman amplification at this low pump power level allowed an initial proof that the configuration would be effective.

Considering that the optimal dither frequency would be higher in the case of a Raman amplified signal rather than a high power beam launched at the start of the fibre as a result of the shorter effective Brillouin gain length, the optimal SBS suppression frequency had to be found empirically. This was carried out by conducting the Raman amplification experiment and adjusting the signal modulation frequency as the pump is increased with 74.0kHz used as a starting point. The optimised frequency was reached by maximising output signal power with respect to backscattered power and although the effect of cycle frequency was observed to be much less defined and important in an amplified beam, this frequency was found to be 204kHz. Given an optimised dither frequency, the dither depth was set to 3GHz peak-to-peak and a characterisation was carried out in terms of output amplified signal power as a function of input pump power. The characterisation using the 30dBm EDFA is shown in Figure 4.22. It should be noted that it was more difficult to characterise optimal dither frequency for SBS suppression because the effect of dither frequency on the amplified signal was unexpectedly very weak compared with the dramatic dependence in the case of using a high power narrow band source from the start of the medium.

As shown in Figure 4.22, the pump power inserted into the system was varied between 10 and 800mW (taking account of insertion loss) using the 30dBm (1W) Keopsys EDFA, with powers below 100mW being achieved using in-line attenuation before the pump input port. Backscattered power was minimal throughout the investigation at both pump and signal wavelengths and a signal was amplified from 4mW (using the 5mW DFB) at the start of the Raman fibre to 34mW at the end of the fibre.

Raman amplification of the signal was successful, however in order to produce a meaningful data set for model validation, it was necessary to launch more pump power into the gain medium and hence the experiment was repeated using Seed 2 equipped with the 1531nm CWDM filter to drive the 37dBm EDFA.

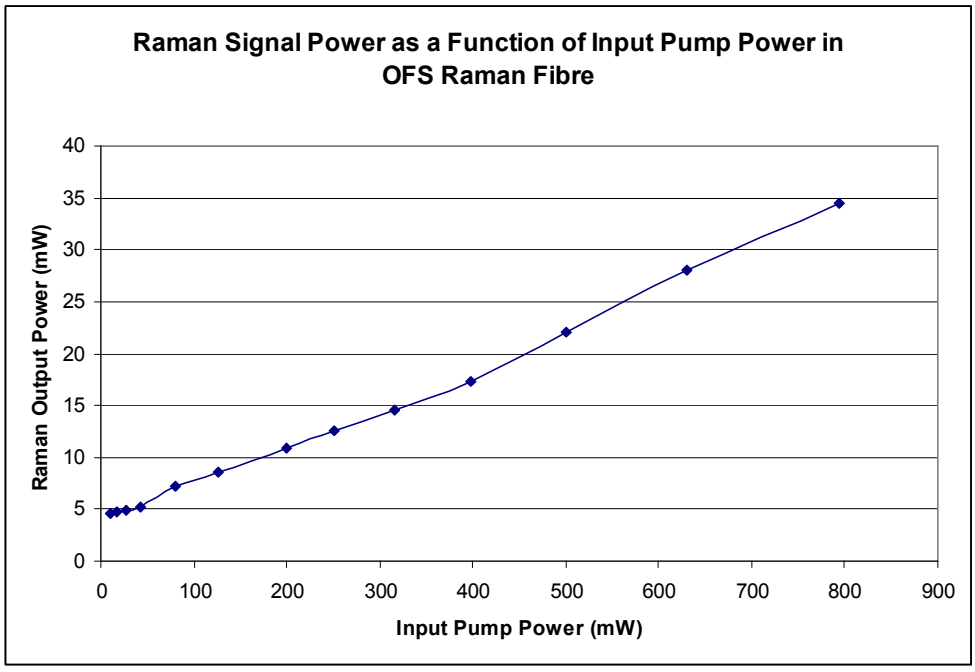

Figure 4.22 Signal power as a function of pump power in the OFS fibre system

Apart from the change in pump configuration, all other apparatus remained the same. In order to aid comparison with theory, values for residual pump were recorded. In this pumping regime with the 37dBm EDFA, it was expected that strong pump depletion would be observed, unlike the low gain case of Figure 4.22.

The results of the high pump power investigation are shown in Figure 4.23. As can be seen, the signal reached an output power of 1.38W before a rapidly increasing backscatter level, which was due to Raman amplified SBS of the signal was observed. In addition, the signal was of very poor quality approaching this power level, with spikes and noise at high levels. These effects began at low levels at around 600mW amplified signal power. Apart from obtaining a substantial signal power, these Raman amplification experiments demonstrated the return of SBS in the signal even with modulation in place and how rapidly the effect increases with pump power after its onset. This was exacerbated by the large amount of residual pump in the system, leading to Raman amplification of the backward travelling Brillouin Stokes wave. The backscattered power is plotted as a function of signal power in Figure 4.24.

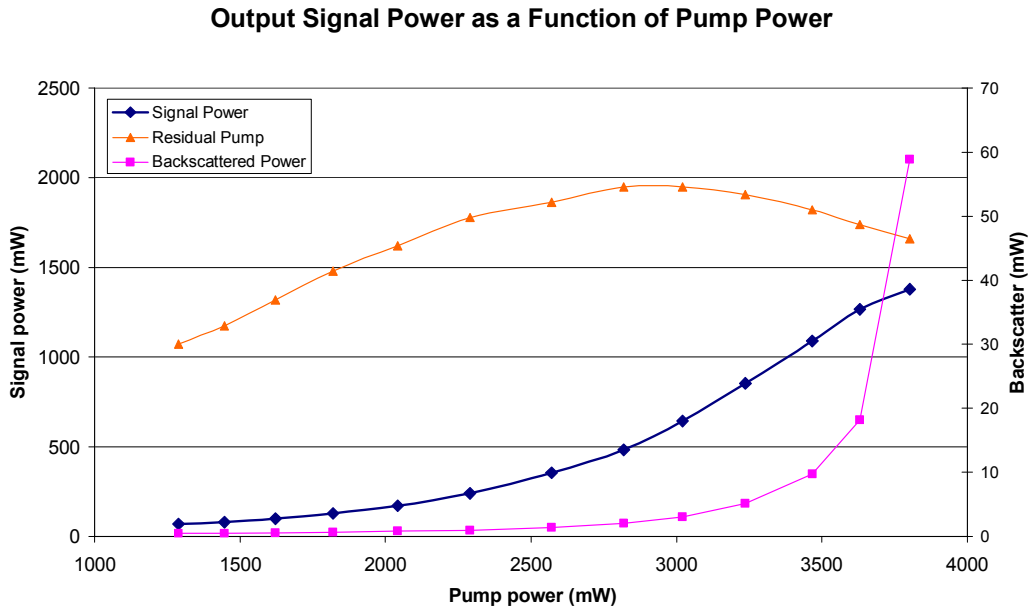

Figure 4.23 Raman output power as a function of input signal power using the 37dBm EDFA

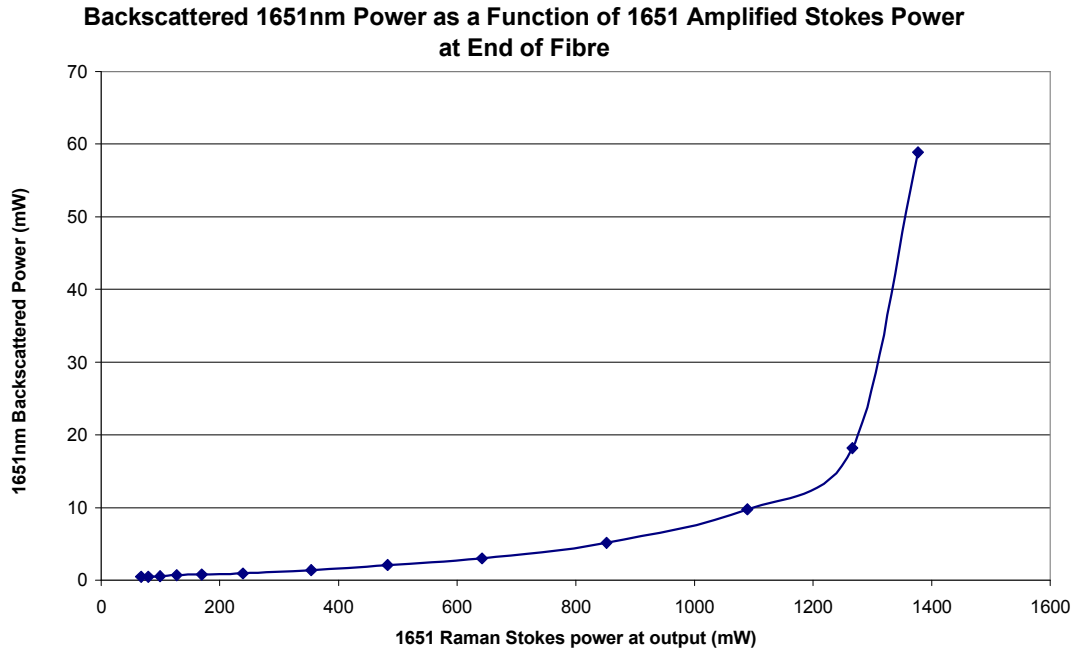

Figure 4.24 Backscattered power as a function of Raman amplified signal power at the end of the gain fibre

The poor signal quality, as measured in the time domain was thought to arise from amplification of Rayleigh, splice and connector backscatter in the system, which led to beat noise in the signal. A fuller discussion of potential signal problems in a Raman amplifier system is included at the end of the chapter. Given the results of this experiment, it can be concluded that the amplifier system built using OFS Raman fibre would exceed the projected (1W) signal power level requirements with the need for only several Watts of input pump power, but some noise issues in the signal would need to be solved if this were to be used as a methane sensing signal source.

4.6.2 Investigation of Polarisation Dependent Gain for Seed 2

In order to provide confirmation that the system carried no significant polarisation dependent gain, the Raman investigations were carried out while varying the state of polarisation of the linearly polarised Raman seed source. This was now possible, given the ability to carry out safe, SBS suppressed Raman amplification experiments over a large range of signal output powers.

A polarisation controller was inserted before the 1650nm input to the system to control the input signal polarisation and a Raman amplification experiment was conducted, maximising and minimising the output signal power via the polarisation controller. The results are shown in Figure 4.25

As can be seen from Figure 4.25, there is little or no dependence on the gain upon the polarisation state of the DFB signal laser. The small discrepancy can be explained by slight variations in the insertion loss while twisting the fibre in the polarisation controller. The implication of this result is that Seed 2 is acceptable as a seed source in terms of suppressing polarisation dependent gain, and this contributes to the realisation of a low noise system. This also allows a meaningful comparison of the results with calculations since a polarisation k value can be used to run the model based on the unpolarised nature of the pump.

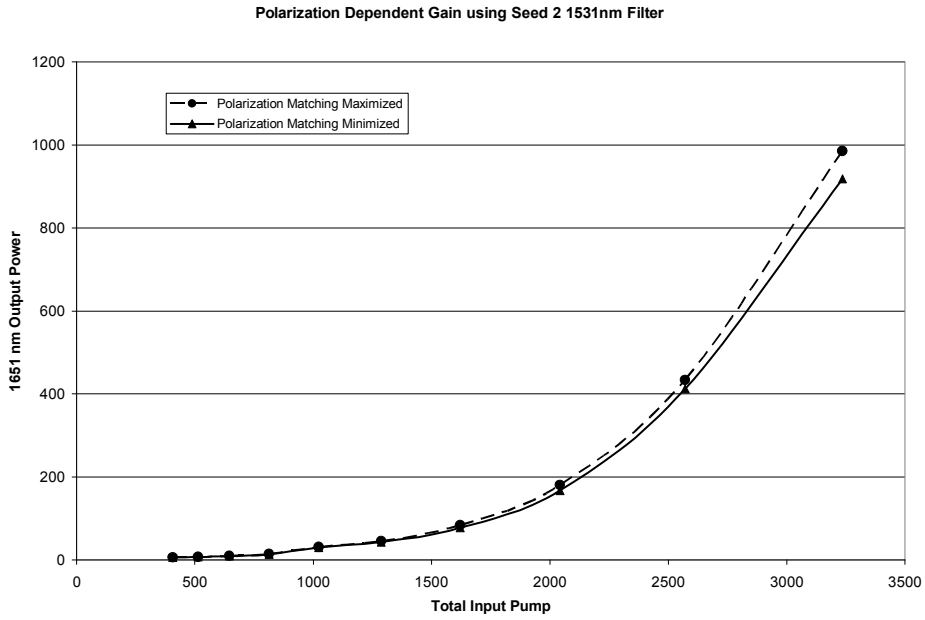

Figure 4.25 Verification of independence of gain with input signal polarisation using seed 2

4.6.3 Comparison of OFS Raman Amplifier Characterisation with Modelled Results

In addition to realising a high power Raman amplifier system, the other main objective was to validate the Raman amplifier models, upon which the design of

further Raman amplifier systems would be based. Given significant Raman amplification from the Raman amplifier, it was possible to compare the modelled Raman results with a meaningful data set. Given that the main uncertainty lay in the effective Raman gain efficiency of the system arising partly from the unpolarised pump, the model was run to provide results for several different effective gain efficiencies. That is to say, that it is uncertain whether the 0.55 value for the k polarisation factor is valid (obtained by averaging orthogonal and parallel k polarisation coefficients), but this comparison of theory and experiment could help to validate this. The comparison of the theoretical and experimental output powers of the OFS Raman fibre system is shown in Figure 4.26.

The theoretical and experimental results are in good accordance for the gain efficiency value 1.4$(W.m)^{-1}$, which equates to a polarisation k value of 0.57. This also agrees very well with the earlier postulation that the unpolarised pump should have an effective k value of around 0.55, see discussion in Section 2.7.4. It should be noted that the error in measurement of power levels is very small (<0.1%) and so uncertainty limits were not included in the figures.

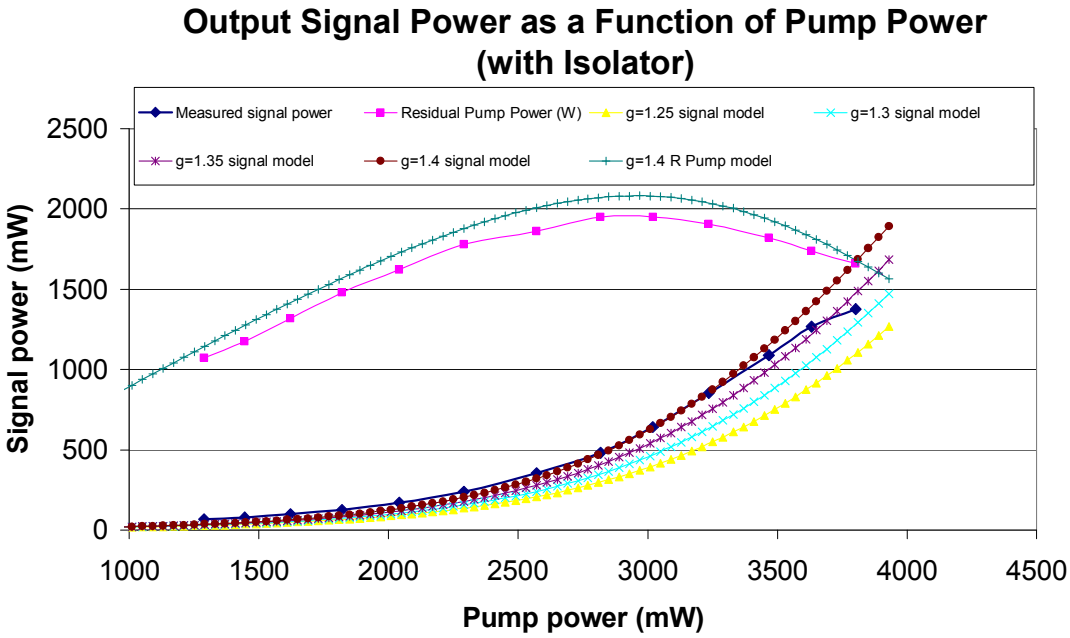

Figure 4.26 Comparison of modelled and actual output power for the OFS Raman amplifier system.

4.6.4 Implications of OFS Raman Fibre Results on Later Designs

In summary, the preliminary investigations and characterisation of the Raman amplifier using OFS specialist Raman fibre have provided the following.

- The Raman amplification models are reliable in the co-pumped configuration for the case of relatively high Raman gain efficiencies until backscattered power begins to rise. This means that further Raman amplifier systems can be designed based upon the model results. However, the Raman amplification models do not predict the onset of signal distortion resulting from amplified double backscatter, nor at what level SBS backscatter levels become unacceptable (without already having constructed the amplifier system). That is to say, although the amplifier system agreed with the calculated output powers up to around 1.2W, the calculated potential of the system was never realised as the pump power could not be increased further due to backscatter and signal distortion. The result is that caution should be exercised when choosing the fibre length, so that achieving the required power is possible, but minimising the gain fibre length is also important to minimise other negative effects. It is also thought that during operation, the fibre provides high gain per unit length arising from the high fibre gain coefficient and also the high level of residual pump in the system. While this is ideal for amplifying a signal, it also makes the system very sensitive to manufacturing defects such as imperfect splicing and connector problems, potentially causing long-term reliability issues. This is because any wave of wavelength within 10nm of the signal wavelength will experience considerable gain regardless of direction of propagation through the fibre. The issue of high residual pump could be removed by using a larger 1651nm seed signal, while the gain coefficient could be reduced using a fibre with a lower gain coefficient.

- SBS would be a major problem in the system if not addressed, but the selected strategies for suppressing SBS in the pump and signal have been demonstrated and characterised satisfactorily. Further SBS suppression may be possible in using a counter-pumped system where the signal power only becomes significant over a shorter length.

- The pump source is essentially unpolarised and hence PDG is not observed in the system

- Over 1W of Raman amplified signal power has been achieved, which was the expected signal power requirement derived from scaling of 10m range systems using the backscatter modelling (see Section 2.3.2)

4.7 Characterisation of Standard Single-Mode Fibre Raman Amplifier Systems

4.7.1 Summary of Desired Benefits of Standard Single Mode Fibre as a Raman Gain Medium

In order to improve and build upon the results obtained in the OFS Raman fibre, a system using standard communications fibre was investigated. The improvements over the OFS based system sought were in terms of signal quality of the 1651nm output signal and reduction of splice loss, reflections from within the fibre system and cost. It was expected that standard single-mode fibre would provide the advantage of more efficient splicing as well as lower backscatter levels from splices as a gain medium. This is because of the improved matching between the fibre optic components, which are commonly made from standard single-mode fibre, and the gain fibre, when compared to attempting insert a highly doped gain fibre into the system. The resulting lower gain coefficient could be exploited to suppress unwanted amplification, aside from the seeded Raman amplification. In addition, a long gain fibre could be used in order to produce a counter-pumped Raman amplifier

system. The advantages that this could provide include an improved signal in terms of improved isolation from Raman ASE (direction) and lower pump to signal noise transfer.

As discussed in Section 2.7.3, counter-pumping could be a method of reducing the effective gain length of SBS of the signal power increases more rapidly towards the end of the fibre compared with co-pumping. This can lower the length of fibre over which the signal power is high, which in turn would lead to a higher SBS threshold. This is clearly illustrated in the DSF fibre modelling, which was conducted both in counter-pumping and co-pumping, which can be found along with the relevant discussion in Section 4.8.3. The cost of standard communications fibre is considerably lower than that of specialist fibres and the splice is much more convenient and readily repeatable. Both of these factors are considerable advantages in terms of producing a commercial system.

4.7.2 Calculation of Optimal Length for Standard Single-Mode Fibre

The process of obtaining the optimal Raman gain fibre length from the Matlab model was repeated. Previously, when selecting an optimal gain fibre length, the main issue was maximising the Raman scattering of the pump without sufficient experience of SBS and other effects. Given the results from the OFS Raman system, it was clear that the best useable Raman amplifier would have a fibre gain length that was a compromise between being short enough to suppress unwanted non-linear effects, but as long as possible to achieve the best possible optical efficiency. This time the gain length was selected so that the theoretical output power requirement (of 1W for 100m leak detection) was exceeded by around 50% rather than 200% like the design of the OFS Raman system. This could still be considered to be a reasonable performance margin to maximise the chances of the overall sensor system being successful, while reducing the need for a very long gain medium.

The optimal gain length for the counter-pumped standard single-mode fibre system was chosen to be 10km, with the signal evolution along the fibre as shown in Figure 4.27. It was acknowledged that such a long gain length used to compensate for the

low Raman gain efficiency could lead to considerable backscatter and SBS, and hence the gain fibre was created from two reels, one of 4.5km and the other of 5.5km. In assembling the system in this way, it was easy to cut the length of the gain medium in order to investigate the effect on system performance.

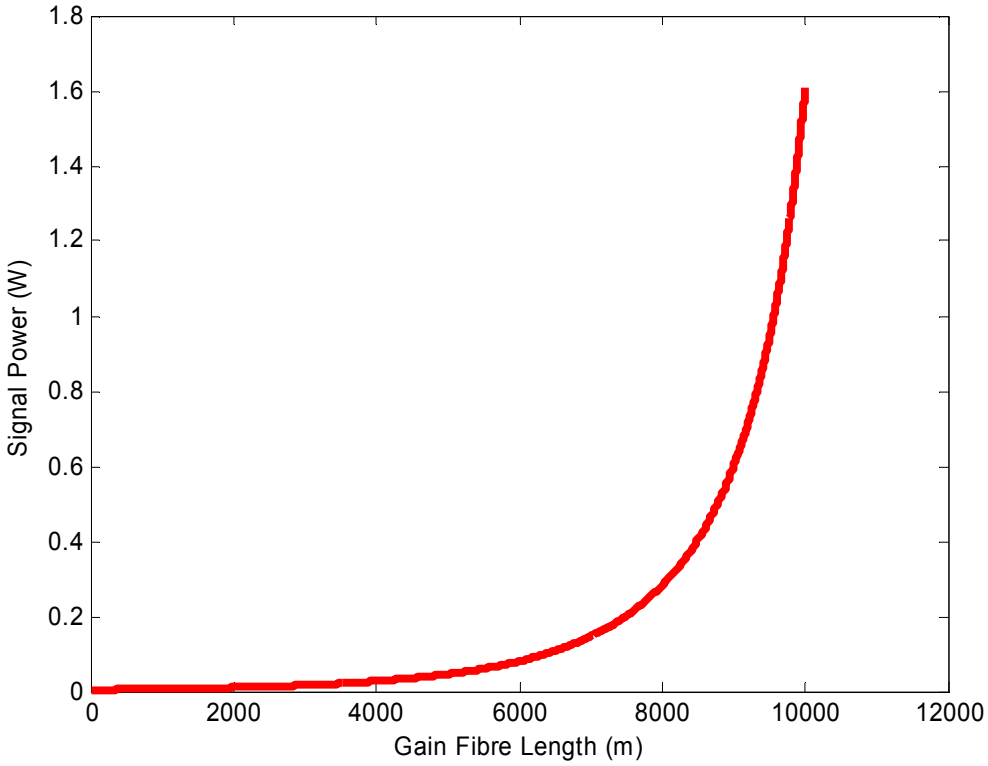

Figure 4.27 Signal power evolution along gain fibre in standard single-mode fibre

4.7.3 Characterisation of Amplified Signal Power as a Function of Input Pump Power for Standard SMF Amplifier Systems

Raman experiments were conducted with the standard single-mode fibre reel, this time only optimising the SBS suppression frequency while conducting Raman amplification (90kHz was chosen). As mentioned previously, the dependence of the effectiveness of SBS suppression by wavelength dither was much less pronounced for the amplified signal case and hence continual optimisation led to no additional benefit. The amplification was conducted firstly in co-pumping followed by counter pumping configurations. Although the system was designed to be counter-pumped, it would be instructive to compare the SBS levels of the system in both co and

counter-propagating configurations in order to help validate the postulation that SBS of the signal experiences a shorter gain length in a counter-pumped system.

During investigations it was apparent that using the 10km system in co-pumping was not a viable system and it did not seem possible to suppress SBS in the signal using the selected techniques with the modulation range available (up to 3GHz dither bandwidth). The results obtained from co-pumping the standard fibre system were as shown in Figure 4.28.

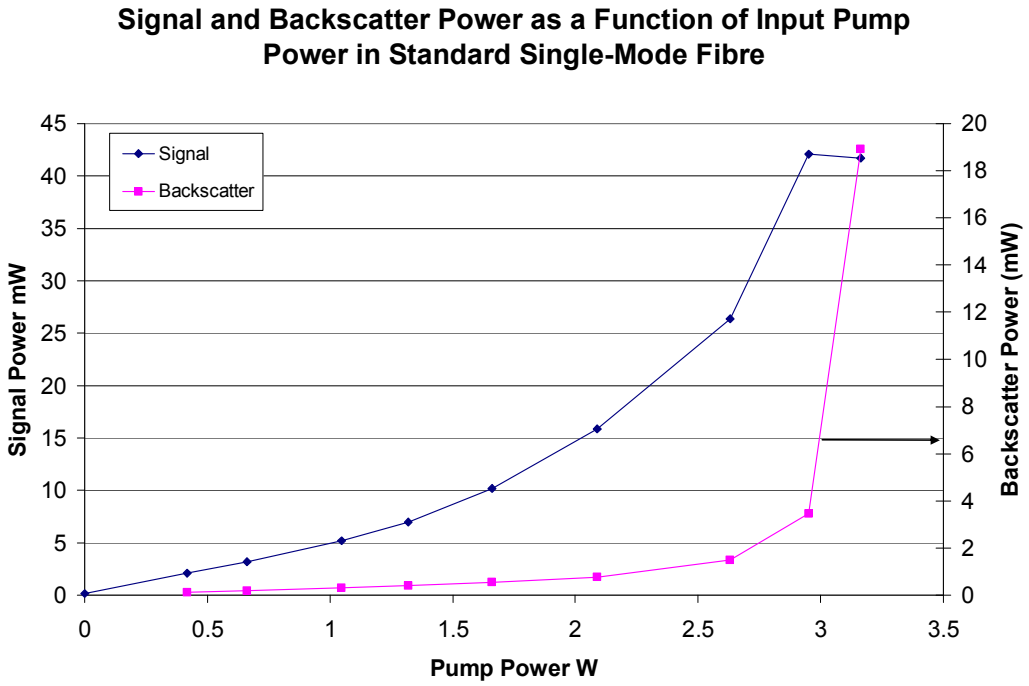

Figure 4.28 Signal and backscattered powers as a function of input pump in a 10km co-pumped standard single-mode Raman amplifier system.

As can be seen in Figure 4.28, the signal power is considerably lower than that expected given the pump power levels and SBS sees strong gain with relatively little signal power. When the signal power reaches 43mW, additional pump power actually leads to decreased signal output as the Brillouin Stokes wave scatters an increased proportion of the signal back out of the fibre. From these results, it could be concluded that this configuration was unsuitable and is considered no further in terms of developing an optimised system.

The Raman amplification experiment was conducted using the 10km standard SMF once more in the counter-propagating configuration, as initially intended. The results of this are shown in Figure 4.29. It can be seen from this, the signal power reached considerably higher levels before SBS led to diminishing signal power with increasing pump power once again. This increase in SBS threshold in the same gain fibre supports the argument that the effective Brillouin gain length can be kept relatively short even in a long gain fibre by concentrating much of the signal gain towards the end of the fibre, in this case by using a counter-pumped configuration. Even given the improvement over a co-pumped standard fibre system, the peak output power at 380mW was insufficient for the purpose of amplifying the signal to the theoretically determined requirement for WMS at 100m range.

Since it was clear that the fibre was too long to be optimal, the 5.5km reel was used alone in the counter-pumping configuration. This configuration was chosen because around ten times more signal was obtainable from the 10km SMF system in the counter-pumped system before SBS became a problem compared with the co-pumped system. It was expected that, even should SBS not pose a problem within the available input powers, insufficient Raman gain would be reached given the pump power available, but the maximum power available in this length of fibre given available sources should be realisable without SBS backscatter beginning to dominate.

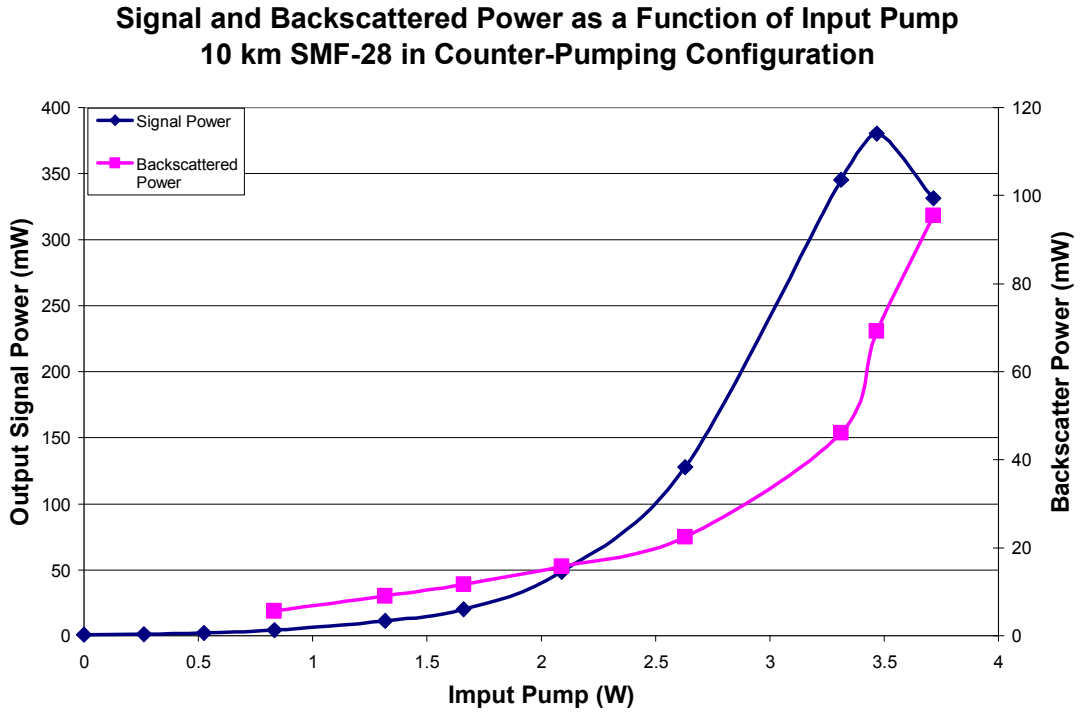

Figure 4.29 Signal and backscattered powers as a function of input pump in a 10km counter-pumped standard single-mode Raman amplifier system.

The larger, 20mW signal DFB was used in order to maximise the Raman gain within the shorter length. This additional signal power was not available for the other standard fibre experiments because the 5.5km fibre was in fact tested at a later date, after the investigations that led to the acquisition of the 20mW DFB laser. This provided 10±1mW 1651nm Raman seed power at the start of the gain fibre under normal operating conditions, rather than 4mW. The laser was not run at full power so that the current modulation still ran the laser at safe, linear limits at all parts of the modulation (i.e. the current limits were not exceeded despite strong modulation).

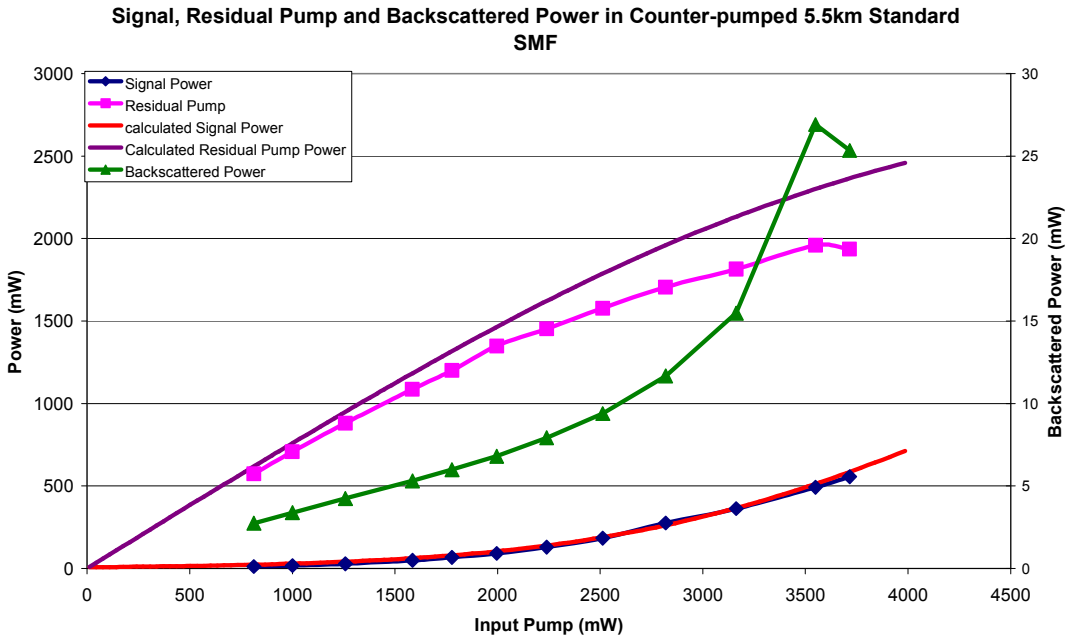

Figure 4.30 Signal and backscattered powers as a function of input pump in a 5.5km counter-pumped standard single-mode Raman amplifier system compared with theory at k=0.55

Although a meaningful, direct comparison between Figure 4.30 and Figure 4.29 cannot be made because of the increased signal seed input power in the 5.5km reel compared to that in the 10km reel, it is instructive to note the relative behaviours of the systems. The model results for the standard SMF parameters and matching experimental are also included in Figure 4.30. From previous results, the polarisation k factor was assumed to be 0.55 directly.

SBS was no longer a limiting factor in the system, despite the strong backscatter when pumping was raised above 3W and the experiment was only limited in range by the maximum output power of the pump EDFA. Given that the growth of the signal power is not adversely affected by the increase in backscatter, the backscattered power is not increasing as sharply as might be expected in the case of SBS, and that at the last point, the backscatter actually decreases, it is thought this backscatter arises from Raman amplified 1651nm Rayleigh, splice and/or connector backscatter. After its onset, SBS becomes very dominant and the continued increase of the signal after threshold is reached is unlikely. It is also highly unlikely that the SBS power level would decrease with extra signal power. The most likely

explanation is that the backscatter experienced less Raman gain as the residual pump power in the gain fibre began to decline because of the increasing signal power (with additional pump power). Finally, the signal power is quite low when compared with other experiments where SBS was suppressed.

The ability to maximise the output of the EDFA while maintaining excellent time-domain resolved signal quality allowed 560mW of signal power to be generated from the standard fibre system. Although this is approximately half of the target signal power level, according to the backscatter models this shortfall should only apply a ~30% penalty to maximum range (i.e. 70m rather than 100m) because of the inverse square relationship between range and backscattered intensity, which makes the system competitive with the current state of art (see Chapter 1). Given excellent output signal quality as observed in the time domain and the relatively low cost of the amplifier system, this was considered to be a reasonable benchmark upon which improvements could be made in terms of high quality output signal power level and hence sensor system range.

The calculated signal power is in excellent accordance with the measured power levels, however the residual pump is not. This could be because, as the backscattered power rises, only a small amount of this is scattering out of the signal and most of it is from the pump via amplification, resulting in unaccounted depletion. This would result in a further gain fibre transit and its associated attenuation (0.22dB/km at 5.5km) and a further set of connector losses before it is read as backscattered power. The other possible cause is a change in 1550nm insertion loss after measurement through bending, splice and connector degradation.

4.8 DSF Fibre as a Raman Gain Medium

4.8.1 Summary of Desired Benefits of DSF as a Raman Gain Medium

DSF fibre was chosen as a compromise between the high gain, high cost, comparatively difficult to splice Raman fibre and the low gain, low cost readily spliced standard fibre in an effort to gain the benefits of practicality of using standard fibre, but with additional gain. It was expected that the best compromise would allow sufficient Raman gain with a moderate gain coefficient, but yet not provide gain to small backscattered signals and SBS. In addition, it was required that sufficient gain could be obtained in a fibre length that would not give rise to high Rayleigh backscatter levels.

4.8.2 Cut-Back Technique for the Practical Realisation of an Optimised Raman Gain Length

Given the results of the investigations with the OFS and standard fibres, it was clear that the length selection was a critical issue in the realisation of an optimised system and that the current strategy of length selection using the mathematical model alone, which did not include terms for SBS and interference, required modifying. By modelling in this way, a gain length that was too long in practical terms when taking SBS into account was chosen and hence an amplifier that would never achieve its projected output power was constructed. Conversely, it was clear that in acquiring a gain fibre that is too short, there was a real possibility of not realising the requisite 1W output power even with the pump amplifier at maximum output.

Although the mathematical models of the Raman systems are instructive in guiding the design of a Raman amplifier system, it is very difficult to create a single model that will predict the exact interplay of all of the parameters. That is to say, it is relatively simple to make a calculation of the SBS threshold of a propagating wave in a known fibre, or the achievable amplified signal power, but when the waves are amplified from small signal levels to the order of Watts this makes the calculation

more complex. In addition, it is not trivial to predict the level at which backscatter problems become an issue in terms of maximum output power and signal quality. The main difficulty is that the Raman amplification and Brillouin scattering parameters are linked. This means that the Brillouin threshold depends upon the Raman signal power profile along the fibre but then, once SBS is initiated and Raman amplified thus backscattering a proportion of the 1651nm signal and depleting the pump, the signal power profile along the fibre changes, resulting in positive feedback.

Taking this into account, the mathematical model would already have become fairly complex but in addition to SBS, there is the problem of amplified Rayleigh, connector and splice backscatter and its interference with the signal. This is a difficult effect to predict and depends upon the splice quality and effective gain of an additional, small backscattered signal while the signal is being amplified. In addition to obtaining these parameters, some threshold for when this backscattered signal begins to cause enough beat noise to be disruptive would need establishing.

With so many interconnected parameters, some of which are based upon physical parameters that are not readily measureable without dismantling the system, the construction of this model would become a major component of the project. Instead, the existing models were kept in place and used as guides to a starting point of an effective empirical investigation. The objective of this investigation was to find an optimal gain length of fibre at which sufficient Raman signal power can be obtained, but also at which SBS and amplified backscatter is effectively suppressed using the dither techniques with modulation parameters conducive to optimised WMS for methane detection.

4.8.3 Calculation of Starting Length for Cut-Back Investigations

With the desired DSF gain fibre sold in 2.1km intervals, a counter-pumped model was run and it was found from the counter-pumping model that a 6.3km would provide acceptable output power using the 5mW signal DFB once more. The more powerful 20mW DFB was not available for the preliminary experiments using the

DSF amplifier system. The counter-pumping model results are shown in Figure 4.31 and additionally the co-pumping results are shown in Figure 4.32. This was included despite the decision to construct this amplifier only in the counter-pumping configuration as it is easier to deduce an optimal length from the resultant plot. The length returned by the co-pumping model is likely to suggest a length shorter than that actually required, but it is better to be conservative to avoid the problems with too much gain medium. If it is found in practice that the gain medium is too short, a different fibre gain medium could be spliced to the end, which would contribute to Raman gain, but not SBS so long as the refractive index of the second fibre is sufficiently different from the first to result in a Brillouin Stokes shifts more than a Brillouin Stokes bandwidth apart. The model of signal power (given a 4mW launch power from the 1651nm DFB and 4W pump power) as a function of distance along fibre was run and returned the results shown in Figure 4.31.

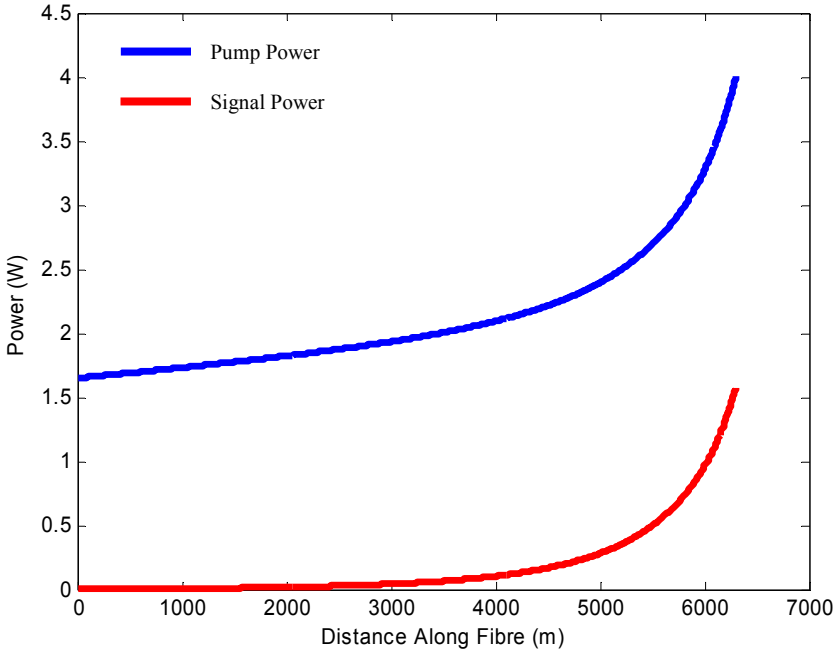

Figure 4.31 Theoretical signal and pump power as a function of distance along DSF fibre in counter-pumping configuration.

It was also thought to be instructive to observe the signal evolution in terms of co-pumping, since it is easier to predict the effects of cutting back the fibre than in the

case of counter-pumping, recalling the relevant discussion in Chapter 2. The results of this are shown in Figure 4.32 for a range of input signal seed powers, 1,3,5 and 10mW corresponding to green, blue, red and purple, or the bottom curve to the upper curve. This suggests that a fibre of down to 4-5km could be acceptable and given that the fibre was sold in intervals of 2.1km, it was considered to be prudent to start with a 6.3km fibre rather than an 8.4km. This was decided on the basis that from experience of previous fibres, the models have generally provided an ideal length that is in fact too long, but that 4.2km could be unnecessarily short. It should also be noted that 10km of standard fibre was too long for the application and this is an indicator for the case of DSF.

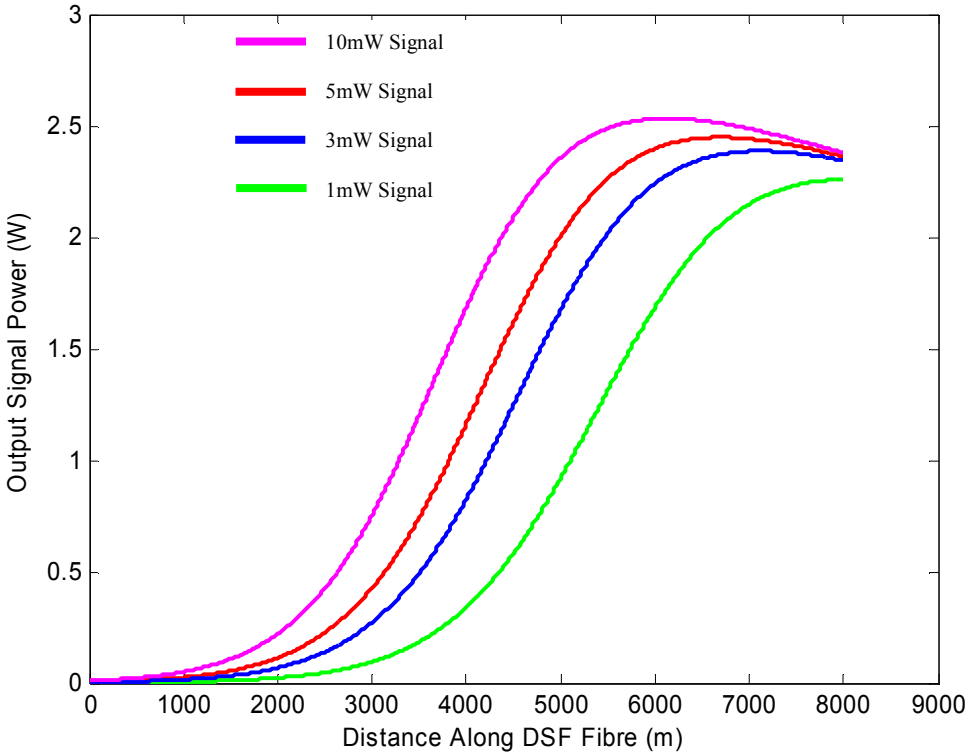

Figure 4.32 Calculated signal power as a function of position along the DSF fibre for a range of input signal powers and a 4W pump in co-pumping

Conducting modelling of the same amplifier for co and counter-pumping is also illustrative of the earlier discussion of the relative signal power evolution along the fibre with respect to distance along the gain medium travelled. It has been observed in the standard fibre experiments that more signal power was generated before SBS

of the signal prevented further gain. This was thought be a result of the shorter length over which counter-pumped amplifiers produce their gain. Comparing the red (5mW) series on the co-pumped model (Figure 4.32) with the signal trace on the counter-pumped model (Figure 4.31) it can be seen that the counter-pumped signal reaches 50% of maximum in the last 600m of the fibre gain medium, whereas in the co-pumped model, the signal reaches 50% of maximum in the last two km. Therefore, it would be expected that there should be a considerable advantage to using a counter-pumped Raman amplifier configuration in terms of maximum achievable signal power through effectively truncating the Brillouin gain length.

4.8.4 The Cut-Back Process

With signal SBS suppressed as far as possible by optimising signal modulation parameters at each cut-back length, Raman amplification was carried out in the counter-pumping configuration using the 5mW 1650nm signal laser while the signal was observed in the time domain to identify problems. With the onset of SBS, the Raman amplification investigation was stopped and the fibre cut back further with the aim of producing an SBS free Raman amplifier system. The fibre was cut back in stages of 600m by spooling sections of the fibre onto an empty reel on a wire winder with a rotations counter until the fibre length was reduced to 4500m.

It was found that at a length of 4500m, SBS was suppressed and there was no impediment to increasing signal power. The backscatter appeared to arise once more from amplified backscatter. However, it was found that there was interference on the output signal despite a moderate output power. The signal output power for the 4.5km reel is shown below in Figure 4.33.

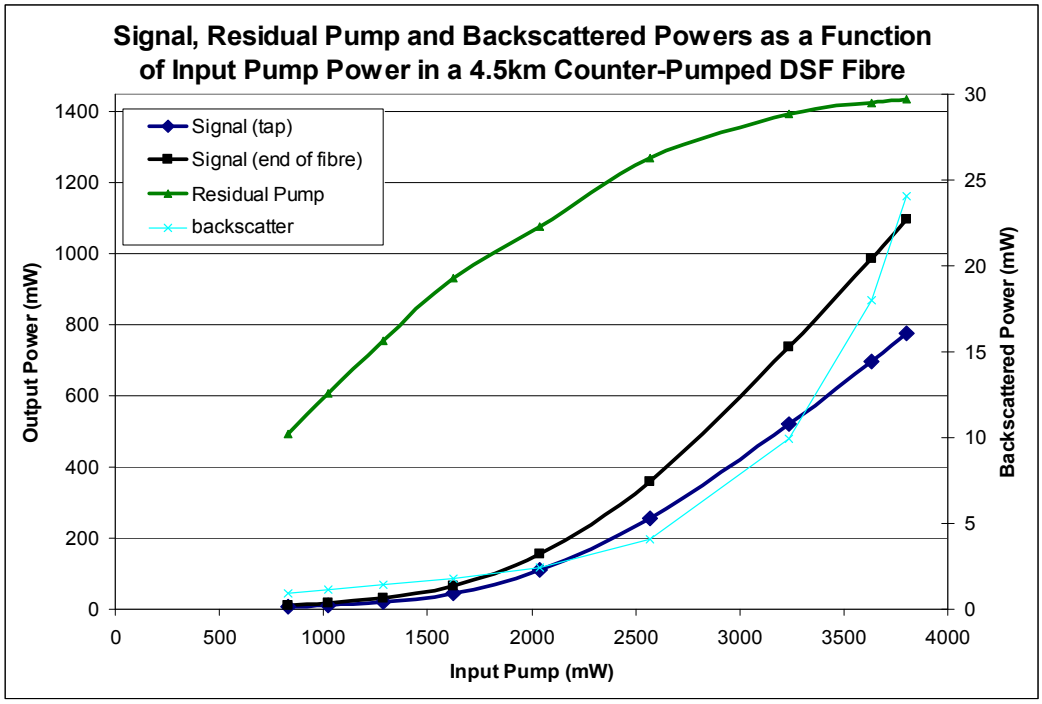

Figure 4.33 Signal power as a function of pump Power for a 4.5km counter-pumped DSF fibre system

It was clear that reducing the length further would not provide any further benefit in terms of signal quality, but would only further reduce 1651nm signal gain. With the 4.5km fibre it was found that the maximum signal power was limited not by SBS but by an unacceptable level of interference in the signal from an amplified double-backscattered 1651nm wave. On further inspection of Figure 4.33, it can be seen from the residual pump series that around half of the pump power is transiting through the fibre unscattered and output as residual pump, meaning that any back-reflections at around 1650nm should experience considerable gain as well as the fact that the system must be sacrificing a great deal of efficiency.

4.8.5 DSF Raman Amplifier Response to Increased Signal Seed Power

One method of suppressing the high gain, while also increasing scattering efficiency into the required Stokes wave was to reduce the residual pump in the system by introducing more 1651nm signal power at the input. Hence, the use of the larger, 20mW signal laser as the Raman seed was investigated in the counter-pumped, 4.5km DSF system.

A Raman amplification experiment was carried out with the EDFA pump set at the maximum power at which a clear, undistorted signal was achieved using the small 5mW laser in the previous investigation (3.8W launched into the gain medium) while the signal power from the 20mW DFB was varied, having been characterised in terms of output signal power as a function of current (see Figure 3.3). The backscatter power, signal power and residual pump were all monitored. The results of this investigation are shown in Figure 4.34

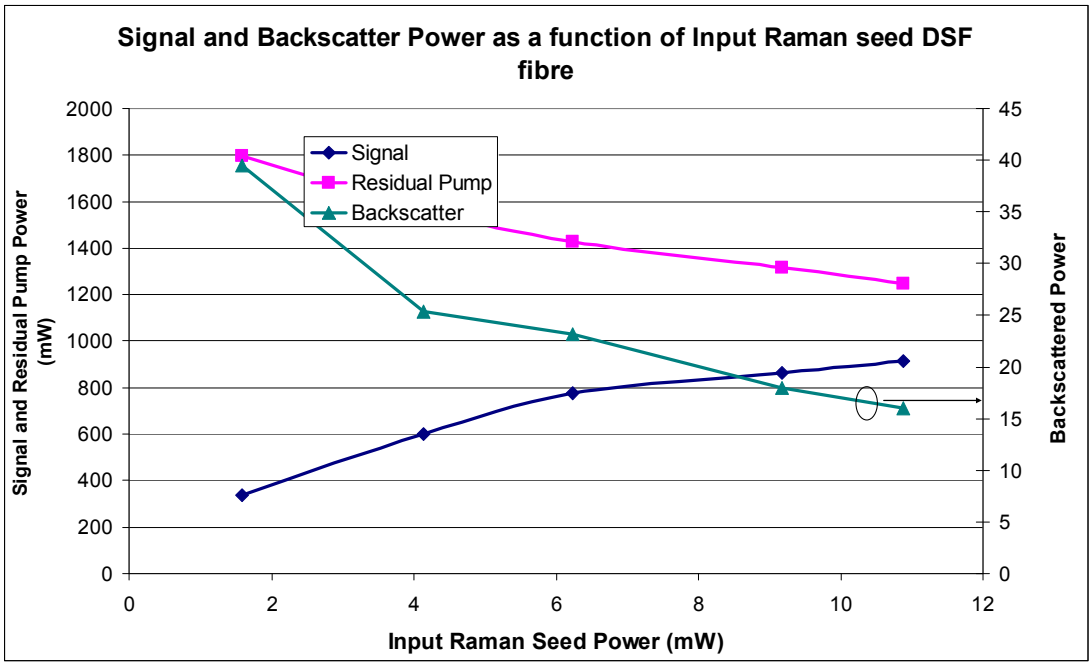

Figure 4.34 Output signal, residual pump and backscattered powers as a function of input Raman seed power, as measured at the output tap.

As can be seen in Figure 4.34, as the input signal power is increased, the output signal power is increased dramatically without any change to the input pump power. Intuitively, this corresponds to a matched decrease in residual pump at the output end of the fibre. Most significantly, the amplified backscatter has been reduced despite the considerable increase in signal power, and this indicates that, as supposed, most of the problematic backscatter power was in fact derived from amplification, rather than the backscatter directly. In other words, most of the backscattered power is in fact scattered 1540nm pump power being seeded by 1651nm backscattered signal. Signal quality was observed to be excellent during the experiment at all input signal powers.

These results led to the inclusion of the larger DFB laser and the signal power as a function of input pump characterisation took place once more to make use of the additional signal power without incurring any penalty to signal quality. The results of the new Raman signal power characterisation, using the 20mW DFB are shown in Figure 4.35. The dither depth was 3GHz and the dither frequency was 337kHz

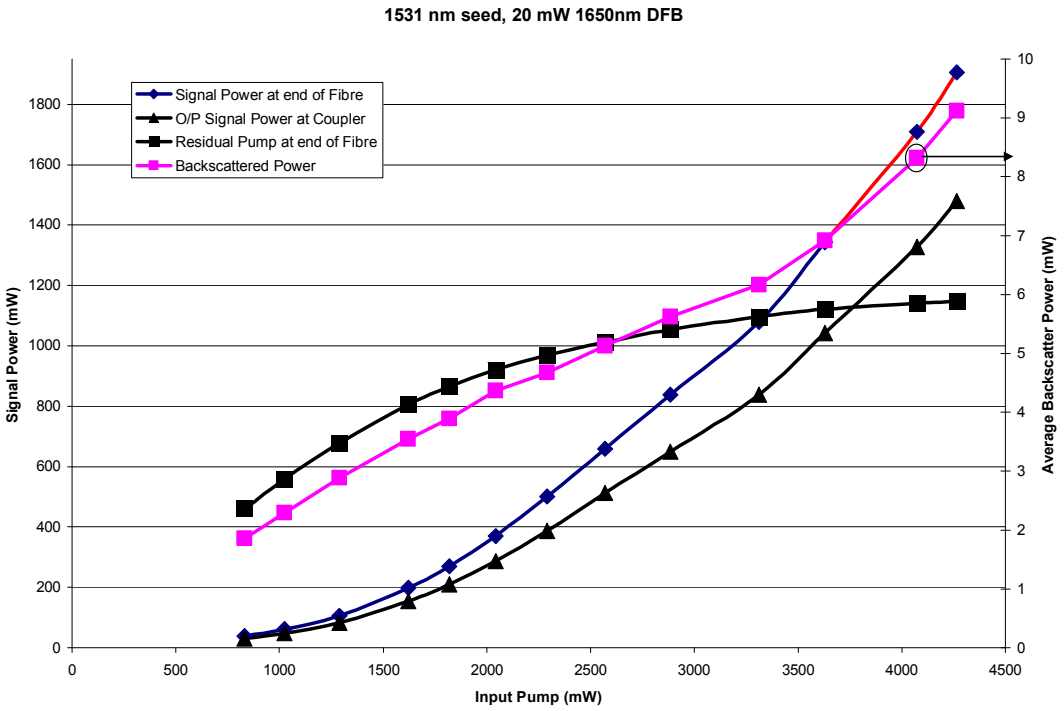

Figure 4.35 Signal, residual pump and backscattered powers as a function of input pump power in 4.5km DSF fibre using the 20mW DFB

The section of the signal series in red indicates the signal level over which there is some signal distortion from interference once more. The implication of these results is that, should the interference add significant noise to a gas signal when the amplifier is used in its application as a high power WMS source, the DSF system can produce over 1W of useable output power (after the taps) without sacrificing sensitivity, whereas if a small amount of interference can be tolerated without a significant change to the quality of the gas sensing signal, 1.4W could be produced.

It should be noted that in this experiment, the signal input connector was replaced because it had become damaged and this increased the available power when compared with the signal response experiment results shown in Figure 4.34. Another note is that during the cutback experiments, part of the fibre at the output side became tangled sharply, leading to a bend loss. As a result of the position of the bend, it was impossible to access without unwinding the entire reel. This bend loss could not be measured directly, but was deduced as being around 1dB from the change in transmission over the entire system. This means that the final demonstrator would be expected to be more efficient than this lab prototype amplifier.

4.9 Characterisation of SBS of a Frequency Dithered Narrow Bandwidth Source in the 4.5km DSF Raman Amplifier System

4.9.1 Characterisation of the Effect of Dither Frequency on SBS Suppression in the 4.5km DSF Raman Amplifier System

While characterising the DSF fibre, it was seen as an opportunity to further test the SBS modelling by conducting the dither frequency and 1% backscatter-bandwidth characterisations. Firstly, an optimal dither frequency was found, again using the 1550nm DFB to seed the EDFA at a constant 170MHz dither depth over a range of dither frequencies while monitoring the backscatter level arising from a constant inserted pump power. The pump bandwidth was maintained at 170MHz so that SBS could be instigated at relatively low power levels so that it could be characterised safely, but also the dither depth would be sufficient so that a noticeable decrease in backscattered power were observed at optimal dither depths

Once more, comparing the theoretical optimal dither frequency for a pump being launched into the fibre gain medium, it is expected that the optimal dither frequency should be around 23.0kHz. In practical investigations it was found to be 27.1kHz.

Some of this disparity could arise from uncertainty in the fibre length after having been cut back and respliced three times.

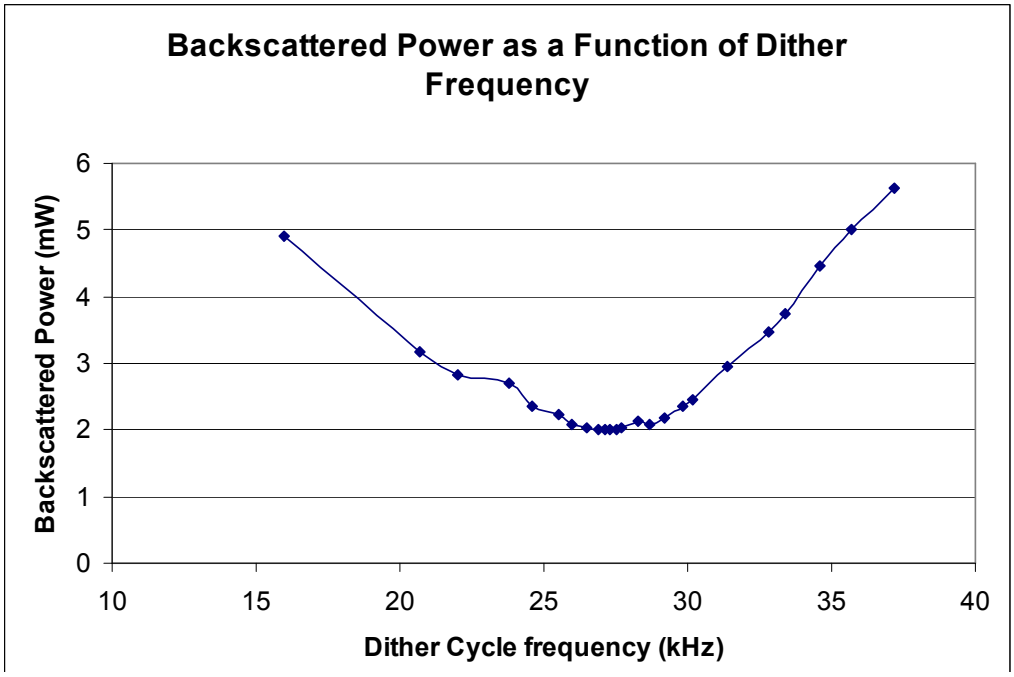

Figure 4.36 Backscatter as a function of dither frequency in DSF Fibre

4.9.2 Characterisation of the Effect of Dither Depth on SBS Suppression in the 4.5km DSF Raman Amplifier System

Using a 27.1kHz cycle frequency, the 1% SBS threshold power was found for an unamplified signal range of dither depths in the same way as in the OFS fibre SBS characterisation. The results of this investigation are shown in Figure 4.37 and using this data shown in Figure 4.37, the 1% thresholds for each dither depth were plotted on a separate chart as a function of pk-pk dither depth and compared with the mathematical modelling. This plot is shown in Figure 4.38.

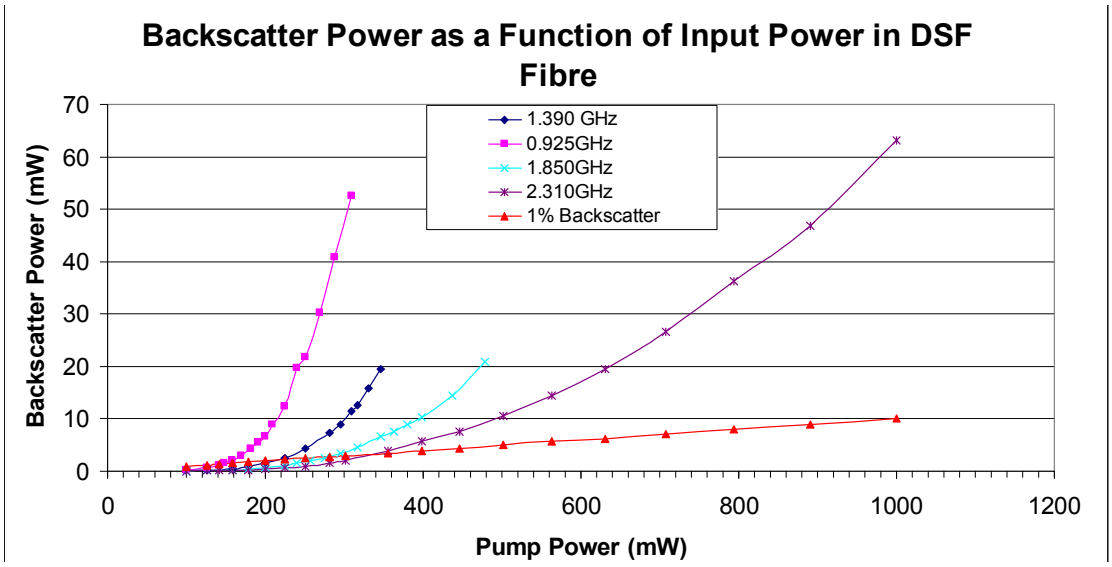

Figure 4.37 Backscatter power as a function of input power for a range of pump bandwidths

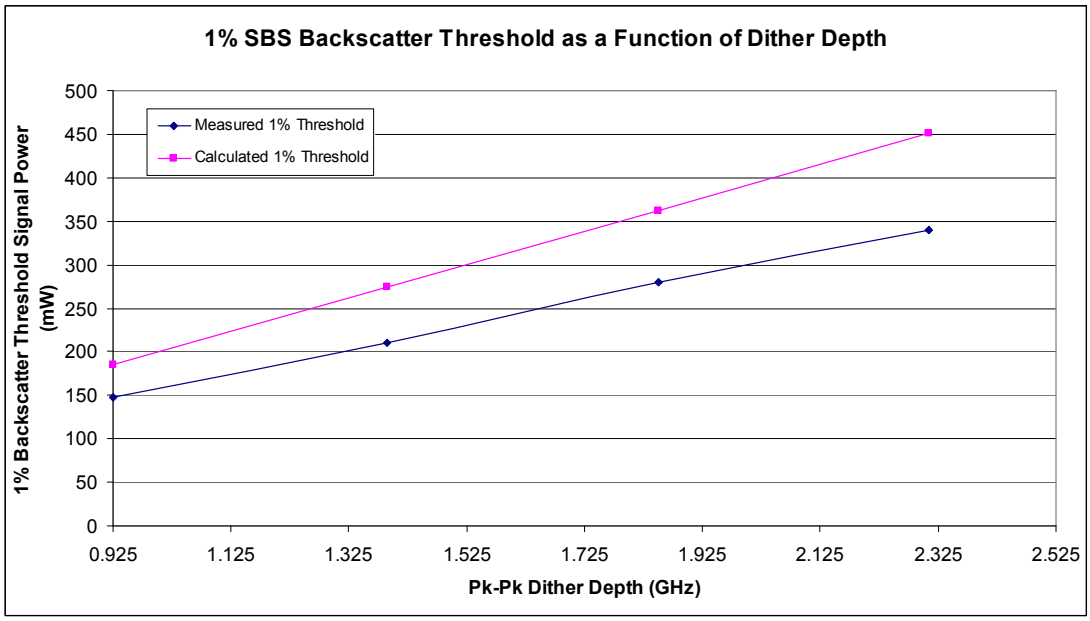

Figure 4.38 1% SBS threshold power as a function of signal dither depth for unamplified signal in 4.5km DSF fibre system.

Once more, the same assumptions were made in the modelling of the SBS threshold in the DSF system, i.e. the Brillioun gain coefficient being similar to those of standard fibre, and approximating the pk-pk dither depth as the signal bandwidth. It is possible that these assumptions have led to some discrepancy between the theoretical and measured values.

This is supported as, once more the expected threshold is higher than that measured, indicating that the disparity is likely to be systemic. Despite the offset, the model results are considered to be accurate enough to make the models useful in designing a system, and with further modification to take account of the effective bandwidth arising from dither depth, could be much more accurate.

4.10 Diagnostics of a Raman Amplifier System

4.10.1 Overview

Over the course of the account of the investigations carried out with the aim of producing an optimised Raman amplifier, several effects that destabilize the output of the amplifier have been alluded to and their method of suppression stated. It is convenient to give a more detailed account of these effects separately, in terms of the evidence sought and verification procedures to identify and suppress them. In all cases, while carrying out a characterisation of the signal power as a function of pump power for an amplifier, the signal was monitored in time and wavelength domains as part of the design procedure. The effects observed and suppressed were Raman ASE, SBS of the signal and signal interference with the amplified, double-backscattered signal and will be dealt with in turn.

4.10.2 Raman ASE

As stated in Chapter 2, Raman ASE occurs when the build-up of spontaneous Raman scattering of the pump becomes sufficient to seed stimulation of Raman scattering of the pump. This was observed while using the 37dBm EDFA with Seed 1 tuned to 1541nm while carrying out the characterisation of signal power as a function of input pump in the 4.5km DSF reel in the counter-pumping configuration. It should be recalled that Seed 1 produced a relatively narrow peak at the selected wavelength that, although of sufficiently broad bandwidth to suppress SBS, it confined sufficient

spontaneous Raman scattering within a narrow enough spectrum for the spontaneous emission at 1650nm to experience significant gain and become ASE. The signal as a function of pump power characterisation where Raman ASE was identified was as follows in Figure 4.39.

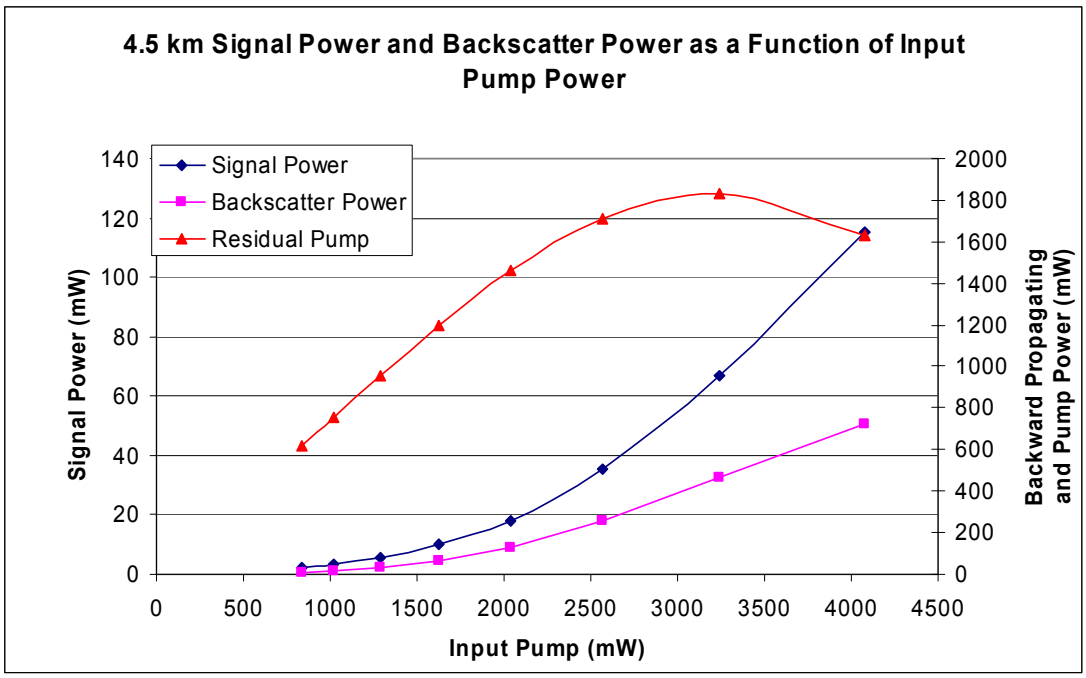

Figure 4.39 Backscatter, residual pump and signal power as a function of input pump power in counter-pumped 4.5km DSF system using Seed 1 to drive the pump EDFA

The most obvious characteristic that indicates that there is a problem with this Raman amplifier system is that there is a very large 1651nm 'backscatter' reading (right hand axis applying to backward travelling light relative to the signal and residual pump) in comparison to the signal power level (left hand axis), i.e. there was a significant amount of 1651nm power travelling in the direction of the pump wave. It should be noted that this was extremely unlikely to be SBS for two reasons, firstly the backward travelling power level is much greater than the wave from which it was generated even at low signal and pump powers and secondly, despite its considerable magnitude, it does not cause signal power to decrease with increasing pump as it would in the case of SBS of the signal. The power is around 1651nm as investigated using an OSA.

Given this evidence, it was supposed that the 1651nm power travelling with the pump must have derived from another effect. Investigating the 1651nm power travelling with the pump in the time domain using an oscilloscope revealed a strong noise reading, and investigation using an OSA shows a broad bandwidth peak around 1650nm. It was concluded, therefore that the forward propagating 1650nm power (relative to the pump) was ASE arising from the relatively narrow bandwidth pump peak.

Since the tuneable filter was used in this investigation, it was possible to provide additional verification that the observation was indeed Raman ASE. The wavelength of the seed and hence the pump peak output wavelength was varied via the tuneable filter, resulting in the range of pump spectra shown between Figure 4.11 and Figure 4.13, and the ~1651nm ASE peak could be observed to shift in wavelength with the changing pump wavelength on the OSA. This would not be the case if the Raman Stokes wave were seeded by a laser source of fixed wavelength (or performing a dither of the order of a few GHz), the signal wavelength would remain the same. Instead, as the pump wavelength changed the scattering efficiency to the signal output wavelength would change by an amount depending upon the Raman gain spectrum and the magnitude of the wavelength shift. It was found that the ASE peak was strongly suppressed when the tuneable filter was set at a wavelength (around 1530nm) that provided very little control over the output of the EDFA pump, resulting in a broad bandwidth ASE pump spectrum without any strong peaks.

This was one of the observations that demanded the construction of Seed 2 with a CWDM filter in place. This action removed any Raman ASE from the system, yet controlled the pump more efficiently than tuning the tuneable seed out of the EDFA peak range. It should be noted that if Raman ASE is present in a co-pumped system, the high power level at the backscatter tap will not be present (as a result of the ASE). The ASE power will emerge deceptively through the same output as signal power from the test bed used in these investigations and cannot be distinguished using power meters alone, instead it can be distinguished from amplified signal

power in two ways. Firstly, in the time domain any AM signal applied to the DFB (via the current dither) will appear to have considerable noise on top of it and perhaps be of small magnitude compared to what might be expected given the output power as measured on the optical power meters if significant ASE is present. Secondly, on an OSA, the 1650nm signal will appear as a narrow bandwidth spike on top of a broad bandwidth ASE peak (assuming a broad bandwidth source compared to the signal laser is being used to pump the Raman system), which will follow the shape of the pump peak from which it has seeded. The pump and signal spectra were monitored during Raman amplification experiments, and an example of a good signal spectrum is shown in Figure 4.40.

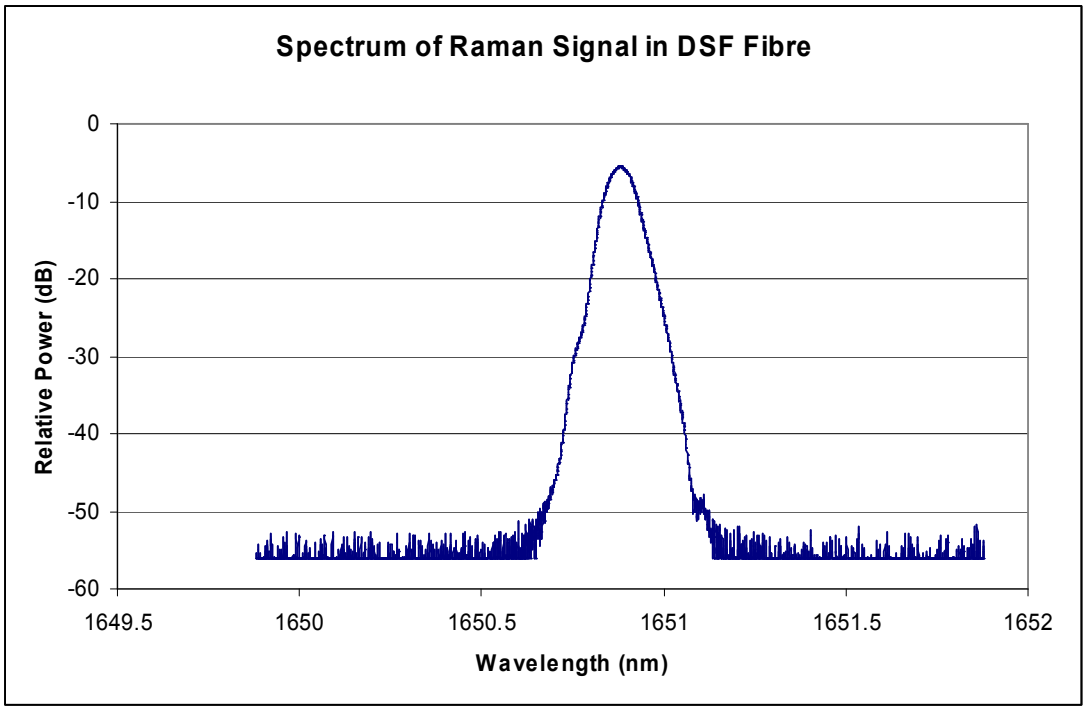

Figure 4.40 Wavelength Spectrum of methane sensing signal output

In addition, although this is inadvisable in practice, there will be an unexpectedly insignificant change in the signal output power level if the DFB signal laser is switched off if the signal is dominated by ASE (again assuming the co-pumping regime). The occurrence of this effect underlines the importance of monitoring signals in the time domain for early identification of such effects.

4.10.3 SBS

This has been covered in more detail while providing an account of the results, but the most obvious limitation SBS applies is the impediment to increasing gain via pump power either by scattering dangerous levels of power back to the source or by actually reducing the signal power level. The signal power can decrease with increasing pump because as the pump power is increased, more signal power is generated, and more of this is scattered in the backward direction, which in turn depletes the pump as it experiences SRS. This has been observed most dramatically in the 10km standard single mode system, see Figure 4.29.

Suppressing SBS was one of the major considerations within the project, it requires a strategy for suppression as it is an inevitable consequence of attempting to evolve high power, narrow bandwidth signals in a standard type optical fibre. Should the limits of the suppression strategies be exceeded by the onset of SBS, there are several strategies available. Firstly, the fibre can be cut back, as with the DSF fibre. This reduced length increases the SBS threshold, but also decreases the Raman gain of the system. If sufficient Raman gain is still available, the cutting back can be ceased and the amplifier used, if the output power is not sufficient, it should be possible to splice on further fibre reels, which have sufficiently different refractive indices and core areas, resulting in different Brillouin frequency shifts. If these shifts are more than a Brillouin gain band apart, they allow further Raman amplification without contributing cumulatively to the effective Brillouin gain length.

4.10.4 Signal Interference with Double Backscatter

With SBS suppressed, it was possible to run the Raman amplifier system at maximum pump power without risk of high backscatter levels. However, multipath interference (MPI) imposed a limit upon the available signal output power by adding noise to the signal. Its onset, as viewed when monitoring the time domain signal output using a photoreceiver is shown in Figure 4.41, where a small fluctuation can be seen in the AM signal. This was observed in all of the fibre systems in which

SBS was fully suppressed, and signal power levels at which this distortion is present are denoted as the red section of the signal power series in Figure 4.35.

This fluctuation normally occurs at high signal power levels (~W), but can also occur at lower power levels if there is a problem with a splice or a connector that increases the reflectivity of the fibre system. At its onset, the distortion is small, but increased signal power levels result in a rapid increase in the size of the distortion, resulting in the signal becoming almost unrecognisable as a sinusoid.

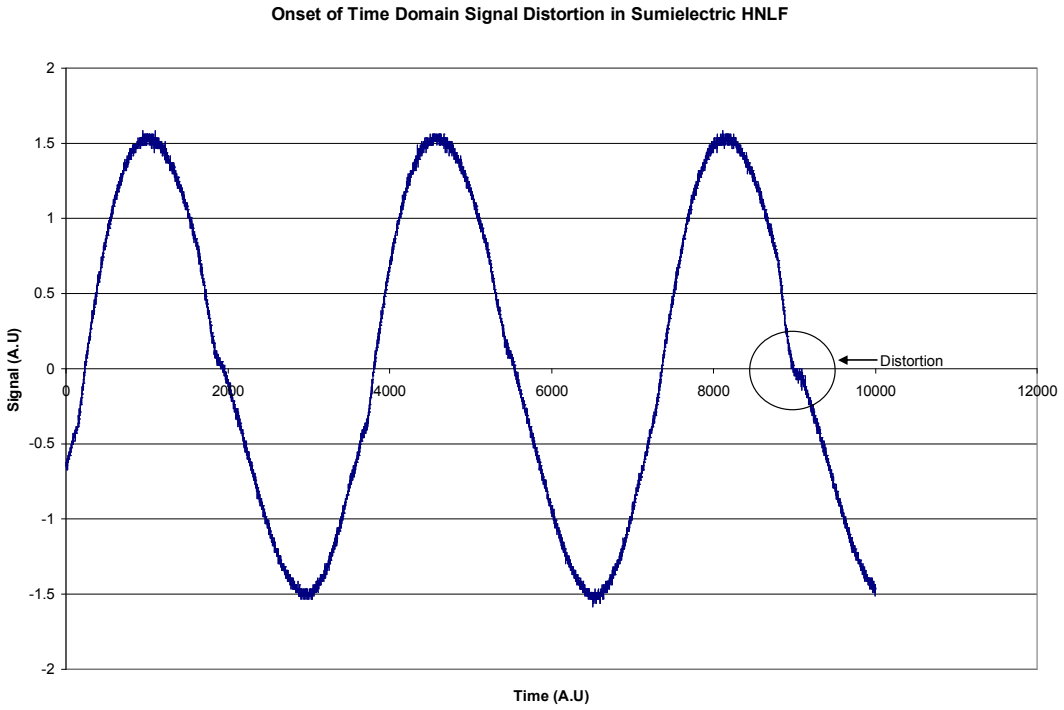

Figure 4.41 Amplified backscattered signal-signal interference.

In order to support the supposition that this effect was a result of MPI, the effect was replicated by launching an unamplified 1550nm DFB into the OFS fibre system and fitting a loop mirror to the 1550nm high power tap output (residual pump 99% output), while observing the 1550nm low power tap (1% 1550nm monitor tap) output, which would usually have been used for monitoring the residual pump output. A current dither similar to that used in the Raman amplifier systems was applied and the result observed was the same as that in Figure 4.41.

Given the evidence observed in the behaviour of the system whilst affected by MPI, an account is made of the processes occurring. Essentially MPI noise occurs as a result of amplitude fluctuations of the narrow bandwidth signal caused by interference between the single-pass and double-backscattered signal at the photodetector. Double-backscatter occurs because the signal is backscattered continuously throughout the fibre via the elastic Rayleigh scattering and also at scattering centres such as the splices and connector end faces. This backscattered light experiences Raman amplification within the gain fibre and this amplified backscattered signal power is backscattered a second time through the same processes (i.e. double-Rayleigh scattering (DRS) and connectors and splices again). This experiences Raman gain once more while co-propagating with the signal. The photodetector at the output of the system incurs both the single-pass and triple pass signal components simultaneously and how they interact depends upon the signal and fibre system conditions. Firstly, recall that the sinusoidal current dither applied to the DFB laser results in modulation of both the wavelength and amplitude of its output, and this means that the single and triple pass signals coincide in wavelength twice per dither cycle, resulting in two interference spikes in each complete sinusoidal dither.

It was observed that the spikes were particularly prevalent at certain dither frequencies and that increasing the dither depth suppressed the effect to an extent. For optimised interference (hence exacerbating the problem) to occur when the wavelengths match, the electromagnetic waves must be in phase or anti-phase at the detector. The phase separation between the multi-pass wave and the signal depends upon two things, firstly the round trip optical path length difference, a parameter related to the fibre system that determines the time delay between the waves (dt). Secondly the phase separation depends upon the dither frequency, which determines the phase angle swept through in the time interval dt. Hence it would be expected that adjustment of the dither frequency would change the strength of the interference measured at the detector. The other observed effect dither parameters had on the

interference spikes was that increasing dither bandwidth suppressed the interference spikes. The suspected reason for this was that by increasing the wavelength dither depth, the time over which the interference condition is met at the detector is shorter compared with the scan period of the photoreceiver circuit, resulting in the observation of a smaller amplitude fluctuation. It should be recalled that the bandwidth of even the Thorlabs photoreceiver was only in the range of MHz, so with a modulation frequency of hundreds of kHz, it is possible that this could have an effect. An investigation was carried out in the 4.5km counter-pumped DSF system in order to form a relationship between signal power and threshold dither bandwidth for the onset of interference as shown in Figure 4.42.

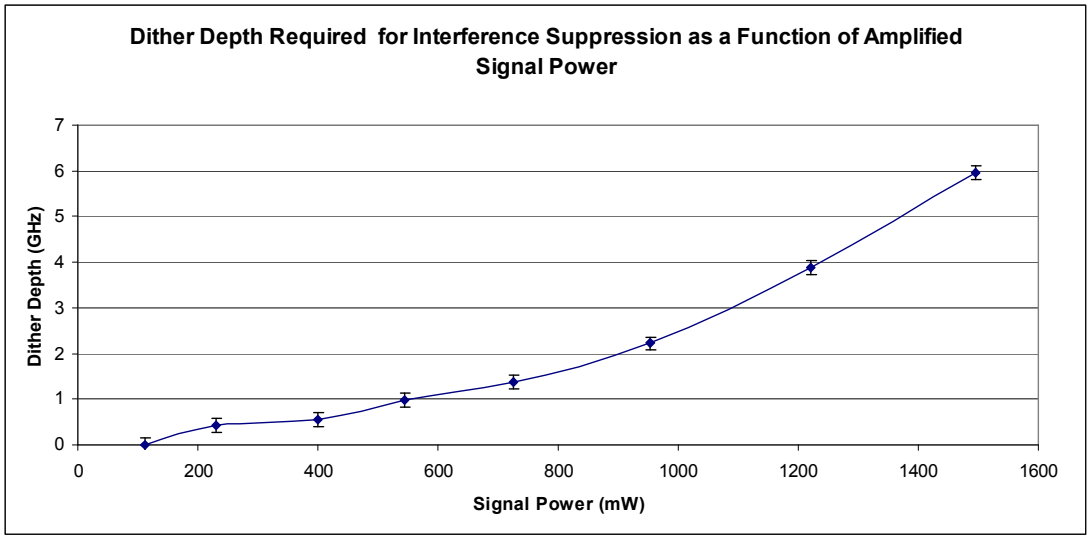

Figure 4.42 Threshold dither depth for suppression of interference in DSF fibre system as a function of signal power

For a dither depth of 3GHz, the preferred modulation depth for WMS, the lab based Raman amplifier could produce an optimised WMS signal of ~1.1W without measureable interference in the signal. It was expected that, in the construction of a full prototype system, more effort could be applied to minimising scattering centres during splicing. It would therefore follow that the interference threshold for the prototype system would be offset towards higher power for a given dither bandwidth compared to those in Figure 4.42

Given the observations of the behaviour of the interference and the resultant suppositions, a strategy was formed to maximise signal power while suppressing the interference. In overall terms, this involves two types of approach; building the system with lower effective reflectivity and optimising the modulation parameters. The first preventative is self-explanatory, in that by reducing the amount of backscatter, the signal-double-backscatter interference is reduced. Considering that the backscatter and double-backscatter experience Raman amplification when they become significant, the effect of reducing the origins of scattering within the system should have a strong effect on suppressing MPI. In order to achieve this, the system should be built with careful consideration of splice reflections. This applies to care when choosing fibre gain media to reduce Fresnel reflections at the splice, taking care to make an excellent cleave and splice on fusing the fibres, minimising the number of splices over which high powers are transmitted, regularly checking and cleaning connector end-faces and ensuring that all fibre ends are terminated or cleaved and folded into a tight loop.

Secondly, modulation depth should be maximised in terms of acceptable WMS limits. Even if a smaller modulation depth is adequate for SBS suppression, the interference can be more difficult to suppress. Also, within the band of modulation frequencies acceptable for WMS and SBS suppression, there are optimal and poor frequencies in terms of suppressing the interference and so a dither frequency that suits all three requirements needs to be found. This applied a third set of criteria to the WMS modulation frequency in addition to the SBS suppression requirements. A suitable frequency in the 4500m DSF fibre for suppressing SBS and interference while being useable for WMS was found to be 337kHz.

4.11 Conclusion of Design of Raman Amplifier System and Summary

4.11.1 Conclusion of Raman Amplifier Design and Performance of Prototype

It was decided that an optimal system had been realised in the 4.5km counter-pumped DSF system, achieving more than 1W of good quality output signal. This system was reproduced by a partner organisation and received for characterisation and field testing. One change that had been made by the company was that the 1531nm CWDM filter in the seed source had been replaced with a 1551nm CWDM filter. This was replaced with the 1531nm CWDM filter after characterisation of the system showed that this was detrimental to efficiency. The performance of the system in terms of output power was investigated for pump profiles resulting from the two different filters and the results are as follows in Figure 4.43

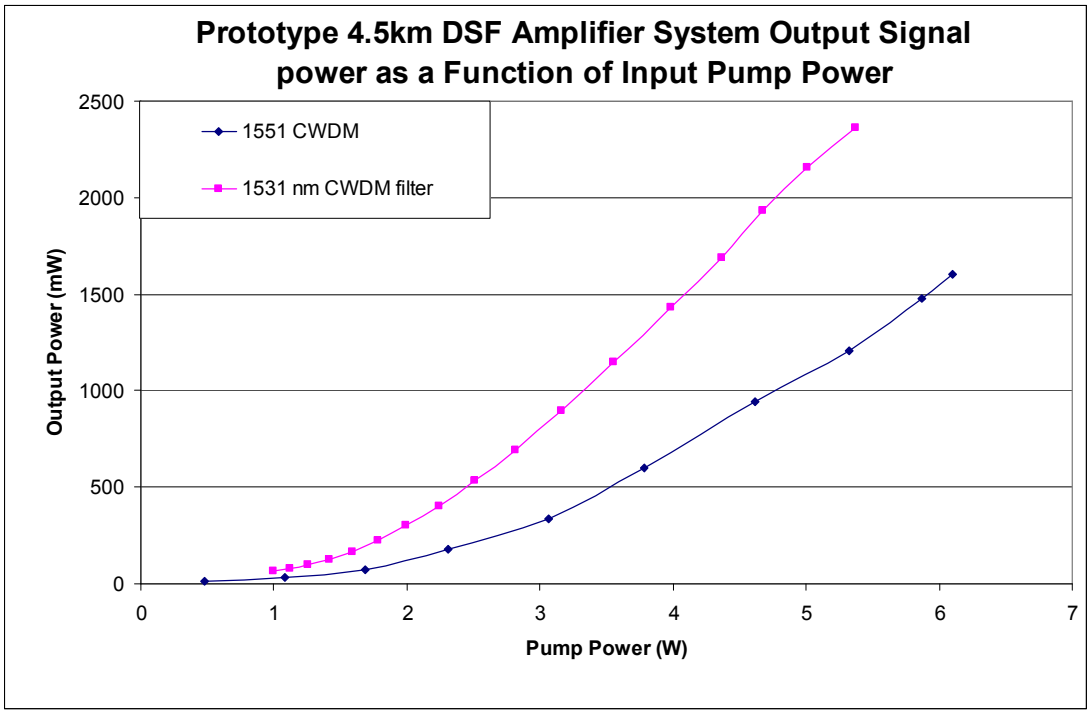

Figure 4.43 Signal power as a function of input pump power in final prototype amplifier system (assembled in factory, modified and tested in Strathclyde University)

It can be deduced from Figure 4.43 that the splice and bend losses have been optimised in comparison to the lab demonstrator system. Furthermore, given the improved splice quality, interference only began to appear (occasionally) at the final data point on each trace, meaning that the system was capable of consistently producing a 2.16W WMS signal of excellent quality at the output coupler as measured by a pyrometer. It was required that the system should be energy efficient and therefore the scattering efficiency from 1540nm to 1651nm was characterised in terms of output signal power given input pump power as shown in Figure 4.44.

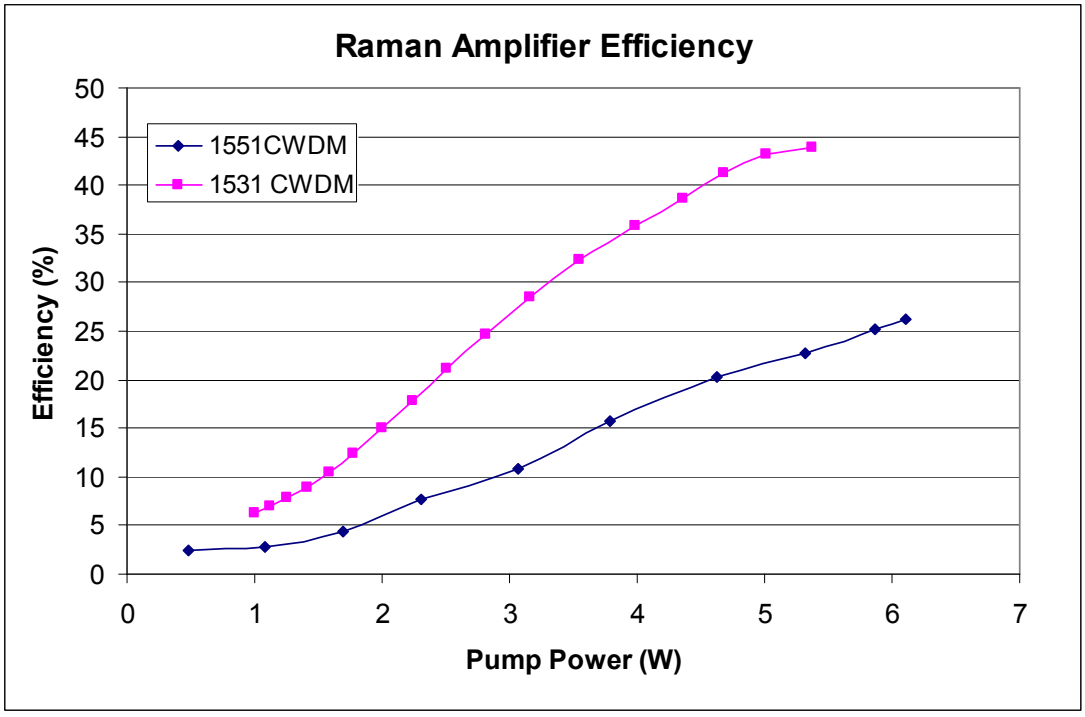

Figure 4.44 Characterisation of efficiency of prototype amplifier system as a function of input pump power

4.11.2 Summary

The aims of the investigations were to validate the mathematical modelling of Raman amplifier systems in terms of Raman amplified power and SBS. In doing so, this would help form a method for the design and characterisation of a Raman amplifier system. On completion of both a design method, an optimised demonstrator was to be constructed and tested and the successful design sent to the fibre specialist partner organisation to be reconstructed to factory standard.

The Raman amplification models were in excellent accordance with measured values for both co and counter-pumping investigations, particularly with regard to the prediction of output signal power, meaning that the Raman models were valid, as was the treatment of polarisation dependent gain in the modelling process. It was found that restraint was required when using the models to determine a desired length for a Raman gain medium as the model did not take account of some unwanted effects arising from excessive gain length. Given this, it was convenient to use the model to calculate an approximate length and then optimise the gain length empirically using the cutback technique while monitoring signal power levels in the time and wavelength domains in stages together with the diagnostics detailed above. For large scale Raman amplifier design for many different amplifiers, it may be worth designing or purchasing a fuller modelling package that would take account of all of the factors involved with producing a high power WMS signal via Raman amplification in fibre. The data contained within this chapter might be a good starting point for such a package, which would have considerable commercial value.

The SBS modelling was in reasonable agreement with the experimental data, but the actual measured 1% SBS threshold level was always found to be lower than the calculated level. The SBS models could still be used as an excellent guide to optimal dither frequency (for a wave with gain ~0) and a fair guide to threshold signal power level given a signal bandwidth. However, they require some refinement to provide a higher degree of accuracy.

In terms of the production of an optimised Raman amplifier system, a range of fibres were successfully tested in co and counter-pumping configurations with SBS, Raman ASE and backscatter-signal interference being observed, identified and suppressed to the extent that the target signal power could be comfortably exceeded. An optimised amplifier system was realised by the end of the investigations, with a system being designed with a common communications fibre gain medium (DSF fibre was readily available and inexpensive because of its use in telecommunications) and fibre components. The system produced a good quality 1651nm WMS signal in excess of

1.1W (at the output connector). In addition, the system would be cheap, robust and easily manufactured without using time consuming specialised diffusion splicing techniques. It was realised that the reconstructed system would perform much better because there was an irresolvable tangle on the DSF fibre reel, leading to a bend loss.

The final prototype system was constructed according to the lab demonstrator design and its performance was found to exceed that of the lab demonstrator through the minimisation of splice loss and lower reflections allowing more interference-free power to be evolved (see Figure 4.43). This CW, silica fibre Raman amplifier system represents a significant advance in spectroscopic sources, providing high gain (>23dB, or a factor of 200) and power (~2.2W), high efficiency (~44%), low noise and low cost associated with this device. The system was considered to be ready for testing in the application of long range methane detection and this is discussed from initial backscatter and short range methane measurements (using the lab demonstrator) to full field trials (using the prototype system) in Chapter 5.

4.12 References

[4.1] R. Billington "Measurement Methods for Stimulated Raman and Brillouin Scattering in Optical fibres" NPL report (June 1999) Obtained from www.npl.co.uk in April 2007

[4.2] B. Culshaw, G. Stewart, F. Dong C. Tandy D. Moodie, "Fibre optic techniques for remote spectroscopic methane detection—from concept to system realization" Sensors and Actuators B 51 (1998) 25–37

Chapter 5 Methane Leak Sensing at 100m Range

5.1 Introduction

This chapter presents the results of the preliminary methane sample measurements, leading to the full range testing of the sensor system. These include a backscatter power level characterisation of a range of surfaces to form a basis for the expected received powers at 100m as well as short range gas measurements using a scaled signal power to investigate the minimum power required at the detector to measure a given methane concentration. Both of these investigations were carried out using a lab demonstrator configuration, whose schematic is shown in Figure 3.12. The amplifier source for this configuration was the final, cut-back DSF FRA. Given these preliminary methane sensing results, the expected performance of the system was investigated and the fully packaged prototype was used for long range field trial gas sensing investigations.

5.2 Validation of the Inverse Square Relationship between Range and Backscattered Intensity

It is supposed that the only difference between detecting methane leaks at short range ~10m and at long range ~100m is the output signal power required to provide the requisite backscattered power at the detector to produce a useable gas signal. Given this, if a relationship between range and received backscattered signal can be established, the required output signal power to achieve a specific range or the maximum range given the available signal power can be extrapolated based upon short range gas measurements. The relationship between backscattered intensity and range was considered to be an inverse square law, based upon the radar equation while assuming that the output beam is small compared with its target. (see Section 2.3)

In order to carry out a validation of this relationship experimentally, the backscatter configuration was arranged (recall Figure 3.12) and a diffuse reflector, in this case a concrete garden block, was initially mounted at 9m from the receiver and 42mW from the Raman amplifier was directed normally onto its surface via the Tx telescope. The send receive (Tx Rx) configuration can also be viewed in the photograph supplied (see Figure 5.3), showing the collimator, to which the high power signal is fed before being split at the glass slide, with the reflection passing through the variable attenuator set between the telescope lenses. The resulting photoreceiver voltage due to backscatter was measured on an oscilloscope at each of a series of ranges, which were set using a measuring tape. In addition, the output photoreceiver voltage from background light was measured to be subtracted from each of the readings. The ranges chosen were between 9m and 24m at 3m intervals. The actual backscattered power falling on the detector, as focussed by the 30cm diameter Fresnel lens (the area of which was taken to be the collector area) was calculated from the measured output voltage of the photoreceiver and can be seen as a function of range in Figure 5.1.

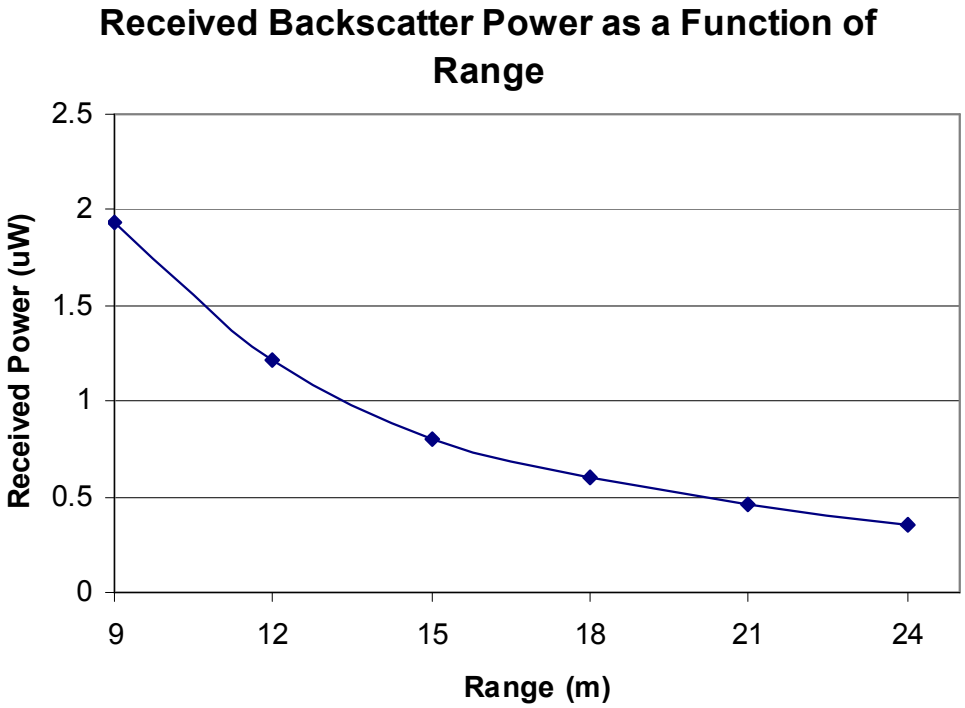

Figure 5.1 Received backscatter power from a concrete block as a function of range

These power measurements were normalised to the received power at 9m (the closest range measured) and plotted together with a theoretical plot that assumes that received power (at a fixed collector of known area) is inversely proportional to the square of range (distance between detector and target.) This theoretical plot is also normalised to the received power at 9m. The comparison of this theoretical plot and the measured power at the detector as a function of range should determine whether it is valid to use Eqn 2.6 (whose significance is that it states that backscattered intensity is proportional to the inverse square of range from surface to detector) to calculate the backscattered power at the detector from diffuse surfaces, and whether the maximum range of the sensor system can be calculated using it.

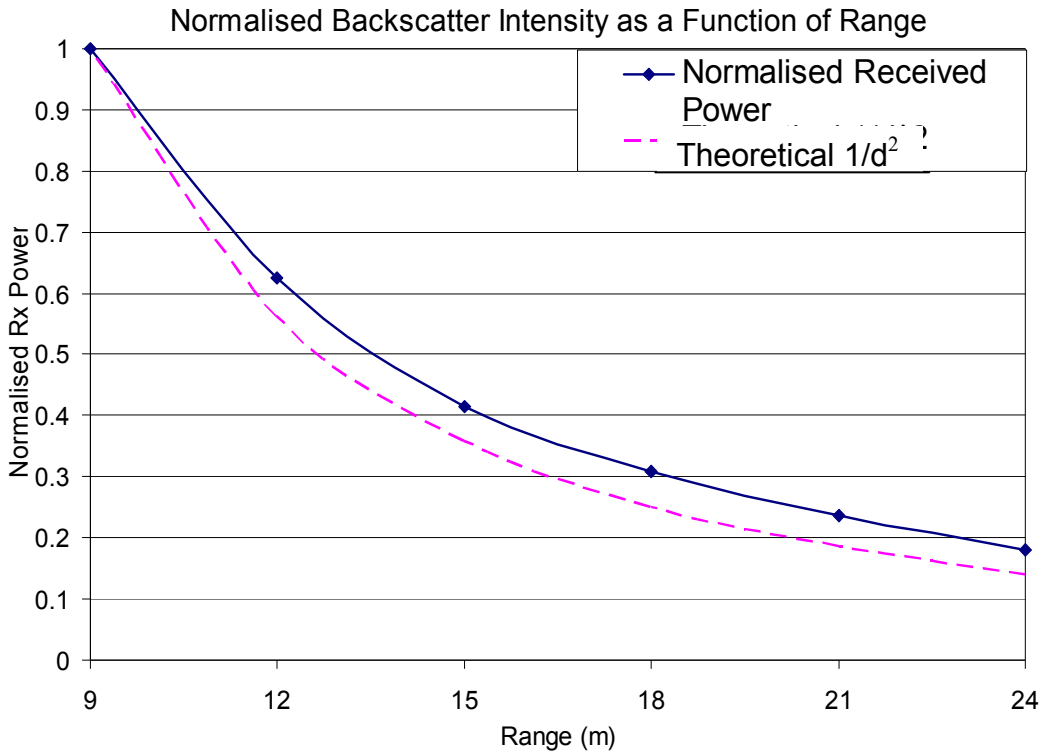

Figure 5.2 Comparison of normalised backscatter power at the detector as a function of range and expected backscatter power at detector assuming radar equation holds

The normalised comparison of the measured power at the receiver and the expected values according to the radar equation is shown in Figure 5.2. From these results it is reasonable to say that backscatter intensity (or the received power falling on a set collection area) is a function of the square of distance and extrapolations of long range gas sensing performance can be made using this in conjunction with short range sensing results. Although the data set range is relatively small, it is considered to be useful in determining whether the system is ready to take to long range testing.

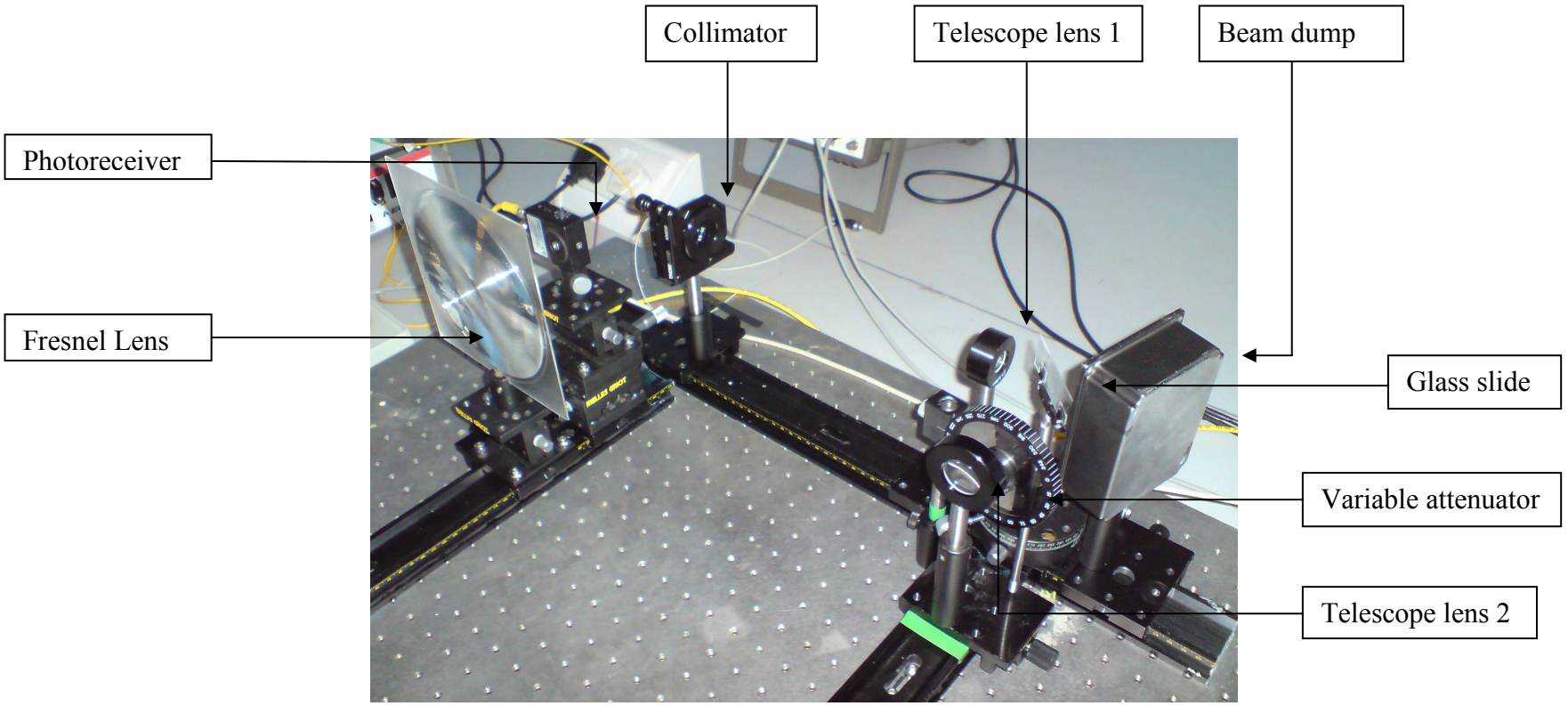

Figure 5.3 Photograph of backscatter/gas sensing configuration

5.3 Additional Configuration Information for Methane Sensing Investigations

5.3.1 Gas Cells

Further to the description of the gas sensing and backscatter configuration described in Chapter 3, this chapter outlines some of the details involved in producing short range methane and surface backscatter power levels for testing the system's ability to act as a methane sensor system in controlled conditions and to make an extrapolation of its maximum range. The gas leaks were simulated using gas cells, which were filled with varying concentrations of methane and then placed directly in front of the receiver's collection lens. Two different types of gas cell were used, one an in-house built clear Perspex box and the other a Tedlar bag.

5.3.2 Perspex Cell

The Perspex box cell was a transparent box with window dimensions 288mm X 288mm as shown in the schematic in Figure 5.4. The windows were 3mm thick and fixed to provide a 100mm path through the interior of the box. This cell was used in all of the lab based gas measurements, mainly because of the ease of flushing for re-use and durability with regard to be refilled many times compared to the Tedlar bags. Its main disadvantage was its high insertion loss (66%) of 1651nm signal power.

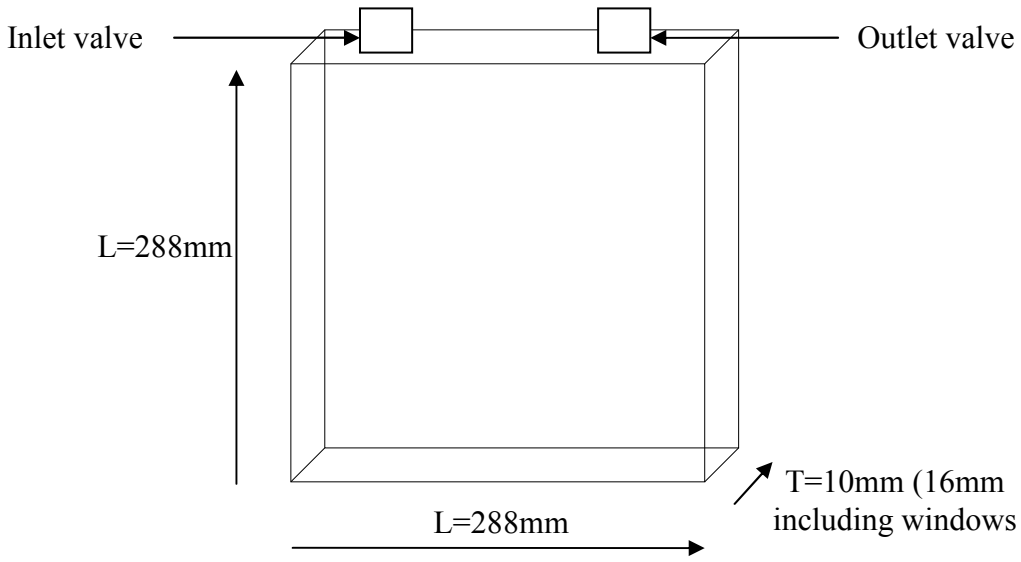

Figure 5.4 Schematic of Perspex gas cell

5.3.3 Tedlar Bag

The Tedlar bag is a cell commonly used in environmental monitoring as a sampling tool [5.1]. The benefits of using them as gas sample bags include, their thin walls, relatively low absorption in the near-IR, low permeability (meaning that the gas concentration should not change significantly over the course of an investigation.) The Tedlar bags were used in the final, long-range gas sensing experiments because of their superior integrity (with respect to gas containment), leading to an increased reliability of measurement. When filled, the Tedlar bags also had a path length of 100mm (with the incident beam at normal incidence), except at the edges, where the bag narrowed slightly at its seams. This was considered to be acceptable because when the bag was suspended in front of the receiver lens, the path length was only less than 0.1m at the very edges of the collector lens, where the surface backscatter collection is relatively small.

5.4 Short Range Gas Measurements Using the Lab Demonstrator Methane Sensor System

5.4.1 Details of Gas Signal Measurement Investigation

Using the backscatter/gas sensing configuration of Figure 5.3 once more, the ramp and dither were applied to the amplified DFB laser, so that a 5Hz, 1V (33GHz) sweep was applied in addition to the 3.8V sinusoid (M=2) for 1f detection or 4V (M=2.2) for 2f detection at 377kHz dither frequency. The 1651nm WMS signal, amplified in the counter-pumped DSF Raman system (lab demonstrator), was directed at a range of surfaces and the resulting backscattered radiation was focussed onto a Thorlabs photoreceiver via a 30cm diameter Perspex Fresnel lens. The methane samples of concentration 10%, 1% and 0.1% in nitrogen and path length 0.1m were placed before the Fresnel lens in turn, using the Perspex cell.

The initial gas sensing experiments were conducted to find the minimum received power at the photoreceiver a 3:1 SNR for each methane concentration and various backscatter surfaces. As described with the discussion of the apparatus, the launched signal power was attenuated to emulate longer range by using the reflection of a glass slide to obtain around 5%, then the variable attenuator characterised in Figure 3.15 and shown in position in Figure 5.3. This limit was determined based on a single scan of the 1f and 2f signals, but the gas signal traces shown were averaged over 2 and 32 scans on the oscilloscope for the observation of a clearer gas signal. In particular, the 2 scan rather than single scan was captured because of the digitised nature of the screen grab operation, which leads to deceptively poor traces for a single scan. The 32 and 2 scan averaged traces, using a concrete block as the surface backscatter target with the range of methane samples are shown for illustration. This was carried out using a variety of surfaces, but the 3:1 SNR gas signals are indistinguishable in appearance between surfaces.

5.4.2 Short Range Detection of 10000ppm.m Methane Sample

Figure 5.5 shows the 1f gas signal arising from the 10% sample (10000ppm.m) for a range of 11m. The characteristic shape is present, with the maxima and minima corresponding to the maximum gas line gradients and the 0V point corresponds to

the peak of the methane absorption line. The peak to peak amplitude is taken to be the amplitude of the gas signal and the noise amplitude is taken to be the visually observed noise level at the baseline. The ratio of the gas signal magnitude to the noise amplitude must be greater than 3:1 to be of use. The 2 scan trace is shown in Figure 5.6

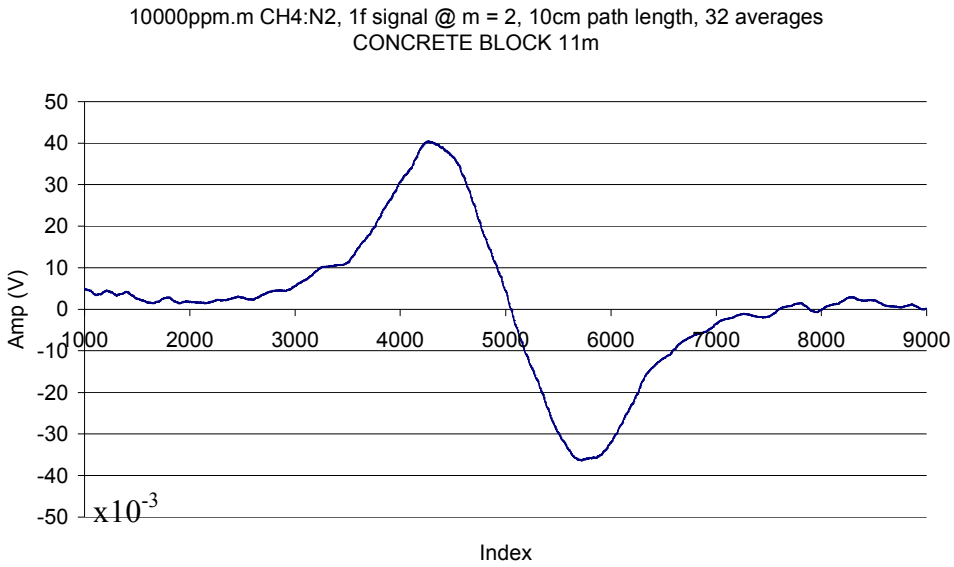

Figure 5.5 1f Gas signal from 10000ppm.m methane sample at 11m range from a concrete garden block surface - 32 scan average

In order to achieve the gas signals shown in Figure 5.5 and Figure 5.6, 270µW launch power was required, resulting in the collection of 350nW of backscatter power at the photoreceiver. The SNR of the gas signal is in considerable excess of 3:1, but this launch power was the smallest achievable using the backscatter measurement configuration while running the amplifier at full power. The launched signal power was measured before reaching the bulk variable attenuator using the pyrometer and the actual launch power calculated using the characterisation of the variable attenuator (Figure 3.15) to avoid the inaccuracy of measuring sub-mW power levels with the available apparatus. Given that in a real gas leak detection system the gas would be free floating and not contained within a cell, it was considered reasonable to discount the insertion loss of the cell against the required

signal output power to generate the 3:1 SNR. The cell attenuated around 67% of the 1650nm signal and therefore the required transmitted signal power was corrected to be one third of that actually transmitted when the Perspex cell was in place. The actual launched signal power is shown in brackets after each quoted transmit power. Therefore, the actual transmitted signal power was 810µW for all of the 1f and 2f 10000ppm.m results, rather than 270µW, which will hence follow the notation 270µW (810µW).

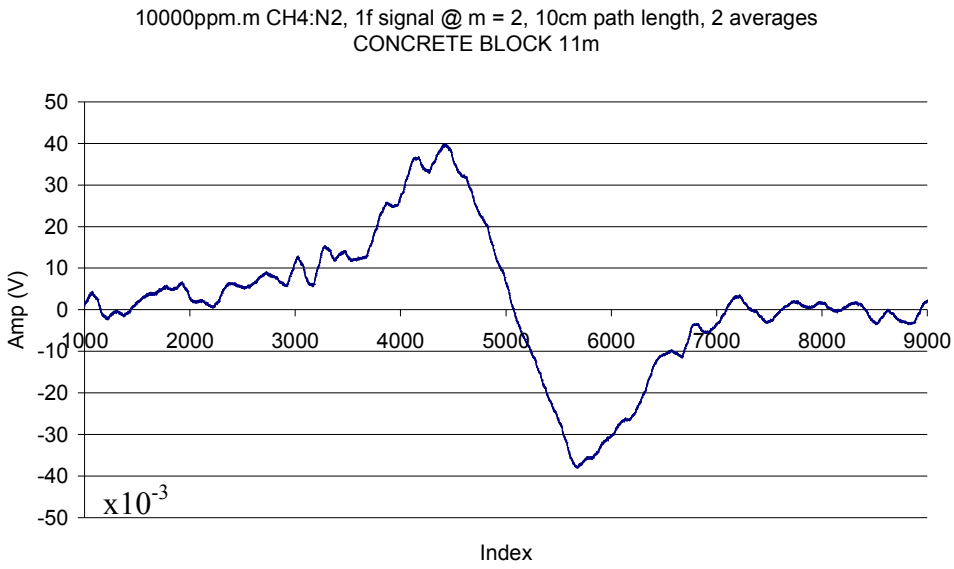

Figure 5.6 1f Gas signal from 10000ppm.m methane sample at 11m range from a concrete garden block surface - 2 scan average

Figure 5.7 is the 32 scan averaged 2f gas signal, using the same 10000ppm.m gas sample as before with the same send and resultant received power as for the 1f signal. The magnitude of the 2f signal is proportional to the second derivative of the gas line, therefore rather than being proportional to the gradient of the slopes of the absorption line, it is proportional to the curvature at the peak absorption. Hence, the peak of the 2f gas signal corresponds to the peak of the methane absorption line with respect to wavelength.

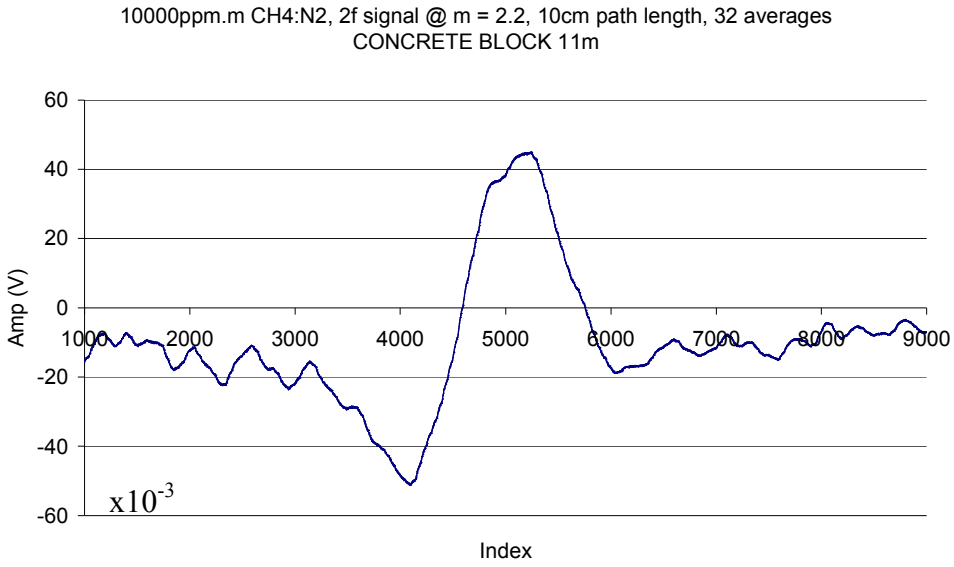

Figure 5.7 2f Gas signal from 10000ppm.m methane sample at 11m range from a concrete garden block surface - 32 scan average

Figure 5.8 is the 2 scan averaged 2f signal trace of the 10000ppm.m sample, where, as before the transmit power is 270µW (810µW). It can be seen when comparing Figure 5.8 and Figure 5.6 that although the corresponding 2f signal still has a SNR better than 3:1, it has a lower SNR than the 1f signal with the same received signal power. As discussed in Chapter 1, it is commonly the case that the 2f is preferred to 1f because in the absence of the DC background resulting from RAM it can be further amplified in the LIA to greater amplitude than the 1f before saturation, despite the smaller magnitude of the second harmonic signal from the detector. The 1f and 2f signals were compared for the remaining 1% and 0.1% concentration sample bags with 2 and 32 scan averaged traces.

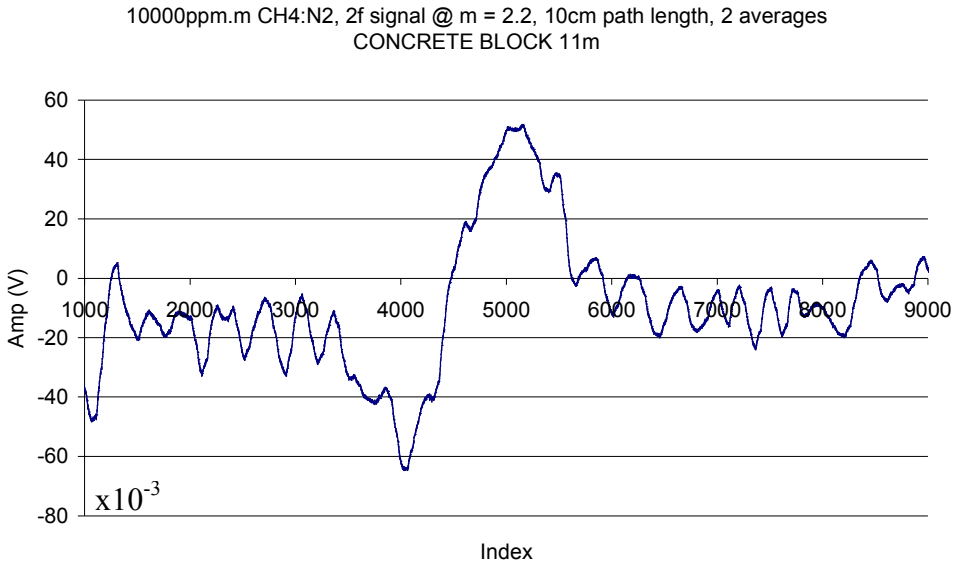

Figure 5.8 1f Gas signal from 10000ppm.m methane sample at 11m range from a concrete garden block surface - 2 scan average

5.4.3 Short Range Detection of 1000ppm.m Methane Sample

In the case of the 1f and 2f gas signals taken from the 1000ppm.m gas sample, the corrected launched signal power was 1.44mW (4.32mW) for the concrete target as shown in Figure 5.9 - Figure 5.12. Figure 5.9 and Figure 5.10 show the 32 and 2 scan averaged 1f methane signals of the 1000ppm.m sample respectively. Once more, the signals are of higher SNR than 3:1 with a small increase of transmit and receive power compared to the detection of 10000ppm.m. On these occasions 380nW was measured at the photodectector to obtain a clear >3:1 SNR at 1000ppm.m. Using the same parameters, the 2f signal was captured and the 32 and 2 scan averages are shown in Figure 5.11 and Figure 5.12 respectively.

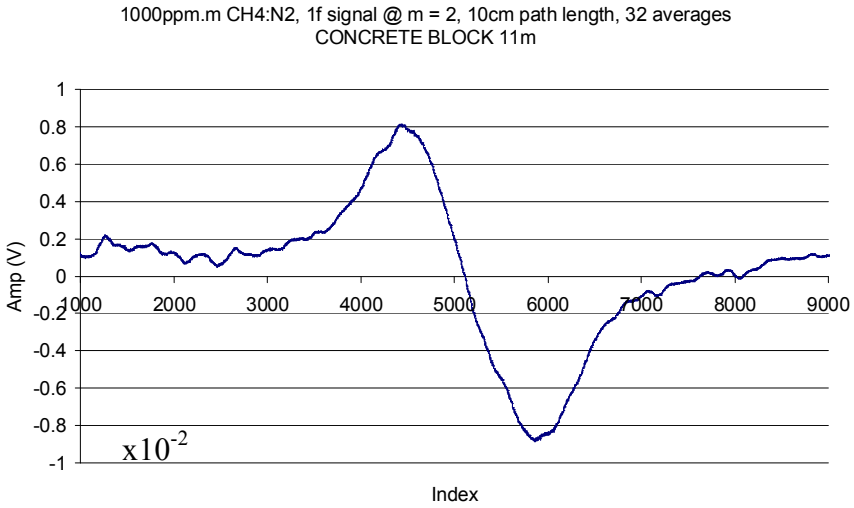

Figure 5.9 1f Gas signal from 1000ppm.m methane sample at 11m range from a concrete garden block surface - 32 scan average

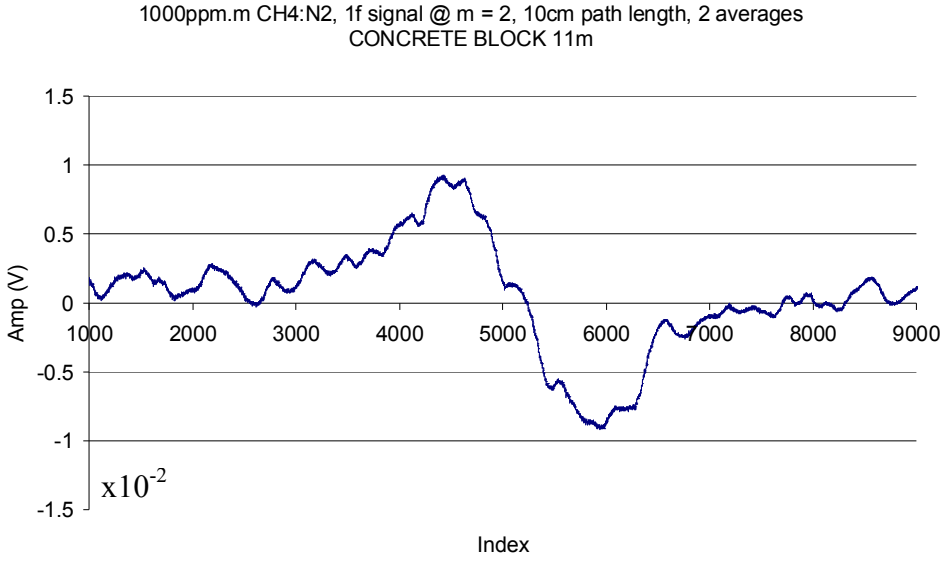

Figure 5.10 1f Gas signal from 10000ppm.m methane sample at 11m range from a concrete garden block surface - 2 scan average

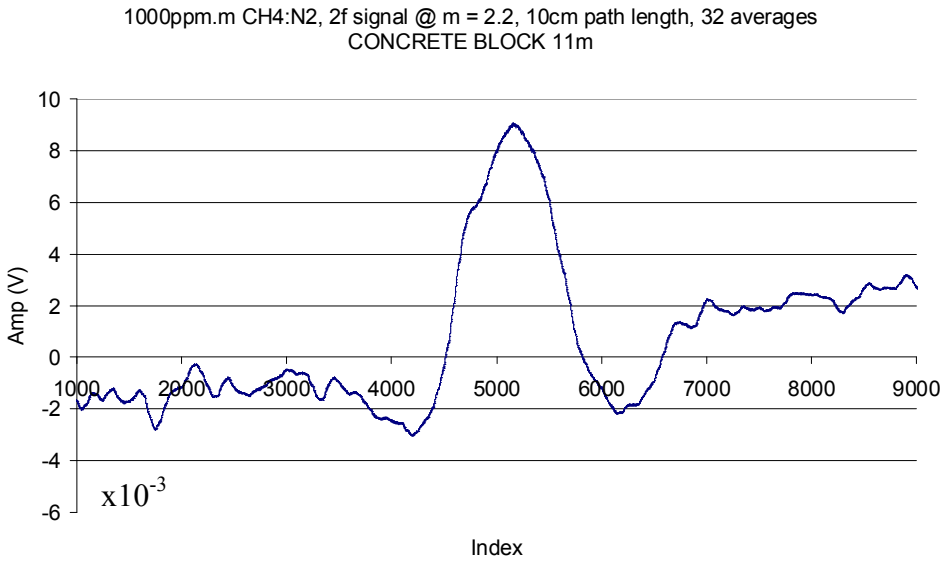

Figure 5.11 2f Gas signal from 1000ppm.m methane sample at 11m range from a concrete garden block surface - 32 scan average

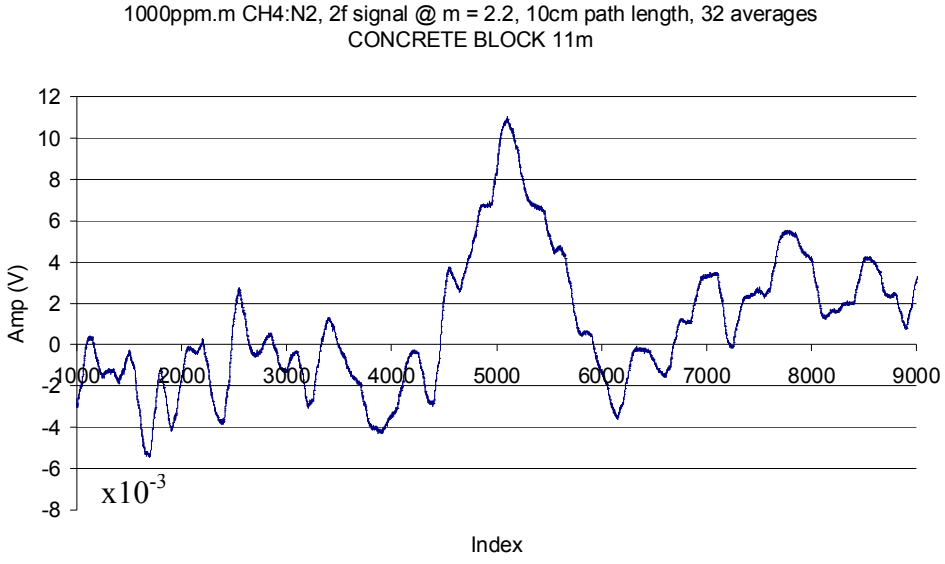

Figure 5.12 2f Gas signal from 1000ppm.m methane sample at 11m range from a concrete garden block surface - 2 scan average

5.4.4 Short Range Detection of 100ppm.m Methane Sample

In order to test the sensitivity of the methane sensor system in the context of various current sensor systems (see Chapter 1), it was necessary to investigate the signal

strength at 100ppm.m integrated path concentration. This is the required sensitivity limit, hence the received power required to detect this concentration is the critical measurement parameter in these investigations, as this will be used to determine the extrapolated maximum range of the system given a maximum Raman amplifier output power and backscatter study.

Figure 5.13 and Figure 5.14 show the corresponding 32 and 2 scan averaged 1f detection traces respectively. The required power falling on the receiver in this case was measured to be 420nW, which in turn required a 3.8mW (11.4mW) launch power. The shape of the 2 scan 1f trace is heavily distorted by noise, yet the SNR is in excess of 3:1 and is considered to be useable.

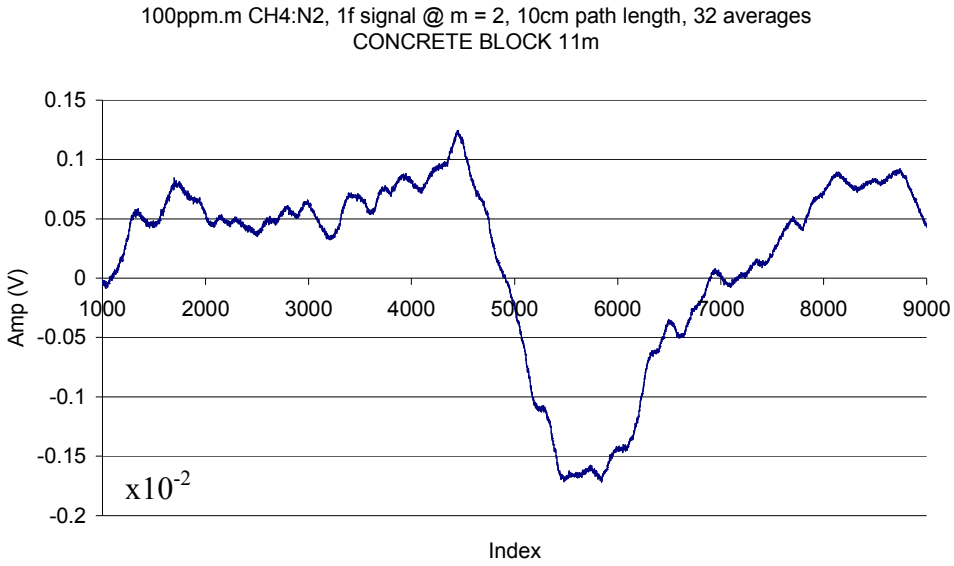

Figure 5.13 1f Gas signal from 100ppm.m methane sample at 11m range from a concrete garden block surface - 32 scan average

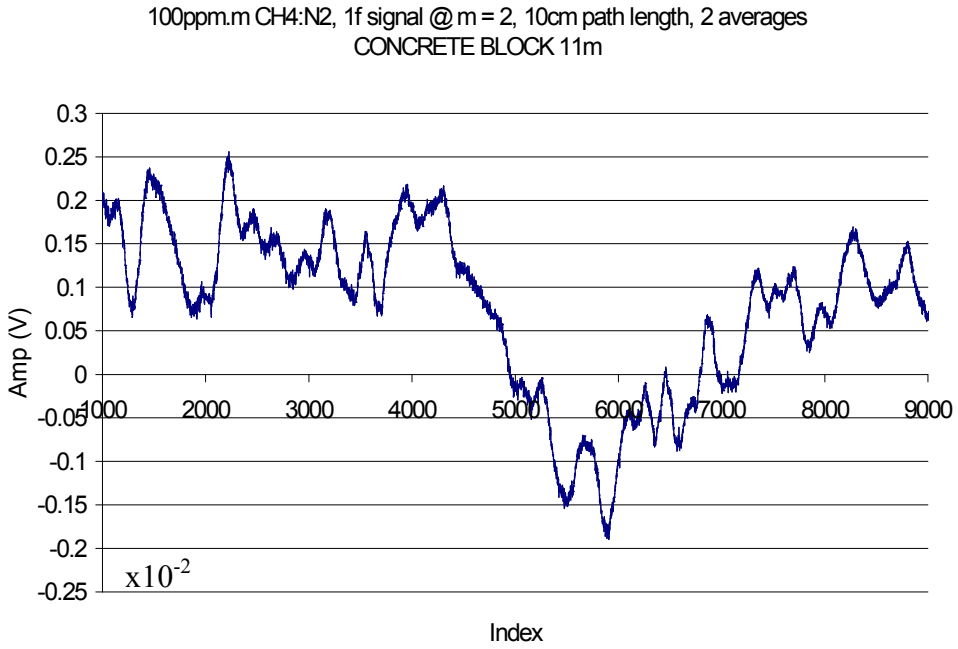

Figure 5.14 1f Gas signal from 100ppm.m methane sample at 11m range from a concrete garden block surface - 2 scan average

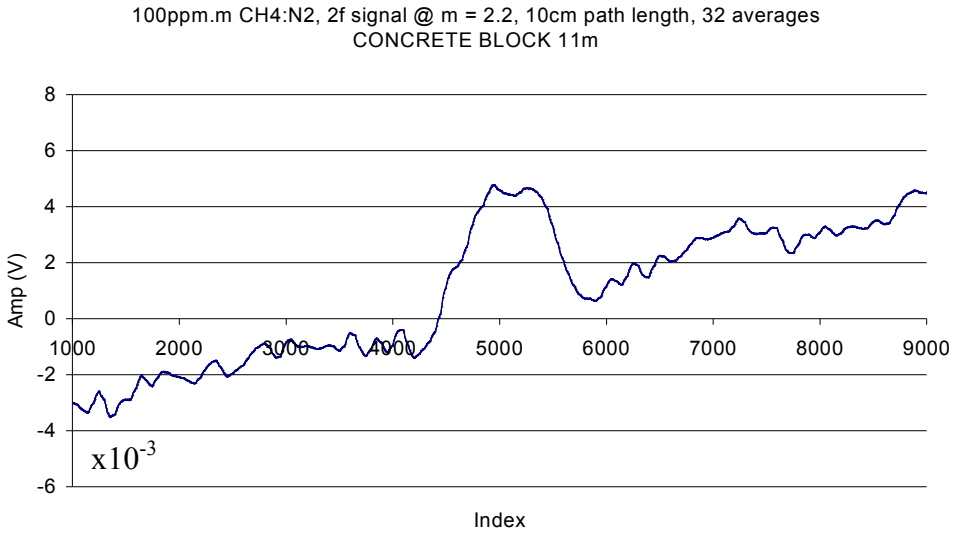

Figure 5.15 2f Gas signal from 100ppm.m methane sample at 11m range from a concrete garden block surface - 32 scan average

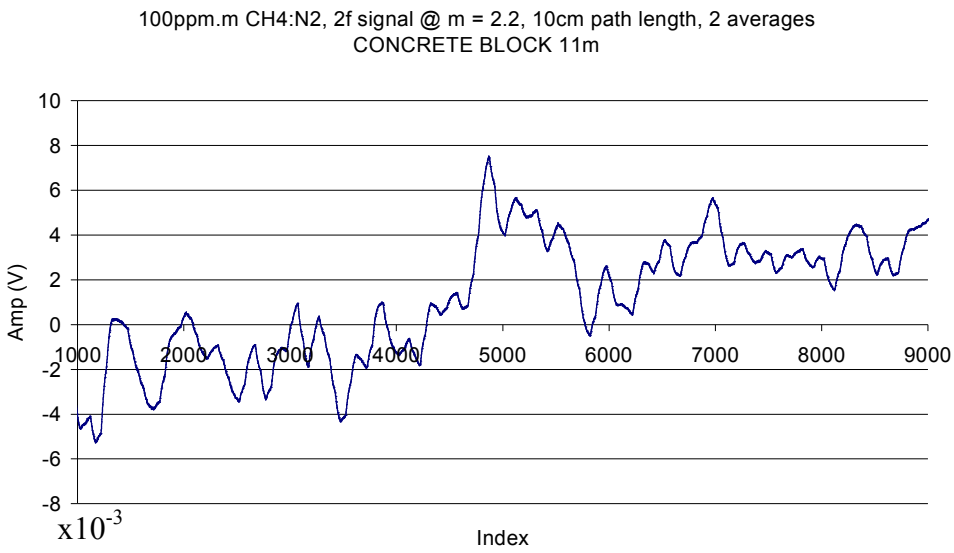

Figure 5.16 2f Gas signal from 100ppm.m methane sample at 11m range from a concrete garden block surface - 2 scan average

Figure 5.15 and Figure 5.16 show the 100ppm.m 32 and 2 scan averaged 2f gas signals respectively, once more using the same transmit and receive power as the 1f signal measurements for comparison. In the case of the 2 scan 2f trace (Figure 5.16), the SNR appears to be closer to 2:1 SNR, demonstrating that 2f detection is less sensitive while using this technique with this configuration.

5.5 Comparison of Minimum Transmitted Power Required for Methane Sample Detection

The 3:1 SNR gas signal was also found using the same concentration range for a rusty metal plate and a piece of white card in addition to the concrete block and the results are tabulated in Table 5.1.

Considering the 10000ppm.m results, it can be seen that this integrated path concentration was detectable using the minimum transmit power from any of the test surfaces. However, the 1000ppm.m set is more significant, in that the rusty plate and the concrete showed similar reflectivity, the white card required less incident power

to provide the same gas signal power. This is expected, since white card is more reflective than rust or concrete. Most significant of all are the 100ppm.m results, since these are most relevant to the required system performance limits. In this set the rusty plate target unexpectedly provides a better backscatter surface than the white card. Based upon these results it was suspected that, with small, unrusted spots on the rusty metal plate, this target had a significant specular component and was therefore caused more alignment sensitivity in terms of collecting the backscattered signal. The same argument was used for the unexpectedly poor performance of white card. It is suspected that the specular component was optimised for the metal plate in the 100ppm.m results and poorly aligned in the case of the white card. Of all of the target surfaces, it appeared that the concrete garden block provided the most consistent, diffuse backscatter, even if it appeared to be the worst in terms of backscattered proportion.

Integrated Path Conc. Methane in N_2	**Target Backscatter Surface**	**Minimum Transmit Power For >3:1 SNR**
10000ppm.m	Concrete block	270µW (810µW)
	Rusty plate	270µW (810µW)
	White card	270µW (810µW)
1000ppm.m	Concrete block	1.44mW (4.32mW)
	Rusty plate	1.44mW (4.32mW)
	White card	1.25mW (3.75mW)
100ppm.m	Concrete block	3.77mW (11.31mW)
	Rusty plate	1.72mW (5.16mW)
	White card	3.54mW (10.62mW)

Table 5.1 Minimum transmitted power to achieve 3:1 SNR in gas signal with respect to surface and methane concentration using lab demonstrator system.

5.6 Conclusion of Lab Based Stand-off Methane Sensing Investigations

Taking the data in Table 5.1 together with the validation of the distance squared dependence of diffuse backscatter intensity the ability of the sensor system to detect a 100ppm.m methane cloud at longer ranges can be extrapolated. Taking the worst, but most consistent surface, the concrete garden block, and the required incident signal power upon its surface of 3.77mW (4.32mW) at 11m range (once more assuming that the attenuation resulting from the Perspex cell is not present in a real scenario) the output signal power required to detect 100ppm.m methane at 100m can be calculated. This was conducted using the following simple relationship

$$P_{\mathrm{Re}q} = P_{lab} \times \left(\frac{R_{\mathrm{Re}q}}{R_{lab}} \right)^2 \qquad \text{Eqn 5.1}$$

Where P_{Req} is the transmitted power required for a given, required range $R_{Req,}$ P_{lab} is the necessary transmitted power to achieve a 3:1 SNR for a given range short range R_{lab}. In order to detect a 100ppm.m methane cloud using concrete as a backscatter surface, this implies that ~310mW optical power is necessary for this configuration. Eqn 5.1 can be rearranged, so that with knowledge of the maximum available output signal power (reports on the concurrent construction of the prototype Raman amplifier system at the factory suggested that ~2W was achieveable), a projected maximum range for the detection of a 100ppm.m methane cloud can be calculated. This was found to be ~260m, again based upon the worst case scenario target surface, concrete.

5.7 Short Range Methane Sensing Using the Finalised Sensor System

5.7.1 Description of the Prototype System

The prototype system was essentially the same as the lab demonstrator, using the same Tx-Rx (send/receive) optics, which were simply transferred across from one system to the other and the Raman amplifier system was a reproduction of the lab based Raman amplifier. The only significant difference between the system's configurations is the fact that, given that the methane sensor would have to be vehicle mounted, it was necessary to build a unit that consisted of one package and a send receive head, rather than an array of instruments and controllers. Although not directly significant with respect to the results, a discussion of the differences between the lab demonstrator and fully packaged prototype systems is included in this section.

A labelled photograph of the fully packaged prototype system, which was built to the specification of the final lab system (i.e. counter-pumped 4.5km DSF FRA) is shown Figure 5.17. The main difference is that, rather than an array of benchtop instruments, these devices have been produced in-house and integrated into the 'control unit.' Those incorporated directly include the current and temperature controls for the DFB laser, the modulation controls and bias T as well as the LIA. This allowed total control of the system via a PC rather than each instrument or controller having a separate adjustment and display. Using the program designed in Labview, it was possible to control signal temperature, current and modulation parameters.

The in-house built LIA was connected to a 'Picoscope' which displays the signal traces on the PC, serving the function of an oscilloscope. Apart from the control and measurement controls, both the pump EDFA (along with its broad bandwidth seed source) and Raman amplifier were contained within this control unit. A compact, broad bandwidth seed was incorportated into the system and spliced directly into the EDFA unit for pump spectrum control. As in the lab demonstrator amplifier system, the prototype system had 20dB (1%) monitor tap couplers at the signal output port,

allowing signal monitoring at low power as well as a high power signal output when required. In the case of the short range lab experiments, the 1% signal tap was fed to the send optics in the Tx-Rx head and the 99% into a beam dump. During long range, high power gas sensing experiments, the 99% signal tap was fed to the Tx head and the 1% tap to a photoreceiver to monitor signal level and quality in the time domain. The high power signal output was connected to the Tx telescope via fibre connection through a bulkhead mounted at the back of the Tx-Rx casing. The high power signal link was originally provided by an FC-APC connector as received from the factory, but was replaced with an E2000PS connector in order to provide improved reliability and safety in field trials.

The Tx-Rx head unit is an aluminium cubic box of side 400mm in which to mount the send and receive lenses systems (see Figure 5.17). The output transmit lens and the 30cm Fresnel collector lens are mounted on its faceplate. Within the Tx-Rx head, there was originally a Thorlabs telescope, which was to be incorporated as the Tx system for reliable beam expansion and collimation. It was found that the antireflection coating on the output lens attenuated much of the 1651nm power. Hence the in-house, rail mounted telescope system used to test the lab demonstrator, was set up inside the Tx-Rx head (the schematic is shown in Figure 3.16). The difference between the schematic of the demonstrator transmit optics and the actual prototype system in scaled power mode, as constructed within the Tx-Rx head was the removal of the glass slide from the demonstrator configuration. Originally the glass slide was put in place for the lab demonstrator to perform scaled power investigations by splitting ~5% of the signal from the high power signal tap for transmission rather than using the 1% available from the low power signal tap. This was because it was originally uncertain whether 1% of the amplifier output would be sufficient to detect all gas concentrations from all surfaces. This was not necessary with the prototype system because of the extra output power available and so the 1% tap could be fed directly to the Tx optics and the final output power was once again controlled via the bulk variable attenuator (placed after the collimator) during scaled power investigations at short range. This allowed a suitable, scaled down signal output power range of around 270μW to around 20mW for the short range

backscatter experiments. In the case of full power/range investigations, the bulk attenuator was removed and the 99% tap fed directly to the Tx system.

On receiving the factory designed amplifier system, some improvements were made. Briefly, these included the removal of the malfunctioning EDFA system and the installation of the rack mountable Keopsys benchtop model (as used to pump the lab demonstrator) into the control unit. The high power signal output connector (for the 99% signal output tap) was replaced with a ruggedised E2000PS connector and the EDFA seed system was altered with the insertion of the 1531nm CWDM to replace the 1551nm CWDM that was previously installed.

Given the modifications, the system was able to produce 2.36W of interference-free 1651nm WMS signal power while suppressing SBS using the 5W Keopsys EDFA and the 20mW signal DFB laser.

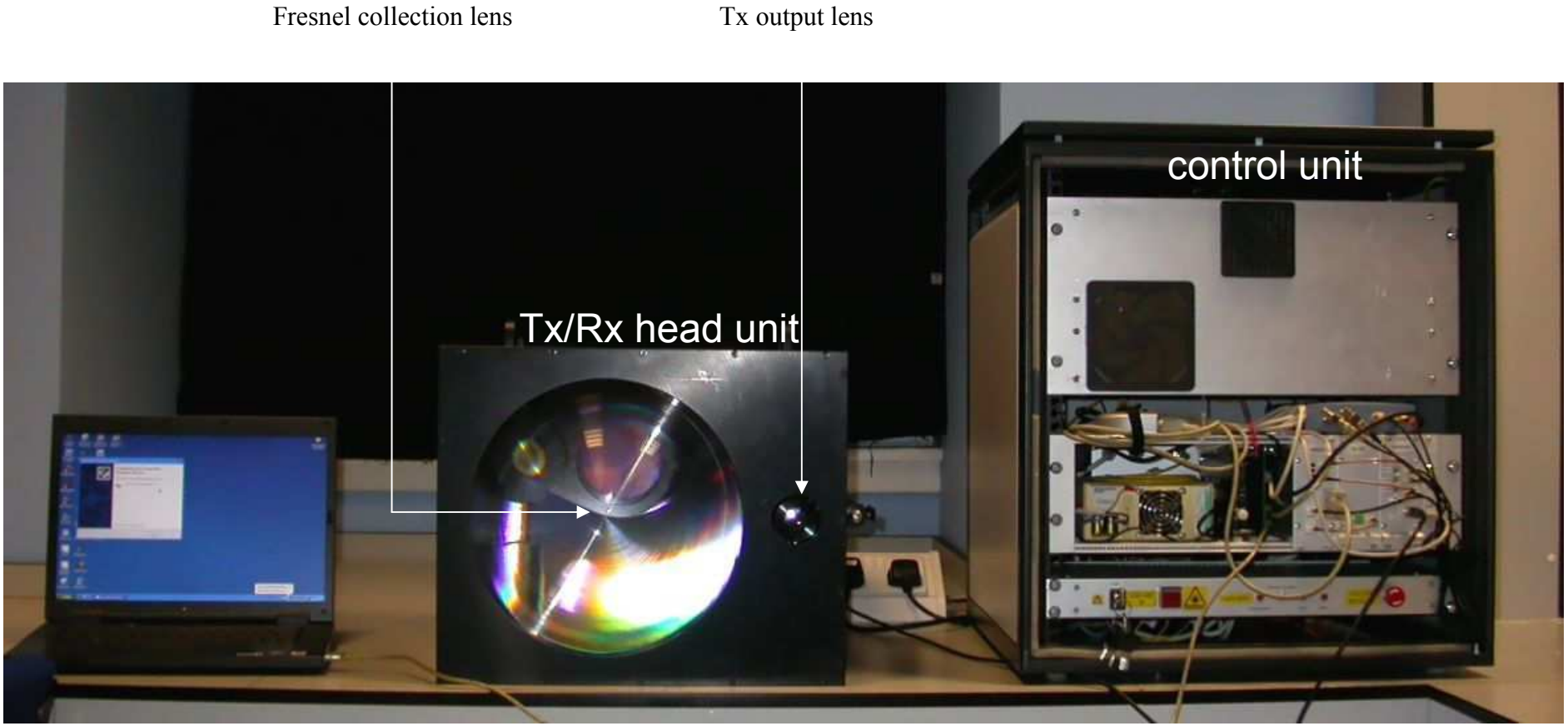

Figure 5.17 Photograph of fully packaged prototype unit (Tx Rx head centre, control unit RHS)

5.7.2 Measurement of Minimum Required Signal Launch Power to Obtain a 3:1 SNR Gas Signal in 11m Stand-off Methane Sensing Investigations

On receipt of the finalised remote sensor system, it was necessary to ensure that its methane sensing performance was similar to or better than that of the lab demonstrator. In order to investigate this, short range methane measurements were carried out using the fully packaged system. If the results were comparable, it could be concluded that the system was ready for field testing.

The 1f and 2f 2-scan averaged gas signals are shown at the 3:1 SNR limit for the 10000ppm.m, 1000ppm.m and 100ppm.m methane samples with concrete as the backscatter surface in Figure 5.18, Figure 5.19 and Figure 5.20 respectively. Their respective minimum required transmit powers were 270µW (810µW) for 10000ppm.m, 660µW (1.98mW) for 1000ppm.m and 3.3mW (9.9mW) at 100ppm.m. The Perspex cell was used to contain the methane samples and the surface target was mounted 11m from the receiver as before.

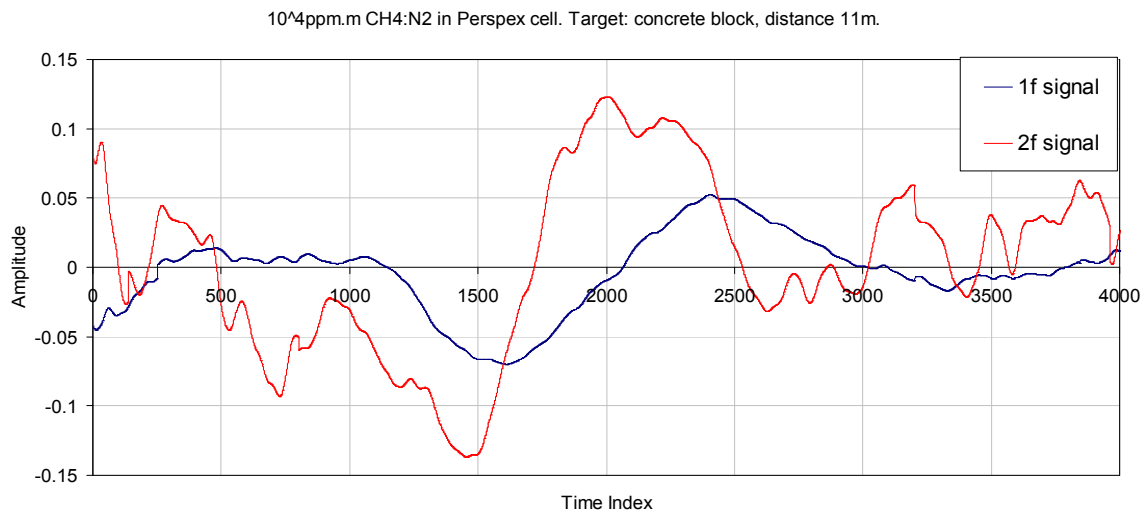

Figure 5.18 1f and 2f gas signals from finalised, packaged prototype system for 10000ppm.m methane at 11m. 270µW (810µW) signal launch power

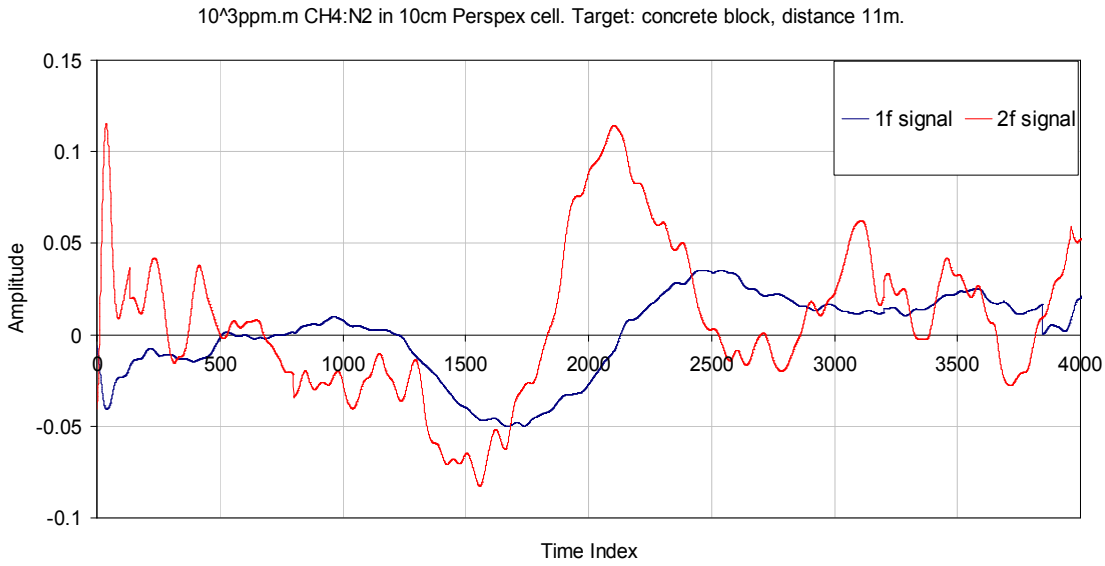

Figure 5.19 1f and 2f gas signals from finalised, packaged prototype system for 1000ppm.m methane at 11m. 660µW (1.98mW) signal launch power

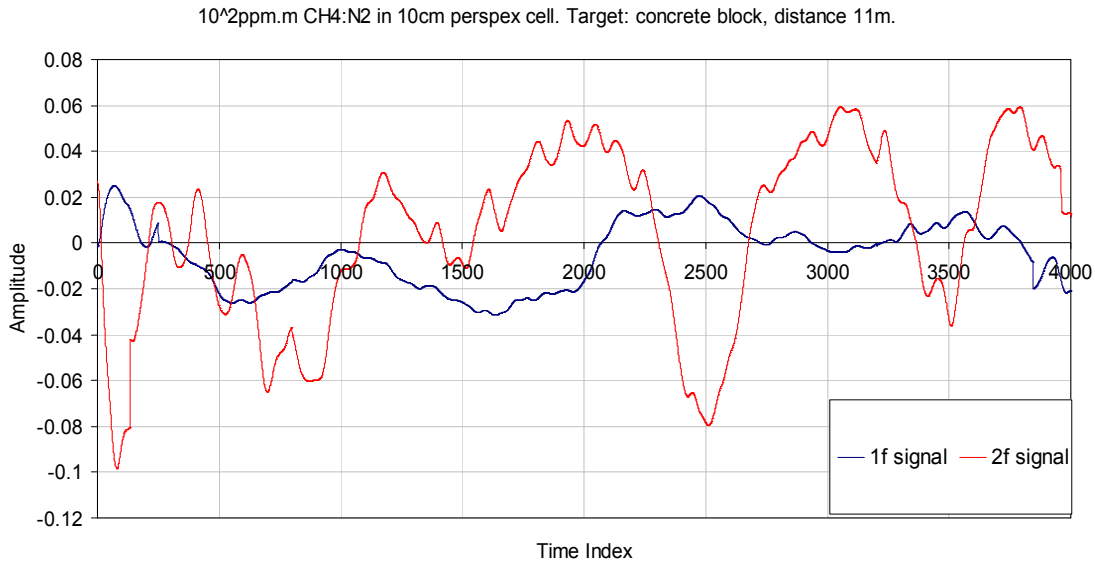

Figure 5.20 1f and 2f gas signals from finalised, packaged prototype system for 100ppm.m methane at 11m. 3.3mW (9.9mW) signal launch power

It can be seen from Figure 5.18 and Figure 5.19 that, although the 1f signal is clearly well in excess of the requisite 3:1 SNR, the transmit power limit has been limited by the 2f signal, which only just meets this SNR requirement in both of those cases. In the case of Figure 5.20, although both 1f and 2f signals meet the requisite 3:1 SNR, it was difficult to measure in the case of the 2f signal because of the heavily distorted

signal shape. It was noted that the 1f signal was of considerably better quality at the same transmit power level, with a SNR of around 5:1, hence in the field trials 1f detection would be preferred and all discussion will focus on these. This investigation was repeated for the rusty plate and the white cardboard and the results were tabulated as shown in Table 5.2

From Table 5.2 it can be seen that the values for minimum transmit power at which the 1f and 2f signals exceed a 3:1 SNR, while using the 100ppm.m methane sample, are very similar to those using the lab demonstrator system, (see Table 5.1). It can also be seen that some of the results appear to be improved over the lab based system, with less transmit power required to detect the 1000ppm.m sample from all surfaces. This could be a result of better lens alignment, better power stability with the reflective glass slide removed or the fact that the receive optics are boxed, thus reducing detector noise from background light. It was expected that the results should be similar, particularly because the same send and receive optics were used for both systems, but it is desirable to test whether the packaged prototype performed as it should along with its control software. Given that the short range methane sensing results were either very similar or better than in the case with the lab demonstrator, it can be concluded that the system should surpass the 100ppm.m sensitivity requirement at 100m by extrapolation (i.e. required projected power for 100ppm.m sensitivity at 100m based upon 11m range data in Table 5.2 is ~272mW, c.f. 2.36W available results in a projected range of 294m).

Integrated Path Conc. Methane in N_2	Target Backscatter Surface	Minimum Transmit Power For >3:1 SNR
10000ppm.m	Concrete block	<270μW (<810μW)
	Rusty plate	<270μW (<810μW)
	White cardboard	<270μW (<810μW)
1000ppm.m	Concrete block	660μW (1.98mW)
	Rusty plate	500μW (1.5mW)
	White cardboard	500μW (1.5mW)
100ppm.m	Concrete block	3.3mW (9.9mW)
	Rusty plate	3.3mW (9.9mW)
	White cardboard	3.3mW (9.9mW)

Table 5.2 Minimum transmitted power to achieve 3:1 SNR in gas signal with respect to surface and methane concentration using final system

5.8 Field Testing of Prototype System

5.8.1Configuration Notes

The system was considered ready to test at full power and full design range in outdoor conditions. The Tx-Rx system was maintained as before in the lab trials, except the 99% arm (with E2000 connector) was fed to the Tx optics rather than the 1% and the variable attenuator (previously mounted inside the Tx-Rx box) was removed. The methane samples were placed in the Tedlar bags, with each test sample concentration being given a separate bag. This was considered to be a more reliable test condition than flushing the cell with nitrogen for every change of concentration required, because of the elimination of the risk of sample contamination. This is aside from the practical issue of attempting to flush a cell in a field environment, far from the gas lab. Additionally, the Tedlar bags were considered to be less permeable than the in-house made Perspex box cell, meaning that they could be filled before taking the system out for testing, and should maintain their integrated path concentration throughout the day. There was no power

attenuation correction in the field trials, but it should be remembered that even a clean Tedlar bag added at least 1dB insertion loss that would not be expected in an actual gas leak.

The entire sensor system was powered using a petrol generator, and the Tx-Rx head was aimed at the mounted target, which was positioned 105m away, from the back of the van in which it was transported as shown in Figure 5.21. The target placement is shown in Figure 5.22 The target alignment was supposed to be conducted using a laser pointer on a mount fitted to the side of the Tx-Rx head. The position of the laser pointer was adjusted to coincide with that of the output signal beam along a long (85m) corridor, using an IR card to follow the path of the signal. This was not effective in during field trials because the cold conditions prevented the laser pen from working. Instead, the beam was directed to the target by manually moving the Tx-Rx head while monitoring the 10000ppm.m methane (highest concentration available) signal, with the Tedlar bag placed over the Fresnel collector lens using full signal power. Confirmation that the target surface was responsible for the signal backscatter, as apposed to the ground for example, was obtained by moving the target away while keeping the Tx-Rx head in position, if the gas signal did not change, then the alignment had to be carried out once more. This was the best way of conducting the alignment because it was difficult to see the expanded signal beam at the target using the IR cards in daylight.

The signal launch power was maintained at 1.9W despite the highest available power being in the region of 2.36W because at the maximum output power, the onset of multi-path interference was much easier to initiate, with dirt on connectors etc. Hence 1.9W was used because this was found to be an output power at which the system could be considered to be robust even in outdoor conditions.

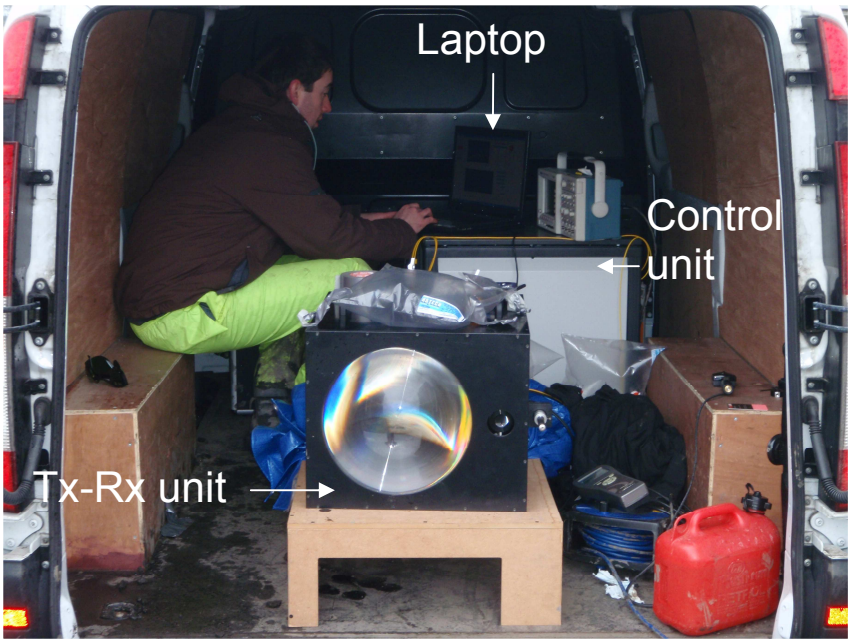

Figure 5.21 Photograph of the prototype sensor system in use from the back of a van

Each of the Tedlar bag gas samples, with the same integrated path concentration range as in the lab experiments were taped in front of the receiver Fresnel lens, and the backscatter from a range of target surfaces placed on a stand at 105m was received via the gas sample onto the collector lens. This would simulate a single pass through a gas cloud of the given integrated path concentration.

Figure 5.22 Photograph of target placement during field trials

5.8.2 Characterisation of Target Surfaces

The target surfaces used were ply wood, a large concrete paving slab and a large, smooth matt finish laminate board. Note that the concrete paving slab was not that used in the lab experiments, because larger targets were required at the long range to compensate for the difficulty in beam alignment. The paving slab is known as 'concrete slab', and the concrete garden block as 'concrete'. The backscatter levels for the range of target surfaces were compared by comparing the (modulation induced) AM signal arising from each of the surfaces at 105m with the signal power maintained at 1.9W. The comparison was as shown in Figure 5.23

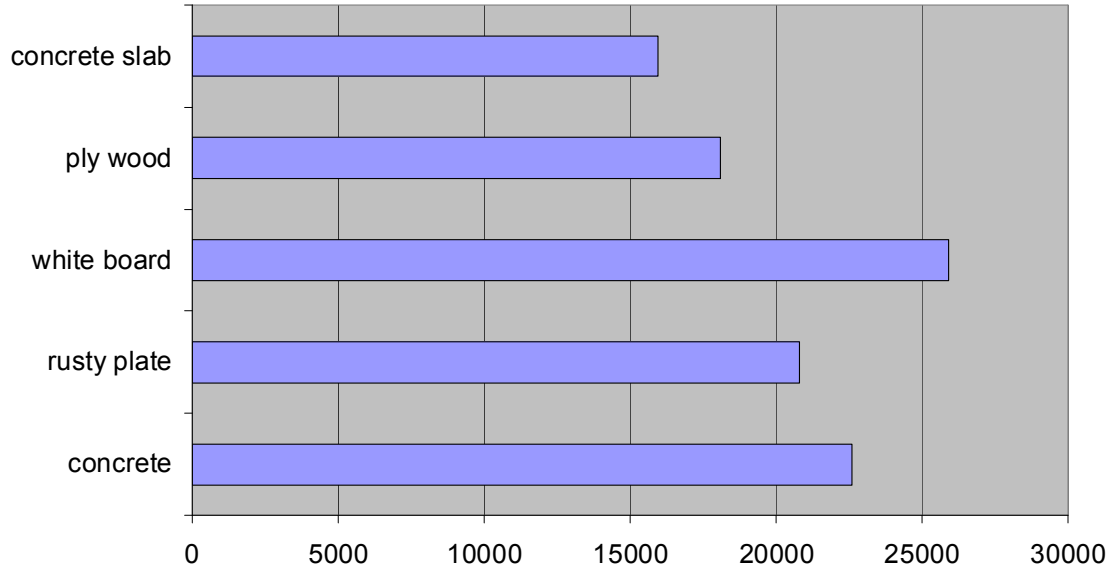

Figure 5.23 Relative RAM signals (arbitrary units) from target backscatter surfaces at 105m with 1.9W signal power.

From Figure 5.23, it can be seen that the new concrete slab is the least efficient backscatter surface, which is illustrative in demonstrating the potential difference in signal quality arising from different terrain. Unsurprisingly, the white board control target provided the most backscatter with plywood in between, providing similar performance to the rusty plate in the lab experiments.

5.8.3 Detection of Simulated 10000ppm.m Gas Cloud at 105m

With the surface backscatter characterised qualitatively, gas measurements were taken, with the signal power set to 1.9W once more. The 10000ppm.m 1f signals using the white board, plywood and concrete backscatter surfaces are shown below in Figure 5.24, Figure 5.25 and Figure 5.26 respectively. In the case of all of the backscatter surfaces tested, the 1f gas signal from 10000ppm.m is very strong, with a visual SNR measurement not feasible because of the relative size of the signal to the noise on it.

As can be seen from the concrete slab backscattered gas signal results in Figure 5.26, this surface is worse in terms of backscattered signal than the others tested, displaying the worst SNR. This is expected, given the results from the backscatter analysis Figure 5.23.

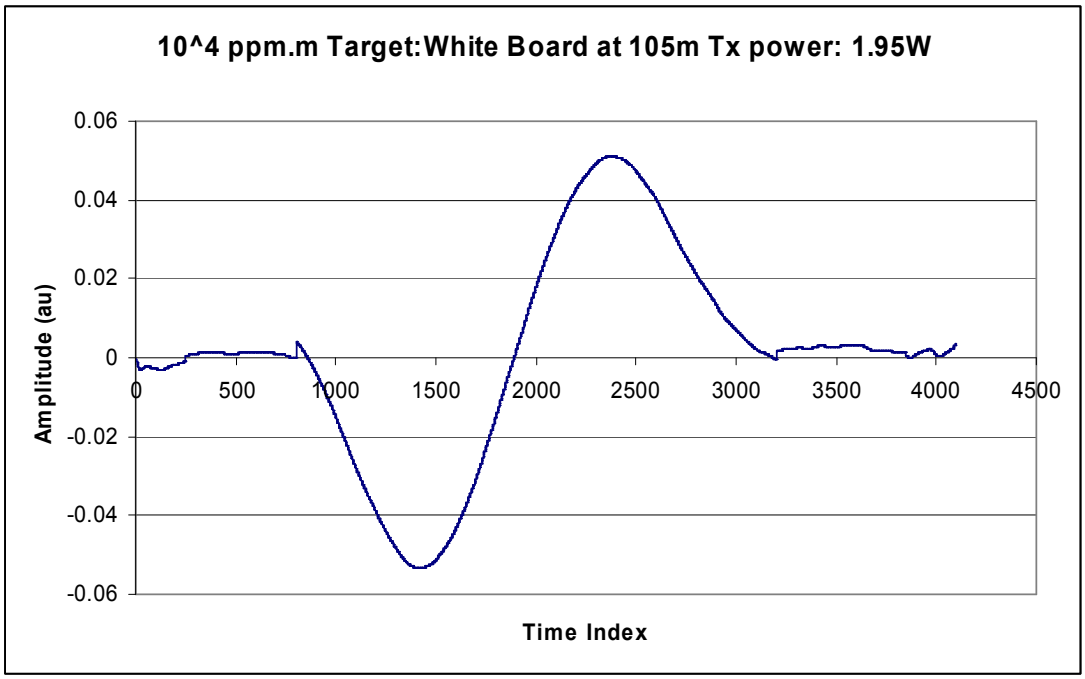

Figure 5.24 10000ppm.m gas signal from white board at 105m range using final packaged sensor system

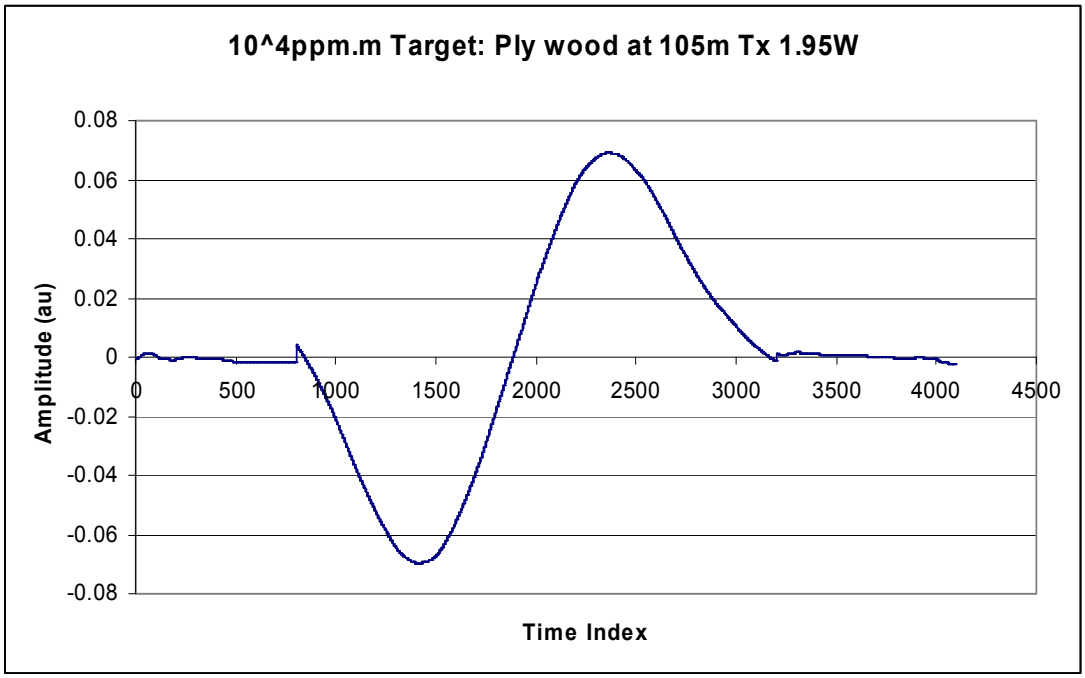

Figure 5.25 10000ppm.m gas signal from ply wood at 105m range using final packaged sensor system

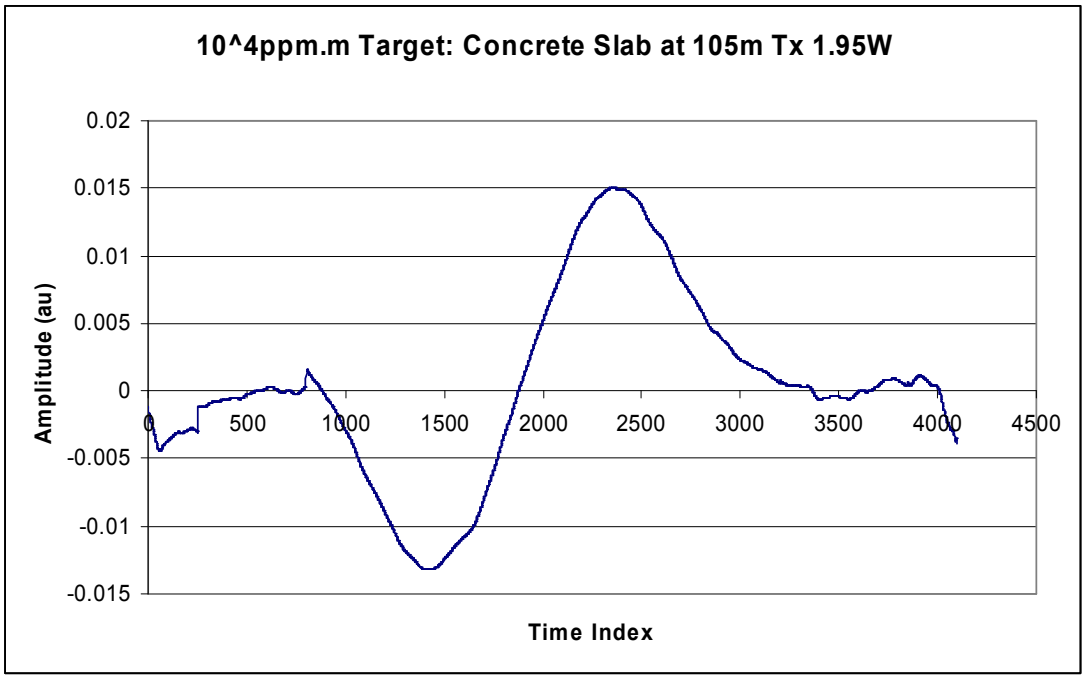

Figure 5.26 10000ppm.m gas signal from concrete slab at 105m range using final packaged sensor system

5.8.4 Detection of Simulated 1000ppm.m Gas Cloud at 105m

The same target surfaces were used in the same sequence as with the 10000ppm.m investigation while monitoring the gas signal from the 1000ppm.m methane sample, with the traces shown in Figure 5.27, Figure 5.28 and Figure 5.29 (white board, plywood and concrete). The output power was maintained at 1.9W

The signals are orders of magnitude greater than the noise except in the case of the concrete slab backscatter target. In this case, the concrete slab's poor backscatter qualities caused a visible degradation to the gas signal compared with other surfaces. Even taking this into account, the 3:1 SNR requirement is easily surpassed.

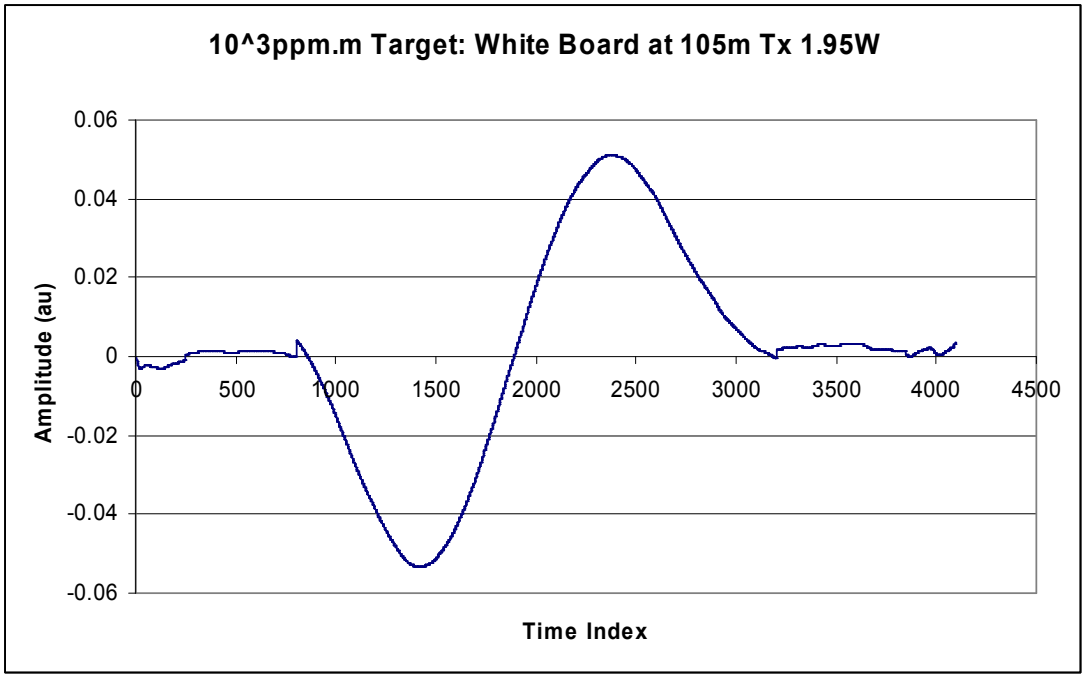

Figure 5.27 1000ppm.m gas signal from white board at 105m range using final packaged sensor system

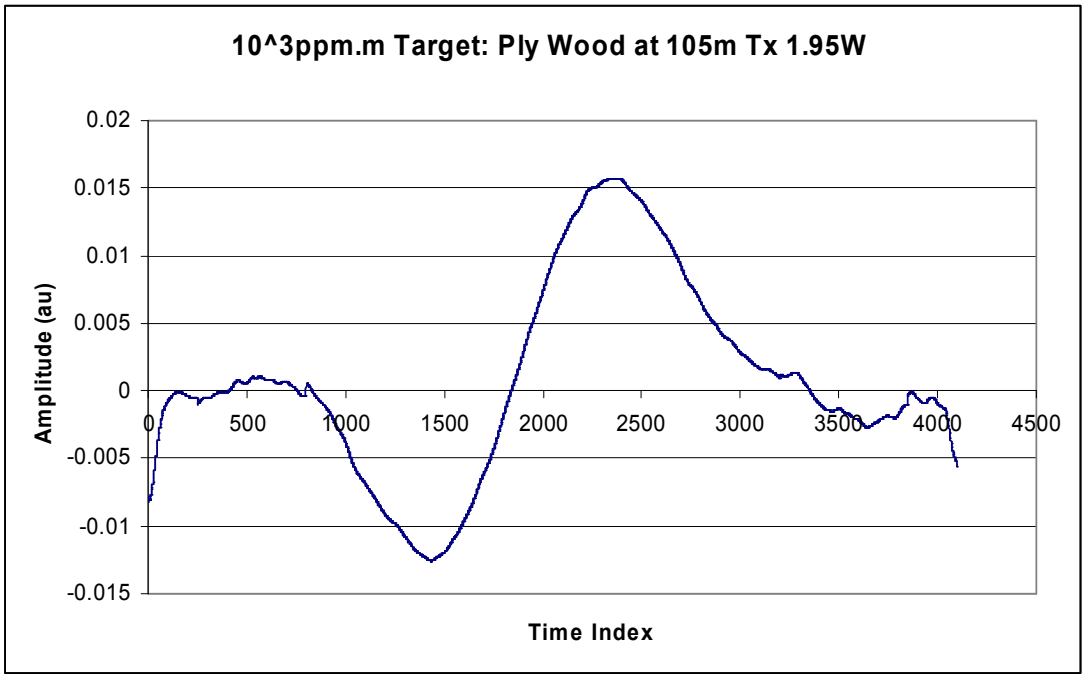

Figure 5.28 1000ppm.m gas signal from ply wood at 105m range using final packaged sensor system

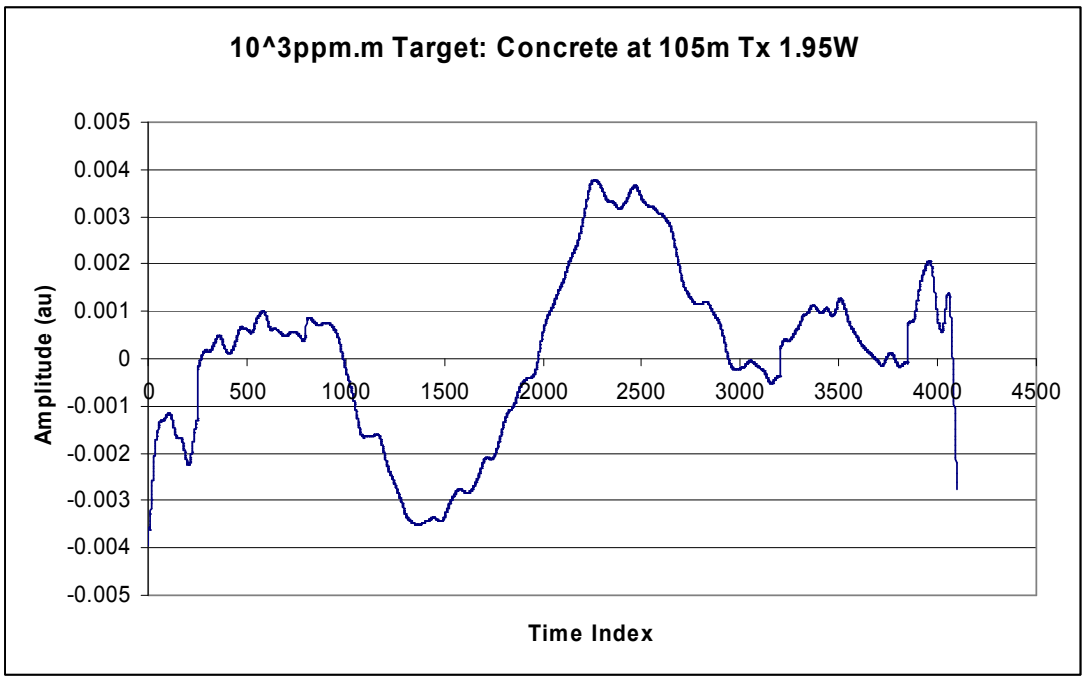

Figure 5.29 1000ppm.m gas signal from concrete slab at 105m range using final packaged sensor system

5.8.5 Detection of Simulated 100ppm.m Gas Cloud at 105m

The final 100ppm.m sample bag was put into place and the surfaces white board, plywood and concrete were mounted in turn as shown in Figure 5.30, Figure 5.31

and Figure 5.32 respectively. This is the most critical set of methane measurements, since performance at detecting this integrated path concentration provides the basis of the comparison between this system and current point and hand-held stand-off sensor systems. For the system to be successful, it must provide a >3:1 SNR while inspecting a 100ppm.m methane cloud while using a non-ideal backscatter target.

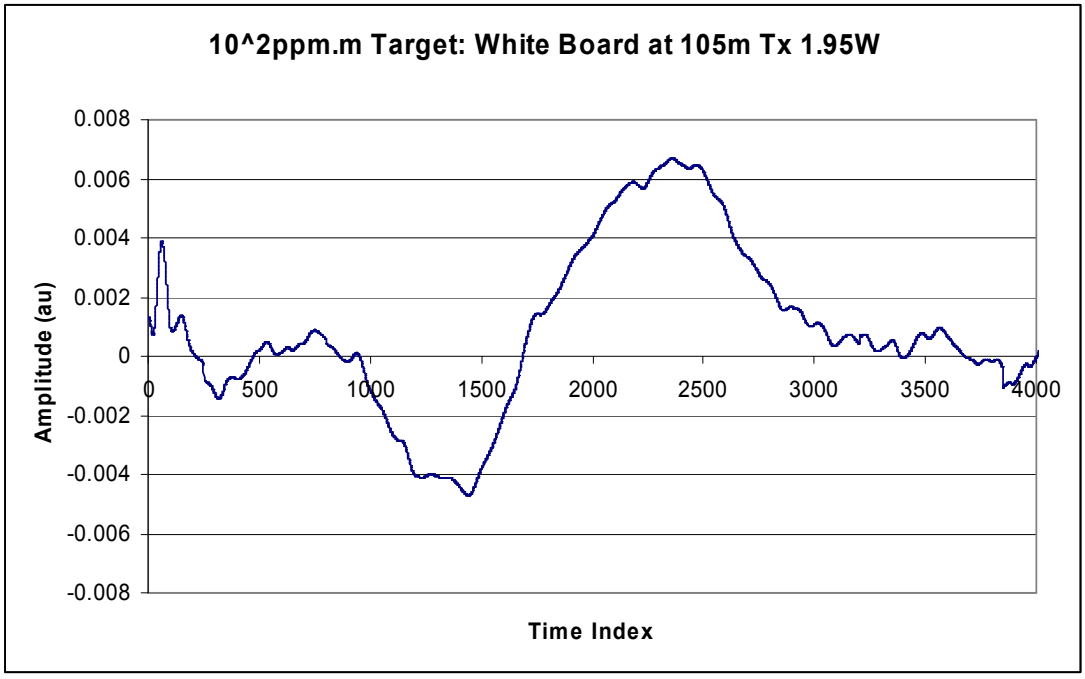

Figure 5.30 100ppm.m gas signal from white board at 105m range using final packaged sensor system

As can be seen in Figure 5.30, the signal is strong and most significantly, easily discernable from noise. Although this is a positive result for the sensor system, it is recognised that this surface was essentially a strongly reflective 'control' surface meaning that the limits of the sensor system have not been fully tested. Considering the backscatter investigation, the results of which are shown in Figure 5.23, plywood could (in a very simplistic approximation) be considered to be a common target surface because it represents the middle of the range of surfaces tested in terms of backscatter efficiency. The 1f gas signal using plywood as the target is shown in Figure 5.31 and has a SNR considerably in excess of 3:1, demonstrating that for a non-optimised backscatter surface, the sensor system easily exceeds the required

sensitivity and range. Once more, the 2f signal, despite being discernable is of poor quality.

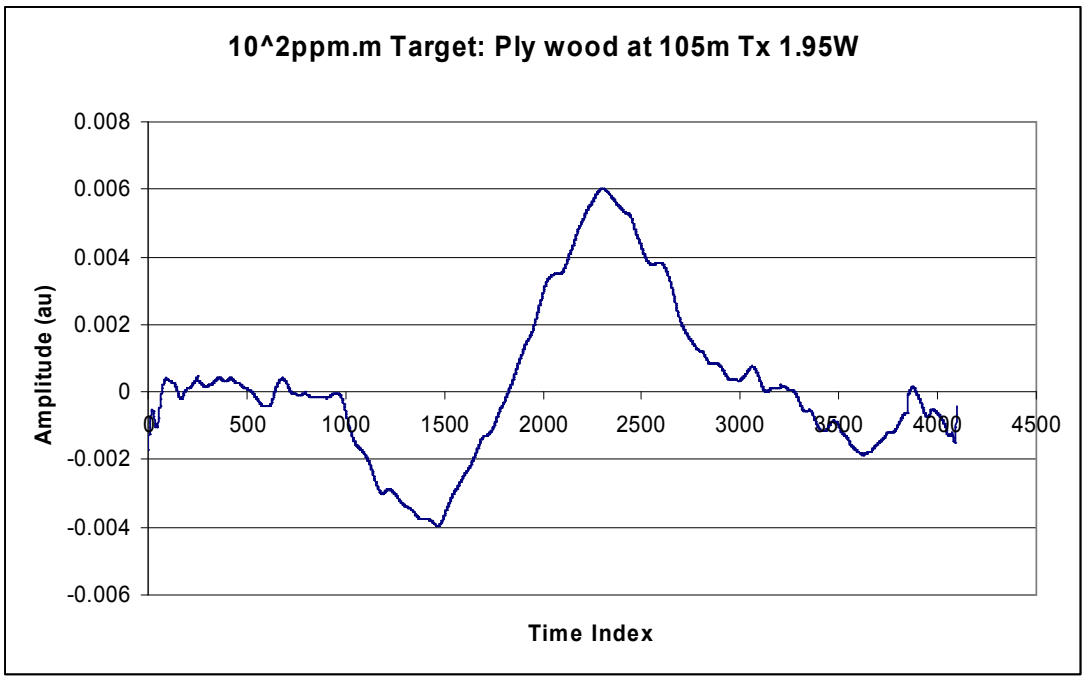

Figure 5.31 100ppm.m gas signal from plywood at 105m range using final packaged sensor system

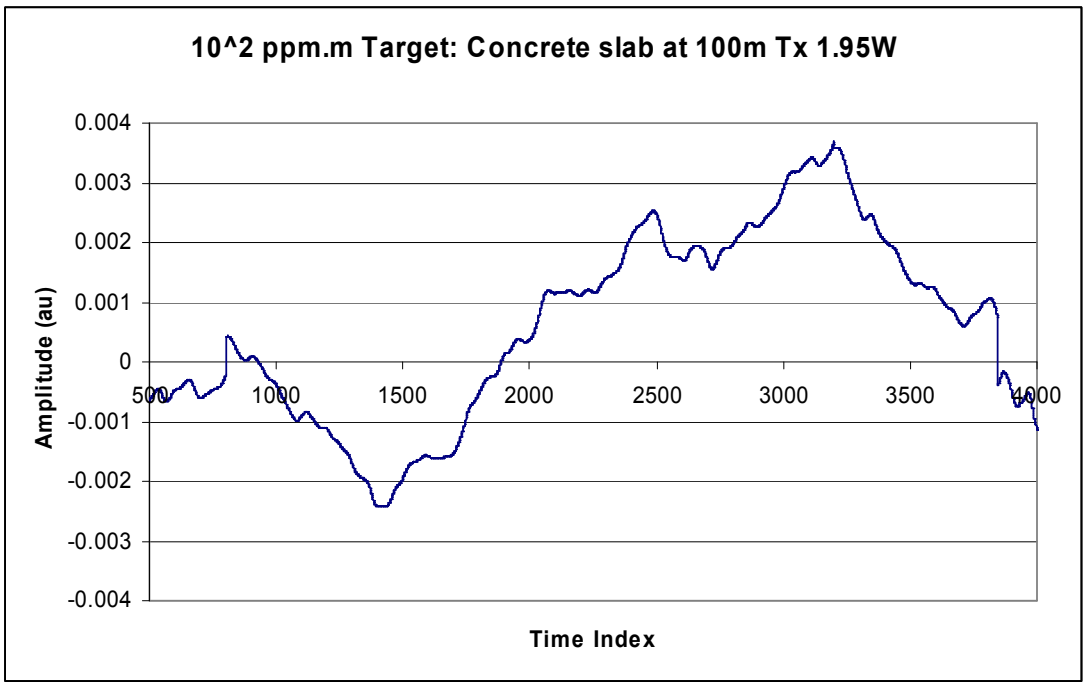

Figure 5.32 100ppm.m gas signal from concrete slab at 105m range using final packaged sensor system

Finally the worst target surface available (concrete slab) was tested with the 100ppm.m sample as shown in Figure 5.32. In this measurement, the signal does still exceed a 3:1 SNR, taking the average noise peak to be around 0.001 and the signal to be around 0.004 arbitrary linear units. This 1f signal does look different than those before, with a large peak at around 3000 on the time scale. Bearing in mind that the ramp and modulation parameters were constant throughout the investigation, this value on the time scale is almost off-line. However, it is not congruent with the rest of the noise peaks, hence it was assumed to be the wind moving the taped Tedlar bag slightly, thus allowing more optical power to fall on the detector, which may in turn have caused some destabilisation of the gas signal. The gas signal magnitude was measured as the peak to peak difference between the minimum at 1500 and maximum at 2400 on the time index.

In addition to the Tedlar bag methane samples, background methane tends to be around 1.6ppm as discussed in Chapter 1. Therefore, on top of every sample, there is a ~340ppm.m background methane level in the long range experiments. It was therefore of interest to investigate the background methane level signals to compare with the sample readings. Once more the backscatter targets were white board, plywood and the concrete slab shown in Figure 5.33, Figure 5.34 and Figure 5.35 respectively.

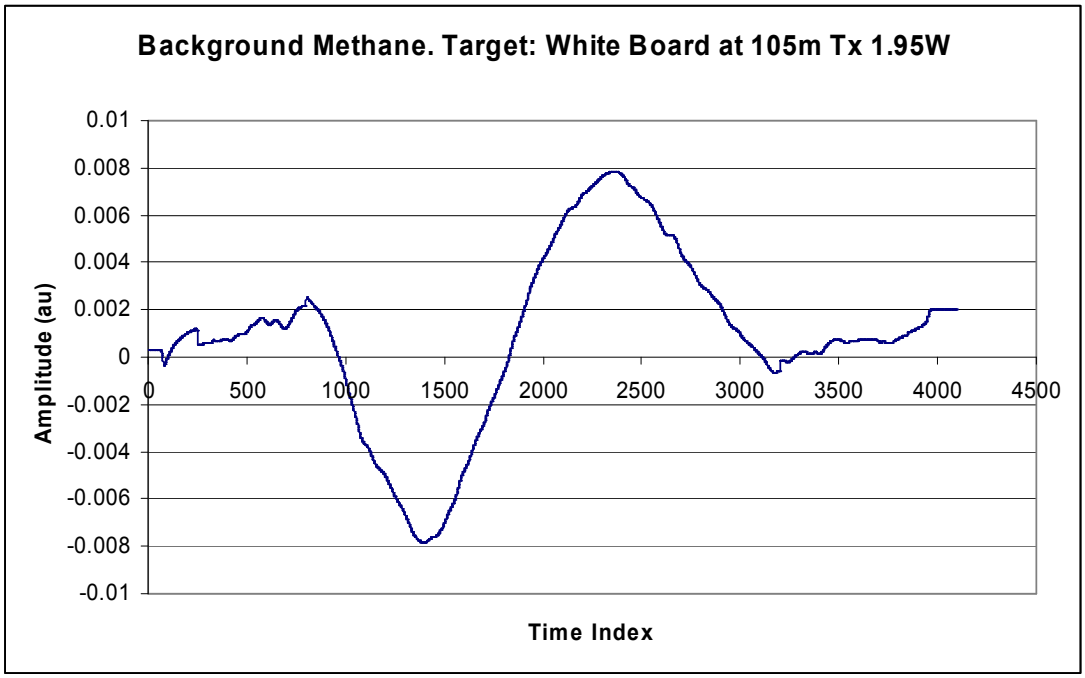

Figure 5.33 Background gas signal from white board at 105m range using final packaged sensor system

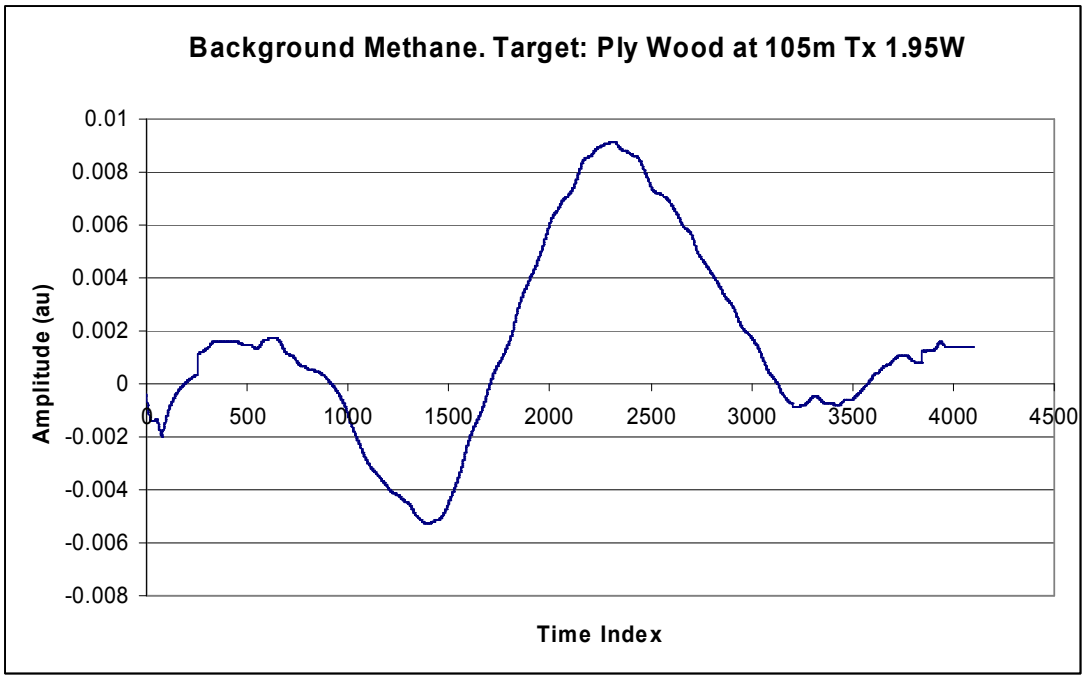

Figure 5.34 Background gas signal from ply wood at 105m range using final packaged sensor system

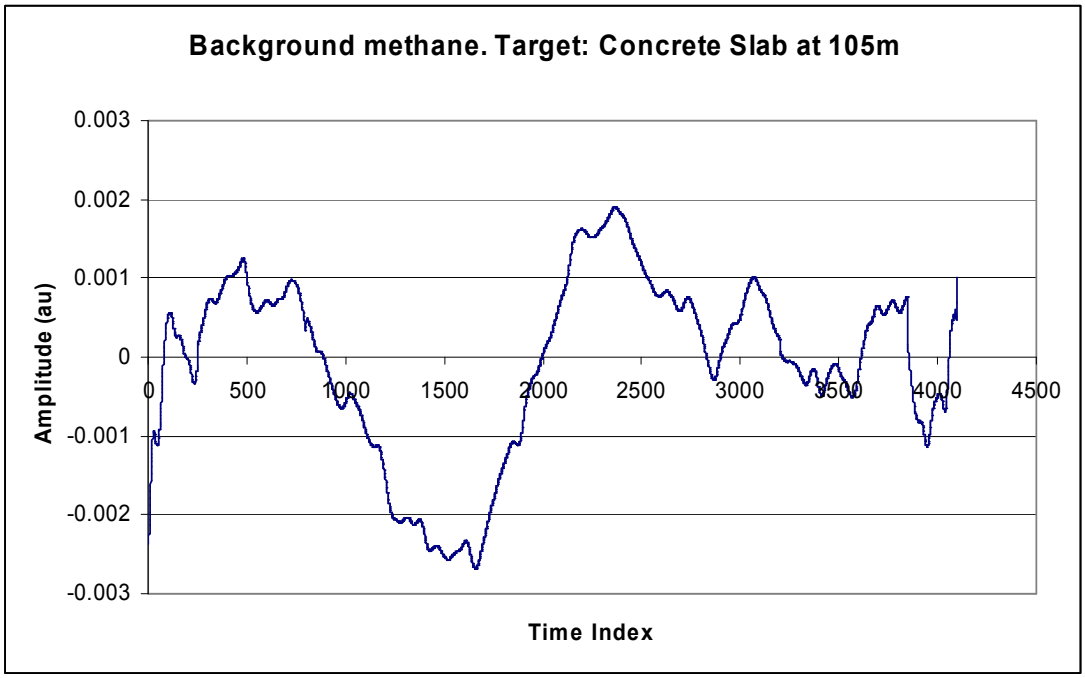

Figure 5.35 Background gas signal from concrete slab at 105m range using final packaged sensor system

The 100ppm.m gas signals are all well above the requisite 3:1 SNR, using the white board, concrete slab and plywood targets. Taking all of the background readings together, the aspect that is immediately striking is that the gas signals appear to be stronger for background than when the 100ppm.m samples were in place if the backscatter surfaces are compared directly. This indicates that the attenuation from the Tedlar bags causes more of a detriment to the amplitude of the gas signal than the increase resulting from additional 100ppm.m integrated path concentration. From this, three facts can be deduced.

Firstly, the sensor system is able to detect a strong 1f background signal at 105m from all surfaces tested. Secondly, it is expected that with the removal of any attenuating cell for the gas leaks, the sensor system should operate considerably more efficiently than in the simulated case. Thirdly, it was not possible to deduce from the field trials whether the sensor system genuinely had 100ppm.m sensitivity (i.e. it could distinguish a 100ppm.m rise in methane level from background.) In conclusion to the field trial methane detection results, it could be concluded that the sensor system prototype was successful, with 3:1 SNR achieved from all test surfaces and available concentration levels, one of which was the worst in terms of backscatter

that was tested in lab and field trials. There are many improvements that could be made to increase methane sensing performance and these will be discussed in Chapter 6. As further background to the results, there were many difficulties in obtaining optimal results. Strong winds continually shook the mounted target and the van, which undoubtedly added noise to the signals. On many occasions there was rain, causing scattering centres on lenses, Tedlar bags and through the air. The extreme cold stopped the laser pointer from working, meaning that although great care was taken to align the targets using signal feedback at the detector, this was not the most reliable method. Another effect arising from the cold conditions was that the petrol generator continually struggled and was unlikely to have supplied a constant voltage level to the equipment, possibly leading to an increased noise level. Although a fully commercialised sensor system would be expected to operate through such conditions, this was a proof of principle investigation, where more benign conditions were assumed. However, despite this, the desired performance criteria were met.

5.9 Demonstration of 100ppm.m Sensitivity to Methane

During the field trial investigations, the removal of the 100ppm.m Tedlar bag in order to measure background level gas signals resulted in an increased gas signal. One of the goals of testing background methane and background methane +100ppm.m was to observe an increased signal in the higher integrated path concentration case to prove that the system achieved the requisite sensitivity. This meant that a further investigation was necessary to demonstrate 100ppm.m sensitivity of the system.

The prototype system was set up in the 11m lab once more, with the 1% tap fitted to the Tx optics and the variable attenuator put back in place. The plywood target was mounted at 11m range from the receiver. In order to recreate the 105m conditions for methane sensing, the power was attenuated so that the 100ppm.m gas signal amplitude was comparable to that observed in the field trial given the same sample

and target surface. Having acquired this, a method to compensate for the bag attenuation had to be devised. Hence, when testing the 100ppm.m sample, an unfilled Tedlar bag was be placed in front of the collection lens in addition to the gas sample for the 100ppm.m measurement. In addition to this, a second Tedlar bag was used as a second 100ppm.m sample so that a 200ppm.m path was available. While testing the 200ppm.m sample of two bags, the unfilled Tedlar bag was removed from the collection lens. This allowed a direct comparison of 100ppm.m and 200ppm.m gas signals with the same signal power falling onto the receiver. The result of this investigation is shown in Figure 5.36, which shows a clear increase in signal amplitude for the 200ppm.m integrated path concentration compared to the 100ppm.m sample. Additionally, it can be seen that, given the same LIA and scope settings the ratio of the signal amplitudes is approximately 2:1, the same as that of the ratio of integrated path concentrations. In conclusion, this investigation was considered to be successful in terms of demonstrating the 100ppm.m sensitivity and also that the signal amplitude follows the theoretical direct proportionality to integrated path concentration.

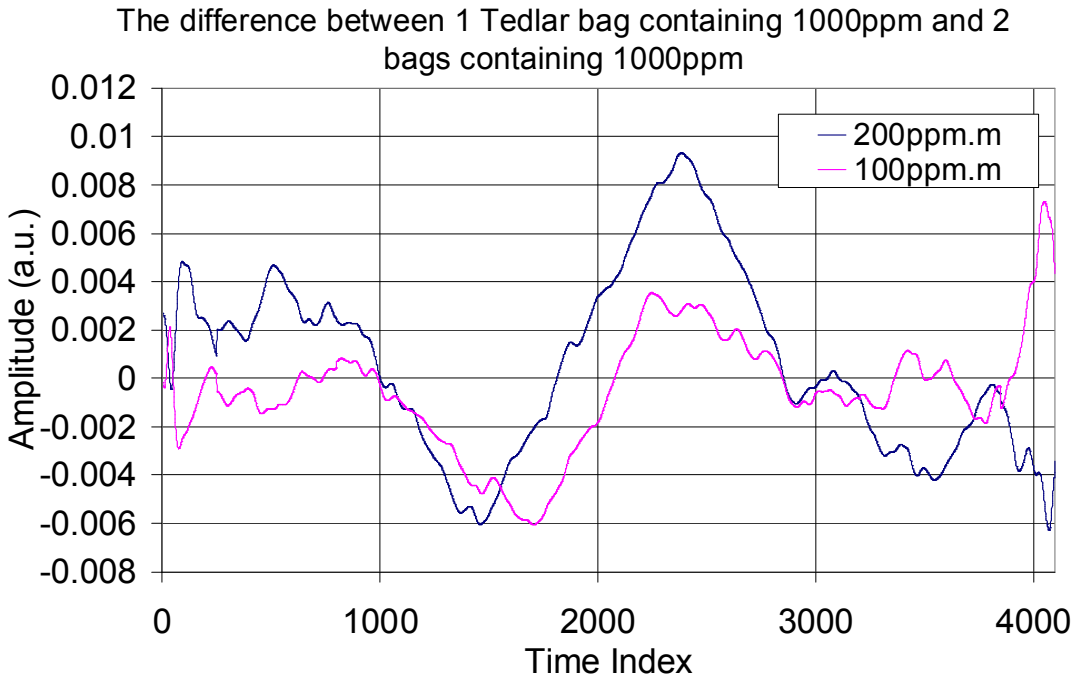

Figure 5.36 100ppm.m and 200ppm.m 1f gas signals with the same power at the receiver from plywood target at 11m (attenuated send power)

5.10 Summary

The aims of this chapter was firstly to present the gas sensing results of the system in order to show that the system as a whole met its ultimate requirements (100ppm.m above background at 100m range. In order to do this, the short range scaled power gas results at a range of concentrations down to 100ppm.m from a range of rough surfaces were presented along with a validation of the dependence of backscattered power as a function of range. Together with knowledge of the capabilities of the Raman amplifier system in terms of output power, this allowed a theoretical range to be calculated for the required sensitivity. Given these results, the prototype system was taken for field trials at full range, where it performed to the requirements of 100ppm.m sensitivity above background, and also achieved a clear background methane signal at 100m from all backscatter surfaces. These results proved that the system exceeded its required specifications, as will be discussed in more detail in Chapter 6.

5.11 References

[5.1] http://www.sigmaaldrich.com/analytical-chromatography/analytical-products.html?TablePage=16369234

Chapter 6 Conclusion of the Design and Testing of the Long Range Methane Leak Sensor System

6.1 Introduction

This chapter summarises the conclusions arising from this work and discusses some of the possibilities of further development work, or improvements that could be made to the final system. The discussion includes the conclusions arising from the Raman amplifier design, followed by the short range gas sensing results. The final conclusions are those arising from the field trials of the prototype system, which will be discussed in the context of performance compared with initial requirements as well as further work required to create a full, commercial system.

6.2 Raman Amplifier Design Achievements and Conclusions

6.2.1 Motivation for the Development of the Raman amplifier

The motivation for the Raman amplifier system was that, given the demonstration of standoff methane leak detection at 10m using the backscatter from 1651nm DFB diode lasers incident on random scenery, it was hypothesised that with greater launch power, this 10m range could be extended. This would have possible applications in

wide area leak inspections and possibly aerial pipeline inspections, which is a commercially desirable capability. One of the main challenges was that the optimal 1651nm and 1665nm gas sensing signal wavelengths are not currently served by amplifiers, meaning that high CW power at these wavelengths is not readily achievable. With high power C-band amplifiers readily available at 1540-1560nm, an opportunity was seen to exploit Raman scattering (~13.2THz frequency shift, or 110nm in germano-silicate fibres) to scatter the readily available C-band power to the appropriate gas sensing wavelength. It was estimated initially that around 1W of signal power would be required to produce a reliable, long range sensor system, based upon scaling the specification of those designed for short range inspections.

The Raman amplifier was to be constructed of optical communications fibre components and fibres wherever possible to develop a low cost, reliable system. Given that the high power would be propagated and scattered in optical fibre, the suppression of SBS was also a major concern. The suppression of SBS, while maintaining Raman amplification and gas sensing performance represented the main effort in the design of the amplifier system.

6.2.2 Suppression of SBS of the Raman Pump through Spectral Control

Given that SRS has a much broader gain bandwidth than SBS, it was reasonable to use a broad bandwidth pump, that would be efficient at pumping the 1651nm Raman signal, but very inefficient at pumping SBS. This was achieved by building a filtered ASE source to seed the pump EDFA. The filter used to filter the ASE before insertion into the main EDFA played a significant role in controlling the pump spectrum, which in turn determined the SBS and Raman gain characteristics of the pump output as it propagated though the gain fibre.

In choosing a filter, the gain spectra of both the ASE producing EDFA units as well as the main pump EDFA had to be taken into account. The gain peak of the Keopsys EDFA was centred at 1560nm and it was found that for a filter to be suitable, it had to suppress ASE in this wavelength region strongly. If this was not the case, much of the output pump spectrum would centre at this wavelength, which would not be

optimal for Raman scattering to 1651nm. Additionally, the seed had to be designed so that the main EDFA output power was of sufficient bandwidth so that the spectral power density of the 1651nm spontaneous Raman scattering would not be sufficient to experience significant Raman amplification (becoming a significant Stokes wave). A 1531nm CWDM filter was found to be the optimal filter to use to achieve an optimal pump spectrum from those tested. This is because this filter suppressed ASE strongly in the 1560nm region and seeded most of the pump to around 1540nm in a broad bandwidth peak. An alternative 1551nm CWDM was tested, but this resulted in significant emission at around 1560nm. Additionally a 1540nm DWDM filter was investigated, but when used in the seed system it gave rise to a very sharp peak in the output spectrum of the main EDFA and hence was not used in the amplification and gas sensing investigations.

The broad bandwidth seed source was effective at seeding a suitable pump source for the Raman system, did not produce SBS at the pump wavelength nor give rise to significant ASE. Furthermore, it should be noted that the 1551nm CWDM filter could be effective in a seed system configured for pumping a 1665nm signal (which corresponds to strong, alternative methane absorption line) because 1555-1560nm is an effective band over which to pump a 1665nm Raman Stokes wave. This was not carried out during the development process because a 1665nm DFB of sufficient output power was not available, but this could be a relatively simple development to target an alternative methane absorption line at 1665nm. From the investigations, the best results were obtained when around 10mW of Raman seed power was available at the start of the Raman gain medium.

6.2.3 Suppression of SBS of the Raman Signal

In the case of the amplified methane sensing signal, the WMS technique requires that the signal must be of narrow bandwidth compared to the gas absorption line for good sensitivity (See Figure 1.1 and surrounding discussion in Section 1.4). The DFB output is optimal in terms of producing a strong gas signal but its bandwidth is narrower than the Brillouin gain bandwidth. With a considerable increase in bandwidth required to suppress SBS to acceptable levels, it was impractical to

employ a broad bandwidth signal and compromise on gas sensing sensitivity and for this reason, it was necessary to consider other SBS suppression techniques. The most elegant of these was a technique to emulate signal bandwidth broadening via wavelength modulation, which essentially distributes the spectral power of the signal over the modulation bandwidth with respect to the entire gain fibre length. (See description in Section 2.10.4) This technique was conceived to suppress SBS in high capacity optical communications links, where a wavelength dither is applied on top of any signal modulation (i.e. bit sequence). The elegance of this solution with respect to a WMS signal propagating in an optical fibre is that the WMS signal modulation itself can be optimised for the purpose of SBS suppression with no detriment to gas sensing performance, thus serving two purposes simultaneously. This essentially meant that the WMS signal could be amplified to high power while conducting its normal operation without the need for special or multiple gain fibres, components or external techniques, thus maintaining low cost and simplicity. This was a significant milestone in the system development.

The effect of dither depth on SBS backscatter was then characterised for the main fibre gain media. Although only around 3GHz peak to peak modulation depth was available, limited by the gas sensing modulation requirements, this was sufficient to suppress SBS in the signal up to high power. This was made possible because efforts were made to confine the high signal power propagation within the shortest possible length by using both the shortest useable length of gain fibre and a counter-pumping configuration. The theoretical analysis of the gain dynamics of the signal in co and counter-pumping configurations suggests that the majority of gain occurs closer to the end of the fibre in the counter-pumping configuration compared with co-pumping, thus reducing the effective Brillouin gain length. The fact that counter-pumping increases SBS threshold has been demonstrated through the fact that SBS was more restrictive in the co-pumping configuration for the same length of gain fibre during experiments for standard SMF fibre systems (see Section 4.7.3 comparing Figures 4.26 and 4.27). Together, through the techniques applied in the design and modulation scheme, a multi-Watt narrow bandwidth signal was amplified within the amplifier without significant SBS.

6.2.4 Final Raman Amplifier System

The finalised Raman amplifier system was constructed from communications components, and the relatively common DSF fibre. This meant that a reliable, low loss fibre system was constructed at a low cost. The maximum signal power achieved was 2.36W (1.9W used in field trials to avoid multi-path interference MPI arising from connectors requiring cleaning and improve reliability) with an optical efficiency of 44%. This could be rectified by protecting the optics more efficiently. The maximum output power achieved was limited by the maximum output power of the pump EDFA. The conclusion is that the amplifier system represents a significant technological advance in the field of remote natural gas leak detection. Furthermore, the additional power beyond the requisite 1W further increases the feasibility of the system as an airborne leak detector system. One of the main limitations of this configuration is that scanning the ground at speed, which is potentially made up from a continuum of slightly different backscatter surfaces, leads to additional noise through rapidly changing received power levels but the extra power could help to overcome this to achieve an acceptable gas SNR.

6.3 Conclusions of the Short Range Stand-off Methane Detection and Backscatter Investigations

Short range standoff methane measurements were made with the purpose of establishing the send and receive power requirements at this range for a range of integrated path methane concentrations. These, in conjunction with a practical confirmation of the dependence of backscatter intensity with the square of range, established the send and receive power requirements for the 100m leak detection field trial. It was found that with the Tx-Rx (send-receive) system employed that around 300mW would be required to detect a 100ppm.m methane cloud at 100m using the worst surface tested in the short range investigations (concrete garden block). This was determined from a required 3.3mW launch power (using the prototype at short range) at an 11m range to achieve the requisite 380nW at the detector, resulting in a 3:1 SNR by visual assessment. Given that up to 2.36W would

be obtained from the final sensor system, this implied that a range of 294m should be possible.

6.4 Conclusions of the Field Trials

The prototype system, whose design was essentially a packaged version of the lab demonstrator, was taken to field trials and tested at 105m from the back of a van. Methane samples of 10000ppm.m, 1000ppm.m and 100ppm.m were placed in front of the Fresnel lens in addition to background level at approximately 350ppm.m and gas signals were recovered from a variety of surfaces. It was found that a SNR of >3:1 was recoverable in the single scan limit for integrated path concentration levels down to background (350ppm.m) from all of the backscatter surfaces tested using 1f detection.

The demonstration of the detection of 100ppm.m was required, but showing gas signals of 100ppm.m methane samples at 100m range did not demonstrate this alone because over this long return path, background methane added 350ppm.m integrated path concentration to the 100ppm.m sample. Furthermore, the comparison of background level (with no Tedlar bag) and background plus 100ppm.m in a Tedlar bag was not useful because of the additional signal attenuation due to the Tedlar bag. Hence, the 100ppm.m sensitivity was demonstrated in the lab, using received powers comparable to those received during the field trials (by comparing the gas signal magnitudes for a known methane concentration from the same surface as was taken to the field trials). Hence, to take account of the Tedlar bag attenuation, the investigation was simply carried out with one 100ppm.m and one unfilled Tedlar bag and compared with two 100ppm.m Tedlar bags placed one after the other in front of the Fresnel lens, while using return powers available from the worst surface tested at 105m. The demonstration of this level of sensitivity was successful and hence the system met or exceeded all of its specified requirements. Furthermore, most of the results were achieved in unfavourable conditions (unstable power supply, strong

winds, rain and mud on lenses, targets and sample bags) with what was essentially a makeshift Tx-Rx unit.

6.5 Summary of Conclusions

Recall that the overall aims of the project were to design a long-range (>100m), open-path, single-ended methane leak sensor system with a 100ppm.m sensitivity (above background) using a CW Raman amplifier of output power in excess of 1W. These aims have all been exceeded as discussed below.

A 2.36W, 1651nm WMS source based around a counterpumped FRA was developed using dispersion shifted fibre, which is commonly used in telecommunications, as the gain medium. SBS was suppressed through spectral control of the pump source and optimisation of the WMS wavelength dither for the narrow bandwidth 1650nm signal and did not limit the output power of the system. MPI did appear intermittently at the maximum signal output level, but this could be dealt with by more careful design of the Tx fibres and optics. This source was projected to be effective at producing a gas signal for methane concentration paths down to 100ppm.m with received powers much less than those expected with the source running at full power directed at a diffuse surface at 100m range (through scaled power investigations). Given the power available from the Raman amplifier system, knowledge of the transmitted signal power levels required to obtain a 3:1 SNR gas signal from a variety of surfaces and the verification of the relationship between backscattered intensity (at the detector) with range, a maximum effective range for 100ppm.m methane detection was calculated to be 294m for one of the worst surfaces investigated (concrete). Furthermore, the prototype system was tested at 105m using a simple Tx-Rx head and a 1.9W transmit power for a full demonstration of this performance. A SNR of 3:1 was exceeded for all gas samples, including background at ~340ppm.m from all surfaces tested.

6.6 Further Work to Move from Prototype Sensor System to Commercialisation

6.6.1 Further Work in the Raman Amplifier System

The first possible improvement to the amplifier system would be to further optimise the signal for methane sensing. Given that the 1f signals tended to be much stronger than the 2f signals in the methane measurements, it is particularly desirable to make best use of the 1f signal. The main problem with using the 1f signal is the DC level from the RAM background, which limits the gain that can be applied by the LIA before it saturates. The RAM is generally separated as much as possible from the signal by the LIA using the fact that the amplitude modulation and frequency modulation (which leads to the gas signal) are phase separated, but unless the signals are in quadrature, there is still some RAM component on the gas signal. It should be possible to suppress RAM in the design of the amplifier system, or in particular the signal source.

Currently, the WM modulation is applied to the DFB via current modulation which leads to both wavelength and amplitude modulations. However, injection locking of a communications DFB laser in order to achieve pure AM or pure FM signals has been demonstrated [6.1]. The principle of the required pure FM technique is that if a DFB laser incurs some light into its cavity close to its centre wavelength, the DFB can lock onto this signal. With sufficient input optical power passing through its isolator into the cavity, it is possible to cause the output of the DFB to follow a wavelength modulation applied to the incoming light. This causes very little amplitude modulation of the output from the laser, which is ultimately responsible for the non-zero baseline of the 1f gas signal, compared with modulation via the current.

Given the application of this technique, it would be necessary to normalise the gas signal (i.e. remove the dependence of gas signal amplitude on received power so that it depends only on gas parameters) by some other means than the RAM amplitude. This could be done by applying a chopper to the residual pump power and

transmitting this onto the same surface as the WMS signal, or by normalising the 1f signal to another harmonic gas signal.

6.6.2 Proposed Improvements to the Send-Receive Head

The main area for improvement can be found in the Tx-Rx unit. In the final prototype this unit is a large and rather heavy (20kg) plate aluminium cube. There is no immediate advantage to making such a robust construction when considerable effort has been allocated to the design of a light weight fibre amplifier system. It could be made much smaller and lighter in a custom built package. If the entire system is made to be very light it could conceivably be mounted on an unmanned aircraft on a pre-designated monitoring route. This would further increase the economic advantages of the system.

The collector lens and the transmit output lens are placed side by side on the faceplate of the box, which means that the receiver position relative to the collector lens must be optimised on an XYZ stage if the target is moved. This resulted in the need to open the send receive head to adjust the position of the receiver with every measurement during the lab and field trials, leading to inconvenience and possible inaccuracy of gas measurement. The best way to arrange the transmission and collection optics is for them to share an optical axis and in this way the receiver is always properly aligned. This improvement (or one that obtains the same effect) is regarded as absolutely mandatory in terms of commercialising the system, since otherwise it confines the use of the sensor system to applications where the beam is directed across a long, fixed path with a stationary backscatter surface.

In addition to the alignment of the send telescope and receiver, the Fresnel lens could be replaced by a parabolic mirror (focussing onto a backward facing detector). This could be advantageous because Perspex is not optimal at transmitting 1651nm and the Fresnel lens was found to have an attenuation of more than 1dB >20%. Again, with significant effort applied to the maximisation of the output signal power, it is counter-intuitive to waste so much in the receive optics. In contrast, the reflectivity of the surface of a parabolic mirror could be around 99% at 1651nm, thus improving

the collection efficiency considerably. In order to further increase collection efficiency, a cone concentrator could be fixed to the front of the photodetector.

In order to reduce detector noise and saturation in strong sunlight, a filter was included in front of the photodetector. A UV filter was used because these could be obtained relatively conveniently and cheaply. However, the use of a narrow band pass filter with good transmission properties around 1651nm could reduce noise considerably, increase 1651nm transmission and hence increase sensitivity and might be worth additional cost in a fully commercialised system.

6.6.3 Further Applications and Modifications

Considering the system in its primary aerial natural gas detection role, it would be possible to make a scan pattern for the output beam that could provide methane concentration information as a function of position on a scan grid. This could be matched up with GPS positioning and an image from a camera, thus allowing operatives to 'see' gas leaks in order to locate leaks more effectively.

It can also be seen that, with the development of a long range sensor system, with essentially two broad gain bandwidth amplifiers available, it should be a reasonably small step to make the system applicable to numerous species for a range of environmental monitoring roles for security, industrial sensing and emissions control and inspection roles. The EDFA can amplify signals between around 1530-1570nm and the Raman amplifier stage can scatter this power to between 1620-1680nm, both with reasonable efficiency and CW signal power levels of the order of Watts obtainable. The output wavelength is determined by the signal laser and its potential power (if Raman scattered) depends upon the pump spectrum available via the seed source.

Using a VCSEL with a movable MEMS cavity mirror would allow broad wavelength tuning of a WMS signal source, or alternatively, a range of standard DFB lasers could be combined and activated as required. Their output could be channelled to the EDFA or the Raman amplifier system using optical switches similar to those used in communications, as could the output from the EDFA (i.e. the output of the EDFA

might need to feed to the Raman system to act as a pump or directly to the Tx system if the signal is in the EDFA gain band.) The seed spectrum could be adjusted with the use of a suitable, electronically controlled, broad bandwidth tuneable filter while using the EDFA to pump the Raman amplifier stage.

Although these suggested improvements add some complexity and redundancy to the system, it would be much more economical than employing many different sensor systems and conducting separate inspections in areas that require monitoring for numerous species. Some examples of species that could be monitored apart from methane include CO, CO_2, CH_2CL_2, NH_3 and H_2S. Hence, with only an improvement to the Tx-Rx head and some work on the packaging, the sensor system would be likely represent the state of art in long-range methane leak detection and with some or all of these improvements, it could represent the state of art in wide area environmental monitoring for a broad range of applications from health and safety to security and defence as well as greenhouse gas/carbon emission monitoring.

6.7 References

[6.1] L Th´evenaz, S Le Floch, D Alasia and J Troger "Novel schemes for optical signal generation using laser injection locking with application to Brillouin sensing" Meas. Sci. Technol. 15 (2004) 1519–1524

Appendix: Publications

Conference Papers

D. Mitchell, K. Duffin and W. Johnstone, *"Remote methane sensor using tuneable diode laser spectroscopy (TDLS) via a 1W Raman source"*, Twentieth Conference on Optical Fibre Sensors, Edinburgh, UK, 5-9 October 2009. DOI: 10.1117/12.835810

D. Mitchell, K. Duffin and W. Johnstone, *"Remote methane sensor using TDLS via a high power Raman amplified source"*, International Conference on Field Laser Applications in Industry and Research, Grainau, Germany, 6-11 September 2009.

D. Mitchell, K. Duffin and W. Johnstone, *"Remote methane sensor using Raman amplified open path TDLS"*, 7th International Conference on Tunable Diode Laser Spectroscopy (TDLS), Zermatt, Switzerland, 13-17 July 2009.

D. Mitchell, K. Duffin and W. Johnstone, *"Remote tuneable diode laser spectroscopy (TDLS) via a 1W Raman source"*, SPIE Optical Sensors 2009, Prague, Czech Republic, April 2009. DOI: 10.1117/12.820567

W. Johnstone, K. Duffin and. D Mitchell, *"Remote gas detection using tunable diode laser spectroscopy with high power rare earth and Raman fibre amplifiers" Invited Paper*, Photonics 2008, New Delhi, India, December 2008.